Award Number: W81XWH-11-1-0716

TITLE: Development of a Novel Synthetic Drug for Osteoporosis and Fracture Healing

PRINCIPAL INVESTIGATOR: Hiroki Yokota, PhD

CONTRACTING ORGANIZATION: Indiana University
INDIANAPOLIS, IN 46202

REPORT DATE: NOVEMBER 2015

TYPE OF REPORT: Final Report

PREPARED FOR: U.S. Army Medical Research and Materiel Command
Fort Detrick, Maryland 21702-5012

REPORT DOCUMENTATION PAGE

Form Approved
OMB No. 0704-0188

1. REPORT DATE	2. REPORT TYPE	3. DATES COVERED
NOVEMBER 2015	Final Report	22AUG2011 - 21AUG2015

4. TITLE AND SUBTITLE
Development of a novel synthetic drug for osteoporosis and fracture healing

5a. CONTRACT NUMBER

5b. GRANT NUMBER
W81XWH-11-1-0716

5c. PROGRAM ELEMENT NUMBER

6. AUTHOR(S)

Hiroki Yokota, PhD

E-Mail: hyokota@iupui.edu

5d. PROJECT NUMBER

5e. TASK NUMBER

5f. WORK UNIT NUMBER

7. PERFORMING ORGANIZATION NAME(S) AND ADDRESS(ES)
Indiana University
Biomedical Engineering, 723 W. Michigan St., Indianapolis, IN 46202
Anatomy and Cell Biology, 635 Barnhill Drive, Indianapolis, IN 46202

8. PERFORMING ORGANIZATION REPORT

9. SPONSORING / MONITORING AGENCY NAME(S) AND ADDRESS(ES)
U.S. Army Medical Research and Materiel Command
Fort Detrick, Maryland 21702-5012

10. SPONSOR/MONITOR'S ACRONYM(S)

11. SPONSOR/MONITOR'S REPORT NUMBER(S)

12. DISTRIBUTION / AVAILABILITY STATEMENT
Approved for Public Release; Distribution Unlimited

13. SUPPLEMENTARY NOTES
None

14. ABSTRACT

This 4-year study strongly supported salubrinal's therapeutic action on the prevention of bone loss by elevating bone formation and inhibiting bone resorption. The observed dual role of salubrinal is unique, and currently no therapeutic drugs provide these dual functions. In the animal experiments for evaluating the effects of salubrinal on osteoporosis, osteonecrosis and bone fracture healing, salubrinal presented its anabolic and anti-catabolic effects. In *in vitro* experiments, the mechanisms of salubrinal's action through genome-wide mRNA and micro RNA analyses revealed that salubrinal induces its unique functions through novel targets in bone remodeling, which are mediated by eukaryotic translation initiation factor 2 alpha (eIF2a) signaling. The U.S. patent for use of salubrinal in treatment of bone diseases was issued in 2015.

15. SUBJECT TERMS Nothing listed

16. SECURITY CLASSIFICATION OF:			17. LIMITATION OF ABSTRACT	18. NUMBER OF PAGES	19a. NAME OF RESPONSIBLE PERSON
					USAMRMC
a. REPORT	b. ABSTRACT	c. THIS PAGE			19b. TELEPHONE NUMBER *(include area code)*
U	U	U	UU	177	

Main Report

1. INTRODUCTION

This 4-year research project (W81XWH-11-1-0716; Development of a novel synthetic drug for osteoporosis and fracture healing) was conducted at Indiana University, Indianapolis, IN from September 2011 to August 2015, as a collaborative project among the Departments of Biomedical Engineering (PI, Hiroki Yokota, PhD), Anatomy and Cell Biology (co-I, Teresita Bellido, PhD), Medicine (co-I, Munro Peacock, MD, Division of Endocrinology), and Orthopaedic Surgery (Jeffrey Anglen, MD). The project was also conducted in collaboration with Indiana University Research and Technology Corporation that handled intellectual properties and assisted commercialization planning.

The project mainly focused on the characterization and examination of salubrinal ($C_{21}H_{20}Cl_3N_4OS$; 479.8 Da), a novel drug candidate, for treatment of bone diseases such as osteoporosis and osteonecrosis, as well as healing of bone fracture. The research team employed *in vitro* systems (bone cell cultures including osteoblasts and osteoclasts) and a mouse model of osteoporosis, osteonecrosis, and bone fracture.

2. KEYWORDS

Osteoporosis, osteonecrosis, bone fracture, drug candidate, salubrinal, guanabenz, bone formation, bone resorption, apoptosis, osteoblasts, osteoclasts, eukaryotic translation initiation factor 2 alpha (eIF2α)

3. ACCOMPLISHMENTS

Major Goals: The major goal of this proposal was to develop salubrinal as a novel small-molecule drug for enhancing bone formation, and stimulating bone fracture healing. Salubrinal is a synthetic chemical agent, which is known to prevent de-phosphorylation of eukaryotic initiation factor 2 alpha (eIF2α). However, a potential linkage of the regulation of eIF2α to bone metabolism has not been well understood. This project was directed at "osteoporosis and related bone disease" in the FY10 PRMRP topic areas.

This project was aimed to test the hypothesis:

> *A novel synthetic agent, salubrinal, can be administered through multiple routes (oral, subcutaneous injection, intravenous injection, and local deposition) with superior efficacy compared to existing drugs for enhancing bone formation and stimulating bone fracture healing.*

Accomplishments: In this 4-year research project, the key accomplishments are as follows:

(a) Pharmacokinetics and model systems

- A formulation for salubrinal (49.5% PEG – polyethylene glycol 400 and 0.5% Tween 80) was determined.
- An effective dosage for *in vivo* (0.5 – 1.5 mg/kg body weight) and *in vitro* (5 – 20 μM) studies was identified.

(b) Mechanistic study

- *Ex vivo* experiments using bone marrow derived cells showed that salubrinal inhibits osteoclast development and stimulates osteoblast development.
- Genome-wide mRNA expression analysis reveals that both salubrinal and guanabenz downregulate NFATc1 transcription factor, which activates bone resorption, in a novel eIF2α mediated pathway.
- Salubrinal and guanabenz significantly changes the expression levels of micro RNAs (e.g., miR-221, miR-222).
- There is a cross talk between salubrinal and alendronate (bisphosphonate) in the responses to glucocorticoid that induces osteonecrosis.

(c) Pre-clinical animal studies

- *In vivo* experiments using ovariectomized mice revealed that administration of salubrinal reduces fat weight, and prevents reduction in uterus weight and BMD/BMC.
- The decrease in bone mass and bond formation rate and the increase in osteoblasts and osteocyte apoptosis, which is induced by glucocorticoid at 1.4 mg/kg/day, are abolished by treatment with salubrinal.
- Administration of salubrinal elevates bone formation at the site of tibia fracture by increasing BMD (bone mineral density) and BMC (bone mineral content).

(d) Intellectual properties

- A U.S. patent (Method for treatment of bone diseases and fractures; 13/055,399) was issued in June 2015.

Two review articles on potential use of salubrinal for treatment of skeletal diseases were published (**Appendices 3 & 4**). Below are the detailed descriptions of accomplishments with supporting data for the tasks in SOW.

Task #1 – Develop formulations for four routes of administration (oral, subcutaneous – s.c., intravenous – i.v., and local immobilization in implantable matrix), and determine pharmacodynamics.

Subtasks 1a and 1b: Develop salubrinal formulation

A formulation screen was performed to identify physiological conditions compatible with injection and oral administration with satisfactory salubrinal solubility. A total of 25 candidates were prepared in a phosphate buffer or water, in which a selection of surfactants, co-solvents, and complexing agents was tested. A rapid, stage-appropriate HPLC-UV (high performance liquid chromatography - ultra violet) method was developed for the quantitation of salubrinal concentration in solution. The quantification of salubrinal solution concentration in the subsequent studies was carried out relative to a single external standard containing 0.1 mg/mL salubrinal, using an average peak area of triplicate injections. The results are presented in **Table 1**. The greatest solubility of salubrinal was achieved in vehicles containing PEG (polyethylene glycol) 400 and TPGS (vitamin E d-α-tocopheryl polyethylene glycol 1000 succinate).

Seven formulations were identified with salubrinal concentrations from 0.3 to 1.8 mg/ml (**Table 2**). A number of vehicles suitable for i.v. and oral administration of salubrinal were prepared with satisfactory active pharmaceutical ingredients (API) concentration and recovery upon dilution into simulated physiological fluids. The vehicles may be ranked based on their concentration in vehicle, composition, and performance in these *in vitro* tests. In the absence of the *in vitro/in vivo* correlation, all parameters are considered equally important. The correlation between the *in vitro* data sets and performance *in vivo* will have to be established as the project progresses into the animal testing phase. Of these, four are appropriate for i.v. administration and six for oral administration. The samples were subsequently diluted into simulated plasma and simulated gastric and intestinal fluids, as appropriate, and were analyzed for percent recovery of API in solution.

Table 1. Salubrinal formulations in simulated gastric fluid (SGF).

Sample #	Vehicle Description (% w/w)[1]	Salubrinal concentration at 24 h, µg/mL	Apparent pH at 24 h
1	20% EtOH	0.6	7.7
2	50% PG	13.6	7.9
3	50% PEG 400	330.8	8.5
4	30% Glycerin	0.4	7.5
5	19.5 % EtOH, 0.5% Tween 80	20.0	7.7
6	49.5% PG, 0.5% Tween 80	74.1	8.0
7	49.5% PEG 400, 0.5% Tween 80	598.4	8.3
8	29.5% glycerin, 0.5% Tween 80	54.3	7.3
9	18% EtOH, 2% DMA	0.7	7.7
10	20% EtOH, 5% TPGS	324.9	7.7
11	18% EtOH, 2% PVP K-15	1.7	7.4
12	48% PG, 2% DMA	17.1	7.8
13	45% PG, 5% TPGS	965.2	7.9
14	48% PG, 2% PVP K-15	24.2	7.4
15	48% PEG 400, 2% DMA	427.5	8.4
16	45% PEG 400, 5% TPGS	1849.9	8.2
17	48% PEG 400, 2% PVP K-15	347.1	7.9
18	10 mM pH 7.4 phosphate buffer	0.0	7.5
19	10 mM pH 3.0 phosphate buffer	0.0	3.7
20	0.25% methylcellulose in water	0.0	6.3
21	0.5% HPMC in water	0.0	7.0
22	10% HPβCD in 10 mM pH 7.4 phosphate buffer	6.2	7.4
23	30% HPβCD in 10 mM pH 7.4 phosphate buffer	40.1	7.5
24	10% Captisol in 20 mM pH 7.4 phosphate buffer	6.0	7.0
25	20% Captisol in 20 mM pH 7.4 phosphate buffer	18.5	6.8

[1] Vehicles 1 – 17 were prepared in 10 mM pH 7.4 phosphate buffer.

Table. 2. Solubility of salubrinal.

Sample #	Vehicle Description (% w/w in 10 mM pH 7.4 phosphate buffer)	Conc. API at 24 h, µg/mL	Apparent pH at 24 h	% Recovery in SP (1:8)	% Recovery in SGF (1:10)	% Recovery in SIF (1:10)[3]
3	50% PEG 400	330.8	8.5	65.3	62.5	12.1
7	49.5% PEG 400, 0.5% Tween 80	598.4	8.3	80.4	76.1	53.6
10	20% EtOH, 5% TPGS[1]	324.9	7.7	n/a	82.4	73.6
13	45% PG, 5% TPGS[1]	965.2	7.9	n/a	75.3	85.4
15	48% PEG 400, 2% DMA[2]	427.5	8.4	81.9	n/a	n/a
16	45% PEG 400, 5% TPGS[1]	1849.9	8.2	n/a	0.0	90.9
17	48% PEG 400, 2% PVP K-15	347.1	7.9	79.6	78.0	15.3

Samples 10, 13, and 16 are identified for oral administration only, while the sample 15 for injection only. Samples 3, 7, and 17 are for both oral administration and injection. Since API of the sample 7 (49.5% PEG400 and 0.5% Tween 80) is the highest among three samples, we decided to use the formulation of this sample hereafter.

Subtask 1C: Develop a procedure for local implantation (**Appendix 11**)

Salubrinal loaded poly lactic-co-glycolic acid (PLGA) (50:50, MW: 30-60 kDa, Sigma) microparticles were prepared using oil-in-water emulsion method. First, 100 mg/ml of PLGA was dissolved in dichloromethane (DCM). Next, 2 mg of salubrinal was added to 1 ml of PLGA/DCM solution, followed by vortexing for 1 minute. The primary emulsion was added to 2 ml of 1% poly(vinyl alcohol) (PVA) solution and vortexed for 3 minutes. The secondary emulsion was poured into 20ml of aqueous solution containing 0.5% PVA and 450 mM sodium chloride. The emulsion was stirred for 4 hours at 700 rpm to allow the evaporation of DCM, and the hardened microparticles were collected by centrifugation (2000 rpm, 5 min) and washed three times with ddH_2O. The drug-loaded PLGA microparticles were then freeze dried and stored at -20°C until use.

In situ cured PEG hydrogels were prepared by reacting four-arm PEG-acrylate (PEG4A, 20 kDa, synthesized using published protocol) and four-arm PEG-thiol (PEG4SH, 10 kDa, purchased from JenKem Technology USA) (**Fig. 1A)** through Michael-type addition reaction (**Fig. 1B**). Briefly, stock solutions of PEG4A and PEG4SH (both at 20 wt%) were mixed at equal volume and pipetted onto the platform of a digital rheometer (CVO 100, Malvern). Eight-mm parallel plate geometry was used, and the gelation was monitored using single frequency rheometry (1 Hz) operated at 5% strain (**Fig. 1C & D**). In one group, PLGA microparticles (10 wt%) were mixed with the PEG solutions prior to *in situ* rheometry measurement.

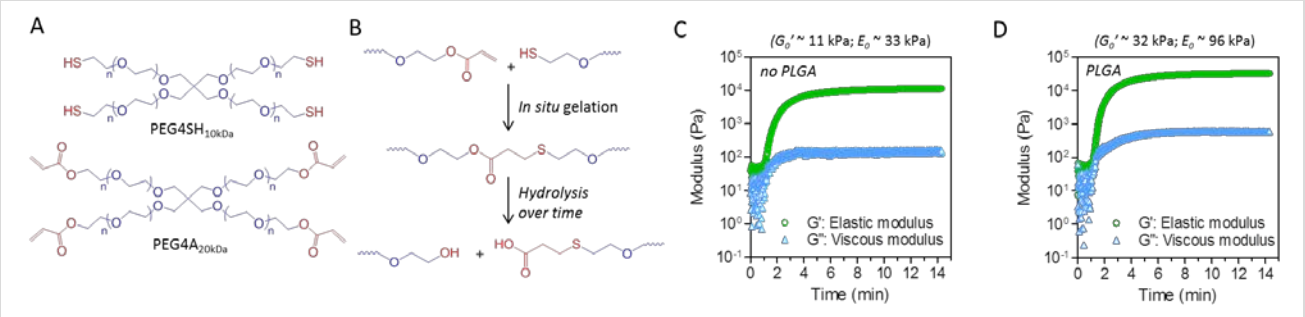

Figure 1. Hydrogel based delivery. (A) Chemical structure of two PEG derivatives (PEG4SH and PEG4A). (B) Chemical reactions for *in situ* gelation and overtime hydrolysis. (C) Changes in moduli during gelation without PLGA particles. (D) Changes in moduli during gelation with salubrinal-loaded PLGA particles.

For the healing of bone fracture (Task 4), we employed hydrogel-based administration of salubrinal.

Subtask 1d: Determine the salubrinal concentrations in serum

Using the formulation identified above, we administered salubrinal by three different routes (SC-subcutaneous, IP – intraperitoneal, and OR – oral gavage) and determined the concentration of

salubrinal in serum. The dosage of salubrinal was 1.25 mg/kg per administration, and blood was drawn at 0 h (prior to administration), 0.5 h, 1 h, 2 h, 4 h, and 8 h. The concentration of salubrinal in serum was determined using mass spectrometry (**Figs. 2 - 4**).

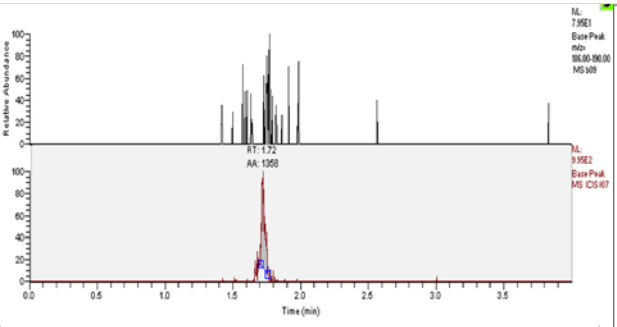

Figure 2. Ion chromatogram of salubrinal detection.

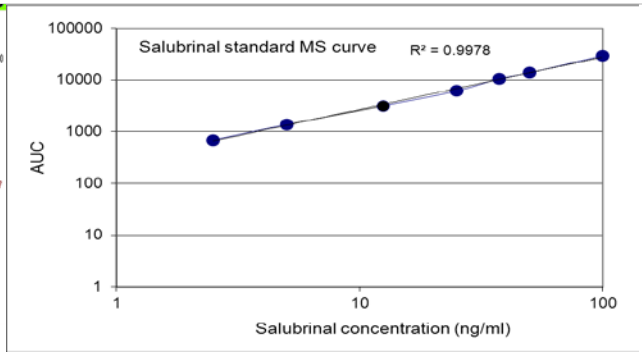

Figure 3. Standard mass spec curve for determining the concentration of salubrinal.

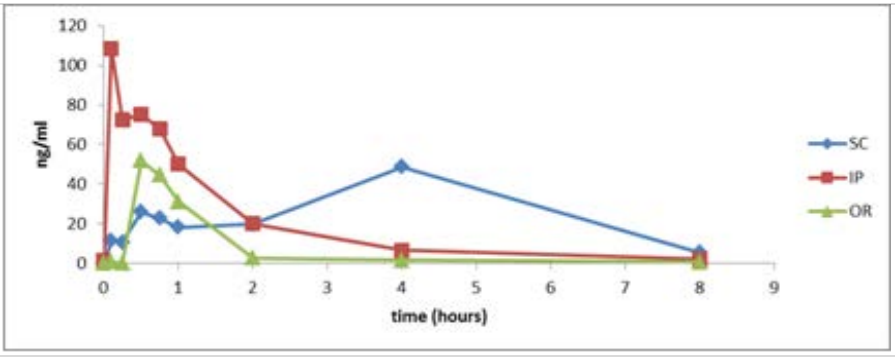

Figure 4. Concentration of salubrinal in serum after administration by three different routes (SC: subcutaneous; IP: intraperitoneal, and OR: oral gavage). Each point represents the average of three measures.

Note that propylene glycol was identified as an excellent solvent of salubrinal, but this agent is a hazardous chemical and we did not use it as a standard formulation.

Task #2 – Evaluate the efficacy of salubrinal on bone formation (Appendices 5, 10). Ovariectomized (OVX) mice demonstrated an increase in body weight over the sham control mice, while subcutaneous administration of salubrinal in weeks 5 to 8 significantly suppressed the OVX-induced increase in body weight ($p < 0.001$) (**Fig. 5A**). Similarly, the uterus weight of OVX mice was significantly decreased compared to sham control mice, while salubrinal administration of OVX mice increased the uterus weight over untreated OVX mice, though this weight was still significantly lower than that of sham control mice (**Fig. 5B**). The percentage of both total fat and abdominal fat was increased in OVX mice when compared to the sham control group and decreased by the administration of salubrinal (**Fig. 5C & D**). OVX mice receiving salubrinal exhibited a statistically significant increase in BMD (bone mineral density) and BMC (bone mineral content) in the lumbar spine, femur, and tibia compared with OVX-only mice (**Fig. 5E & F**). The BMD of the lumbar, femur, and tibia in sham-operated mice were 0.0502 ± 0.0009 g/cm^2, 0.0521 ± 0.0016 g/cm^2, and 0.0492± 0.0009g/cm^2, respectively, while the BMC of the

lumbar, femur, and tibia in sham-operated mice were 0.0693 ± 0.002 g, 0.024 ± 0.0008 g, and 0.0215 ± 0.0029 g.

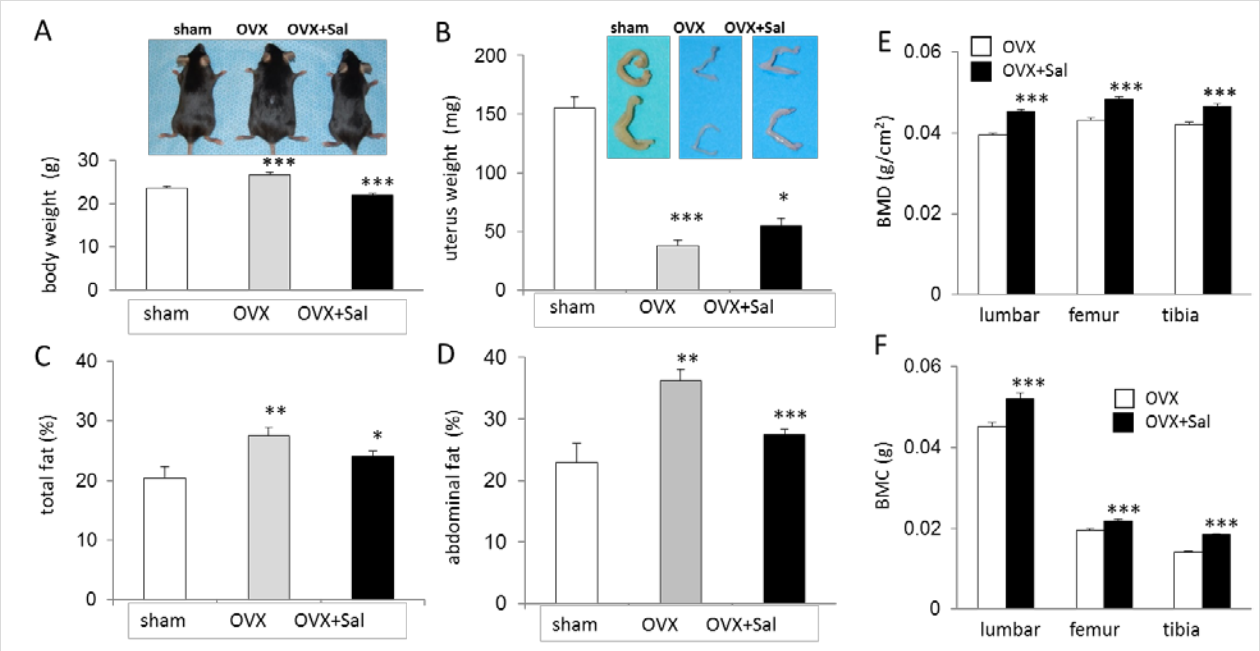

Figure 5. Effects of ovariectomy and salubrinal on body weight, uterus weight, total fat, abdominal fat, BMD, and BMC. (A) Salubrinal-driven suppression of OVX-induced gain of body weight. (B) Salubrinal-driven partial recovery of OVX-induced loss of uterine weight. (C) Salubrinal-induced reduction in total fat (%). Total fat, when compared to sham control, was increased by OVX and decreased by salubrinal. (D) Salubrinal-induced reduction in abdominal fat (%). OVX increased abdominal fat over sham, while salubrinal treatment decreased it. (E and F) Suppression of OVX-induced reduction of BMD and BMC, respectively, in the lumbar spine, femur and tibia. Salubrinal increased BMD compared to OVX in the lumbar spine, femur, and tibia. Asterisks (*, **, and ***) represent statistical significance at $p< 0.05$, $p< 0.01$, and $p< 0.001$, respectively (n=12).

Ovariectomy did not induce a significant change in colony forming units of fibroblasts (CFU-F) or colony forming units of osteoblasts (CFU-OBL) colonies, representing the progenitors of fibroblasts and osteoblasts, respectively, as measured in cultures of bone marrow-derived cells (**Fig. 6A&B**). However, cells derived from OVX mice injected with salubrinal produced more CFU-F and CFU-OBL colonies when compared to cultures established from both sham-operated mice and ovariectomized mice (**Fig. 6A&B**).

To evaluate salubrinal's effect on bone architecture, the BV/TV (bone volume/trabecular volume) ratio in the distal femur was evaluated among these three groups (**Fig. 6C**). Compared to sham-control mice, ovariectomized mice presented a reduction in BV/TV ($p< 0.001$; 32.05 ± 1.5% in sham-control mice, and 19.31 ± 0.82% in OVX mice). However, salubrinal administration significantly restored BV/TV ($p< 0.001$; 25.5 ± 1.03% in salubrinal-treated OVX mice). In response to its daily administration, salubrinal's effects on femoral BMD (bone mineral density) and BMC (bone mineral content) differed between sham-control and OVX mice

(**Fig. 6D**). OVX mice increased BMD and BMC of the femur by 11.8 ±2.7% and 11.8 ±0.8%, respectively. On the other hand, the elevation of BMD and BMC of sham OVX mice was significantly smaller, and they were 3.5 ±1.9% (BMD) and 3.7 ±0.8% (BMC).

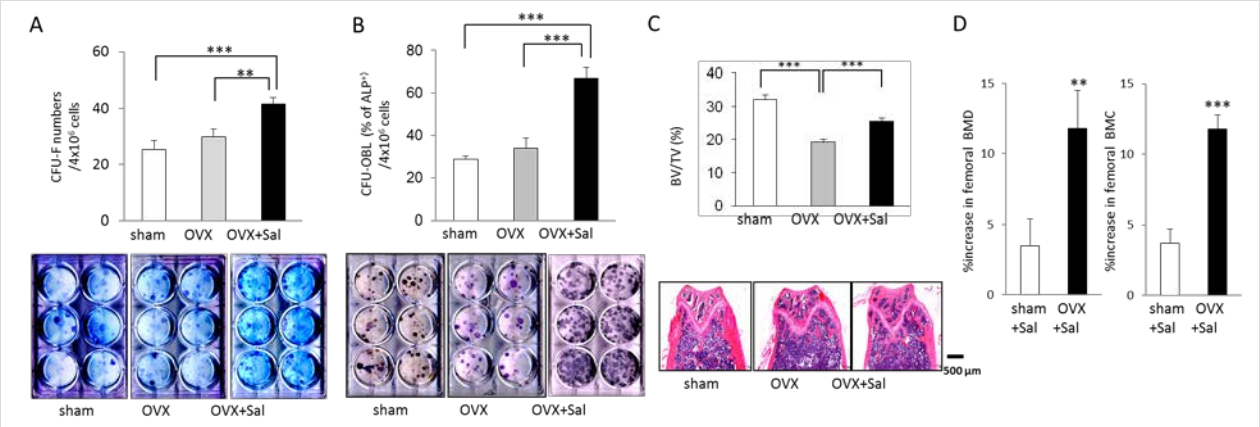

Figure 6. Effects of subcutaneous administration of salubrinal on CFU-F, CFU-OBL, and femoral bone. (A& B) Comparison of CFU-F and CFU-OBL, respectively. Bone marrow-derived cells were isolated from 3 groups of mice (sham, OVX, and salubrinal-injected OVX mice). The representative photographs are shown (n=12). (C) BV/TV ratio in the distal femur (n=6). (D) Comparison of salubrinal-driven increases in femoral BMD and BMC between sham control (n=6) and OVX mice (n=12). Of note, **, and *** for $p< 0.01$ and $p< 0.001$, respectively.

Task #3 – Evaluate the efficacy of salubrinal in preventing bone loss induced by glucocorticoid excess.

Subtask 3a: Evaluate the efficacy of salubrinal in bone loss (**Appendices 7, 8**)
C57BL/6 female mice implanted with pellets containing two different doses of the glucocorticoid (GC) prednisolone (GC1 = 1.4 or GC2 = 2.1 mg/kg/day) received daily injections of salubrinal (1 mg/kg/day). Mice treated with prednisolone exhibited increased apoptosis of osteoblasts in cancellous bone and of osteocytes in both cancellous and cortical bone (**Fig. 7A**). Salubrinal completely blocked GC1-induced apoptosis of both osteoblasts and osteocytes, whereas it only partially prevented the increase in GC2-induced apoptosis of osteoblasts and did not inhibit GC2-induced osteocyte apoptosis. Alendronate effectively prevented GC2-induced apoptosis of both osteoblasts and osteocytes in cancellous bone, although it did not inhibit GC2-induced cortical osteocyte apoptosis. Administration of prednisolone induced a significant decrease in BMD in total body, spine, and femur, at both doses compared to placebo (**Fig. 7B**). Mice implanted with placebo pellets and treated with salubrinal lost significantly less spinal BMD compared to those treated with vehicle. Similarly, mice implanted with GC1 pellets and injected with salubrinal lost significantly less bone compared to mice implanted with GC1 pellets and injected with vehicle. On the other hand, salubrinal did not prevent the loss of bone induced by GC2. In contrast, inhibition of resorption with alendronate not only prevented GC2-induced bone loss, as previously shown, but also increased BMD over placebo treated mice. Moreover, GC1 and GC2 reduced bone formation rate (BFR) in cancellous bone by a combination of reduction in MS/BS (mineralizing surface/bone surface) and in MAR (mineral apposition rate) (**Fig. 7C**).

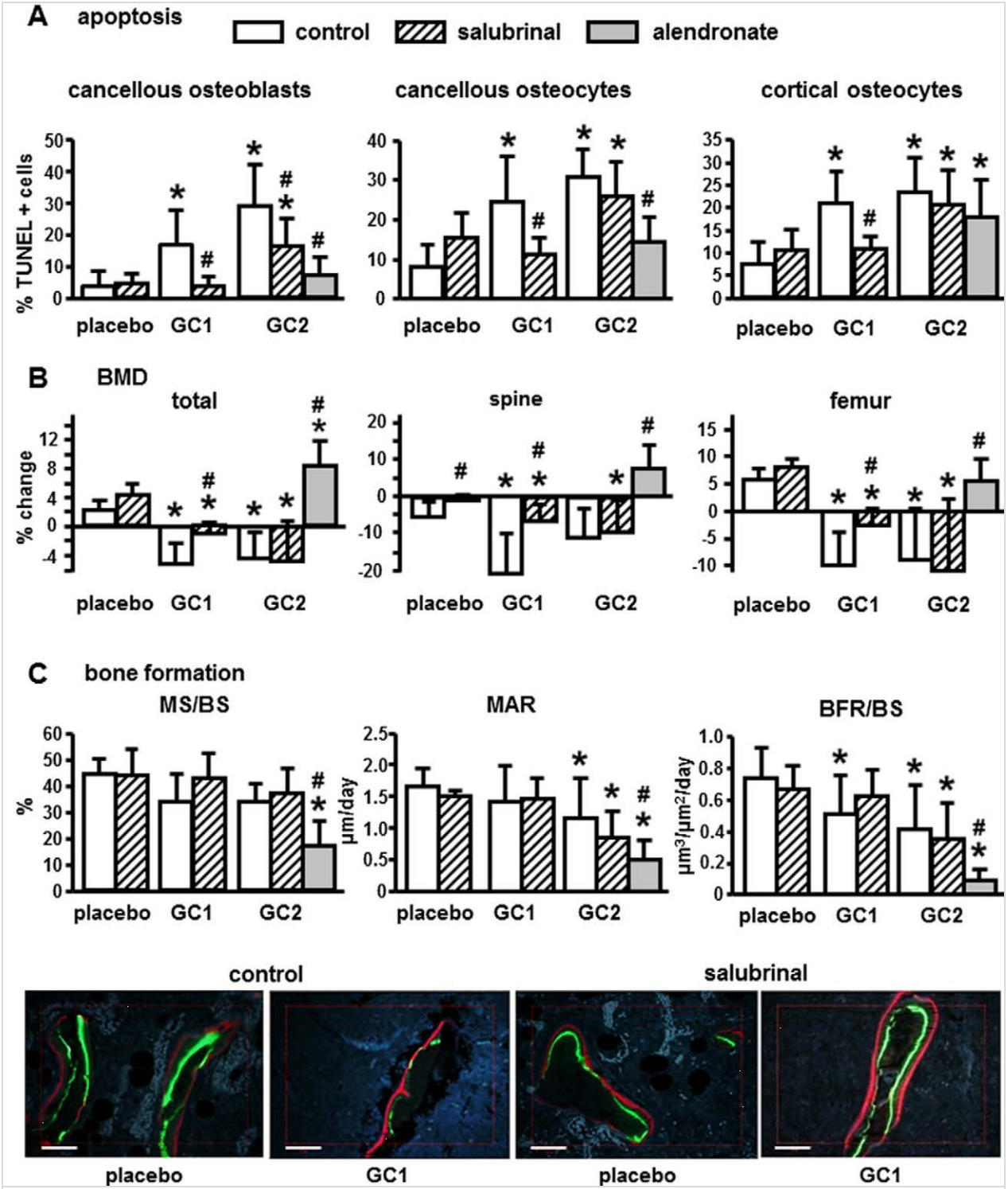

Figure 7. Salubrinal protects against glucocorticoid-induced apoptosis and consequent bone loss in vivo. (A) TUNEL and (C) dynamic histomorphometric data was obtained from longitudinal distal femur sections. Bars correspond to 50 μm. (B) BMD percent changes for placebo, 1.4 mg/kg/day prednisolone (GC1), or 2.1 mg/kg/day prednisolone (GC2) pellet implanted mice with or without salubrinal intervention were determined by DXA (dual energy X-ray absorptionmetry) analysis. Bars represent the

means ± SD of N = 7–10 for (A) and (C) and N = 6–10 for (B). Statistical analysis for placebo, GC1, and GC2 treated mice treated with vehicle (control) or salubrinal was performed by two-way ANOVA. *p < 0.05 vs. placebo mice injected with vehicle (control) or salubrinal. #p < 0.05 vs. the corresponding GC treated mice injected with vehicle (control). The effect of alendronate on GC2 treated mice was analyzed by comparing placebo, GC2, and GC2 plus alendronate by one-way ANOVA. *p < 0.05 vs. placebo mice injected with vehicle (control) and #p < 0.05 vs. GC2 treated mice injected with vehicle (control).

Subtask 3b: Investigate molecular pathways (**Appendices 1, 2, 6**)

Treatment with salubrinal or guanabenz increased mineralization of OB-6 cells (**Fig. 8A & B**). Further, either compound partially prevented the decreased mineralization induced by glucocorticoid (GC) in OB-6 or primary osteoblasts (**Fig. 8**). Thus, salubrinal increased mineral content in cells treated with GC compared to GC alone after 7 and 10 days of culture (**Fig. 8A**). However, salubrinal treatment could not block GC reductions in mineralization after 14 days of GC exposure, but guanabenz remained effective throughout the two week GC treatment period (**Fig. 8A–C**).

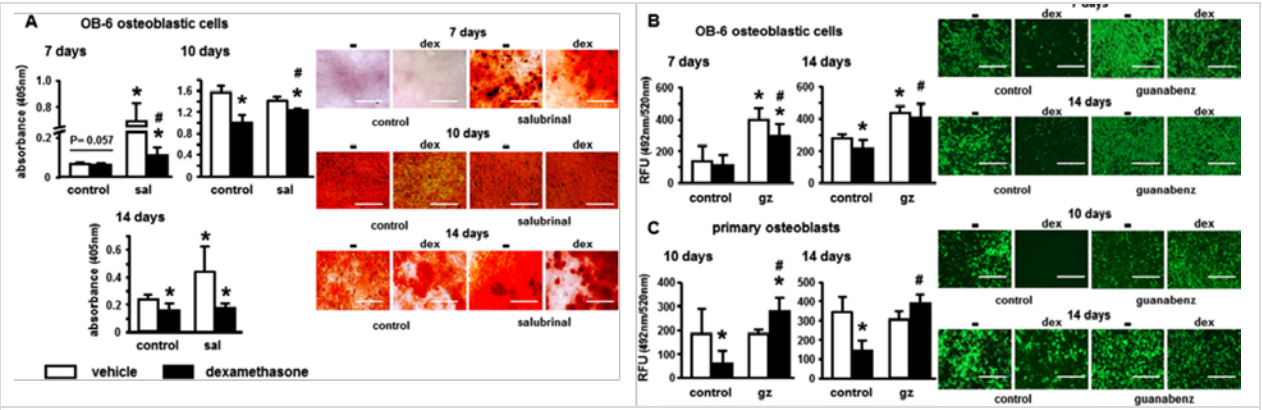

Figure 8. Salubrinal and guanabenz ameliorate the inhibitory effects of GC on matrix mineralization. (A) Mineralization was determined in vehicle (veh) or dexamethasone (dex) treated differentiated OB-6 cells without (control) or with salubrinal (sal) pre-treatment for 7, 10, and 14 days by Alizarin Red S staining. (B) & (C) quantification of mineralization in OB-6 (B) and calvaria-derived (C) osteoblastic cells treated with vehicle or dexamethasone with or without guanabenz (gz) for the indicated incubation periods. Hydroxyapatite accumulation was measured by OsteoImage Mineralization Assay Kit. Lines correspond to 400 μm. Bars represent the means ± SD of N=3 for (A) and N=12 for (B–C). *p < 0.05 vs. vehicle-treated control cells and #p < 0.05 vs. dexamethasone-treated control cells, by one-way ANOVA.

In order to elucidate the mechanism of salubrinal's action on bone-resorbing osteoclasts, we conducted RNA silencing using siRNA specific to Rac1 (Ras-related C3 botulinum toxin substrate 1) (**Fig. 9**). When Rac1 was partially silenced, RANKL (receptor activator of nuclear factor kappa B ligand)-induced stimulation of TRAP (tartrate resistant acid phosphatase) and cathepsin K was partially suppressed. However, RANKL-induced stimulation of NFATc1 (master transcription factor for osteoclast development) was unchanged. Based on the result from this experiment, we proposed the mechanism of salubrinal's action (**Fig. 9C**).

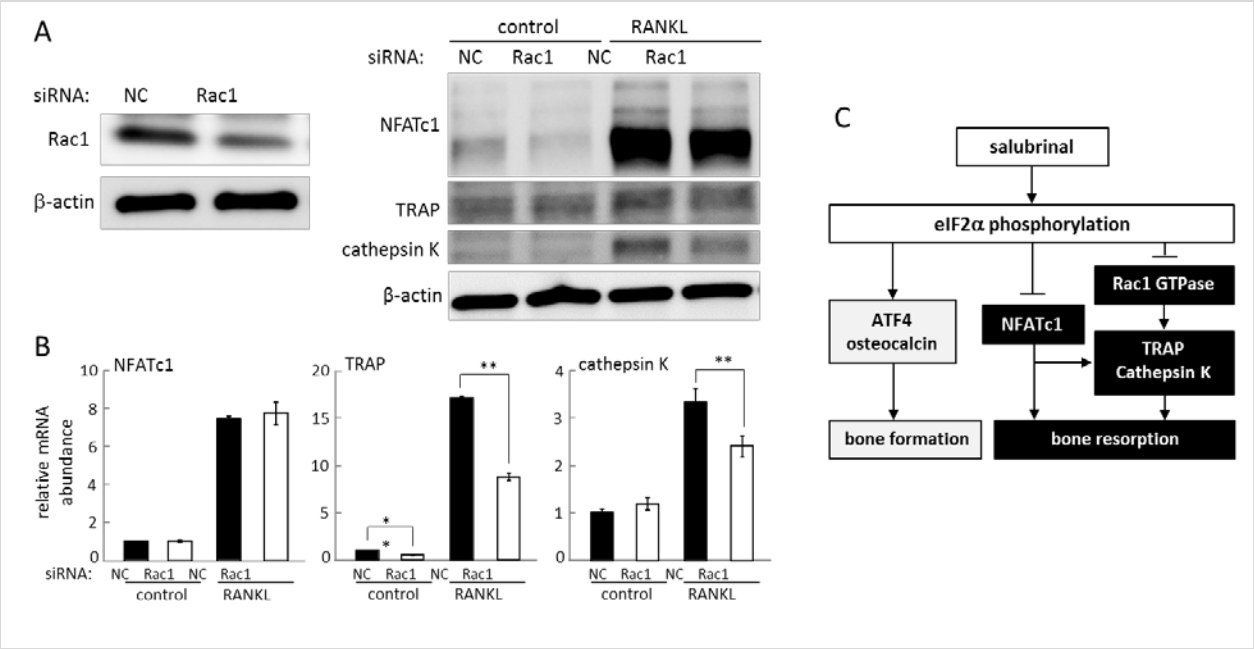

Figure 9. Effects of Rac1 siRNA on expression of NFATc1, TRAP and cathepsin K in RAW264.7 cells. (A) Partial silencing of Rac1 protein level by Rac1 siRNA, and protein expression of NFATc1, TRAP, and cathepsin K. NC = treatment with non-specific control siRNA. (B) Relative mRNA levels of NFATc1, TRAP, and cathepsin K in response to Rac1 siRNA. TRAP and cathepsin K expressions are reduced by Rac1 siRNA, but NFATc1 expression remains unchanged. (C) Proposed mechanism of salubrinal's action in bone remodeling.

Regulation of micro RNA by salubrinal (**Appendix 9**)
In response to RANKL treatment of RAW264.7 pre-osteoclasts for 2 days, expression levels of ~20 miRNAs (micro RNAs) were significantly altered in the microarray-based assay (**Fig. 10**). In particular, the heat map of the selected miRNAs (signal value > 500 and $p < 0.05$) shows that miRNAs such as miR-221-3p and miR-222-3p were downregulated by RANKL, while miRNAs such as miR-125b-5p and miR-182-5p were upregulated (**Fig. 10A**). Principal component analysis (PCA), a statistical technique for finding representative axes in multidimensional data, was used to examine 6 miRNA samples (C1-C3, and R1-R3) to reveal that three RANKL-treated samples had a larger value in the second principal axis than three control samples (**Fig. 10B**). Among 17 miRNAs in **Fig. 10A** that significantly altered their expression levels by RANKL with high signal values (max signal > 500), two miRNAs (miR-221-3p and miR-222-3p) were positioned with the smallest second principal component values (**Fig. 10C**).

To evaluate the role of c-Src (proto oncogene tyrosine protein kinase Src) in RANKL-driven osteoclastogenesis, we employed siRNA specific to c-Src and determined the protein levels of NFATc1, TRAP, and cathepsin K. The significant reduction in the mRNA and protein levels of c-Src was confirmed. The result with c-Src siRNA showed that the protein level of NFATc1 was not significantly altered. However, in response to RANKL treatment, the protein levels of TRAP and cathepsin K were significantly reduced by c-Src siRNA. Of note, the expression of miR-221-3p or miR-222-3p was not significantly affected by c-Src siRNA treatment. TRAP staining

revealed that the number of multi-nucleated osteoclasts was significantly reduced in the presence of c-Src siRNA (**Fig. 11A&B**). Furthermore, an osteoclast activity assay showed that the number of pits, formed by active osteoclasts, was lowered by c-Src siRNA treatment (**Fig. 11C&D**).

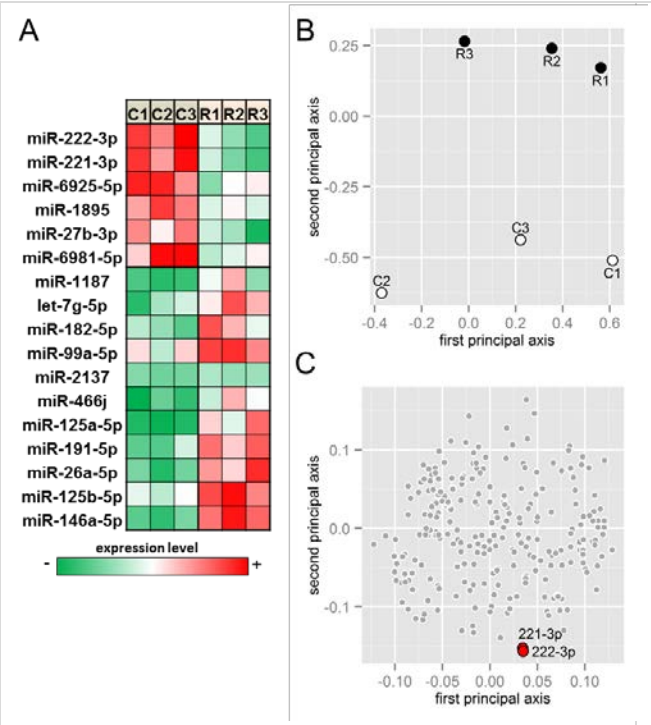

Figure 10. Microarray-based miRNA expression analysis. Cells were stimulated with 20 ng/ml RANKL for 2 days. (A) Heat map of the selected miRNAs (signal values < 500 and $p < 0.05$) in response to RANKL. The green and red colors indicate downregulation and upregulation, respectively. Of note, C1, C2, and C3 are control samples, and R1, R2, and R3 are RANKL-treated samples. (B) PCA for 6 samples (C1-C3, and R1-R3) in the first and second principal plane. (C) PCA for miRNAs in the first and second principal plane. Two miRNAs (221-3p and 222-3) are positioned with the smallest values along the second principal axis.

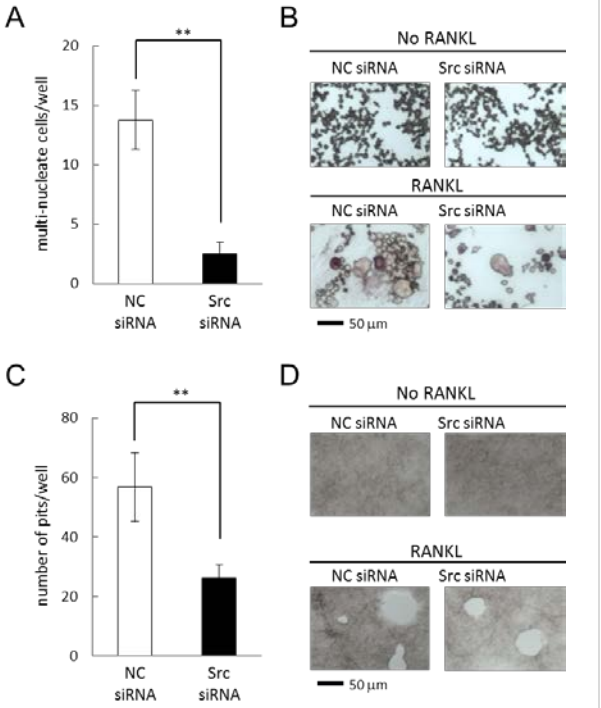

Figure 11. TRAP staining and osteoclast activity in the presence of c-Src siRNA. NC = non-specific control siRNA. (A & B) Number of multi-nucleated cells and TRAP staining in the presence and absence of 50 ng/ml RANKL for 4 days. (C & D) Number of pits and their images in the presence and absence of 50 ng/ml RANKL for 5 days.

Task #4 – Evaluate the efficacy of salubrinal on bone fracture healing.

Seventy-two C57BL/6 female mice (14 weeks, body weight ~20 g; Harlan Sprague–Dawley Inc.) were used in the study. All procedures performed in this study were approved by the Indiana University Animal Care and Use Committee and were in compliance with the Guiding Principles in the Care and Use of Animals endorsed by the American Physiological Society. Five mice were housed together in a cage. Animals were fed with standard laboratory chow and water *ad libitum*, and they were allowed to acclimate for 1 week before

experimentation. Mice were allowed full unrestricted cage activity, and they were weighed weekly. We employed visual inspection of food and water consumption, any signs of inflammation or infection, and walking patterns. Mice were divided into 6 groups, in which group 1 was treated as normal control (no induction of tibia fracture). Groups 2 and 3 were used for testing hydrogel-based administration of placebo and salubrinal (experiment 1), while groups 4-6 for examining subcutaneous injection of placebo, BMP2 and salubrinal (experiment 2). Experiments 1 and 2 were conducted separately using different batches of animals. Prior to the induction of closed fracture in the right tibia, mice were anesthetized using 1.5% isoflurane. To mice in groups 2-5, a stainless steel wire (30-gauge needle) was inserted into the intramedullary cavity of the right tibia through its proximal end (Fig. 12). The wire extending beyond the tibia condyles was cut, and the patella was properly repositioned. A closed diaphyseal fracture was then induced in the right distal tibia using a custom made 3-point bending device with a consistent force (**Fig. 12A & B**). Radiographic images were taken (Faxitron, Tucson, AZ) on day 0, as well as weeks 1, 2, 3 and 4 after fracture induction (**Fig. 12C & D**).

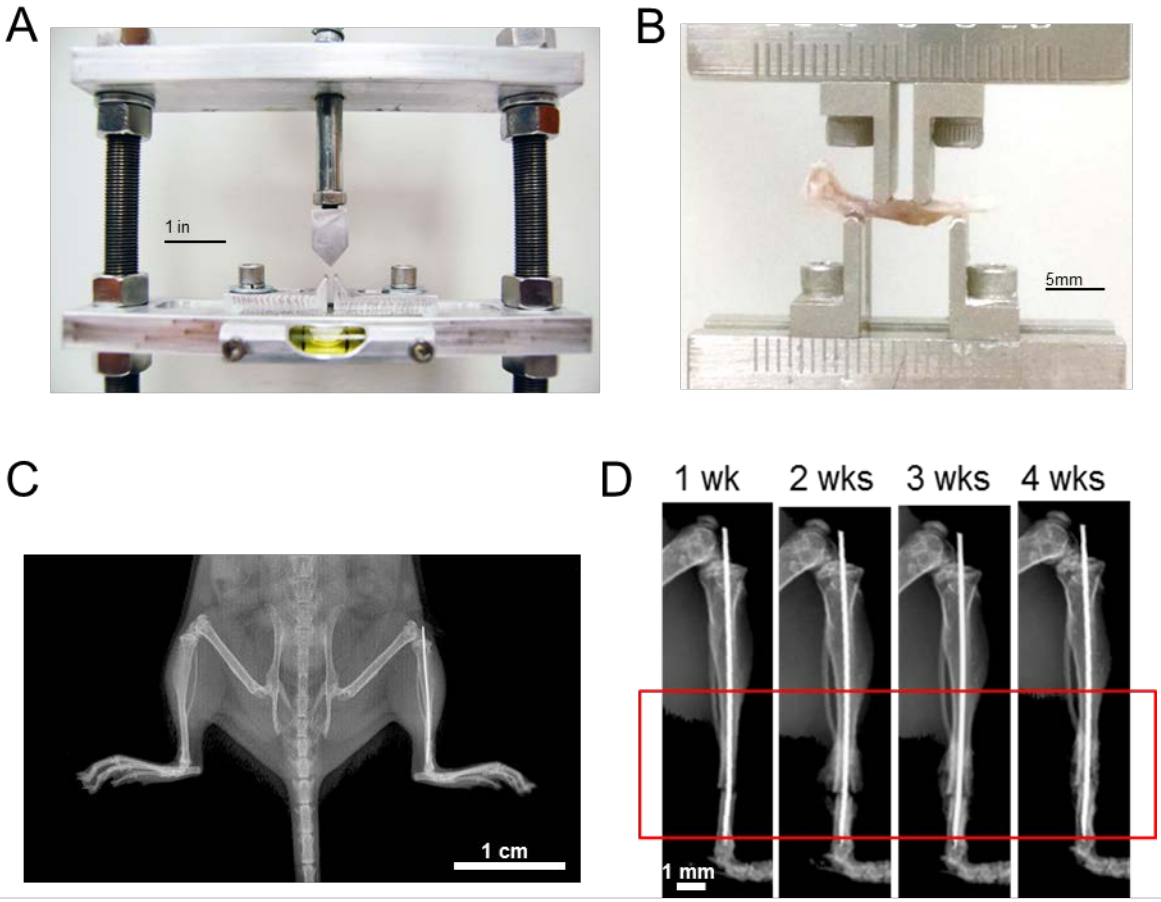

Figure 12. Tibia fracture study. (A) Custom-made 3-point bending device for inducing closed tibia fracture. (B) Four-point bending setup for mechanical testing. (C & D) X-ray images of the fractured tibiae. Of note, a stainless steel rod was inserted in the medullary cavity of the tibia.

Subtask 4a: Evaluate the efficacy of salubrinal using s.c. administration (**Appendix 11**)

In experiment 2 with daily subcutaneous injection of vehicle (group 4), BMP2 (bone morphogenetic protein 2) (group 5), and salubrinal (group 6), the fracture score was determined for weeks 0 to 4 using longitudinal X-ray images (**Fig. 13A & B**). Images collected by PIXImus densitometer were used for determining BMD and BMC (**Fig. 13C & D**). The image analysis revealed that no statistical difference was detected among three groups for the fracture score, BMD, and BMC. Mechanical test using 4-point bending revealed that ultimate force and stiffness were significantly elevated in group 5 (subcutaneous BMP2), but no statistical difference was detected between group 4 (subcutaneous control) and group 6 (subcutaneous salubrinal). Between experiments 1 and 2, no direct comparison of the mechanical testing results is possible since two experiments were conducted independently using different batches of animals.

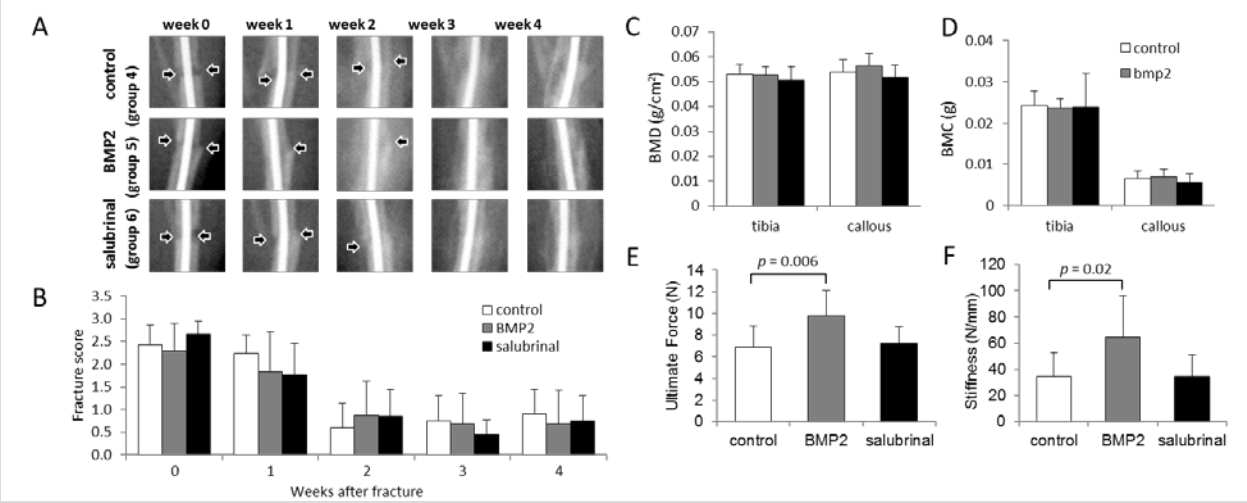

Figure 13. Administration of BMP2 and salubrinal as subcutaneous injection near the fracture site in experiment 2. (A) X-ray images of the fractured tibiae for the subcutaneous control (group 4), subcutaneous BMP2 (group 5), and subcutaneous salubrinal (group 6) in weeks 0, 1, 2, 3, and 4. (B) Fracture score in weeks 0 – 4 for the subcutaneous control, BMP2, and salubrinal groups. (C & D) BMD and BMC of the fractured tibia, respectively. (E) Ultimate force of the subcutaneous control, BMP2, and salubrinal samples. (F) Stiffness of the subcutaneous control, BMP2, and salubrinal samples.

Subtask 4b: Evaluate the efficacy of salubrinal using local administration (**Appendix 11**)

In experiment 1 with hydrogel-based administration of salubrinal, X-ray images in weeks 1, 2, 3, and 4, as well as micro CT (computed tomography) images of the representative tibia samples after harvest in week 4 were captured (**Fig. 14A - D**). Although X-ray images in week 4 indicated a complete bridge of the fracture site with calcified tissue, the sagittal sections of micro CT images revealed discontinuous cortical bone at the fracture site. The BMD and BMC measurement of the entire tibia in week 4 did not show any significant changes in the hydrogel placebo (group 2) and salubrinal (group 3) samples. The same measurement in the restricted callus region in week 4 presented a tendency of increase in the salubrinal treated group, but the difference was not statistically significant (p = 0.2 for BMD, and p = 0.09 for BMC) (**Fig. 14E & F**).

The fracture score, which indicated the degree of discontinuity in the cortical bone at the fracture site, decreased in groups 2 and 3 (**Fig. 15A**). No statistical difference was observed during the 4-week healing period between the two groups except for week 2.

The force-displacement relationship for 3 groups showed a distinctively different profile in response to a sinusoidal load (0.5 Newton force, peak-to-peak) at 0.5, 1, and 2 Hz (**Fig. 15**). The ascending and descending loads exhibited the same pattern, in which the intact control (group 1) was the stiffest and the hydrogel placebo (group 3) was the softest with the hydrogel salubrinal (group 2) in between. The ultimate force was 11.64 ± 5.48 N (hydrogel placebo, n = 12) and 16.99 ± 5.41 N (hydrogel salubrinal, n = 12) with $p = 0.03$, while stiffness was 81.55 ± 23.58 N/mm (hydrogel placebo, n = 12) and 106.73 ± 32.81 N/mm (hydrogel salubrinal, n = 12) with $p = 0.05$.

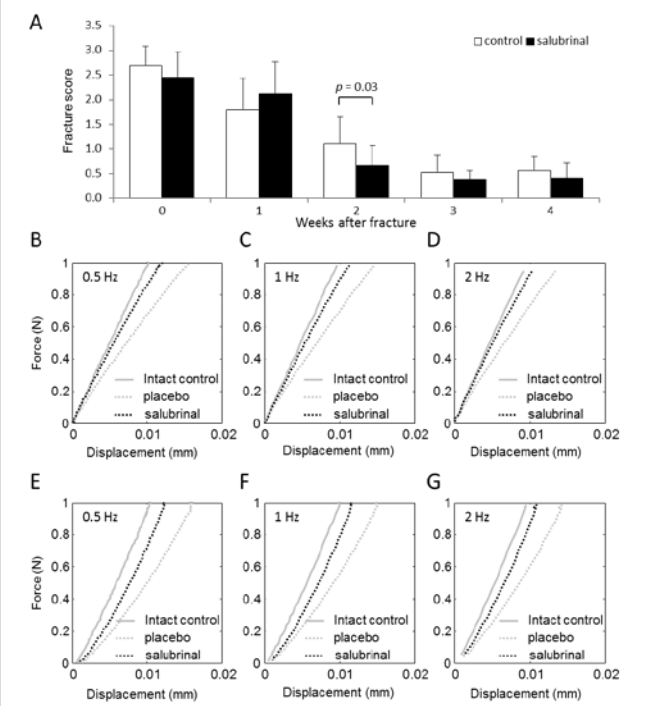

Figure 14. Fracture score and force-displacement relationship for experiment 1. (A) Fracture score in weeks 0 – 4 for the hydrogel control and hydrogel salubrinal groups. Of note, fracture score = "0" (no obvious fracture), "1" (minor fracture), "2" (moderate fracture), and "3" (severe fracture). (B – D) Force-displacement relationship for groups 1-3 in response to an increasing sinusoidal force (0.5 N, peak-to-peak) at 0.5, 1, and 2 Hz, respectively. (E – G) Force-displacement relationship for groups 1-3 in response to a decreasing sinusoidal force (0.5 N, peak-to-peak) at 0.5, 1, and 2 Hz, respectively.

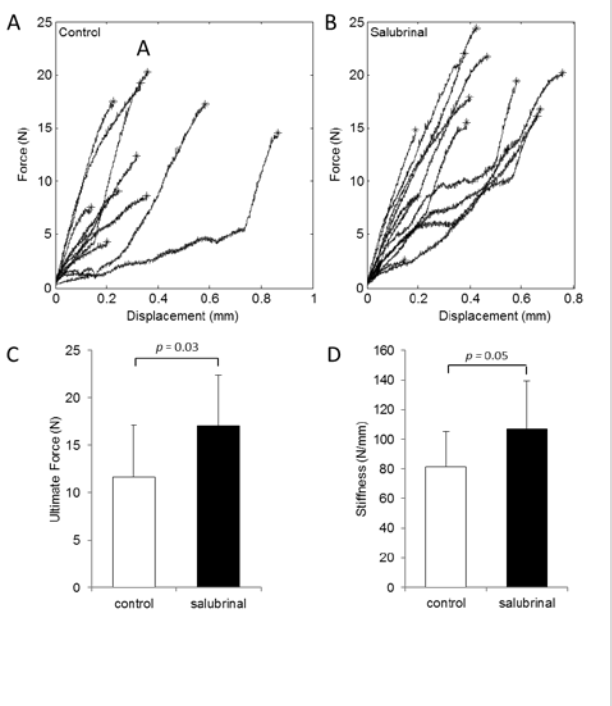

Figure 15. Mechanical strength 4 weeks after fracture induction for experiment 1. (A) Force-displacement relationship for the hydrogel control group in response to a linearly increasing displacement. The cross indicates the site of ultimate force. (B) Force-displacement relationship for the hydrogel salubrinal group. (C) Ultimate force of the hydrogel control and hydrogel salubrinal groups. (D) Stiffness of the hydrogel control and hydrogel salubrinal groups.

Opportunities for Training and Professional Development: The research team included three graduate students, as well as four postdoctoral fellows (See the section 7: PARTICIPANTS & OTHER COLLABORATING ORGANIZATIONS).

Results Disseminated to Communities: The research project was highlighted in Kelley School of Business at Indiana University as a case study for medical marketing. This class activity was introduced in a local newspaper, The Indianapolis Star, as an article, "IU course brings dose of real world to the lab," on March 12, 2010.

Plan to Do during the Next Reporting Period: N/A

4. IMPACT

Impact on Principal Disciplines

- A pilot grant from Indiana CTSI (Clinical and translational Sciences Institute) Research Intervention and Scientific Commercialization (Title: Novel pharmacological treatment of osteogenesis imperfecta, $25,000, 07/01/14 – 06/30/15) was funded for the application of salubrinal and guanabenz in treatment of brittle bone diseases.

Impact on Other Disciplines

- A clinical trial for strengthening bone with guanabenz for patients with bone metastasis from breast cancer is being conducted at Indiana University Hospital in 2015 (PI, Kathy Miller, MD).

Impact on Technology Transfer

- A U.S. patent (Method for treatment of bone diseases and fractures; 13/055,399) was issued in June 2015.
- An international patent application (compositions and methods for treating bone diseases, PCT/US2014/021682) was filed on March 7, 2014.

Impact on Society

- A small company, Ossa Biomedical LLC, was founded in 2013 by J.R. Renbarger (CEO) and Alex Brethauer (CTO) for developing a commercialization plan for salubrinal and guanabenz.

5. CHANGES/PROBLEMS

Changes in Approach

Three changes were implemented in the second year. First, to evaluate efficacy of salubrinal for treatment of osteoporosis, the research team modified the animal model. In the original procedure, mice in a normal physiological condition were proposed to be employed. In the amended procedure, ovariectomized mice that mimicked postmenopausal osteoporosis were added. This amendment allowed the research team to evaluate the effects of salubrinal on bone remodeling in normal and osteoporotic background.

Second, usage of cell lines for osteoblasts and osteoclasts was included in the original project, but use of primary cells was not included. To confirm the results obtained with cell lines, the research team added use of primary bone marrow derived cells.

Third, guanabenz (synthetic small molecule; 231 Da) was included as an additional control agent. Guanabenz upregulates the phosphorylation level of eIF2α.

Actual Problems
None.

Changes and Impact on Expenditures
None.

Significant Changes in Animals
To achieve three major changes in the animal procedure, the amendment for the procedure in the animal study was submitted to Indiana University IACUC and approved. After the approval by Indiana University IACUC, the amendment request was submitted to ACURO and approved during the project.

6. PRODUCTS

Publications

1. Hamamura K, Chen A, Tanjung N, Takigawa S, Sudo A, Yokota H. (2015). *In vitro* and in silico analysis of an inhibitory mechanism of osteoclastogenesis by salubrinal and guanabenz. *Cellular signaling* 27:353-362.
2. Hamamura, K., Tanjung, N., Yokota, H. (2013). Suppression of osteoclastogenesis through phosphorylation of eukaryotic translation initiation factor 2 alpha. *J. Bone Miner. Metab*. 31:618-628.
3. Hamamura K, Chen A, Uto Y, Yokota H (2015). Potential therapeutic applications of salubrinal for skeletal diseases and beyond. J. *Nature Sci* 1:e151.
4. Chen AB, Hamamura K, Tanjung N, Yokota H (2014). Principal component analysis of the regulation of osteoclastogenesis by salubrinal and guanabenz. 2014 *Annual Meeting of Biomedical Engineering Society*, October 22-25, 2014, San Antonio, TX.
5. Zhang P, Chen A, Dodge T, Tanjung N, Zheng Y, Fuqua C, Yokota H. Salubrinal regulates bone remodeling and fat metabolism in ovariectomized mice. *Abstract to the 2013 annual meeting of Orthopedic Research Society*.
6. Yokota, H., Hamamura, K., Chen, A., Dodge, T.R., Tanjung, N., Abedinpoor, A., Zhang, P. (2013). Effects of salubrinal on development of osteoclasts and osteoblasts from bone marrow-derived cells. *BMC Musculoskeletal Disorders* 14:197.
7. Sato A, Plotkin LI, Bellido T. Prevention of glucocorticoid induced-apoptosis of osteoblasts and osteocytes by protecting against endoplasmic reticulum (ER) stress. The 35th Annual Meeting of the American Society for Bone and Mineral Research. Minneapolis, MN, USA. *Journal of Bone and Mineral Research* 28 (Supl. 1):S403 201.

8. Sato AY, Tu X, McAndrews KA, Plotkin LI, Bellido T (2015). Prevention of glucocorticoid induced apoptosis of osteoblasts and osteocytes by protecting against endoplasmic reticulum stress in vitro and in vivo in female mice. *Bone* 73:60-68.
9. Takigawa S, Chen A, Wan Q, Na S, Sudo A, Yokota H, Hamamura K. Role of miR-222-3p in c-Src-mediated regulation of osteoclastogenesis. *Intl. J. Molecular Sci*. (accepted).

Websites: N/A

Inventions, Patent Applications, and Licenses

A small business company, Ossa Biomedical LLC, was established with the objective of commercializing salubrinal and guanabenz-linked IP. Through Indiana University Research and Technology Cooperation, two key personnel (J.R. Renbarger and Alexander Brethauer) were recruited. Renbarger serves as President and CEO and he is responsible for business strategy and financial support for Ossa Biomedical. Alexander Brethauer serves as CTO and he is responsible for product development, regulatory strategy, and IP strategy.

7. PARTICIPANTS & OTHER COLLABORATING ORGANIZATIONS

Individuals on the Project:

Name	Hiroki Yokota, PhD
Project Role	PI
Nearest person month worked	15 months
Contribution	organize the project and disseminate the results
Other Funding Support	NIH

Name	Teresita Bellido, PhD
Project Role	co-I
Nearest person month worked	14 months
Contribution	design experiments and interpret data
Other Funding Support	NIH

Name	Jeffrey Anglen, MD
Project Role	Co-I
Nearest person month worked	2 months
Contribution	interpret data and provide advice from a clinical side
Other Funding Support	DOD

Name	Munro Peacock, MD
Project Role	co-I
Nearest person month worked	2 months
Contribution	interpret data and provide advice from a clinical side
Other Funding Support	NIH

Name	Ping Zhang, MD
Project Role	collaborator
Nearest person month worked	22 months
Contribution	design and conduct animal experiments
Other Funding Support	NIH

Name	Kazunori Hamamura, DDS/PhD
Project Role	collaborator
Nearest person month worked	6 months
Contribution	design and conduct in vitro experiments
Other Funding Support	NIH

Name	Xiaolin Tu, PhD
Project Role	collaborator
Nearest person month worked	13 months
Contribution	design and conduct animal experiments
Other Funding Support	NIH

Name	Gaurav Swarnkar, PhD
Project Role	Postdoctoral Fellow
Nearest person month worked	8 months
Contribution	design and conduct animal experiments
Other Funding Support	NIH

Name	Jeffrey Benson
Project Role	Technician
Nearest person month worked	2 months
Contribution	assist animal experiments and data interpretation
Other Funding Support	None

Name	Simon Shim, PhD
Project Role	Postdoctoral Fellow
Nearest person month worked	11 months
Contribution	design and conduct animal experiments
Other Funding Support	NIH

Name	Liming Zhao, MD
Project Role	Research Associate
Nearest person month worked	3 months
Contribution	design and conduct animal experiments
Other Funding Support	NIH

Name	Akinobu Nishimura, MD/PhD
Project Role	Research Assistant
Nearest person month worked	10 months
Contribution	conduct in vitro experiments
Other Funding Support	None

Name	Andy Chen
Project Role	Graduate Student
Nearest person month worked	6 months
Contribution	assist animal experiments
Other Funding Support	None

Name	Jialing Li, PhD
Project Role	Faculty
Nearest person month worked	1 month
Contribution	assist animal experiments
Other Funding Support	None

Name	Chien-Chi Lin, PhD
Project Role	Faculty
Nearest person month worked	1 month
Contribution	assist animal experiments
Other Funding Support	NIH, NSF

Name	Shinya Takigawa, MD
Project Role	Research Associate
Nearest person month worked	8 months
Contribution	conduct in vitro experiments
Other Funding Support	ISDH

Name	Nancy Tanjung
Project Role	Graduate Student
Nearest person month worked	11 months
Contribution	assist in vitro experiments
Other Funding Support	None

Name	Wenxiao Xu, MD
Project Role	Research Assistant
Nearest person month worked	10 months
Contribution	design and conduct animal experiments
Other Funding Support	None

Name	Aysan Abedinpoor
Project Role	Graduate Student
Nearest person month worked	3 months
Contribution	assist in vitro experiments
Other Funding Support	None

Other Organizations: N/A

8. SPECIAL REPORTING REQUIREMENTS

Collaborative Awards: N/A

Quad Charts: N/A

9. APPENDICES

Appendix 1: Hamamura K, Chen A, Tanjung N, Takigawa S, Sudo A, Yokota H. (2015). In vitro and in silico analysis of an inhibitory mechanism of osteoclastogenesis by salubrinal and guanabenz. Cellular signaling 27:353-362.

Appendix 2: Hamamura, K., Tanjung, N., Yokota, H. (2013). Suppression of osteoclastogenesis through phosphorylation of eukaryotic translation initiation factor 2 alpha. *J. Bone Miner. Metab*. 31:618-628.

Appendix 3: Hamamura K, Chen A, Uto Y, Yokota H (2015). Potential therapeutic applications of salubrinal for skeletal diseases and beyond. *J. Nature Sci* 1:e151.

Appendix 4: Chen AB, Hamamura K, Tanjung N, Yokota H (2014). Principal component analysis of the regulation of osteoclastogenesis by salubrinal and guanabenz. 2014 *Annual Meeting of Biomedical Engineering Society*, October 22-25, 2014, San Antonio, TX.

Appendix 5: Zhang P, Chen A, Dodge T, Tanjung N, Zheng Y, Fuqua C, Yokota H. Salubrinal regulates bone remodeling and fat metabolism in ovariectomized mice. *Abstract to the 2013 annual meeting of Orthopedic Research Society*. TX.

Appendix 6: Yokota, H., Hamamura, K., Chen, A., Dodge, T.R., Tanjung, N., Abedinpoor, A., Zhang, P. (2013). Effects of salubrinal on development of osteoclasts and osteoblasts from bone marrow-derived cells. *BMC Musculoskeletal Disorders* 14:197.

Appendix 7: Sato A, Plotkin LI, Bellido T. Prevention of glucocorticoid induced-apoptosis of osteoblasts and osteocytes by protecting against endoplasmic reticulum (ER) stress. The 35th Annual Meeting of the American Society for Bone and Mineral Research. Minneapolis, MN, USA. *Journal of Bone and Mineral Research* 28 (Supl. 1):S403 201.

Appendix 8: Sato AY, Tu X, McAndrews KA, Plotkin LI, Bellido T (2015). Prevention of glucocorticoid induced apoptosis of osteoblasts and osteocytes by protecting against endoplasmic reticulum stress in vitro and in vivo in female mice. *Bone* 73:60-68.

Appendix 9: Takigawa S, Chen A, Wan Q, Na S, Sudo A, Yokota H, Hamamura K. Role of miR-222-3p in c-Src-mediated regulation of osteoclastogenesis. *Intl. J. Molecular Sci*. (accepted).

Appendix 10: Zhang P, Hamamura K, Chen A, Dodge TR, Wan Q, Na S, Peacock M, Bellido TM, Yokota H. Salubrinal attenuates bone loss in a mouse model of postmenopausal osteoporosis (to be submitted to *Osteoporosis International*).

Appendix 11: Xu W, Chen A, Zhang Y, Li J, Lin CC, Yan J, Yokota H. Hydrogel-based local release of salubrinal stimulates healing of mouse tibia fracture (in preparation).

Cellular Signalling 27 (2015) 353–362

Contents lists available at ScienceDirect

Cellular Signalling

journal homepage: www.elsevier.com/locate/cellsig

In vitro and *in silico* analysis of an inhibitory mechanism of osteoclastogenesis by salubrinal and guanabenz

Kazunori Hamamura [a,*], Andy Chen [a], Nancy Tanjung [a], Shinya Takigawa [a,b], Akihiro Sudo [b], Hiroki Yokota [a,c]

[a] Department of Biomedical Engineering, Indiana University—Purdue University Indianapolis, Indianapolis, IN 46202, USA
[b] Department of Orthopaedic Surgery, Mie University Graduate School of Medicine, Mie 514, Japan
[c] Department of Anatomy and Cell Biology, Indiana University School of Medicine, Indianapolis, IN 46202, USA

ARTICLE INFO

Article history:
Received 22 October 2014
Accepted 21 November 2014
Available online 27 November 2014

Keywords:
Osteoclasts
NFATc1
c-Fos
JunB
Salubrinal
Guanabenz

ABSTRACT

Inactivating bone-resorbing osteoclasts is a prime therapeutic strategy for the prevention of bone loss in patients with osteopenia and osteoporosis. Synthetic agents such as salubrinal and guanabenz, which attenuate stress to the endoplasmic reticulum, are reported to inhibit development of osteoclasts. However, the mechanism of their inhibitory action on osteoclasts is largely unknown. Using genome-wide expression profiles, we predicted key transcription factors that downregulated nuclear factor of activated T-cells, cytoplasmic 1 (NFATc1), a master transcription factor for osteoclastogenesis. Principal component analysis (PCA) predicted a list of transcription factors that were potentially responsible for reversing receptor activator of nuclear factor kappa-B ligand (RANKL)-driven stimulation of osteoclastogenesis. A partial silencing of NFATc1 allowed a selection of transcription factors that were likely to be located upstream of NFATc1. We validated the predicted transcription factors by focusing on two AP-1 transcription factors (c-Fos and JunB) using RAW264.7 pre-osteoclasts as well as primary bone marrow cells. As predicted, their mRNA and protein levels were elevated by RANKL, and the elevation was suppressed by salubrinal and guanabenz. A partial silencing of c-Fos or JunB by RNA interference decreased NFATc1 as well as tartrate-resistant acid phosphatase (TRAP) mRNA. Collectively, a systems-biology approach allows the prediction of a RANKL-salubrinal/guanabenz-NFATc1 regulatory axis, and *in vitro* assays validate an involvement of AP-1 transcription factors in suppression of osteoclastogenesis.

1. Introduction

The inhibition of de-phosphorylation of eukaryotic translation initiation factor 2 alpha (eIF2α) stimulates bone formation by osteoblasts [1–3] and suppresses bone resorption by osteoclasts [1,2,4]. This dual role of eIF2α signaling in bone remodeling presents a unique advantage for developing treatment of bone diseases such as osteoporosis, since few existing drugs are able to not only elevate bone formation but also prevent bone resorption [1,2]. It is reported that the stimulation of bone formation through eIF2α signaling is caused by translational activation of activating transcription factor 4 (ATF4) [1]. However, the regulatory mechanism for eIF2α-driven suppression of bone resorption has not been clarified.

Salubrinal and guanabenz are potent chemical agents for the inhibition of protein phosphatase 1 (PP1) that specifically de-phosphorylate eIF2α [5,6]. Through upregulating the phosphorylated level of eIF2α and reducing translational efficiency of most proteins except for a limited set of proteins, such ATF4, these agents attenuate stress to the endoplasmic reticulum [5,6]. Gene regulation by salubrinal and guanabenz, however, not only takes place at the level of translation but also at the level of transcription [2]. In osteoclasts, it has been shown that administration of salubrinal and guanabenz suppresses receptor activator of nuclear factor kappa-B ligand (RANKL)-driven activation of nuclear factor of activated T-cells, cytoplasmic 1 (NFATc1) [1,2], which is a master transcription factor of osteoclastogenesis [7].

Using genome-wide microarray expression analysis, the prime aim of this study was to determine an inhibitory mechanism of NFATc1 transcription by salubrinal and guanabenz. In order to predict potential transcription factors that downregulate RANKL-driven activation of NFATc1, we employed principal component analysis (PCA) [8]. PCA allowed us to evaluate the inhibitory effects of salubrinal and guanabenz through a mathematical procedure called singular value decomposition. When a principal component axis derived from singular value decomposition is aligned along a RANKL-salubrinal/guanabenz-NFATc1 regulatory axis, transcription factors that predominantly contribute to the suppression of osteoclastogenesis could emerge along a principal component axis. We predicted and validated transcription factors that regulate the RANKL-salubrinal/guanabenz-NFATc1 axis.

* Corresponding author at: Department of Biomedical Engineering, Indiana University—Purdue University Indianapolis, SL155, 723 West Michigan Street, Indianapolis, IN 46202, USA. Tel.: +1 317 274 1350; fax: +1 317 278 2455.
E-mail address: hamamurk@iupui.edu (K. Hamamura).

http://dx.doi.org/10.1016/j.cellsig.2014.11.020
0898-6568/

Table 1
Real-time PCR primers used in this study.

Target	Forward primer	Backward primer
Cathepsin K	5′-CAGCTTCCCCAAGATGTGAT-3′	5′-AGCACCAACGAGAGGAGAAA-3′
NFATc1	5′-GGTGCTGTCTGGCCATAACT-3′	5′-GCGGAAAGGTGGTATCTCAA-3′
TRAP	5′-TCCTGGCTCAAAAAGCAGTT-3′	5′-ACATAGCCCACACCGTTCTC-3′
GAPDH	5′-TGCACCACCAACTGCTTAG-3′	5′-GGATGCAGGGATGATGTTC-3′

2. Materials and methods

2.1. Cell culture

Mouse bone marrow cells isolated from long bones (femur and tibia) as well as RAW264.7 mouse pre-osteoclast cells were cultured in αMEM containing 10% fetal bovine serum and antibiotics (50 units/ml penicillin and 50 μg/ml streptomycin; Life Technologies, Grand Island, NY, USA) [9]. Cells were maintained at 37 °C and 5% CO_2 in a humidified incubator.

2.2. Osteoclastogenesis and TRAP (tartrate-resistant acid phosphatase) staining

Bone marrow cells were plated at 1.2×10^5 and 1.0×10^6 cells into 12-well or 60 mm dishes, respectively, and cultured with 10 ng/ml M-CSF (macrophage colony-stimulating factor; PeproTech, Rocky Hills, NC, USA) for 3 days. The surface-attached cells were used as osteoclast precursors. These precursors were cultured with 10 ng/ml M-CSF and 50 ng/ml RANKL (PeproTech). RAW264.7 cells were plated at 1.0×10^5 cells into a 60 mm dish and cultured with 20 or 50 ng/ml RANKL in the presence and absence of salubrinal or guanabenz (R&D

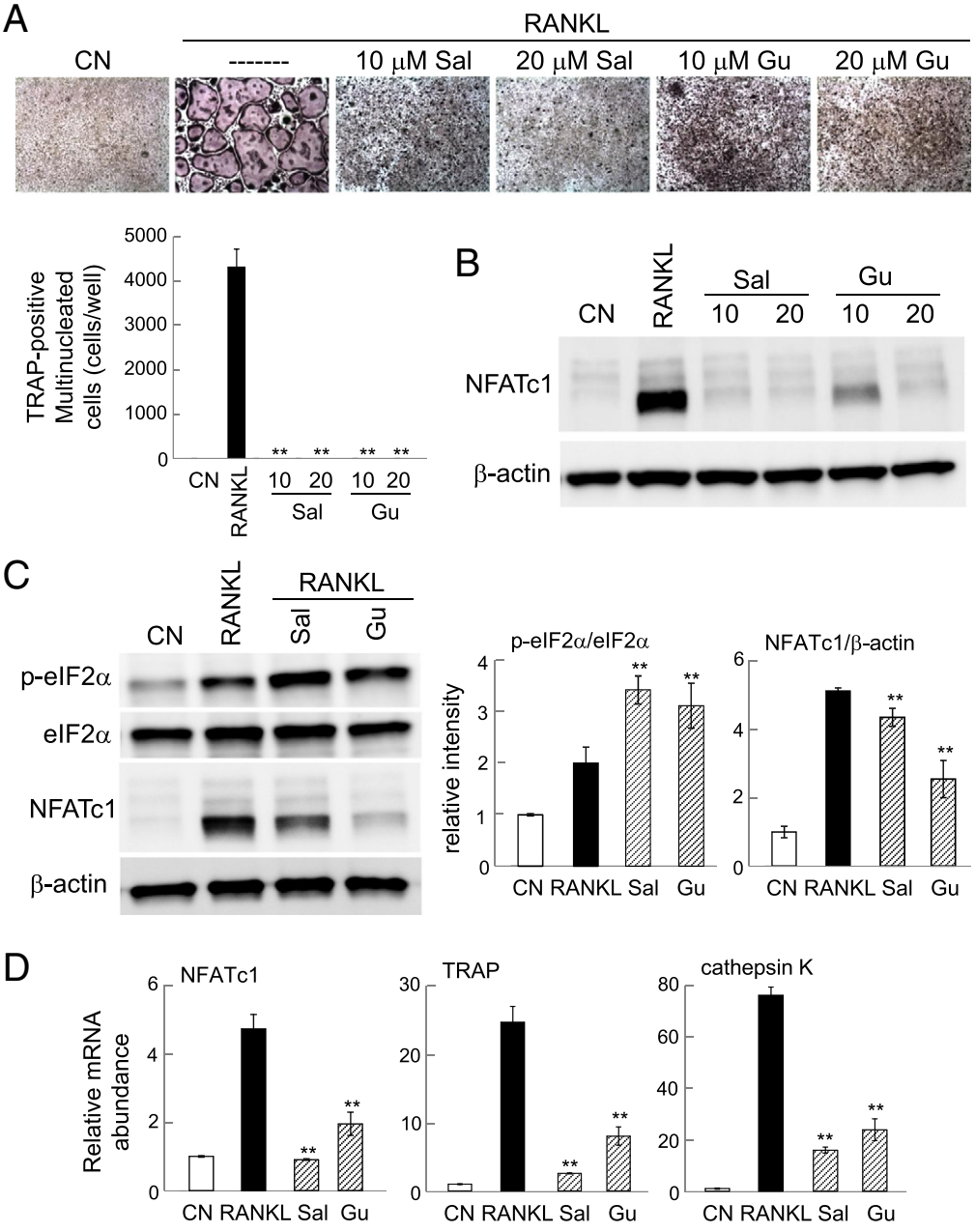

Fig. 1. Inhibitory effects of salubrinal and guanabenz on development of osteoclasts. (A) Dose-dependent suppression of TRAP-positive multinucleated osteoclasts by salubrinal and guanabenz in bone marrow cells. Note that the double asterisk indicates $p < 0.01$. (B) Salubrinal and guanabenz-driven inhibition of NFATc1 on day 2 in bone marrow cells. (C) Elevation of p-eIF2α and reduction of NFATc1 by salubrinal and guanabenz on day 1 in RAW264.7 cells. (D) Salubrinal- and guanabenz-induced reduction of mRNA expression levels of NFATc1, TRAP, and cathepsin K on days 1 in bone marrow cells.

Systems, Minneapolis, MN, USA). After 2-day treatment with RANKL, cells were treated for TRAP staining using an acid phosphatase leukocyte kit (Sigma). The number of TRAP-positive cells containing three or more nuclei was determined.

2.3. Microarray analysis

Two sets of microarray experiments were conducted using RAW264.7 cells. In the first set, we employed 4 groups (3 samples per group; Illumina MouseWG-6 v2.0): CN (control), RL (20 ng/ml RANKL), Sal (20 μM salubrinal with 20 ng/ml RANKL), and Gu (20 μM guanabenz with 20 ng/ml RANKL). Cells were harvested 4 h after incubation with the above agents. In the second set, cells were treated with siRNA (nonspecific control or specific to NFATc1) in the presence and absence of 50 ng/ml RANKL. The four groups (3 samples per group; Affymetrix Mouse Gene 2.0 ST arrays) were: CN_{nc} (nonspecific control siRNA), RL_{nc} (nonspecific siRNA with RANKL), CN_{NFATc1} (NFATc1 siRNA), and RL_{NFATc1} (NFATc1 siRNA with RANKL). Cells were harvested 12 h after incubation with siRNA and/or RANKL.

2.4. Principal component analysis (PCA)

Microarray expression data was normalized using a Robust Multiarray Average procedure. The genes in the first microarray experiment with salubrinal and guanabenz were mapped to unique Entrez gene IDs using annotation data of probe quality [10], while the genes in the second microarray experiment with NFATc1 siRNA were mapped using a custom Chip Definition File [11]. The two microarray datasets were then consolidated by common Entrez gene IDs. After per-gene scaling of the expression data, principal component analysis (PCA) was performed on the salubrinal/guanabenz microarray by applying singular value decomposition to generate 3 matrices: an eigenarray matrix, a diagonal matrix of eigenvalues, and an eigengene matrix [8]. This decomposition defines 12 principal component axes on which each gene can be mapped. The samples were plotted in the plane of the first two principal axes. The eigenarray values for each gene in the principal component axes were also generated. PCA was also performed on a subset of the microarray data that corresponds with genes identified as transcription factors [12].

The NFATc1 siRNA microarray data was used to identify candidate genes upstream of NFATc1. A linear model was applied to the data to identify the relative effects of NFATc1 siRNA, RANKL treatment, and their interaction. This generated a set of false discovery rate (FDR) q values. Candidate activator genes (transcription factors) were those that were upregulated by RANKL ($q < 0.05$) with fold change > 2, did not present significant siRNA-RANKL interaction ($q > 0.05$), and showed siRNA + RANKL group's gene expression greater than the RANKL group's gene expression. Similarly, candidate inhibitor genes were those that were downregulated by RANKL ($q < 0.05$) with fold change < −2, did not induce significant siRNA-RANKL interaction ($q > 0.05$), and exhibited siRNA + RANKL group's expression less than RANKL gene expression. From the above candidate genes, 10 most positive and negative regulators (candidate activator and inhibitor genes) were chosen along the first principal component axis.

2.5. Quantitative real-time PCR

Total RNA was extracted using an RNeasy Plus mini kit (Qiagen, Germantown, MD, USA). Reverse transcription was conducted with high capacity cDNA reverse transcription kits (Applied Biosystems,

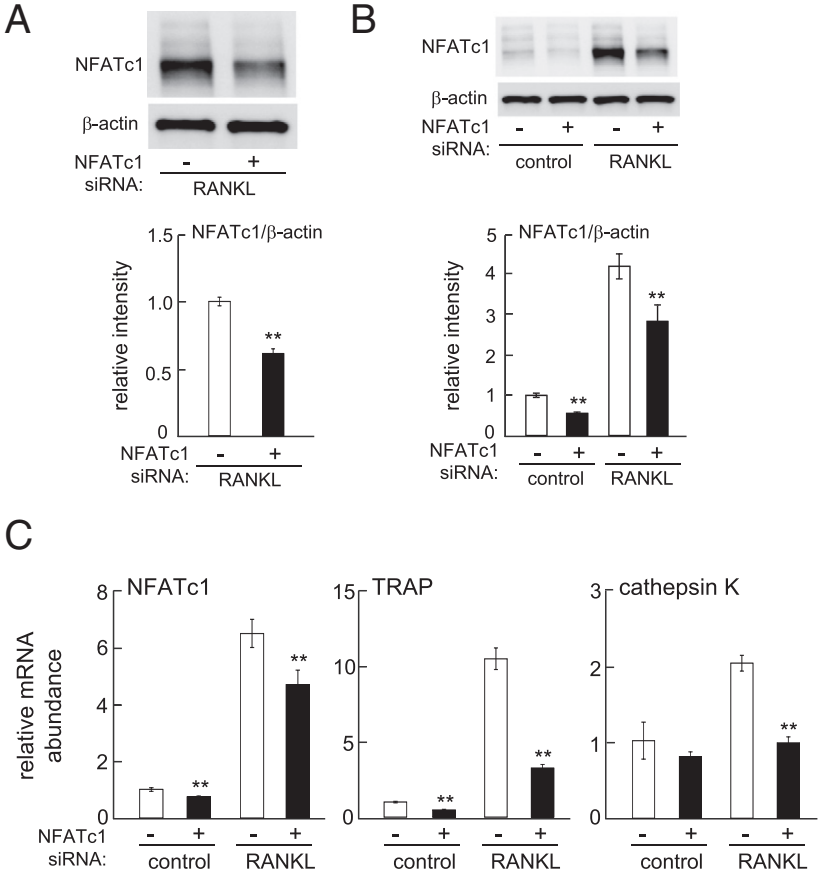

Fig. 2. Suppression of RANKL-driven osteoclast-linked genes by NFATc1 siRNA in RAW264.7 cells. (A) Partial silencing of NFATc1 in the presence of RANKL. (B) Partial silencing of NFATc1 in the presence and absence of RANKL. (C) Levels of NFATc1, TRAP, and cathepsin K mRNAs in response to non-specific control (NC) and NFATc1 siRNAs. The single and double asterisks indicate $p < 0.05$ and $p < 0.01$, respectively.

Carlsbad, CA, USA), and quantitative real-time PCR was performed using ABI 7500 with Power SYBR green PCR master mix kits (Applied Biosystems). We evaluated mRNA levels of cathepsin K, NFATc1 (nuclear factor of activated T-cells, cytoplasmic 1), and TRAP with the PCR primers listed in Table 1. GAPDH was used for internal control.

2.6. Western blot analysis

Cells were lysed in a radioimmunoprecipitation assay (RIPA) buffer containing protease inhibitors (Santa Cruz Biotechnology, Santa Cruz, CA, USA) and phosphatase inhibitors (Calbiochem, Billerica, MA, USA). Isolated proteins were fractionated using 10% SDS gels and electro-transferred to Immobilon-P membranes (Millipore, Billerica, MA, USA). The membrane was incubated with primary antibodies followed by incubation with goat anti-rabbit or anti-mouse IgG conjugated with horseradish peroxidase (Cell Signaling, Danvers, MA, USA). We used antibodies against c-Fos (Santa Cruz), eIF2α (Cell Signaling), p-eIF2α (Thermo Scientific, Waltham, MA, USA), JunB (Cell Signaling), NFATc1 (Santa Cruz), and β-actin (Sigma). Protein levels were assayed using a SuperSignal west femto maximum sensitivity substrate (Thermo Scientific).

2.7. Knockdown of c-Fos and JunB by siRNA

RAW264.7 were treated with siRNA specific to c-Fos (5′-CUA CUU ACA CGU CUU CCU U-3′; Life Technologies), JunB (5′-GCA UCA AAG

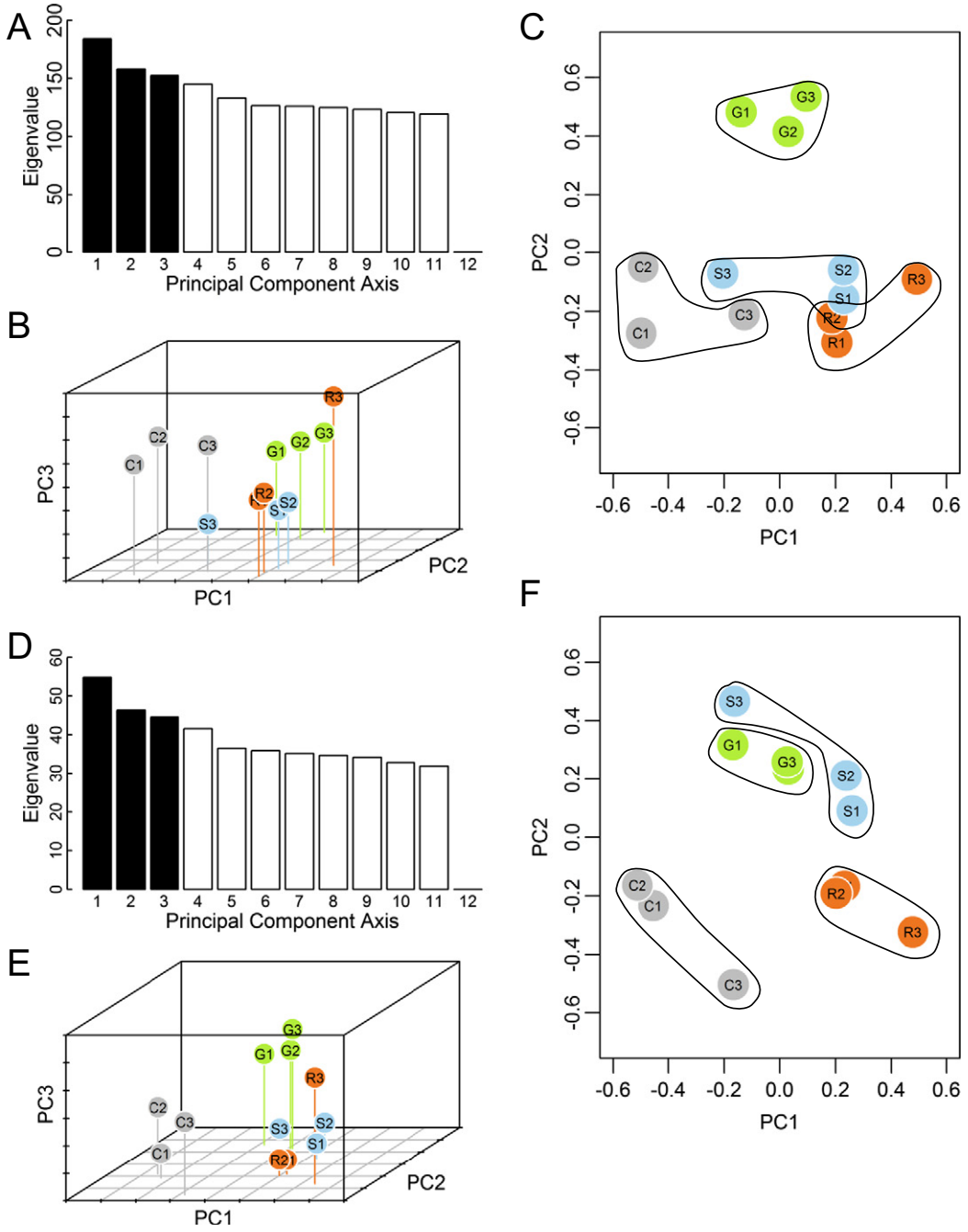

Fig. 3. PCA of the salubrinal/guanabenz microarray. (A) Eigenvalues for the full list of genes. (B & C) Four groups for the full list of genes, plotted in the plane of the first-three (PC1–PC3) and first-two (PC1, PC2) principal component axes, respectively. (D) Eigenvalues for transcription factors. (D & E) Four groups for transcription factors, plotted in the plane of the first-three (PC1–PC3) and first-two (PC1, PC2) principal component axes, respectively.

UGG AGC GAA A-3′; Life Technologies), or a nonspecific control (NC) (5′-UGU ACU GCU UAC GAU UCG G-3′, Life Technologies). Cells were transiently transfected with siRNA in Opti-MEM I medium with Lipofectamine RNAiMAX (Life Technologies). The efficiency of silencing was assessed with immunoblotting or quantitative PCR 48 h after transfection.

2.8. Statistical analysis

For *in silico* analysis, a linear model of differential expression was applied using the *limma* package [13] in R (version 3.1.1), and Student's *t*-test with empirical Bayesian adjustment with Benjamini–Hochberg False Discovery Rate (FDR) correction was used to calculate FDR *q* values of significance for each interaction. For *in vitro* assays, three or four independent experiments were conducted, and data were expressed as mean ± S.D. For comparison among multiple samples, statistical significance was evaluated using Student's *t*-test at $p < 0.05$. The single and double asterisks indicate $p < 0.05$ and $p < 0.01$, respectively. To determine intensities in immunoblotting, images were scanned with Adobe Photoshop CS2 (Adobe Systems, San Jose, CA, USA) and quantified using Image J.

3. Results

3.1. Inhibitory effects of salubrinal and guanabenz on osteoclastogenesis

In response to RANKL-induced development of bone marrow cells, salubrinal and guanabenz suppressed osteoclastogenesis in a dose-dependent manner. The number of TRAP-positive multinucleated osteoclasts and the level of NFATc1 protein were significantly reduced by salubrinal and guanabenz (Fig. 1A & B). The decrease in NFATc1 was associated with an increase in the level of eIF2α phosphorylation

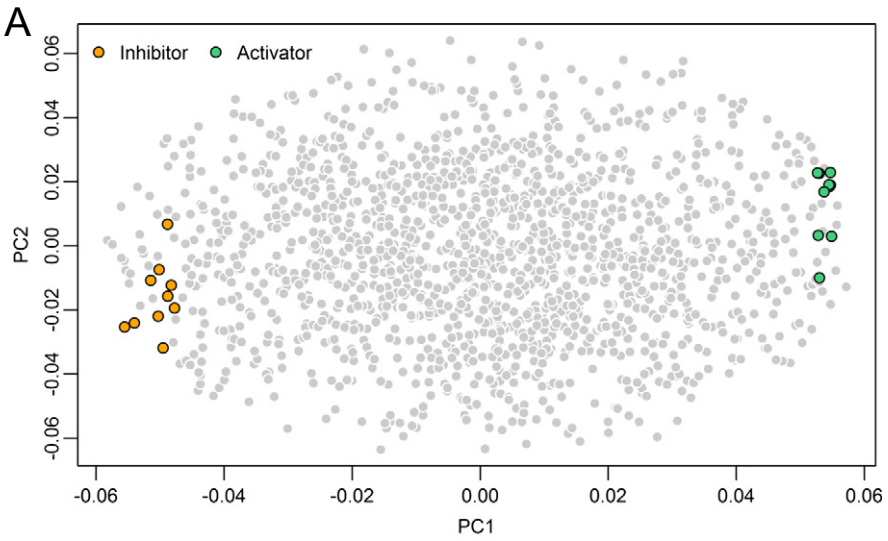

B

Transcription Factor	u1	CN	RANKL	Gu	Sal
NFkB1	0.055				
Jdp2	0.055				
Bcl3	0.055				
Fos	0.055				
JunB	0.054				
Ell2	0.054				
Sertad1	0.053				
Hmga1	0.053				
Nop2	0.053				
Pogk	0.053				

C

Transcription Factor	u1	CN	RANKL	Gu	Sal
Zfpm1	-0.056				
B930041F14Rik	-0.054				
Xbp1	-0.051				
Rfc1	-0.050				
Hes6	-0.050				
Tshz3	-0.050				
Osgin1	-0.049				
Fli1	-0.049				
Cdkn2c	-0.048				
Ing4	-0.048				

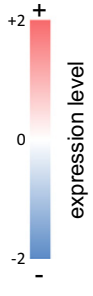

Fig. 4. Candidate stimulatory and inhibitory transcription factors for osteoclastogenesis. (A) Transcription factors plotted on the plane of the first two principal component axes. The 10 most stimulatory and inhibitory candidate transcription factors are highlighted based on the NFATc1–siRNA microarray data. (B) Candidate activators of NFATc1 in response to salubrinal and guanabenz. (C) Candidate inhibitors of NFATc1 in response to salubrinal and guanabenz.

(Fig. 1C). Consistent with the suppression of NFATc1, the mRNA levels of TRAP and cathepsin K were also reduced (Fig. 1D). In RAW264.7 pre-osteoclast cells, partial silencing of NFATc1 reduced the mRNA levels of NFATc1, TRAP, and cathepsin K compared to treatment with non-specific control (NC) siRNA (Fig. 2).

3.2. Principal component analysis of salubrinal/guanabenz microarray

Using PCA on the first set of microarray data (salubrinal and guanabenz), we generated 12 eigenvalues for 12 samples in 4 groups and evaluated eigengene vectors as well as eigenarray vectors. In

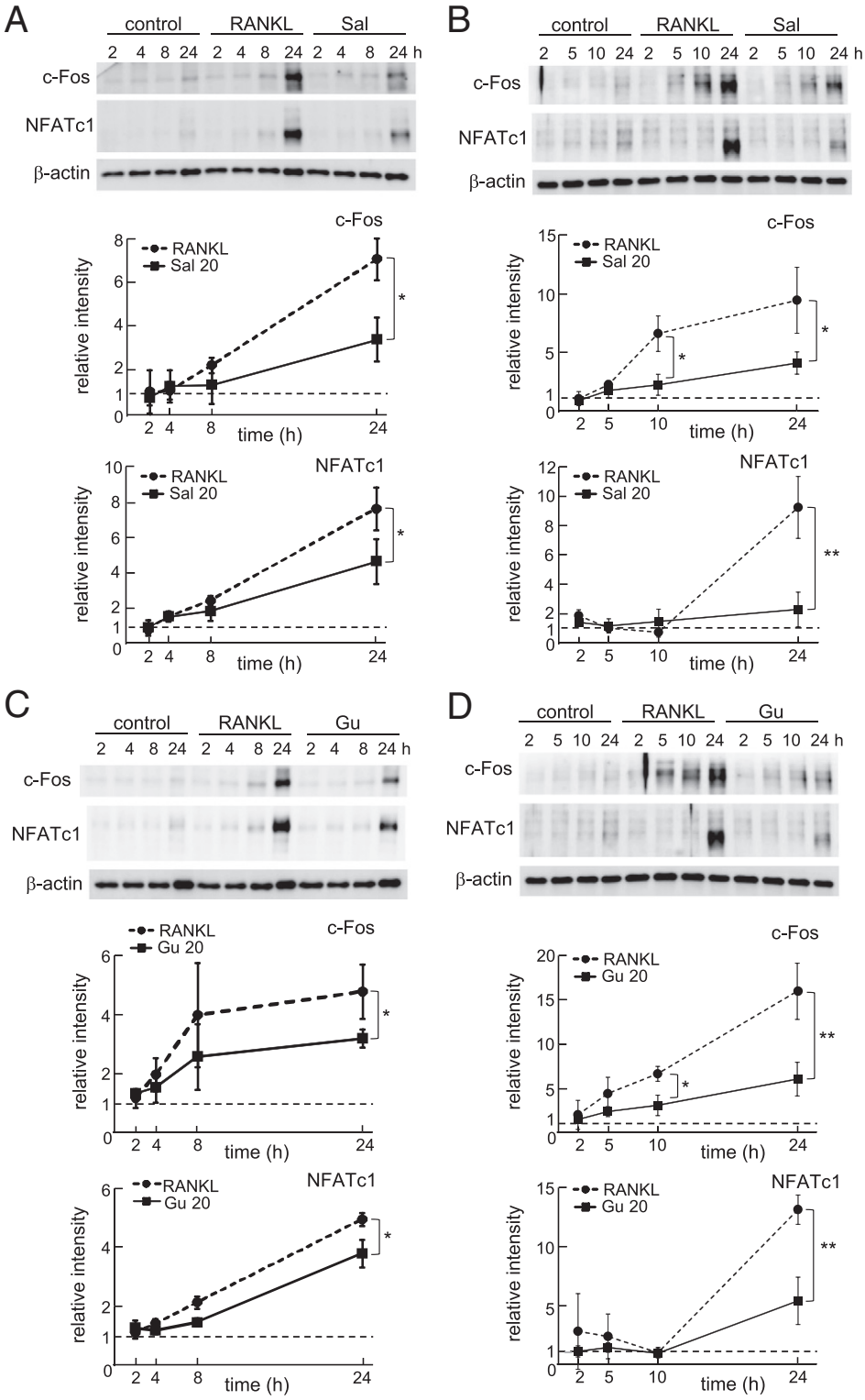

Fig. 5. Salubrinal- and guanabenz-driven reduction in c-Fos. The single and double asterisks indicate $p < 0.05$ and $p < 0.01$, respectively. (A&B) Protein levels of c-Fos and NFATc1 in the presence of salubrinal in RAW264.7 cells (2, 4, 8, and 24 h) and bone marrow cells (2, 5, 10, and 24 h), respectively. (C&D) Protein levels of c-Fos and NFATc1 in the presence of guanabenz in RAW264.7 cells (2, 4, 8, and 24 h) and bone marrow cells (2, 5, 10, and 24 h), respectively.

comparison of the relative variance of each principal component, the first principal component was significantly larger than the other 11 components, although the 2nd to 11th axes showed strong components (Fig. 3A). Using the eigengene vectors, 4 groups were clustered in the first-three (PC1, PC2, and PC3, solid bars in Fig. 3A) and first-two (PC1 and PC2) component axes, respectively (Fig. 3B & C). Along the first principal component axis (PC1), 4 groups were lined up in the order of CN, Sal/Gu, and RL, indicating that PC1 is aligned to the RANKL-driven stimulation of osteoclastogenesis. PCA was also performed on a subset of the first set of microarray data containing only transcription factors (Fig. 3D–F). Consistent with the results in Fig. 3A–C, the first principal component axis (PC1) corresponded with the phenotypic trend of osteoclastogenesis. The RANKL samples were more positive, while the samples treated with salubrinal and guanabenz moved back in the direction of the control groups.

Using the eigenarray vectors, transcription factors were located on the first-two (PC1 and PC2) component axes (Fig. 4A). The color coded transcription factors were identified based on the second set of microarray experiment as top 10 potential activators (Fig. 4B) or inhibitors (Fig. 4C). The mRNA expression levels of these transcription factors were not significantly altered by treatment with NFATc1 siRNA. Among the potential activators responsive to salubrinal and guanabenz were NFκB1, as well as Jdp2, c-Fos and JunB, which belong to AP-1 family genes. The potential inhibitors included Xbp1, which is inducible in response to stress to the endoplasmic reticulum [14]. Hereafter, we focused on the examination of the predicted role of c-Fos and JunB in RANKL-driven osteoclastogenesis.

3.3. Salubrinal- and guanabenz-driven reduction in c-Fos and JunB

The protein levels of c-Fos and NFATc1 were downregulated by salubrinal both in RAW264.7 cells and bone marrow cells (Fig. 5A & B). The downregulation of c-Fos and NFATc1 proteins was also detected in response to guanabenz (Fig. 5C & D). Furthermore, the level of JunB protein was significantly reduced by salubrinal and guanabenz in RAW264.7 cells and bone marrow cells (Fig. 6).

3.4. Suppression of RANKL-driven TRAP and cathepsin K by c-Fos siRNA and JunB siRNA

In RAW264.7 cells, partial silencing of c-Fos suppressed RANKL-driven elevation of NFATc1, TRAP, and cathepsin K mRNAs (Fig. 7). Compared to treatment with nonspecific control siRNA, partial silencing of JunB using siRNA specific to JunB also significantly reduced the mRNA levels of NFATc1 and TRAP (Fig. 8).

3.5. Potential feedback link between NFATc1 and c-Fos

Partial silencing of NFATc1 for 12 h in RAW264.7 cells does not significantly alter the protein levels of c-Fos and JunB (Fig. 9A). After

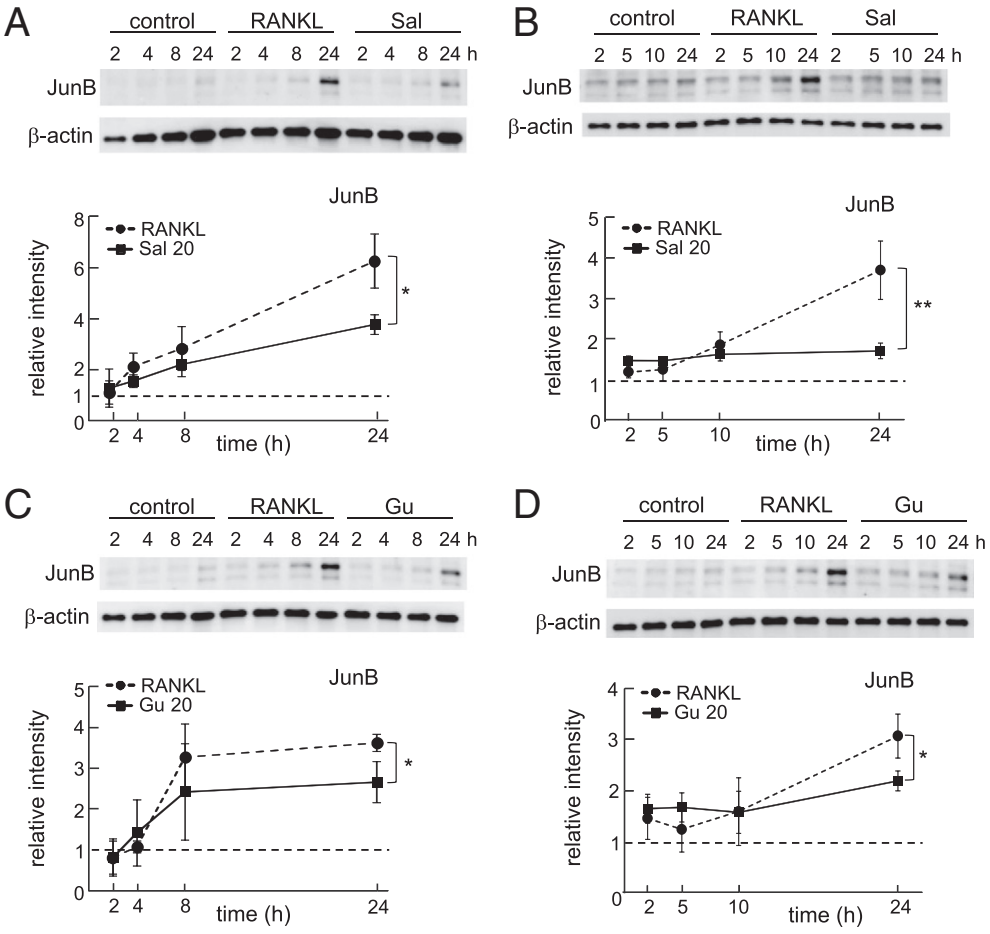

Fig. 6. Salubrinal- and guanabenz-driven reduction in JunB. The single and double asterisks indicate $p < 0.05$ and $p < 0.01$, respectively. (A&B) Protein levels of JunB in the presence of salubrinal in RAW264.7 cells (2, 4, 8, and 24 h) and bone marrow cells (2, 5, 10, and 24 h), respectively. (C&D) Protein levels of JunB in the presence of guanabenz in RAW264.7 cells (2, 4, 8, and 24 h) and bone marrow cells (2, 5, 10, and 24 h), respectively.

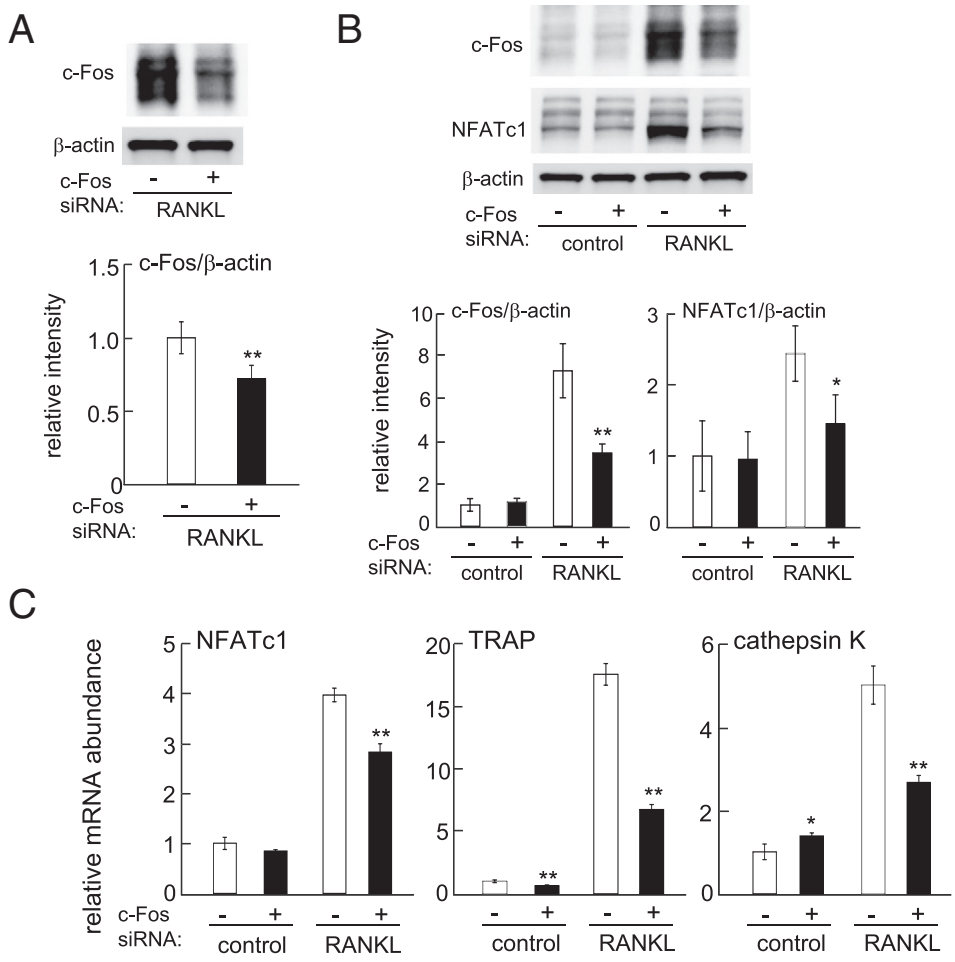

Fig. 7. Suppression of RANKL-driven osteoclast-linked genes by c-Fos siRNA in RAW264.7 cells. (A) Protein levels of c-Fos with c-Fos siRNA in the presence of RANKL. (B) c-Fos and NFATc1 protein levels by c-Fos siRNA treatment. (C) Levels of NFATc1, TRAP, and cathepsin K mRNAs in response to non-specific control (NC) and c-Fos siRNAs. The single and double asterisks indicate $p < 0.05$ and $p < 0.01$, respectively.

24 h, however, the level of c-Fos protein was detectable (Fig. 9B). However, the level of JunB protein was not affected by NFATc1 siRNA for 24 h (Fig. 9B).

4. Discussion

We present in this study that salubrinal and guanabenz, two chemical agents that suppress stress to the endoplasmic reticulum, significantly modulate mRNA expression levels of various transcription factors. PCA analysis revealed that PC1, the first principal component, best explains the expression profiles of the effects of salubrinal and guanabenz on osteoclastogenesis. Along PC1, control samples are most negative and RANKL-treated samples are most positive. Consistent with the phenotypic observations with TRAP staining, the groups treated with salubrinal and guanabenz lay between the control and RANKL groups. Using eigenarray values, we chose candidate transcription factors that are responsive to these agents and significantly alter the expression of NFATc1. The involvement of c-Fos and JunB was predicted by PCA in RAW264.7 cells, confirmed by PCR and Western blotting in RAW264.7 as well as primary bone marrow cells, and validated using RNA interference.

Of the candidate regulators predicted by PCA, we focused on two AP-1 proteins, c-Fos and JunB, and validated their roles in the suppression of RANKL-driven osteoclastogenesis in response to salubrinal and guanabenz. Both proteins responded in cell line cultures (RAW264.7) and primary bone marrow cells. A partial silencing of c-Fos and JunB decreased the mRNA and protein levels of NFATc1. Furthermore, there was a feedback loop in which a decrease in c-Fos by salubrinal reduced NFATc1 expression, and the reduction in NFATc1 further attenuated the level of c-Fos protein. AP-1 proteins are known to play a critical role in osteoclast differentiation. It is reported that mice lacking c-Fos are osteopetrotic due to abnormal development of osteoclasts [15–17]. Osteoclast abnormality was also observed in mice lacking JunB [18]. Together with a pivotal role of Jdp2 in the dimerization of AP-1 proteins, these studies are consistent with our results in which partial knockdown of c-Fos and JunB attenuates the expression of osteoclast-linked genes.

Besides AP-1 proteins, PCA predicted other transcription factors that are potentially involved in regulating osteoclastogenesis in response to salubrinal and guanabenz. NFκB1 (p50) was predicted to be an activator whose expression was downregulated by these agents. This prediction is consistent with a report in which overexpression of each of p50, p65, p52, and RelB proteins in an NFκB family accelerates osteoclast development [19]. As a transcription factor associated with stress to the endoplasmic reticulum [14], Xbp1 was predicted to be inhibitory to osteoclastogenesis. It is reported, however, that Xbp1 stimulates production of RANKL in osteoblasts [20]. The prediction in this study is based on genome-wide expression data in RAW264.7 pre-osteoclasts, and it is possible that the predicted transcription factors may have different roles in other types of cells and different time points.

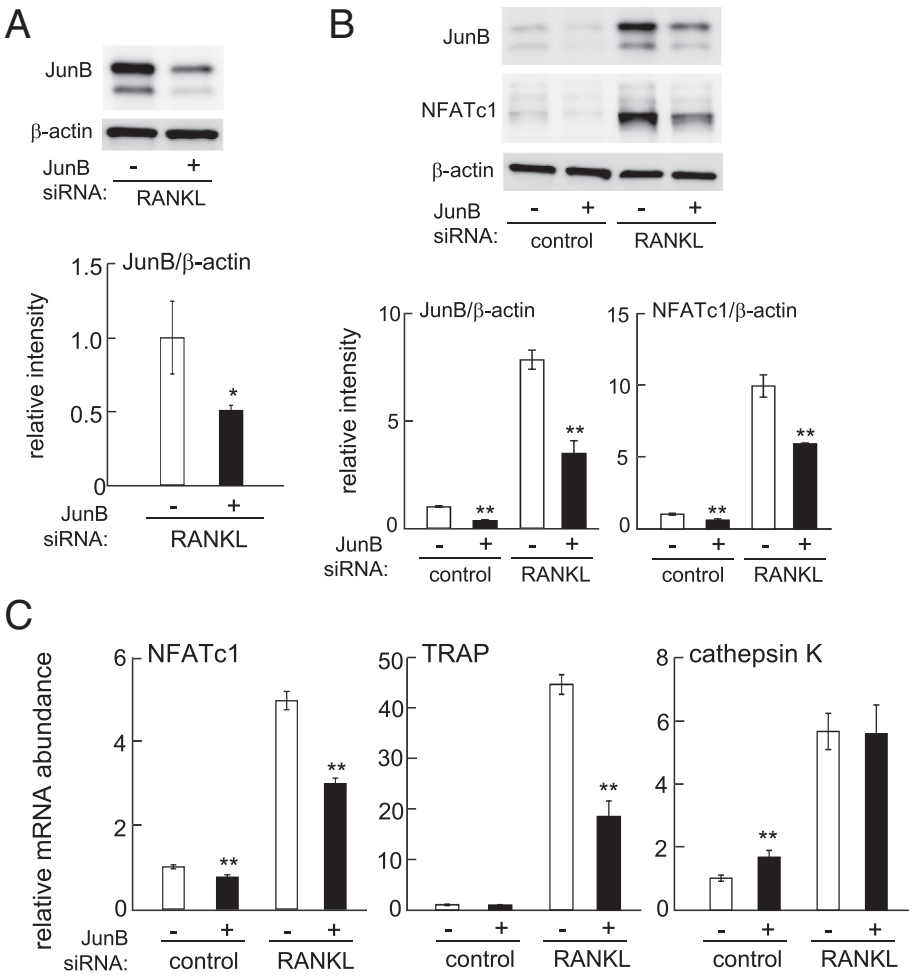

Fig. 8. Suppression of RANKL-driven osteoclast-linked genes by JunB siRNA in RAW264.7 cells. (A) Protein level of JunB with JunB siRNA in the presence of RANKL. (B) JunB and NFATc1 protein levels by JunB siRNA treatment. (C) Levels of NFATc1, TRAP, and cathepsin K mRNAs in response to non-specific control (NC) and JunB siRNAs. The single and double asterisks indicate $p < 0.05$ and $p < 0.01$, respectively.

Though PC1 is the principal component axis that most closely aligns with the observed phenotype among the samples, the other principal components also had significant contributions to eigenvalues. The PC2 values for the samples in the control and RANKL groups were negative, while they were positive for the samples in the salubrinal/guanabenz-treated groups. In PC3, however, the salubrinal and guanabenz samples were on opposite sides of PC3 axis. This observation may relate to differential effects of salubrinal and guanabenz, which are not associated with osteoclastogenesis. For example, guanabenz is reported to be an agonist of the adrenergic receptor alpha 2, but salubrinal is not [21].

In this study we predicted candidate mediators of salubrinal and guanabenz in the regulation of osteoclastogenesis; however, there are limitations that should be carefully considered. First, we used RAW264.7 pre-osteoclasts and bone marrow cells at specific time points (4 h and 12 h post-treatment). These two time points were chosen to help identify genes that were upstream mediators (at 4 h) and co-modulators (at 12 h) of NFATc1. However, some of the predicted genes may not continue their regulatory role at later time points such as 24 h and 48 h. Also, interactions with other types of cells such as osteoblasts might alter the overall role of any transcription factor. Second, we validated a hypothesis that was novel in terms of the responses to salubrinal and guanabenz but known in terms of their role in osteoclastogenesis. The described systems-biology approach can be extended to identify genes whose involvement in the regulation of osteoclastogenesis has yet to be shown.

Because of their dual roles in bone formation and bone resorption, salubrinal and guanabenz can potentially add a new dimension to treatment of patients with osteopenia and osteoporosis [1,2,4]. The mechanism of their action, particularly eIF2α-mediated translational regulation, has been well documented [1]. However, a mechanism of transcriptional regulation in NFATc1-driven osteoclastogenesis has been elusive. Using genome-wide mRNA expression with PCA followed by *in vitro* assays with specific RNA silencing, we herein demonstrated that salubrinal and guanabenz alter the expression pattern of a wide spectrum of genes that are not necessarily linked to stress to the endoplasmic reticulum. Besides the involvement of c-Fos and JunB in the RANKL-salubrinal/guanabenz-NFATc1 regulatory axis, novel targets of salubrinal and guanabenz may be identified by additional validation assays and contribute to our basic understanding of osteoclastogenesis and the development of therapeutic agents for bone diseases.

Acknowledgments

The authors appreciate M. Hamamura for technical assistance. All authors state that they have no conflicts of interest. This study was supported by grant DOD W81XWH-11-1-0716.

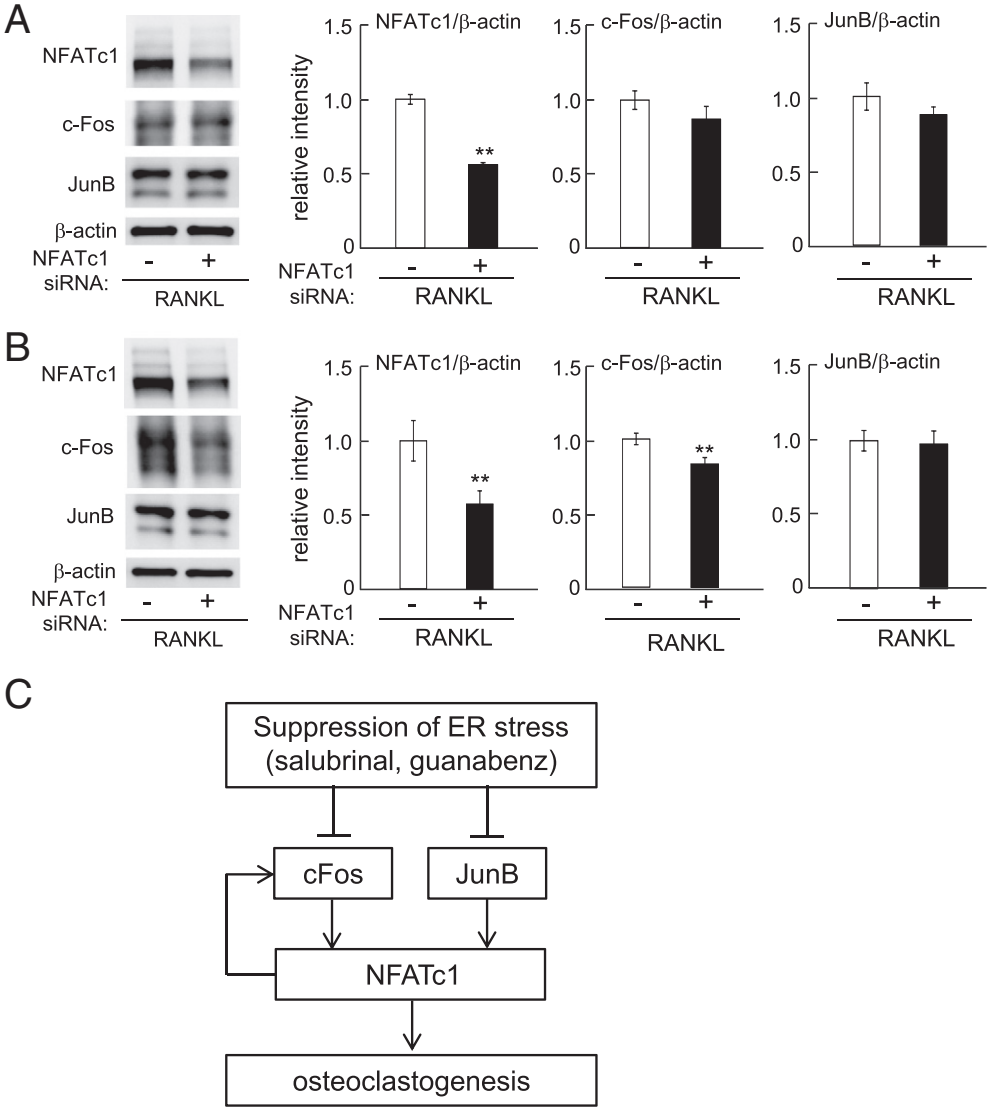

Fig. 9. Suppression of c-Fos protein by NFATC1 siRNA in RAW264.7 cells. (A) Protein levels of c-Fos and JunB after treatment with NFATc1 siRNA in the presence of RANKL for 12 h. (B) Protein levels of c-Fos and JunB after treatment with NFATc1 siRNA in the presence of RANKL for 24 h. (C) Proposed inhibitory mechanism of osteoclastogenesis in response to salubrinal and guanabenz.

References

[1] L. He, J. Lee, J.H. Jang, K. Sakchaisri, J. Hwang, H.J. Cha-Molstad, K.A. Kim, I.J. Ryoo, H.G. Lee, S.O. Kim, N.K. Soung, K.S. Lee, Y.T. Kwon, R.L. Erikson, J.S. Ahn, B.Y. Kim, Cell. Signal. 25 (2013) 552–560.
[2] K. Hamamura, N. Tanjung, H. Yokota, J. Bone Miner. Metab. 31 (2013) 618–628.
[3] A. Chen, K. Hamamura, P. Zhang, Y. Chen, H. Yokota, IET Syst. Biol. 4 (2010) 52–63.
[4] H. Yokota, K. Hamamura, A. Chen, T.R. Dodge, N. Tanjung, A. Abedinpoor, P. Zhang, BMC Musculoskelet. Disord. 14 (2013) 197.
[5] M. Boyce, K.F. Bryant, C. Jousse, K. Long, H.P. Harding, D. Scheuner, R.J. Kaufman, D. Ma, D.M. Coen, D. Ron, J. Yuan, Science 307 (2005) 935–939.
[6] P. Tsaytler, H.P. Harding, D. Ron, A. Bertolotti, Science 332 (2011) 91–94.
[7] H. Takayanagi, S. Kim, T. Koga, H. Nishina, M. Isshiki, H. Yoshida, A. Saiura, M. Isobe, T. Yokochi, J. Inoue, E.F. Wagner, T.W. Mak, T. Kodama, T. Taniguchi, Dev. Cell 3 (2002) 889–901.
[8] O. Alter, P.O. Brown, D. Botstein, Proc. Natl. Acad. Sci. U. S. A. 97 (2000) 10101–10106.
[9] K. Hamamura, A. Chen, A. Nishimura, N. Tanjung, A. Sudo, H. Yokota, Cell. Signal. 26 (2014) 2358–2369.
[10] M. Dunning, A. Lynch, and M. Eldridge, illuminaMousev2.db: Illumina MouseWG6v2 annotation data (chip illuminaMousev2), R package version 1.22.1.
[11] M. Dai, P. Wang, A.D. Boyd, G. Kostov, B. Athey, E.G. Jones, W.E. Bunney, R.M. Myers, T.P. Speed, H. Akil, S.J. Watson, F. Meng, Nucleic Acids Res. 33 (2005) e175.
[12] M. Kanamori, H. Konno, N. Osato, J. Kawai, Y. Hayashizaki, H. Suzuki, Biochem. Biophys. Res. Commun. 322 (2004) 787–793.
[13] G.K. Smyth, Stat. Appl. Genet. Mol. Biol. 3 (2004).
[14] N.N. Iwakoshi, A.H. Lee, P. Vallabhajosyula, K.L. Otipoby, K. Rajewsky, L.H. Glimcher, Nat. Immunol. 4 (2003) 321–329.
[15] Z.Q. Wang, C. Ovitt, A.E. Grigoriadis, U. Mohle-Steinlein, U. Ruther, E.F. Wagner, Nature 360 (1992) 741–745.
[16] E.F. Wagne, Ann. Rheum. Dis. 61 (2002) ii40–ii42.
[17] E.F. Wagner, K. Matsuo, Ann. Rheum. Dis. 62 (2003) ii83–ii85.
[18] L. Kenner, A. Hoebertz, F.T. Beil, N. Keon, F. Karreth, R. Eferl, H. Scheuch, A. Szremska, M. Amling, M. Schorpp-Kistner, P. Angel, E.F. Wagner, J. Cell Biol. 164 (2004) 613–623.
[19] M. Yu, X. Qi, J.L. Moreno, D.L. Farber, A.D. Keegan, J. Immunol. 187 (2011) 1797–1806.
[20] G. Xu, K. Liu, J. Anderson, K. Patrene, S. Lentzsch, G.D. Roodman, H. Ouyang, Blood 119 (2012) 4205–4214.
[21] R.S. Shah, B.R. Walker, S.K. Vanov, R.H. Helfant, Clin. Pharmacol. Ther. 19 (1976) 732–737.

J Bone Miner Metab (2013) 31:618–628
DOI 10.1007/s00774-013-0450-0

ORIGINAL ARTICLE

Suppression of osteoclastogenesis through phosphorylation of eukaryotic translation initiation factor 2 alpha

Kazunori Hamamura · Nancy Tanjung · Hiroki Yokota

Received: 4 January 2013 / Accepted: 28 February 2013 / Published online: 28 March 2013

Abstract In response to various stresses including viral infection, nutrient deprivation, and stress to the endoplasmic reticulum, eukaryotic translation initiation factor 2 alpha (eIF2α) is phosphorylated to cope with stress induced apoptosis. Although bone cells are sensitive to environmental stresses that alter the phosphorylation level of eIF2α, little is known about the role of eIF2α mediated signaling during the development of bone-resorbing osteoclasts. Using two chemical agents (salubrinal and guanabenz) that selectively inhibit de-phosphorylation of eIF2α, we evaluated the effects of phosphorylation of eIF2α on osteoclastogenesis of RAW264.7 pre-osteoclasts as well as development of MC3T3 E1 osteoblast-like cells. The result showed that salubrinal and guanabenz stimulated matrix deposition of osteoblasts through upregulation of activating transcription factor 4 (ATF4). The result also revealed that these agents reduced expression of the nuclear factor of activated T cells c1 (NFATc1) and inhibited differentiation of RAW264.7 cells to multi-nucleated osteoclasts. Partial silencing of eIF2α with RNA interference reduced suppression of salubrinal/guanabenz-driven downregulation of NFATc1. Collectively, we demonstrated that the elevated phosphorylation level of eIF2α not only stimulates osteoblastogenesis but also inhibit osteoclastogenesis through regulation of ATF4 and NFATc1. The results suggest that eIF2α-mediated signaling might provide a novel therapeutic target for preventing bone loss in osteoporosis.

Keywords Osteoclasts · Salubrinal · Guanabenz · eIF2α · NFATc1

Introduction

Osteoblasts and osteoclasts are the two major types of bone cells in bone remodeling. Osteoblasts are bone-forming cells originated from mesenchymal stem cells, while osteoclasts are bone-resorbing cells derived from hematopoietic stem cells. These two types of cells orchestrate a complex remodeling process, in which mineralized bone matrix is degraded by osteoclasts and newly formed by osteoblasts [1, 2]. In order to maintain proper bone mass, exercise and calcium rich diets are recommended. However, a failure of the coordinated action such as in osteoporosis, which is a common form of bone loss prevailing among postmenopausal women, increases risk of bone fracture [3]. In order to develop therapeutic drugs for treatment of osteoporosis, an understanding of signaling pathways that govern osteoclastogenesis—development of pre-osteoclasts (monocyte/macrophage) to multi-nucleated osteoclasts—is required. In this paper, we examined a signaling pathway for osteoclastogenesis that is mediated by eukaryotic translation initiation factor 2 alpha (eIF2α).

A protein complex, eIF2, is a heterotrimer essential for protein synthesis, and eIF2α is one of its major components together with eIF2β and eIF2γ [4]. In response to various stresses such as oxidation, radiation, and stress to the

Electronic supplementary material The online version of this article (doi:10.1007/s00774-013-0450-0) contains supplementary material, which is available to authorized users.

K. Hamamura (✉) · N. Tanjung · H. Yokota
Department of Biomedical Engineering, Indiana University-Purdue University Indianapolis, SL155, 723 West Michigan Street, Indianapolis, IN 46202, USA
e-mail: hamamurk@iupui.edu

H. Yokota
Department of Anatomy and Cell Biology, Indiana University School of Medicine, Indianapolis, IN 46202, USA

endoplasmic reticulum that potentially lead to cellular apoptosis, a serine residue of eIF2α is phosphorylated. This action would initiate a pro-survival program by lowering general translation efficiency except for a group of genes that includes activating transcription factor 4 (ATF4) [5]. The ATF4 is a transcription factor critical for osteoblastogenesis and bone formation [6]. In osteoblasts elevation of phosphorylated eIF2α (p-eIF2α) is reported to stimulate the expression of ATF4 [7, 8]. Little is known, however, about potential effects of p-eIF2α on development of osteoclasts.

Herein we addressed a question: Does elevation of p-eIF2α alter cellular fates of pre-osteoclasts? Osteoblasts and osteoclasts extensively interact through molecular pathways including RANK (receptor activator of nuclear factor kappa-B)/RANKL (RANK ligand)/OPG (osteoprotegerin) signaling [9, 10] and Wnt signaling [11]. Therefore, osteoclastogenesis is potentially regulated by signaling molecules that also affect osteoblastogenesis. Furthermore, osteoclastogenesis is influenced by various stresses such as estrogen deficiency and disuse or unloading [12]. Since elevation of p-eIF2α can provide stress-relieving effects on osteoblasts, we hypothesized that elevation of p-eIF2α suppresses differentiation of pre-osteoclasts to multi-nucleated osteoclasts.

In this study, we employed two chemical agents (salubrinal and guanabenz) and examined the effects of elevated p-eIF2α on osteoclastogenesis. These two agents selectively inhibit de-phosphorylation of p-eIF2α by interacting with protein phosphatase 1, PP1 [13, 14]. The signaling pathway, mediated by eIF2α, is not directly linked to known agents for osteoclastogenesis such as calcium binding agents and RANKL. Currently, the most common medications, prescribed for preventing bone loss in patients with osteoporosis, are bisphosphonates. Bisphosphonates preferentially bind to calcium in bone and induce apoptosis of osteoclasts [15]. Other medications using neutralizing antibodies targeted to RANKL would block osteoclastogenesis by mimicking OPG's binding to RANKL [16]. The RANKL is a cytokine belonging to the tumor necrosis factor family, and is involved in T cell-dependent immune responses as well as differentiation and activation of osteoclasts [9, 10]. To our knowledge, no therapeutic agents for osteoporosis have been targeted to eIF2α-mediated signaling.

We employed MC3T3 E1 osteoblast-like cells [17] and RAW264.7 cells [18] to evaluate osteoblastogenesis and osteoclastogenesis, respectively. In the presence and absence of salubrinal and guanabenz, MC3T3 E1 cells were cultured in an osteogenic medium for evaluation of matrix deposition, while RAW264.7 cells were cultured in an osteoclast differentiation medium for evaluation of multi-nucleation. Alizarin Red S staining was performed to evaluate osteoblast mineralization for MC3T3 E1 cells, and TRAP staining was conducted to determine multi-nucleated osteoclasts proliferation for RAW264.7 cells. To analyze molecular signaling pathways, quantitative real-time PCR and Western blot analysis were conducted. The mRNA levels of ATF4, osteocalcin, c-Fos [19], tartrate-resistant acid phosphatase (TRAP) [20], and osteoclast-associated receptor (OSCAR) [21] were determined. The protein expression levels of eIF2α, ATF4, and nuclear factor of activated T cells c1 (NFATc1) [22] were also determined. The NFATc1 is a transcription factor, which is critically important for development and activation of osteoclasts in response to RANKL. The RNA interference using siRNA specific to ATF4 and eIF2α was conducted to evaluate the role of ATF4 in osteoblastogenesis and eIF2α in osteoclastogenesis.

Materials and methods

Cell culture

The MC3T3 E1 mouse osteoblast-like cells (clone 14—MC3T3 E1-14; and no clonal cells in supplementary figures), and RAW264.7 mouse pre-osteoclast (monocyte/macrophage) cells were cultured in αMEM containing 10 % fetal bovine serum and antibiotics (50 U/ml penicillin, and 50 μg/ml streptomycin; Life Technologies, Grand Island, NY, USA). Cells were maintained at 37 °C and 5 % CO_2 in a humidified incubator. Cell mortality and live cell numbers were determined 24 h after the treatment with 20 ng/ml RANKL (PeproTech, Rocky Hills, NC, USA) in response to 0.1–20 μM salubrinal or 1–20 μM guanabenz acetate (Tocris Bioscience, Ellisville, MO, USA). Cells were stained with trypan blue and the numbers of live and dead cells were counted using a hemacytometer.

Quantitative real-time PCR

Total RNA was extracted using an RNeasy Plus mini kit (Qiagen, Germantown, MD, USA). Reverse transcription was conducted with high capacity cDNA reverse transcription kits (Applied Biosystems, Carlsbad, CA, USA), and quantitative real-time PCR was performed using ABI 7500 with Power SYBR green PCR master mix kits (Applied Biosystems). We evaluated mRNA levels of ATF4, Osteocalcin (OCN), NFATc1, c-Fos, tartrate-resistant acid phosphatase (TRAP), and osteoclast-associated receptor (OSCAR) with the PCR primers listed in Table 1. The GAPDH was used for internal control. The relative mRNA abundance for the selected genes with respect to the level of GAPDH mRNA was expressed as a

Table 1 Real-time PCR primers used in this study

Target	Forward primer	Backward primer
ATF4	5′-TGGCGAGTGTAAGGAGCTAGAAA-3′	5′-TCTTCCCCCTTGCCTTACG-3′
OCN	5′-CCGGGAGCAGTGTGAGCTTA-3′	5′-AGGCGGTCTTCAAGCCATACT-3′
NFATc1	5′-GGTGCTGTCTGGCCATAACT-3′	5′-GCGGAAAGGTGGTATCTCAA-3′
c-Fos	5′-AGGCCCAGTGGCTCAGAGA-3′	5′-CCAGTCTGCTGCATAGAAGGAA-3′
TRAP	5′-TCCTGGCTCAAAAAGCAGTT-3′	5′-ACATAGCCCACACCGTTCTC-3′
OSCAR	5′-ACACACACACCTGGCACCTA-3′	5′-GAGACCATCAAAGGCAGAGC-3′
GAPDH	5′-TGCACCACCAACTGCTTAG-3′	5′-GGATGCAGGGATGATGTTC-3′

ratio of $S_{\text{treated}}/S_{\text{control}}$, where S_{treated} is the mRNA level for the cells treated with chemical agents, and S_{control} is the mRNA level for control cells [23].

Western immunoblotting

Cells were lysed in a radioimmunoprecipitation assay (RIPA) buffer containing protease inhibitors (Santa Cruz Biotechnology, Santa Cruz, CA, USA) and phosphatase inhibitors (Calbiochem, Billerica, MA, USA). Isolated proteins were fractionated using 10–15 % SDS gels and electro-transferred to Immobilon-P membranes (Millipore, Billerica, MA, USA). The membrane was incubated for 1 h with primary antibodies followed by 45 min incubation with goat anti-rabbit or anti-mouse IgG conjugated with horseradish peroxidase (Cell Signaling, Danvers, MA, USA). We used antibodies against ATF4, NFATc1 (Santa Cruz), p-eIF2α (Thermo Scientific, Waltham, MA, USA), eIF2α, caspase 3, cleaved caspase 3, p38 and p-p38 mitogen activated protein kinase (MAPK), extracellular signal-regulated kinase (ERK) and p-ERK, nuclear factor kappa B (NFκB) p65 and p-NFκB p65 (Cell Signaling), and β-actin (Sigma). Protein levels were assayed using a SuperSignal west femto maximum sensitivity substrate (Thermo Scientific), and signal intensities were quantified with a luminescent image analyzer (LAS-3000, Fuji Film, Tokyo, Japan).

Knockdown of ATF4 and eIF2α by siRNA

Cells were treated with siRNA specific to ATF4 and eIF2α (Life Technologies). Selected target sequences for knockdown of ATF4 and eIF2α were: ATF4, 5′-GCU GCU UAC AUU ACU CUA A-3′; and eIF2α, 5′-CGG UCA AAA UUC GAG CAG A-3′. As a nonspecific control, a negative siRNA (Silencer Select #1, Life Technologies) was used. Cells were transiently transfected with siRNA for ATF4, eIF2α or control in Opti-MEM I medium with Lipofectamine RNAiMAX (Life Technologies). Six hours later, the medium was replaced by regular culture medium. The efficiency of silencing was assessed with immunoblotting or quantitative PCR 48 h after transfection.

Mineralization assay

Mineralization of extracellular matrix was assayed by Alizarin Red S staining. The MC3T3-E1 cells were plated in 6-well plates. When cells were confluent, 50 μg/ml of ascorbic acid (Wako Chemicals, Richmond, VA, USA) and 5 mM β-glycerophosphate (Sigma) were added. The medium was changed every other day, and staining was conducted after 3 weeks. Cells were washed with PBS twice and fixed with 60 % isopropanol for 1 min at room temperature, followed by rehydration with distilled water for 3 min at room temperature. They were stained with 1 % Alizarin red S (Sigma) for 3 min and washed with distilled water.

Osteoclastogenesis in vitro and TRAP (Tartrate-resistant acid phosphatase) staining

The RAW264.7 cells were plated at a density of $5 \times 10^3/\text{cm}^2$ into a 12-well or a 60 mm dish, and cultured with 20 ng/ml RANKL in the presence and absence of salubrinal or guanabenz. The culture medium was replaced every 2 days. After 5 days of culture, the cells were stained for TRAP staining using an acid phosphatase leukocyte kit (Sigma). The number of TRAP-positive cells containing three or more nuclei was determined.

Statistical analysis

Three or four-independent experiments were conducted and data were expressed as mean ± SD. For comparison among multiple samples, ANOVA followed by post hoc tests was conducted. Statistical significance was evaluated at $p < 0.05$. The single and double asterisks and daggers indicate $p < 0.05$ and $p < 0.01$. To determine intensities in immunoblotting and areas of Alizarin red S staining, images were scanned with Adobe Photoshop CS2 (Adobe Systems, San Jose, CA, USA) and quantified using Image J.

Results

Enhanced mineralization of MC3T3 E1-14 cells by salubrinal

Prior to examining the effects of salubrinal on osteoclastogenesis, we tested its effects on the development of osteoblasts focusing on cell viability, phosphorylation of eIF2α (p-eIF2α), expression of ATF4 and osteocalcin, and matrix mineralization. Administration of 5–20 μM salubrinal to MC3T3 E1-14 cells did not increase cell mortality or inhibit cell proliferation (Fig. 1a). Unlike application of 10 nM thapsigargin, which is a stress inducer to the endoplasmic reticulum that elevates p-eIF2α, incubation with 10 μM salubrinal for 24 h did not elevate the expression level of cleaved caspase 3 (Fig. 1b). After 3-week incubation in an osteogenic medium, Alizarin red S staining area showed that salubrinal enhanced mineralization of MC3T3 E1-14 cells in a dose dependent manner (Fig. 1c). The enhanced mineralization was also observed in non-clonal MC3T3 E1 cells (Supplementary Fig. S1).

ATF4-mediated elevation of osteocalcin mRNA in MC3T3 E1-14 cells

Salubrinal is an inhibitor of de-phosphorylation of eIF2α. Administration of 5 μM salubrinal to MC3T3 E1-14 cells elevated phosphorylation of eIF2α, followed by an increase in ATF4 expression (Fig. 2a). Furthermore, the level of osteocalcin mRNA was increased 3.3 ± 0.5 fold (24 h) and 3.3 ± 0.3 fold (32 h) (Fig. 2b). When expression of ATF4 was significantly reduced by RNA interference (Fig. 2c, d), however, salubrinal-driven elevation of the osteocalcin mRNA level was suppressed (Fig. 2e). Non-clonal MC3T3 E1 cells also presented elevation of p-eIF2α and ATF4, together with an increase in the mRNA levels of ATF4 and osteocalcin (Supplementary Fig. S2). In addition, administration of guanabenz to MC3T3 E1-14 elevated the mRNA level of osteocalcin in a dose dependent manner, consistent with an increase in p-eIF2α and ATF4 (Supplementary Fig. S3).

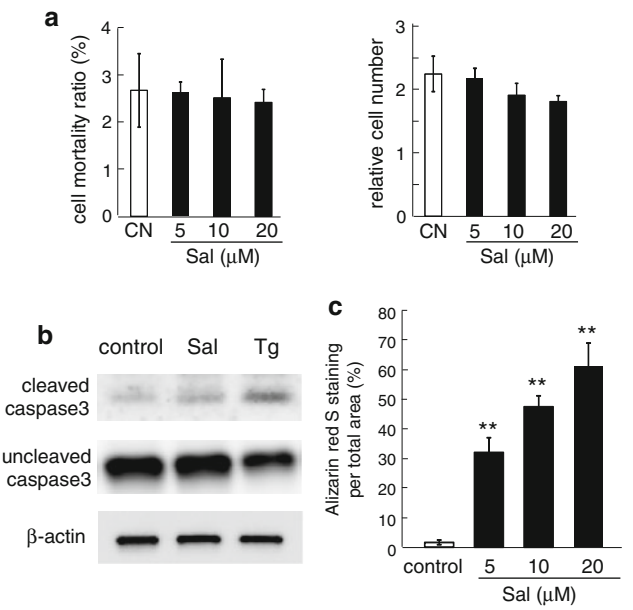

Fig. 1 Osteogenic effects of salubrinal on MC3T3 E1 (clone 14) osteoblast cells. *CN* control, *Sal* salubrinal, and *Tg* thapsigargin. The *double asterisk* indicates $p < 0.01$ in comparison to CN. **a** Cell mortality ratio and relative cell numbers. **b** No activation of cleaved caspase 3 by salubrinal. **c** Alizarin red S staining area in response to 5, 10, and 20 μM salubrinal

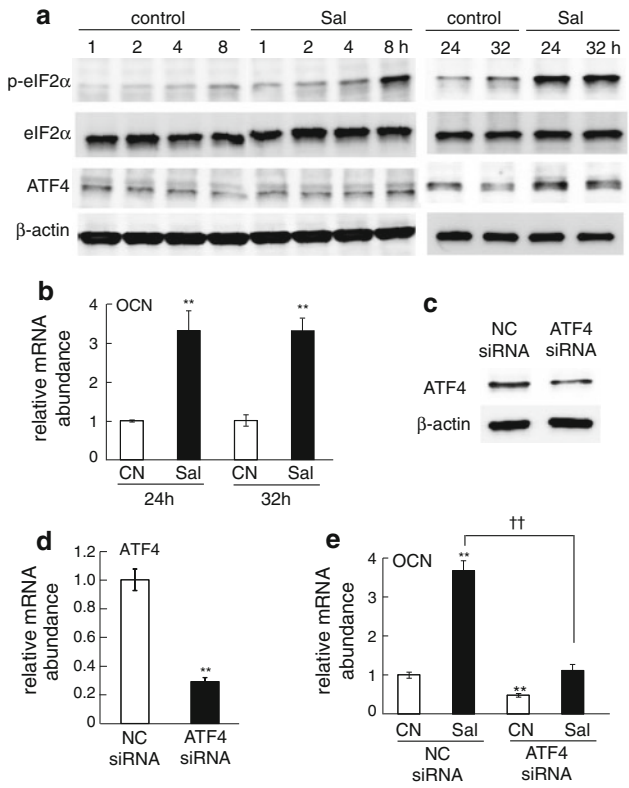

Fig. 2 Upregulation of p-eIF2α, ATF4 and osteocalcin by salubrinal in MC3T3 E1 (clone 14) osteoblast cells in response to 5 μM salubrinal. *CN* control, *Sal* salubrinal, and *NC* non-specific control siRNA. The *double asterisk* indicates $p < 0.01$ in comparison to CN or NC. The *double dagger* indicates with $p < 0.01$ in comparison to the salubrinal-treated NC siRNA cells. **a** Western blot analysis of p-eIF2α and ATF4. **b** Salubrinal driven elevation of osteocalcin mRNA level. **c** ATF4 level after transfecting siRNA specific to ATF4. **d** Relative mRNA levels of ATF4 in response to RNA interference with ATF4 siRNA and non-specific control (NC) siRNA. **e** Relative mRNA levels of osteocalcin (OCN). The *asterisk* is for the comparison to the control with NC siRNA, and the *dagger* is the comparison between the samples transfected with ATF4 siRNA

Inhibition of osteoclastogenesis of RAW264.7 cells by salubrinal

The primary aim of this study is to evaluate the effects of salubrinal on osteoclastogenesis. In response to 0.1–20 μM salubrinal for 24 h, we examined cell mortality and live cell numbers of RAW264.7 pre-osteoclasts. Cell mortality ratio did not present statistically significant differences in the presence and absence of RANKL (Fig. 3a). The number of live cells was increased by ~50 % by incubation with RANKL, and administration of 10–20 μM salubrinal reduced the numbers approximately by 10 % (Fig. 3b). Consistent with the stimulatory role of RANKL, the number of TRAP-positive multi-nucleated cells was substantially increased by the addition of RANKL. However, administration of 0.5–20 μM salubrinal reduced the number of TRAP-positive cells in a dose dependent manner (Fig. 3c, d).

Downregulation of NFATc1 in RAW264.7 cells by salubrinal

The NFATc1 is a transcription factor critical for activating osteoclastogenesis. Addition of RANKL to the culture medium significantly induced NFATc1 expression at day 2 and maintained its elevated level on day 4 (Fig. 4). The RANKL-induced expression of NFATc1 was reduced by administration of 5–20 μM salubrinal on both days, and the effect of salubrinal was dose dependent (Fig. 4).

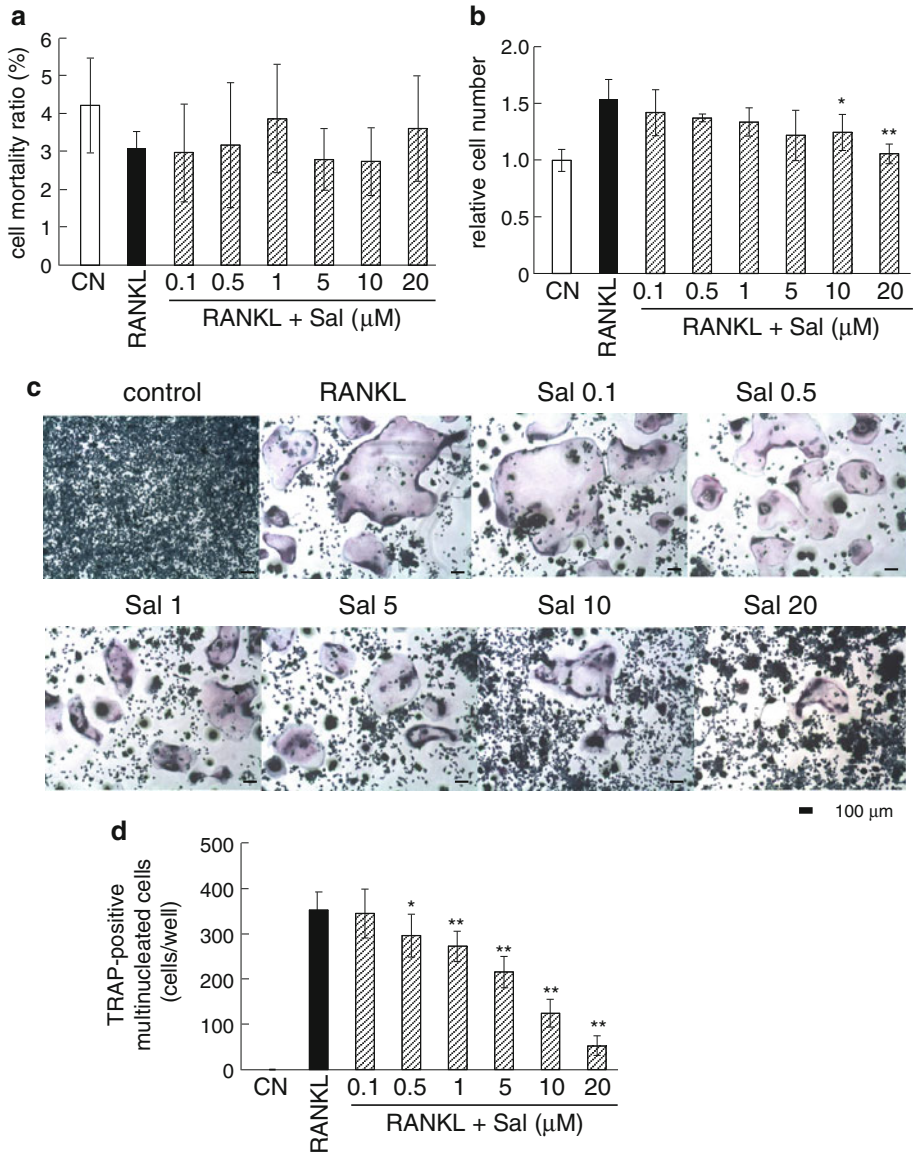

Fig. 3 Inhibitory effects of salubrinal on RAW264.7 pre-osteoclasts. *CN* control, and *Sal* salubrinal. The *single and double asterisks* indicate $p < 0.05$ and $p < 0.01$ in comparison to the RANKL-treated cells, respectively. **a** Cell mortality ratio. **b** Relative cell numbers. **c** Dose-dependent suppression of RANKL driven activation of osteoclasts by salubrinal. **d** Dose-dependent suppression of TRAP-positive multi-nucleated cells by salubrinal

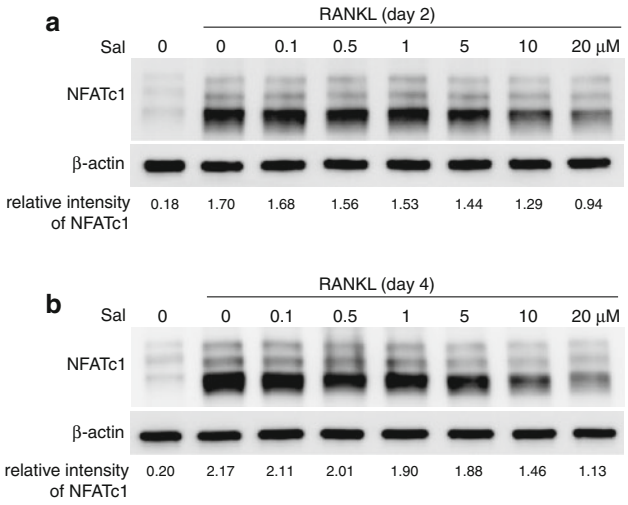

Fig. 4 Reduction of RANKL-induced NFATc1 expression by salubrinal. *Sal* salubrinal. The relative intensity of NFATc1 to β-actin is shown. **a** Expression of NFATc1 (2 days after RANKL administration). **b** Expression of NFATc1 (4 days after RANKL administration)

Partial suppression of mRNA levels of NFATc1, c-Fos, TRAP, and OSCAR by salubrinal

Addition of RANKL increased the mRNA levels of NFATc1, c-Fos, TRAP, and OSCAR, and administration of 20 μM salubrinal significantly reduced their mRNA levels. On day 2, for instance, the RANKL-driven increase was 9.4 ± 0.5 fold (NFATc1), 1.9 ± 0.1 fold (c-fos), 165 ± 4.2 fold (TRAP), and 467 ± 22 fold (OSCAR). The reduction by 20 μM salubrinal was 46 % (NFATc1), 32 % (c-fos), 35 % (TRAP), and 21 % (OSCAR) (Fig. 5a). Consistent with the observed dose response, administration of salubrinal at 0.1–1 μM did not contribute to significant reduction in these mRNA levels except for NFATc1 and c-fos on day 4 (Fig. 5b).

Temporal profile of p-eIF2α and NFATc1

The temporal expression profile revealed that addition of RANKL transiently reduced the phosphorylation level of eIF2α (2–8 h) and elevated NFATc1 by 13.4 ± 3.2 fold (24 h) (Fig. 6). This induction of NFATc1 was partially suppressed by salubrinal with an increase in the level of p-eIF2α. In the early period (2–4 h), administration of 20 μM salubrinal increased the level of p-eIF2α but did not alter the level of NFATc1. In the later period (8–24 h), however, the level of NFATc1 was significantly reduced by 48 % (8 h) and 44 % (24 h). Administration of 20 μM salubrinal did not significantly alter the phosphorylation level of ERK, p38 MAPK, and NFκB (Fig. 6). Note that the normalized level of "1" in Fig. 6c was defined as the level for the cells that were not treated with RANKL without administration of guanabenz.

Inhibitory effects of guanabenz on osteoclastogenesis of RAW264.7 cells

To further examine a potential involvement of p-eIF2α in regulation of osteoclastogenesis, we employed guanabenz that also acts as an inhibitor of de-phosphorylation of eIF2α. Administration of 1 and 5 μM guanabenz did not alter cell mortality and the number of live cells, although its administration at 10 and 20 μM reduced the number of live cells in 24 h (Fig. 7a, b). Consistent with salubrinal's inhibitory action, guanabenz also attenuated osteoclastogenesis of RAW264.7 cells in a dose dependent manner (Fig. 7c, d). Compared to the number of TRAP-positive multi-nucleated cells of 377 ± 39 (RANKL only), guanabenz reduced the number of differentiated osteoclasts to 364 ± 38 (1 μM), 288 ± 51 (5 μM), 189 ± 25 (10 μM), and 73 ± 16 (20 μM).

Reduction of RANKL-induced NFATc1, c-Fos, TRAP, and OSCAR by guanabenz

The induction of NFATc1 by RANKL was suppressed by guanabenz in a dose dependent manner (Fig. 8a). The mRNA levels of NFATc1, c-Fos, TRAP, and OSCAR were also reduced by administration of 20 μM guanabenz. Lower concentrations of guanabenz, 5 and 10 μM, were effective in reducing the levels of TRAP and OSCAR mRNA (Fig. 8b). The temporal expression profile of p-eIF2α and NFATc1 in response to 20 μM guanabenz revealed that p-eIF2α was upregulated in 2 h and NFATc1 was partially suppressed in 8 h (Fig. 9). The normalized level of "1" was defined as the level for the cells that were not treated with RANKL without administration of guanabenz. In the absence of RANKL administration, however, either salubrinal or guanabenz did not significantly alter cell mortality and expression of NFATc1 and TRAP (Supplementary Fig. S4).

Reduction in salubrinal/guanabenz-driven suppression of NFATc1 expression by RNA interference for eIF2α

To evaluate the effects of eIF2α on the expression level of NFATc1, we employed RNA interference specific for eIF2α together with a non-specific control (NC) (Fig. 10). In response to 20 μM salubrinal, RAW264.7 cells transfected with the control siRNA demonstrated a reduction of NFATc1 by 56 %. However, the expression of NFATc1 was reduced only by 20 % in the cells transfected with eIF2α siRNA. Furthermore, 20 μM guanabenz decreased the level of NFATc1 by 43 % in the cells transfected with

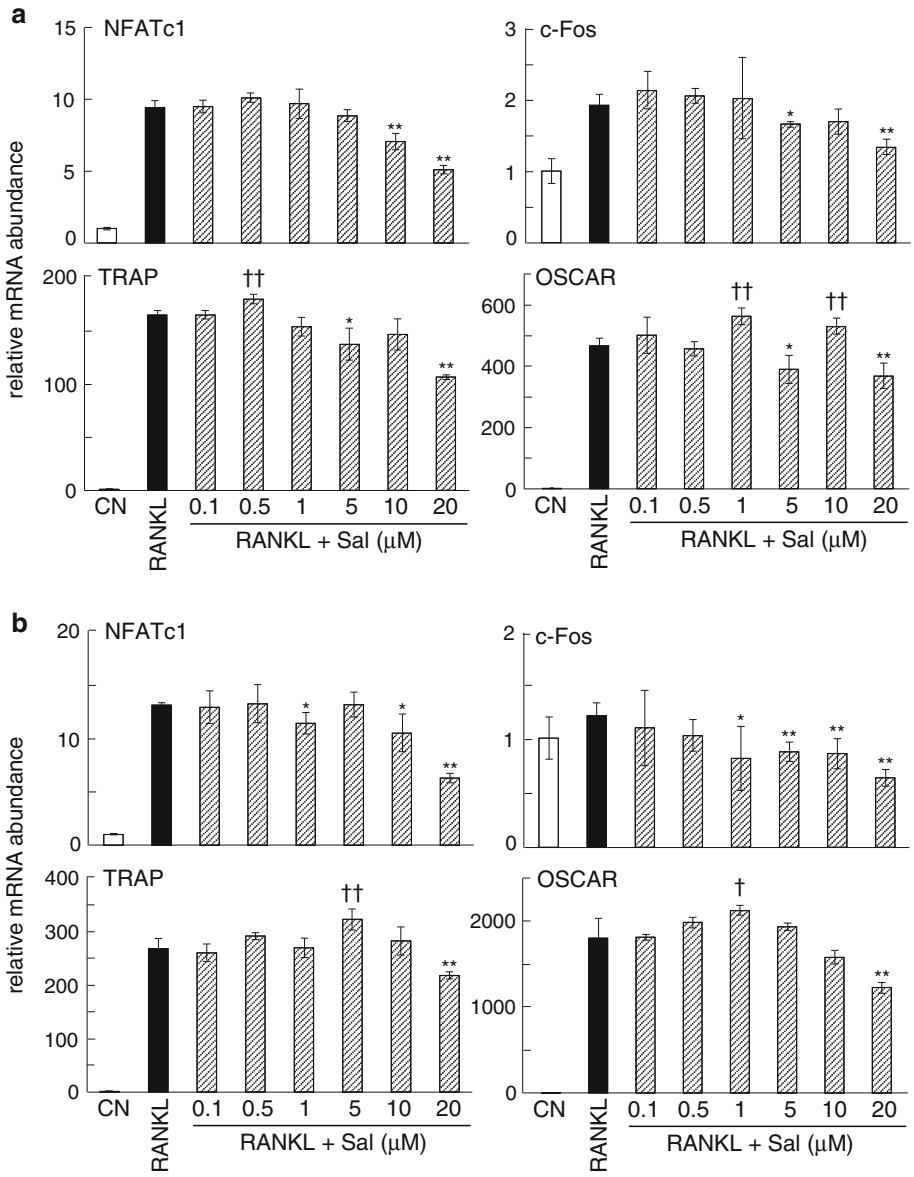

Fig. 5 Effects of salubrinal on mRNA expression levels of NFATc1, c-Fos, TRAP, and OSCAR. *CN* control. The *single and double asterisks* indicate significant decreases with $p < 0.05$ and $p < 0.01$ in comparison to the RANKL-treated cells, respectively. The *single and double daggers* indicate significant increases with $p < 0.05$ and $p < 0.01$ in comparison to the RANKL-treated cells, respectively. **a** Messenger RNA levels (2 days after RANKL administration). **b** Messenger RNA levels (4 days after RANKL administration)

the control siRNA but the transfection of eIF2α siRNA abolished the suppressive effect of guanabenz. The phosphorylation level of NFκB was not significantly altered by transfection with eIF2α siRNA.

Discussion

In this study we demonstrate that differentiation of RAW264.7 pre-osteoclasts to multi-nucleated osteoclasts is inhibited by administration of salubrinal and guanabenz, which block de-phosphorylation of eIF2α and elevate the level of p-eIF2α. The growth area covered by multi-nucleated cells is significantly reduced by salubrinal and guanabenz in a dose dependent manner. Partially silencing eIF2α using RNA interference significantly suppressed salubrinal/guanabenz-driven reduction of NFATc1 expression. Together with the stimulated development of MC3T3 E1 osteoblasts by an increase in ATF4 expression, the results herein suggest that eIF2α mediated signaling may play a physiological role in osteoclastogenesis and osteoblastogenesis.

Both salubrinal and guanabenz interact with PP1 and inhibit its activity of de-phosphorylating p-eIF2α. Guanabenz is reported to bind to PP1R15A subunit [14], while the exact binding site of salubrinal is not known. Guanabenz is also known as an α_2-adrenergic receptor agonist and used to treat hypertension [24]. The observed

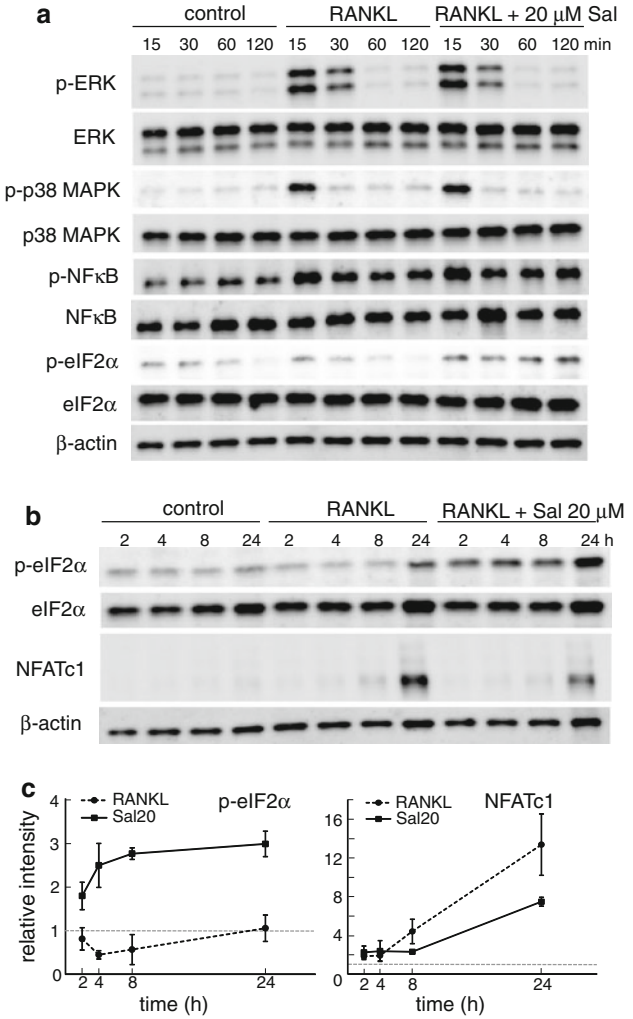

Fig. 6 Temporal expression profile of p-ERK, p-p38 MAPK, p-NFκB, p-eIF2α and NFATc1 in the presence and absence of 20 μM salubrinal. **a** Western blot analysis of p-ERK, p-p38 MAPK, p-NFκB, and p-eIF2α at 15, 30, 60 and 120 min. **b** Western blot analysis of eIF2α-p and NFATc1. **c** Comparison of the expression level of eIF2α-p and NFATc1 with and without 20 μM salubrinal. The normalized level of "1" was defined as the level for the cells that were not treated with RANKL without administration of salubrinal

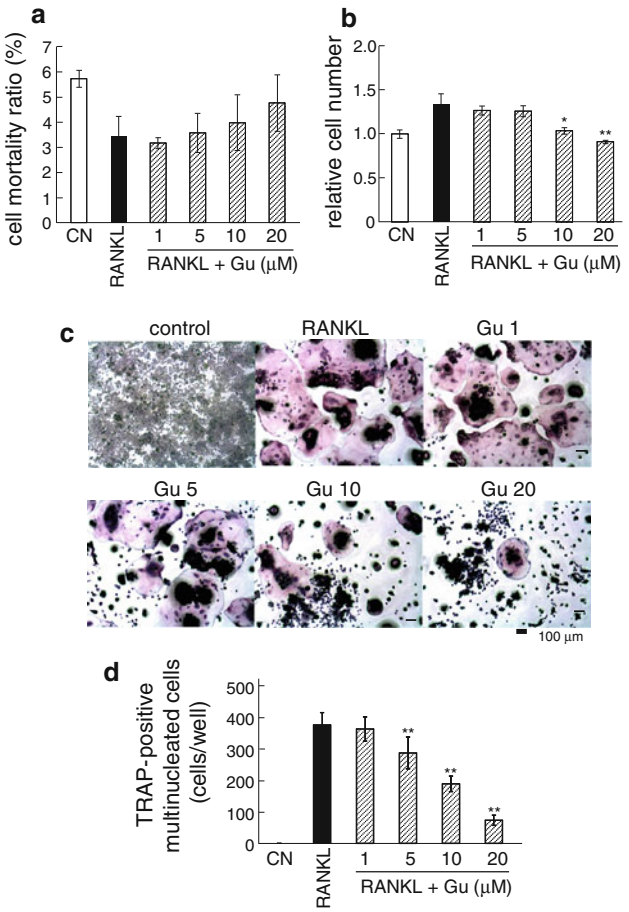

Fig. 7 Inhibitory effects of guanabenz on development of RAW264.7 pre-osteoclasts. *CN* control, *Gu* guanabenz. The *single and double asterisks* indicate significant decreases with $p < 0.05$ and $p < 0.01$ in comparison to the RANKL-treated cells, respectively. **a** Cell mortality ratio. **b** Relative cell numbers. **c** Dose-dependent suppression of RANKL driven activation of osteoclasts by guanabenz. **d** Dose-dependent suppression of TRAP-positive multi-nucleated cells by guanabenz

stimulation of osteoblastogenesis as well as attenuation of osteoclastogenesis by both agents strongly indicates that eIF2α-mediated signaling is central to regulation of ATF4 and NFATc1. This result is also supported by the salubrinal-driven alterations in the mRNA levels of osteocalcin and TRAP, which are representative in development of osteoblasts and osteoclasts, respectively. Osteocalcin is synthesized solely by osteoblasts for matrix mineralization and calcium homeostasis [25], while TRAP is highly expressed in osteoclasts and its overexpression has been observed to cause bone loss in transgenic mice [26].

The elevation of p-eIF2α is reported to enhance the development of osteoblasts and mineralization of extracellular matrix. In response to various stresses such as oxidation, radiation, and stress to the endoplasmic reticulum, cells undergo either survival or an apoptotic pathway [27]. As part of a pro-survival program, the level of p-eIF2α is raised followed by diminished translational efficiency to all proteins except for a limited group including ATF4 [5]. Salubrinal's action mimics the induction of a pro-survival program without imposing damaging stresses, which result in the upregulation of ATF4 without inducing apoptosis. Since ATF4 is a transcription factor critical for osteoblastogenesis and bone formation, we examined the effects of the administration of

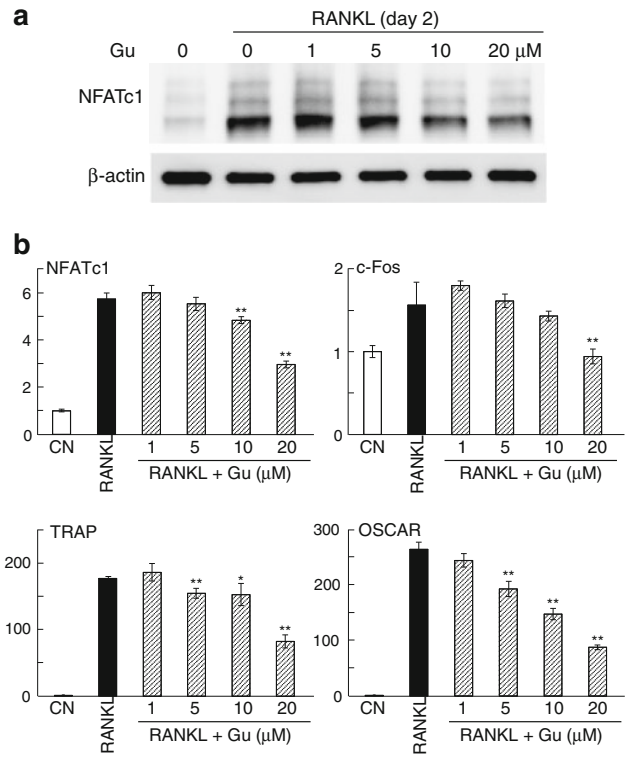

Fig. 8 Reduction of RANKL-induced NFATc1 expression by guanabenz. *CN* control, *Gu* guanabenz. The *single and double asterisks* indicate significant decreases with $p < 0.05$ and $p < 0.01$ in comparison to the RANKL-treated cells, respectively. **a** Expression of NFATc1 (2 days after RANKL administration). **b** Messenger RNA levels of NFATc1, c-Fos, TRAP, and OSCAR (2 days after RANKL administration)

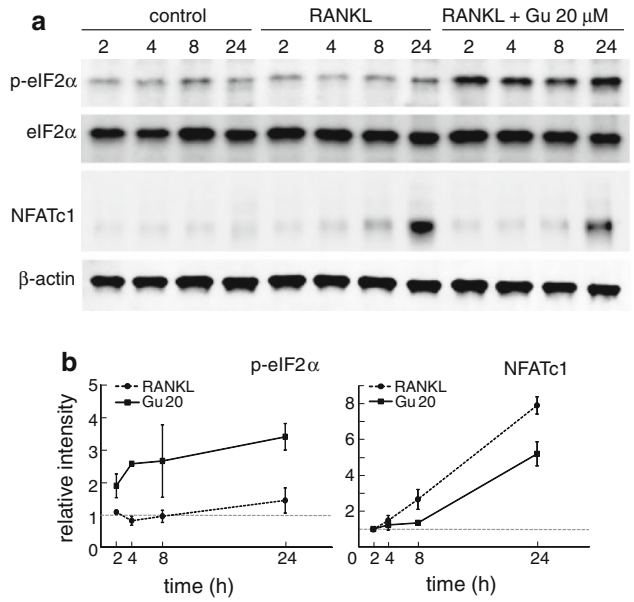

Fig. 9 Temporal expression profile of p-eIF2α and NFATc1 in the presence and absence of 20 μM guanabenz. *Gu* guanabenz. **a** Western blot analysis of eIF2α-p and NFATc1. **b** Comparison of the expression level of eIF2α-p and NFATc1 with and without 20 μM guanabenz. The normalized level of "1" was defined as the level for the cells that were not treated with RANKL without administration of guanabenz

salubrinal and guanabenz on the mRNA level of osteocalcin as well as the mineralization of the extracellular matrix. Silencing ATF4 using RNA interference significantly suppressed salubrinal-driven upregulation of osteocalcin expression. Thus, the result here is consistent with the previously reported role of salubrinal that stimulates new bone formation in the healing of bone wound [8].

A schematic diagram illustrating the proposed pathway of eIF2α-mediated signaling in osteoblastogenesis and osteoclastogenesis is presented (Fig. 11). Through inhibition of de-phosphorylation of eIF2α, salubrinal and guanabenz are capable of enhancing bone formation by activating ATF4, as well as reducing bone resorption by down-regulating NFATc1. Osteoclastogenesis is a complex developmental process, in which active interactions take place between osteoblasts and osteoclasts. In the RANK/RANKL/OPG signaling pathway, for instance, osteoblasts provide RANKL that stimulates osteoclastogenesis. Since binding of RANKL to RANK is known to activate MAPKs and NFκB [28, 29], we evaluated a potential role of ERK, p38, and NFκB in the eIF2α-mediated signaling. In response to administration of 20 μM salubrinal, we examined the levels of p-ERK, p-p38 MAPK, and p-NFκB together with p-eIF2α. However, no detectable changes in the levels of their phosphorylated form were observed. It is possible that salubrinal may activate transcription factors such as MafB (V-maf musculoaponeurotic fibrosarcoma oncogene homolog B), IRF8 (interferon regulatory factor 8), and Bcl6 (B cell lymphoma 6), which are known to be inhibitors of NFATc1 [30–32]. Alternatively, microRNA and epigenetic changes such as histone modification regulate expression of NFATc1 might be involved [33, 34]. For instance, H3K27 demethylase is reported to demethylate the site of H3K27me3 of NFATc1 and stimulate RANKL-induced osteoclastogenesis [34]. The results herein require further analysis on a regulatory mechanism that links elevation of p-eIF2α to the suppression of NFATc1.

A recent study independently reported that salubrinal alters the fate of osteoclasts and bone resorption through eIF2α-mediated translational regulation [35]. Herein, we further examined the regulatory mechanism using not only salubrinal but also guanabenz, which are the inhibitors of PP1. The results revealed that these agents can also regulate expression of NFATc1 at a transcriptional level. A separate in vivo study as well as in vitro studies using

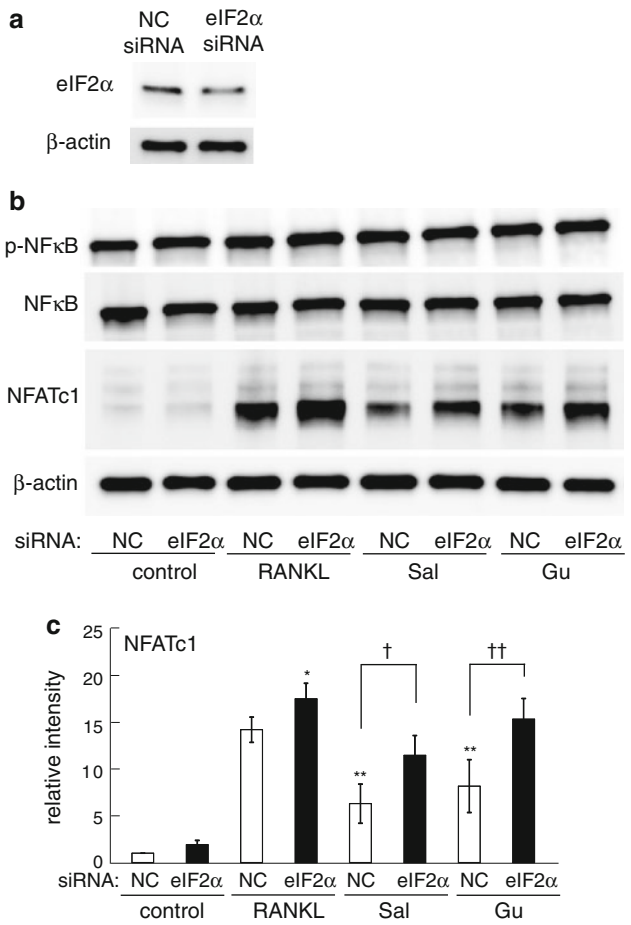

Fig. 10 Reduction in salubrinal/guanabenz driven suppression of NFATc1 expression by RNA interference specific for eIF2α. *Sal* salubrinal, *Gu* guanabenz, and *NC* non-specific control siRNA. The *single and double asterisks* indicate significant changes to the RANKL-treated NC siRNA cells with $p < 0.05$ and $p < 0.01$, respectively. The *single and double daggers* indicate significant changes to the salubrinal or guanabenz-treated NC siRNA cells with $p < 0.05$ and $p < 0.01$, respectively. **a** eIF2α level after transfecting siRNA specific to eIF2α. **b** Western blot analysis of p-NFκB and NFATc1. **c** Comparison of the expression level of NFATc1 between control siRNA and eIF2α siRNA

primary bone marrow derived cells support salubrinal's efficacy on inhibition of bone resorption. In summary, we demonstrate that elevation of p-eIF2α stimulates osteocalcin expression through upregulation of ATF4 in osteoblasts and inhibits TRAP expression via downregulation of NFATc1 in pre-osteoclasts. Silencing eIF2α with RNA interference reduced suppression of salubrinal/guanabenz-driven downregulation of NFATc1. The results in this study support the possibility of regulating bone remodeling through eIF2α-mediated signaling for combatting bone loss in osteoporosis.

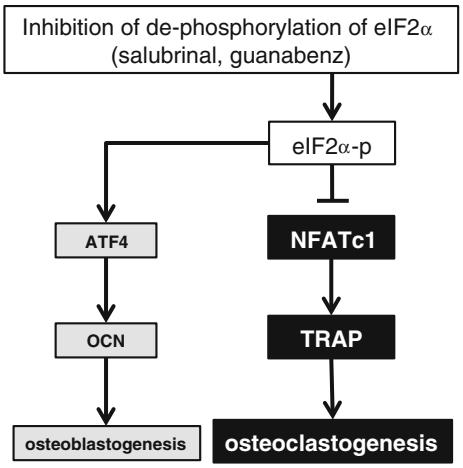

Fig. 11 Proposed mechanism of eIF2α signaling on osteoclastogenesis through NFATc1

Acknowledgments The authors appreciate M. Hamamura's technical assistance. This study was supported by the Grant DOD W81XWH-11-1-0716 to HY. All authors state that they have no conflicts of interest.

Conflict of interest All authors state that they have no conflicts of interest.

References

1. Karsenty G, Wagner EF (2002) Reaching a genetic and molecular understanding of skeletal development. Cell 2:389–406
2. Harada S, Rodan GA (2003) Control of osteoblast function and regulation of bone mass. Nature 423:349–355
3. Manolagas SC (2000) Birth and death of bone cells: basic regulatory mechanisms and implications for the pathogenesis and treatment of osteoporosis. Endocr Rev 21:115–137
4. Kimball SC (1999) Eukaryotic initiation factor eIF2. Int J Biochem 31:25–39
5. Harding HP, Novoa I, Zhang Y, Zeng H, Wek R, Schapira M, Ron D (2000) Regulated translation initiation controls stress-induced gene expression in mammalian cells. Mol Cell 6:1099–1108
6. Yang X, Matsuda K, Bialek P, Jacquot S, Masuoka HC, Schinke T, Li L, Brancorsini S, Sassone-Corsi P, Townes TM, Hanauer A, Karsenty G (2004) ATF4 is a substrate of RSK2 and an essential regulator of osteoblast biology; implication for Coffin–Lowry Syndrome. Cell 117:387–398
7. Hamamura K, Yokota H (2007) Stress to endoplasmic reticulum of mouse osteoblasts induces apoptosis and transcriptional activation for bone remodeling. FEBS Lett 581:1769–1774
8. Zhang P, Hamamura K, Jiang C, Zhao L, Yokota H (2012) Salubrinal promotes healing of surgical wounds in rat femurs. J Bone Miner Metab 30:568–579

9. Yasuda H, Shima N, Nakagawa N, Yamaguchi K, Kinosaki M, et al. (1988) Osteoclast differentiation factor is a ligand for osteoprotegerin/osteoclastogenesis-inhibitory factor and is identical to TRANCE/RANKL. Proc Natl Acad Sci USA 95:3597–3602
10. Lacey DL, Timms E, Tan HL, Kelley MJ, Dunstan CR et al (1998) Osteoprotegerin ligand is a cytokine that regulates osteoclast differentiation and activation. Cell 93:165–176
11. Robling AG, Niziolek PJ, Baldridge LA, Condon KW, Allen MR, Alam I, Mantila SM, Gluhak-Heinrich J, Bellido TM, Harris SE, Turner CH (2008) Mechanical stimulation of bone in vivo reduces osteocyte expression of Sost/sclerostin. J Biol Chem 283:5866–5875
12. Zhang P, Jiang C, Ledet E, Yokota H (2011) Loading- and unloading-driven regulation of phosphorylation of eIF2α. Biol Sci Space 25:3–6
13. Boyce M, Bryant KF, Jousse C, Long K, Harding HP, Scheuner D, Kaufman RJ, Ma D, Coen DM, Ron D, Yuan J (2005) A selective inhibitor of eIF2α dephosphorylation protects cells from ER stress. Science 307:935–939
14. Tsaytler P, Harding HP, Ron D, Bertolotti A (2011) Selective inhibition of a regulatory subunit of protein phosphatase 1 restores proteostasis. Science 332:91–94
15. Hughes DE, Wright KR, Uy HL, Sasaki A, Yoneda T, Roodman GD, Mundy GR, Boyce BF (1995) Bisphosphonates promote apoptosis in murine osteoclasts in vitro and in vivo. J Bone Miner Res 10:1478–1487
16. Furuya Y, Mori K, Ninomiya T, Tomimori Y, Tanaka S, Takahashi N, Udagawa N, Uchida K, Yasuda H (2011) Increased bone mass in mice after single injection of anti-receptor activator of nuclear factor-κB ligand-neutralizing antibody. J Biol Chem 286:37023–37031
17. Sudo H, Kodama HA, Amagai Y, Yamamoto S, Kasai S (1983) In vitro differentiation and calcification in a new clonal osteogenic cell line derived from newborn mouse calvaria. J Cell Biol 96:191–198
18. Xu J, Tan JW, Gao XH, Laird R, Liu D, Wysocki S, Zheng MH (2000) Cloning, sequencing, and functional characterization of the rat homologue of receptor activator of NF-kappaB ligand. J Bone Miner Res 15:2178–2186
19. Wagner EF, Matsuo K (2003) Signaling in osteoclasts and the role of Fos/AP1 proteins. Ann Rheum Dis 62:ii83–ii85
20. Helfrich MH, Thesingh CW, Mieremet RH, van Iperen-van Gent AS (1987) Osteoclast generation from human fetal bone marrow in cocultures with murine fetal long bones. A model for in vitro study of human osteoclast formation and function. Cell Tissue Res 249:125–136
21. Kim N, Takami M, Rho J, Josien R, Choi Y (2002) A novel member of the leukocyte receptor complex regulates osteoclast differentiation. J Exp Med 195:201–209
22. Takayanagi H, Kim S, Koga T, Nishina H, Isshiki M, Yoshida H, Saiura A, Isobe M, Yokochi T, Inoue J, Wagner EF, Mak TW, Kodama T, Taniguchi T (2002) Induction and activation of the transcription factor NFATc1 (NFAT2) integrate RANKL signaling in terminal differentiation of osteoclasts. Dev Cell 3:889–901
23. Hamamura K, Zhang P, Yokota H (2008) IGF2-driven PI3 kinase and TGFβ signaling pathways in chondrogenesis. Cell Biol Int 32:1238–1246
24. Shah RS, Walker BR, Vanov SK, Helfant RH (1976) Guanabenz effects on blood pressure and noninvasive parameters of cardiac performance in patients with hypertension. Clin Pharmacol Ther 19:732–737
25. Galli M, Caniggia M (1984) Osteocalcin. Minerva Med 75:2489–2501
26. Angel NZ, Walsh N, Forwood MR, Ostrowski MC, Cassady AI, Hume DA (2000) Transgenic mice overexpressing tartrate-resistant acid phosphatase exhibit an increase rate of bone turnover. J Bone Miner Res 15:103–110
27. Wang S, Kaufman RJ (2012) The impact of the unfolded protein response on human disease. J Cell Biol 197:857–867
28. Matsumoto M, Sudo T, Saito T, Osada H, Tsujimoto M (2000) Involvement of p38 mitogen-activated protein kinase signaling pathway in osteoclastogenesis mediated by receptor activator of NF-kappaB ligand (RANKL). J Biol Chem 275:31155–31161
29. Zhang YH, Heulsmann A, Tondravi MM, Mukherjee A, Abu-Amer Y (2001) Tumor necrosis factor-alpha (TNF) stimulates RANKL-induced osteoclastogenesis via coupling of TNF type 1 receptor and RANK signaling pathways. J Biol Chem 276:563–568
30. Kim K, Kim JH, Lee J, Jin HM, Kook H, Kim KK, Lee SY, Kim N (2007) MafB negatively regulates RANKL-mediated osteoclast differentiation. Blood 109:3253–3259
31. Zhao B, Takami M, Yamada A, Wang X, Koga T, Hu X, Tamura T, Ozato K, Choi Y, Ivashkiv LB, Takayanagi H, Kamijo R (2009) Interferon regulatory factor-8 regulates bone metabolism by suppressing osteoclastogenesis. Nat Med 15:1066–1071
32. Miyauchi Y, Ninomiya K, Miyamoto H, Sakamoto A, Iwasaki R et al (2010) The Blimp1-Bcl6 axis is critical to regulate osteoclast differentiation and bone homeostasis. J Exp Med 207:751–762
33. Rossi M, Pitari MR, Amodio N, Di Martino MT, Conforti F, Leone E, Botta C, Paolino FM, Del Giudice T, Iuliano E, Caraglia M, Ferrarini M, Giordano A, Tagliaferri P, Tassone P (2012) miR-29b negatively regulates human osteoclastic cell differentiation and function: implications for the treatment of multiple myeloma-related bone disease. J Cell Physiol (in press)
34. Yasui T, Hirose J, Tsutsumi S, Nakamura K, Aburatani H, Tanaka S (2011) Epigenetic regulation of osteoclast differentiation: possible involvement of Jmjd3 in the histone demethylation of Nfatc1. J Bone Miner Res 26:2655–2671
35. He L, Lee J, Jang JH, Sakchaisri K, Hwang JS, Cha-Molstad HJ, Kim KA, Ryoo IJ, Lee HG, Kim SO, Soung NK, Lee KS, Kwon YT, Erikson RL, Ahn JS, Kim BY (2013) Osteoporosis regulation by salubrinal through eIF2α mediated differentiation of osteoclast and osteoblast. Cell Signal 25:552–560

Pharmacology

Potential therapeutic applications of salubrinal for skeletal diseases and beyond

Kazunori Hamamura[1,*], Andy Chen[2], Yoshihiro Uto[3], and Hiroki Yokota[4]

[1]Department of Pharmacology, School of Dentistry, Aichi-Gakuin University, Nagoya 464-8650, Japan. [2]Weldon School of Biomedical Engineering, Purdue University, West Lafayette, IN 47907 USA. [3]Department of Biological Science and Technology, Tokushima University, Tokushima 770-8501, Japan. [4]Department of Biomedical Engineering, Indiana University Purdue University Indianapolis, Indianapolis, IN 46202 USA

Salubrinal is a small synthetic compound that suppresses de-phosphorylation of eukaryotic translation initiation factor 2 alpha (eIF2α) and attenuates stress to the endoplasmic reticulum. It has been reported that salubrinal enhances osteoblastogenesis and suppresses osteoclastogenesis. We have recently reported that salubrinal also presents chondroprotective effects through downregulation of NFκB signaling, and it reduces arthritic inflammation by inhibiting dual-specificity phosphatase 2 (Dusp2). In this review, we summarize salubrinal's beneficial effects on skeletal diseases and suggest its novel therapeutic possibilities. *Journal of Nature and Science, 1(8):e151, 2015*

eIF2α | salubrinal | endoplasmic reticulum | bone

Chemical structure of salubrinal

Salubrinal ($C_{21}H_{17}Cl_3N_4OS$; 479.8 Da) is a synthetic compound with an IUPAC name of (2E)-3-phenyl-N-[2,2,2-trichloro-1-[[(8-quinolinylamino)thioxomethyl]amino]ethyl]-2-propenamide. As outlined in Fig. 1, it is synthesized with *trans*-cinnamamide **1** as a starting material. The first reaction with anhydrous chloral generates chloral cinnamamide **2**. The second reaction transforms into the amine **3** via substitutive chlorination with phosphorus pentachloride followed by treatment with ammonia. Lastly, amine **3** is reacted with 8-isothiocyanatoquinoline to produce salubrinal [1]. Salubrinal's hydrophobic parameter, log[*P*], is 4.56 (pH 7.40) by Pallas 3.0, and its uptake in organs and cells is predicted relatively high.

Salubrinal's action as anti-apoptosis and neuroprotection

Salubrinal inhibits protein phosphatase 1 (PP1) and suppress de-phosphorylation of eukaryotic translation initiation factor 2 alpha (eIF2α). It is known as a suppressor of stress to the endoplasmic reticulum (ER) [2], which can be induced by a multitude of causes, including protein misfolding, UV, and viral infection [3, 4]. ER stress elevates the level of phosphorylated eIF2α (eIF2α-p) [5], and severe ER stress induces apoptosis and tends to worsen systemic disease states [6-8]. Based on its structure-activity relationship, it is suggested that all functional groups except for quinolone moiety are essential to induce protective activity against apoptosis by ER stress [1]. Interestingly, salubrinal in general acts as an anti-apoptotic agent [9-12], although at a high dose it may lead to apoptosis. For instance, salubrinal is reported to prevent glucocorticoid induced-apoptosis in osteoblasts and osteocytes [9]. Salubrinal also protects neurons against apoptotic death by downregulating eIF2α-ATF4-CHOP signaling [10]. Besides protection from apoptosis, salubrinal is reported to generate beneficial effects in animal models for neuronal disorders [13-16]. First, it alleviates neurological dysfunction after cardiopulmonary resuscitation in rats [13]. Second, it provides neuroprotective effects in a mouse model of traumatic brain injury [14]. Third, it inhibits the expression of proteoglycans and increases neurite outgrowth [15]. Lastly, it modulates sleep homeostasis and activates sleep- and wake-regulatory neurons [16].

Salubrinal's stimulation of osteoblastogenesis and inhibition of osteoclastogenesis

In the skeletal system, osteoblasts and osteoclasts play dueling roles in bone remodeling. Osteoblasts are bone-forming cells derived from mesenchymal stem cells, while osteoclasts are bone-resorbing cells derived from myelomonosytic lineage [17]. Differentiation of osteoblasts and osteoclasts are, in part, regulated by transcription factors [18, 19] including activating transcription factor 4 (ATF4). ATF4 is not only one of the key transcription factors for osteoblast maturation but also an essential regulator in stress to the ER [8, 20]. In osteoblasts, ER stress elevates the level of eIF2α-p and stimulates the expression of ATF4 [8]. Salubrinal, on the other hand, increases eIF2α-p by blocking PP1 and enhances matrix deposition through upregulation of ATF4 and osteocalcin [21].

Osteoclast development also involves eIF2α [21-23]. Osteoclastogenesis is induced by administration of receptor activator of nuclear factor kappa-B (RANKL), and RANKL-driven osteoclastogenesis is suppressed by salubrinal. Salubrinal's inhibitory action is consistent with its downregulation of nuclear factor of activated T cells c1 (NFATc1), which is a master gene for osteoclast differentiation [21-23]. Principal component analysis of genome-wide microarray data predicted transcription factors that followed the phenotypic response of salubrinal-driven suppression of osteoclastogenesis. Several of these predicted transcription factors were experimentally validated to conclude that salubrinal downregulates AP-1 proteins such as c-Fos and JunB [24] and suppresses RANKL-driven NFATc1 expression.

Salubrinal-driven prevention of cartilage degradation in osteoarthritis

Osteoarthritis (OA) is the most common joint disease, resulting from multiple factors, including traumatic injury and obesity [25]. Matrix metalloproteinase 13 (MMP13) is one of the most influential collagenases in the destruction of cartilage tissue [26], in which salubrinal is able to attenuate its expression and activity. *In vitro* assays demonstrate that in TNFα and IL1β-treated chondrocytes activation of nuclear factor kappa B (NFκB) signaling is suppressed by salubrinal [27]. In a mouse model of surgically-induced OA, it has been reported that administration of salubrinal alleviates cartilage degradation by downregulating phosphorylated NFκB [28]. Other studies also report that salubrinal acts as an inhibitor of NFκB signaling and attenuates β-amyloid-induced neuronal death and microglial activity [29].

Salubrinal's beneficial effects on inflammatory arthritis

In macrophages, the basal level of phosphorylated eIF2α was higher in old mice than young mice [30]. Our recent study demonstrated that salubrinal suppresses lipopolysaccharide (LPS)-stimulated inflammatory responses in macrophages [31]. Salubrinal is reported to reduce orofacial inflammatory pain [32], and it alleviates colitis through suppression of proinflammatory cytokines [33].

Conflict of interest: No conflicts declared.

* Corresponding Author. Kazunori Hamamura, PhD/DDS. Department of Pharmacology, School of Dentistry, Aichi-Gakuin University
1-100 Kusumoto-cho, Chikusa-ku, Nagoya 464-8650, Japan.
Phone: +81-52-757-6743; Fax: +81-52-752-5988.
Email: hamak@dpc.agu.ac.jp

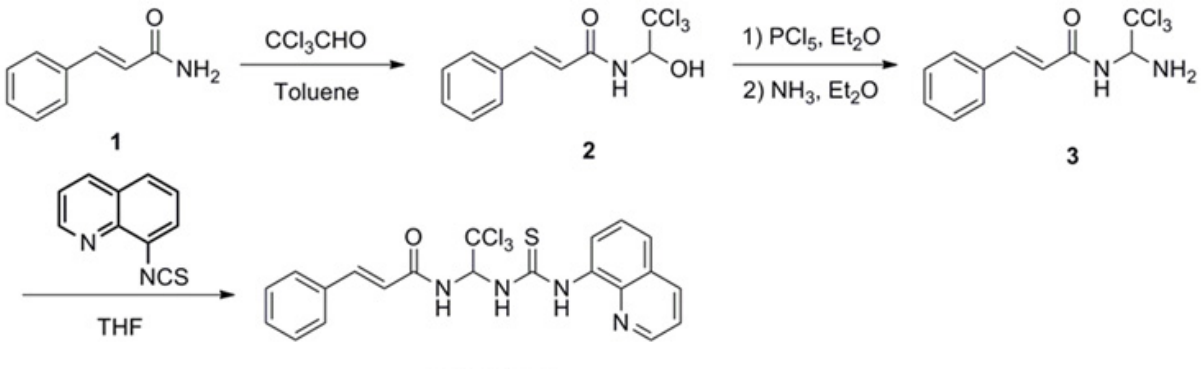

Figure 1. Synthetic route of salubrinal.

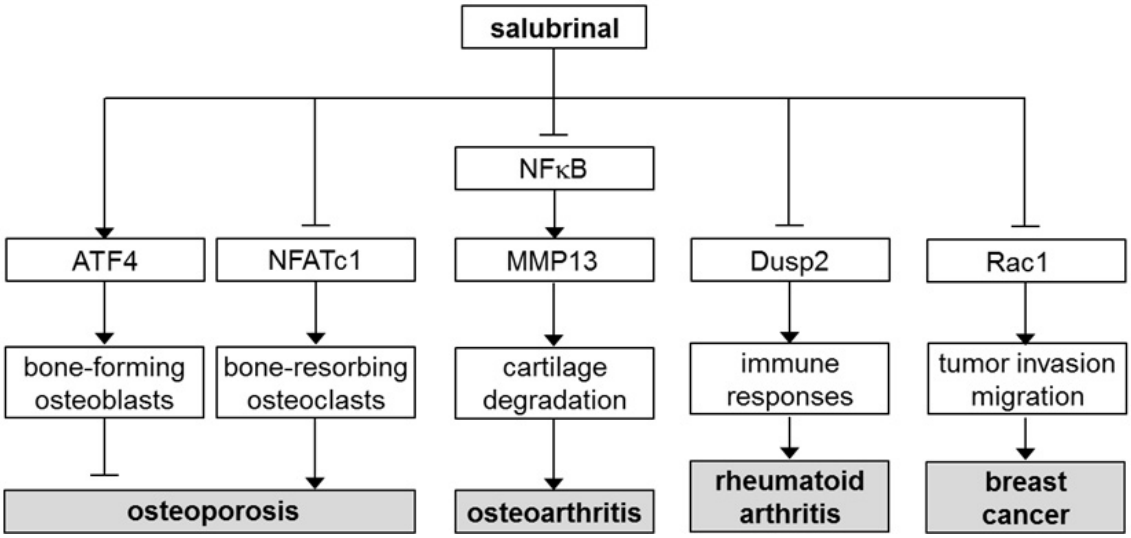

Figure 2. Schematic mechanism of salubrinal's action on skeletal diseases and breast cancer.

We also have reported that salubrinal attenuates inflammatory cytokines such as IL1β, Cox2, IL2, TNF, and IL13 in macrophages, T lymphocytes, and mast cells [31]. Using gene expression microarray data, potential targets of salubrinal were identified by their correlation with the observed phenotype in two cell lines. Of the predicted genes, a potential target, dual-specificity phosphatase 2 (Dusp2), which plays a critical role in the progression of inflammatory arthritis, such as in rheumatoid arthritis, was identified and validated. Dusp2 is highly expressed in activated immune cells, and inflammatory responses are reduced in the K/BxN model of rheumatoid arthritis by deleting Dusp2 [34]. In our study, salubrinal acts as a Dusp2 inhibitor and suppresses inflammatory responses in a mouse model of anti-collagen antibody-induced arthritis [31].

Salubrinal's action through eIF2α and NFκB

Besides salubrinal, guanabenz is another agent that is known as an inhibitor of the de-phosphorylation of eIF2α [35]. These two agents inhibit PP1 by interacting with different subunits of PP1: PP1 alpha for salubrinal and GADD34 for guanabenz. Both agents enhance osteoblastogenesis and suppress osteoclastogenesis through regulating the level of eIF2α–p. However, one of the clear differences between these agents is that salubrinal presents chondroprotective effects through downregulating NFκB signaling, but guanabenz does not [28]. In addition, guanabenz and not salubrinal is known as an agonist of α_2 adrenergic receptor. Further studies are necessary to identify salubrinal's potential binding partner(s) that modulate NFκB signaling.

Other therapeutic possibilities with salubrinal

It is possible that salubrinal may present efficacy to other skeletal diseases we have not yet tested. It has recently been reported using a mouse *in vivo* model that salubrinal is able to attenuate tumor growth and migration by downregulating the activity of Rac1 GTPase [36]. Since salubrinal suppresses osteoclast differentiation, salubrinal may not only suppress proliferation of breast cancer cells but also protect bone from metastasis. Other therapeutic possibilities may include the prevention of bone loss for patients with diabetes and spinal cord injury-induced osteoporosis.

Conclusions & Future Perspectives

Salubrinal has been shown to present various beneficial effects in mouse models of osteoporosis, osteoarthritis, inflammatory arthritis, and breast cancer (Fig. 2). Two major functions in bone remodeling are enhancement of bone formation through upregulation of ATF4 and suppression of bone resorption through downregulation of NFATc1 and AP-1 proteins. Salubrinal also has chondroprotective effects by reducing NFκB signaling and MMP13 activity. Furthermore, it induces anti-inflammatory responses by suppressing Dusp2 and attenuates tumor growth and migration by blocking Rac1 GTPase. Collectively, salubrinal may provide a novel therapeutic possibility for multiple skeletal diseases including breast cancer and bone metastasis. We envision that administration routes, bioavailability, appropriate doses, and patient-related factors such as sex, age, and genetic makeup should be evaluated for each of the potential applications through pharmacokinetics and pre-clinical studies.

Acknowledgment

This work was supported by grants, DOD W81XWH-11-1-0716 and Indiana State Department of Health A70-5-0791036.

1. Long K, Boyce M, Lin H, Yuan J, Ma D: Structure-activity relationship studies of salubrinal lead to its active biotinylated derivative. *Bioorganic & Medicinal Chem Lett* 2005, 15:3849-3852.
2. Boyce M, Bryant KF, Jousse C, Long K, Harding HP, Scheuner D, *et al.*: A selective inhibitor of eIF2alpha dephosphorylation protects cells from ER stress. *Science* 2005, 307: 935-939.
3. Ron D: Translational control in the endoplasmic reticulum stress response. *J Clin Invest* 2002, 110:1383-1388.
4. Marciniak SJ, Ron D: Endoplasmic reticulum stress signaling in disease. *Physiol Rev* 2006, 86:1133-1149.
5. Wek RC, Jiang HY, Anthony TG: Coping with stress: eIF2 kinases and translational control. Biochem Soc Trans 2006, 34: 7-11.
6. Tabas I, Ron D: Integrating the mechanisms of apoptosis induced by endoplasmic reticulum stress. *Nat Cell Biol* 2011, 13: 184-190.
7. Sano R, Reed JC: ER stress-induced cell death mechanisms. *Biochim Biophys Acta* 2013, 1833: 3460-3470.
8. Hamamura K, Yokota H: Stress to endoplasmic reticulum of mouse osteoblasts induces apoptosis and transcriptional activation for bone remodeling. *FEBS Lett* 2007, 581: 1769-1774.
9. Sato AY, Tu X, McAndrews KA, Plotkin LI, Bellido T: Prevention of glucocorticoid induced-apoptosis of osteoblasts and osteocytes by protecting against endoplasmic reticulum (ER) stress in vitro and in vivo in female mice. *Bone* 2015, 73: 60-68.
10. Kim JS, Heo RW, Kim H, Yi CO, Shin HJ, Han JW, et al.: Salubrinal, ER stress inhibitor, attenuates kainic acid-induced hippocampal cell death. *J Neural Transm* 2014, 121: 1233-1243.
11. Wu L, Luo N, Zhao HR, Gao Q, Lu J, Pan Y, *et al.*: Salubrinal protects against rotenone-induced SH-SY5Y cell death via ATF4-parkin pathway. *Brain Res* 2104, 1549: 52-62.
12. Lopez-Hernandez B, Cena V, Posadas I: The endoplasmic reticulum stress and the HIF-1 signalling pathways are involved in the neuronal damage caused by chemical hypoxia. *Br J Pharmacol* 2015, 172: 2838-2851.
13. Zhang J, Xie X, Pan H, Wu Z, Lu W, Yang G: Role of endoplasmic reticulum stress in brain damage after cardiopulmonary resuscitation in rats. *Shock* 2015, in press.
14. Rubovitch V, Barak S, Rachmany L, Goldstein RB, Ziberstein Y, Pick CG, *et al.*: The neuroprotective effect of salubrinal in a mouse model of traumatic brain injury. *Neuromolecular Med* 2015, 17: 58-70.
15. Barrenda-Manso MA, Yanguas-Casas N, Nieto-Sampedro M, Romero-Ramirez L: Salubrinal inhibits the expression of proteoglycans and favors neurite outgrowth from cortical neurons in vitro. *Exp Cell Res* 2015, 335: 82-90.
16. Methippara M, Mitrani B, Schrader FX, Szymusiak R, McGinty D: Salubrinal, an endoplasmic reticulum stress blocker, modulates sleep homeostasis and activation of sleep- and wake-regulatory neurons. *Neuroscience* 2102, 209: 108-118.
17. Karsenty G, Wagner EF: Reaching a genetic and molecular understanding of skeletal development. *Dev Cell* 2002, 2: 389-406.
18. Karsenty G: Transcriptional control of skeletogenesis. *Annu Rev Genomics Hum Genet* 2008, 9: 183-196.
19. Takayanagi H: The role of NFAT in osteoclast formation. *Ann NY Acad Sci* 2007, 1116: 227-237.
20. Yang X, Matsuda K, Bialek P, Jacquot S, Masuoka HC, Schinke T, *et al.*: ATF4 is substrate of RSK2 and an essential regulator of osteoblast biology; implication for Coffin-Lowry Syndrome. *Cell* 2004; 117: 387-398.
21. Hamamura K, Tanjung N, Yokota H: Suppression of osteoclastogenesis through phosphorylation of eukaryotic translation initiation factor 2 alpha. *J Bone Miner Metab* 2013, 31: 618-628.
22. He L, Lee J, Jang JH, Sakchaisri K, Hwang J, Cha-Molstad HJ, *et al.*: Osteoporosis regulation by salubrinal through eIF2a mediated differentiation of osteoclast and osteoblast. *Cell Signal* 2013, 25: 552-560.
23. Yokota H, Hamamura K, Chen A, Dodge TR, Tanjung N, Abedinpoor A, *et al.*: Effects of salubrinal on development of osteoclasts and osteoblasts from bone marrow derived cells. *BMC Musculoskelet Disord* 2013, 14: 197.
24. Hamamura K, Chen A, Tanjung N, Takigawa S, Sudo A, Yokota H: *In vitro* and *in silico* analysis of an inhibitory mechanism of osteoclastogenesis by salubrinal and guanabenz. *Cell Signal* 2015, 27: 353-362.
25. Glyn-Jones S, Palmer AJR, Agricola R, Price AJ, Vincent TL, Weinans H, et al.: Osteoarthritis. *Lancet* 2015, in press.
26. Mitchell PG, Magna HA, Reeves LM, Lopresti-Morrow LL, Yocum SA, Rosner PJ, *et al.*: Cloning, expression, and type II collagenolytic activity of matrix metalloproteinase-13 from human osteoarthritic cartilage. *J Clin Invest* 1996, 97: 761-768.
27. Hamamura K, Lin CC, Yokota H: Salubrinal reduces expression and activity of MMP13 in chondrocytes. Osteoarthritis Cartilage 2013, 21: 764-772.
28. Hamamura K, Nishimura A, Iino T, Takigawa S, Sudo A, Yokota H: Chondroprotective effects of salubrinal in a mouse model of osteoarthritis. *Bone Joint Res* 2105, 4: 84-92.
29. Huang X, Chen Y, Zhang H, Ma Q, Zhang YW, Xu H. Salubrinal attenuates b-amyloid-induced neuronal death and microglial activation by inhibition of the NF-kB pathway. *Neurobiol Aging* 2012, 33: 1007.e9-17.
30. Shirato K, Imaizumi K: Posttranscriptional suppression of lipopolysaccharide-stimulated inflammatory responses by macrophages in middle-aged mice: A possible role for eukaryotic initiation factor 2α. *Int J Inflam* 2014, 292986.
31. Hamamura K, Nishimura A, Chen A, Takigawa S, Sudo A, Yokota H: Salubrinal acts as Dusp2 inhibitor and suppresses inflammation in anti-collagen antibody-induced arthritis. *Cell Signal* 2015, 27: 828-835.
32. Yang ES, Bae JY, Kim TH, Kim YS, Suk K, Bae YC: Involvement of endoplasmic reticulum stress response in orofacial inflammatory pain. *Exp Neurobiol* 2014, 23: 372-380.
33. Okazaki T, Nishio A, Takeo M, Sakaguchi Y, Fukui T, Uchida K, et al.: Inhibition of the dephosphorylation of eukaryotic initiation factor 2a ameliorates murine experimental colitis. *Digestion* 2014, 90: 167-178.
34. Jeffrey KL, Brummer T, Rolph MS, Liu SM, Callejas NA, Grumont RJ, et al.: Positive regulation of immune cell function and inflammatory responses by phosphatase PAC-1. Nat Immunol 2006, 7: 274-283.
35. Tsaytler P, Harding HP, Ron D, Bertolotti A: Selective inhibition of a regulatory subunit of protein phosphatase 1 restores proteostasis. *Science* 2011, 332: 91-94.
36. Hamamura K, Minami K, Tanjung N, Wan Q, Koizumi M, Matsuura N, *et al.*: Attenuation of malignant phenotypes of breast cancer cells through eIF2a-mediated downregulation of Rac1 signaling. *Int J Oncol* 2014, 44: 1980-1988.

Principal Component Analysis of the Regulation of Osteoclastogenesis by Salubrinal and Guanabenz

Andy B. Chen[1], Kazunori Hamamura[2], Nancy Tanjung[2], and Hiroki Yokota[2]

[1]Weldon School of Biomedical Engineering, Purdue University, West Lafayette, IN 47907, USA
[2]Department of Biomedical Engineering, Indiana University Purdue University Indianapolis, Indianapolis, IN 46202, USA

Introduction: Osteoporosis is a common debilitating disease that causes bone loss. Salubrinal and guanabenz, new potential therapeutic agents for treating osteoporosis, have attracted attention since they not only activate bone-forming osteoblasts but also suppress bone-resorbing osteoclasts [1]. They are known to elevate ATF4, one of the known transcription factors for bone formation. However, the mechanism of their action on bone resorption is not fully understood. Focusing on regulation of NFATc1, a master transcription factor of osteoclast development, we analyzed the genome-wide expression data and predicted potential mediators of salubrinal and guanabenz on bone resorption.

Materials and Methods: Principal component analysis (PCA) was conducted [2] using two sets of genome-wide mRNA expression profiles with RAW264.7 mouse pre-osteoclast cells (Figure 1). In the first set (4 groups), cells were treated with placebo, RANKL (stimulator of osteoclastogenesis), salubrinal with RANKL, or guanabenz with RANKL. In the second set (4 groups), cells were treated with control siRNA or NFATc1 siRNA in the presence and absence of RANKL. First, we applied PCA and selected genes that were apparently not regulated by NFATc1, through a comparison between the control and NFATc1 siRNA samples in the presence of RANKL. The genes in the 10th percentile of NFATc1 siRNA-dependent expression, whose components in the first principal axis (PC1) were smaller than others, were chosen. For those genes, we applied PCA for identifying genes responsive to salubrinal and guanabenz. Responsiveness was evaluated based on the components in the first principal axis, which clustered the samples by the degree of osteoclastogenesis. In determining responsiveness, we considered statistical significance (root mean squared combined p-values) among the samples with and without salubrinal or guanabenz treatment.

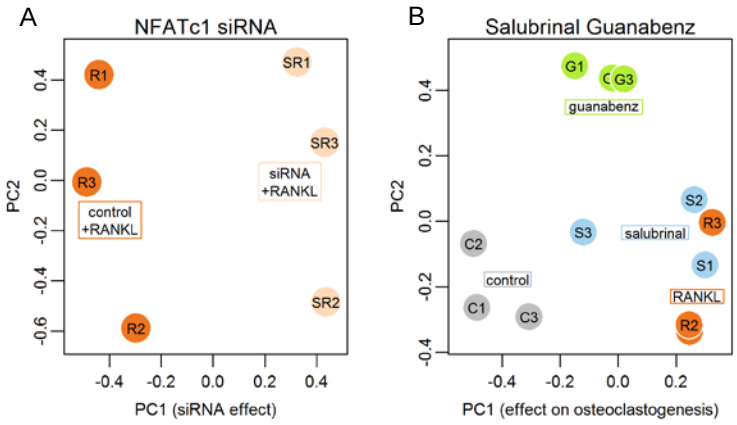

Figure 1. PCA on two data sets. (A) PC1 (first principal axis for siRNA) and PC2 (second principal axis) sort the samples based on the effects of NFATc1 siRNA. (B) PC1 for Sal/Gu clusters 4 sets of samples along the predicted axis of osteoclastogenesis.

Results and Discussion: PCA predicted that Serinc2, Rdx, and Antxr2 are potential activators of RANKL-mediated osteoclastogenesis, whereas Arl11, Zfyve21, and Pcdhb10 are potential inhibitors of RANKL-mediated osteoclastogenesis. These genes were identified to be regulated by salubrinal and guanabenz, but unaffected by the silencing of NFATc1.

Conclusions: In this study, we used PCA to predict potential regulators of salubrinal's and guanabenz's action on RANKL-mediated osteoclastogenesis. The predicted genes are upstream of NFATc1 or unrelated to NFATc1. Further validation of these candidates will be required in order to confirm their activity in regulating osteoclasts. The elucidation of these mechanisms will refine our understanding of osteoclastogenesis and may help direct future targets for drug treatment.

References:

[1] Hamamura, K, et al. J Bone Miner Metab, 2013, vol. 31, pp. 618-628.
[2] Raychaudhuri, S, et al. Pac Symp Biocomput, 2000, vol. 5, pp. 455-466.

TITLE: Salubrinal Regulates Bone Remodeling and Fat Metabolism in Ovariectomized Mice

AUTHORS (LAST NAME, FIRST NAME): Zhang, P[1], Chen, A[1], Dodge, T[1], Tanjung, N[1], Zheng, Y[1], Fuqua, C[1],Yokota, H[1, 2]

INSTITUTIONS (ALL):
1. Department of Biomedical Engineering, Indiana University Purdue University Indianapolis, Indianapolis, IN 46202
2. Department of Anatomy and Cell Biology, Indiana University School of Medicine, Indianapolis, IN 46202

CURRENT PRIMARY CATEGORY: osteoporosis, osteoclasts, osteoblasts

KEYWORDS: salubrinal, bone remodeling, differentiation, osteoclasts, osteoblasts, adipocytes, BMD, BMC

ABSTRACT BODY:

Introduction:
Bone remodeling is conducted by a coordinated action of osteoclasts (bone resorption) and osteoblasts (bone formation), and osteoporosis reflects imbalanced activities of osteoclasts and osteoblasts. It is recently reported that salubrinal, a synthetic chemical agent can accelerate healing of bone wounds [1]. In this study, we address a question: does salubrinal alter differentiation of bone marrow derived cells – progenitor cells to osteoclasts, osteoblasts, and adipocytes? Using ovariectomized (OVX) mice as a model for postmenopausal osteoporosis, we examined a hypothesis that salubrinal not only elevates bone mass but also reduces fat mass and restore OVX-induced obesity through modulation of the fate of bone marrow derived cells.

Methods:
Thirty-six C57BL/6 female mice (~ 12 wks) were used. Twenty-four mice were subjected to OVX (OVX control group, and OVX salubrinal group at 1 mg/kg), and twelve mice were used as the age-match control group. Changes in BMD/BMC in the lumbar spine and abdominal fat were measured by pDEXA. Bone marrow mononuclear cells were harvested, and we examined osteoclast (OCL) lineage (formation, migration, and adhesion) as well as colony formation of osteoclast progenitors with a colony forming unit-macrophage assay (CFU-M). Differentiation of osteoblasts was examined with a colony-forming unit-osteoblast assay (CFU-OBL).

Results:
Attenuation of OVX symptoms: Administration of salubrinal suppressed an increase in body weight and a decrease in uterine weight (Fig. 1A & 1B).
Suppression of osteoclast differentiation: Compared to the age-match control, OVX activated osteoclast formation (Fig. 2A). Administration of salubrinal induced a dosage-dependent inhibition of osteoclast formation at both early and later times (Fig. 2B). Furthermore, salubrinal significantly reduced the migration and adhesion of osteoclasts (Fig. 2C&D; Fig. 3A).
Promotion of osteoblast differentiation: Besides its effects on osteoclasts, salubrinal significantly promoted differentiation of osteoblasts (Fig. 3B).
Reduction in fat and increase in BMC: Salubrinal decreased abdominal fat (%) (Fig. 3C), and increased BMC in the lumbar spine (Fig. 3D).

Discussion:
The current study using OVX mice demonstrates that salubrinal regulates bone remodeling through the promotion of osteoblast differentiation as well as the reduction of osteoclast formation, migration and adhesion. Furthermore, it suppresses OVX-induced increase in body weight and fat storage. A separate study using *in vitro* systems indicate that besides altering the phosphorylation level of eukaryotic translation initiation factor 2a, salubrinal affects the phosphorylation of p38 MAPK and NFκB. Further studies are needed to clarify the molecular mechanism underlying the observed effects.

Significance:
Salubrinal is effective in elevating BMD/BMC and reducing fats in OVX mice, which presented osteoporosis and obesity. It could be considered as a potential therapeutic chemical agent for the regulation of bone remodeling and fat metabolism of patients with postmenopausal osteoporosis.

Acknowledgement:
This study was supported by grant DOD W81XWH-11-1-0716 to HY.

Reference:
[1] Zhang P, et al. (2012) J Bone Miner Metab.

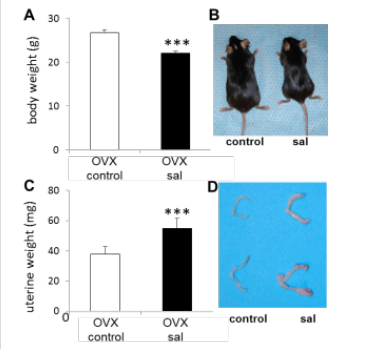

Fig. 1. Effects of salubrinal in body weight and uterine weight in OVX mice. (A-B) Reduction in body weight. (C-D) Increase in uterine weight.

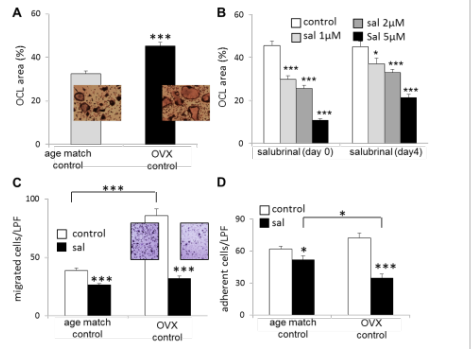

Fig. 2. Effects of salubrinal on osteoclasts (OCL). (A) Increased formation in OVX mice. (B) Dosage-dependent reduction by salubrinal. (C) Reduction in OCL migration. (D) Reduction in OCL adhesion.

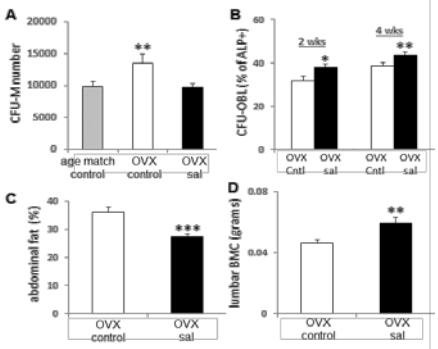

Fig. 3. Effects of salubrinal in OVX mice. (A) Reduction in CFU-M. (B) Increase in CFU-OBL. (C) Reduction in abdominal fat. (D) Increase in BMC in the lumbar spine.

Yokota et al. BMC Musculoskeletal Disorders 2013, 14:197
http://www.biomedcentral.com/1471-2474/14/197

BMC Musculoskeletal Disorders

RESEARCH ARTICLE Open Access

Effects of salubrinal on development of osteoclasts and osteoblasts from bone marrow-derived cells

Hiroki Yokota[1,2*], Kazunori Hamamura[1], Andy Chen[1], Todd R Dodge[1], Nancy Tanjung[1], Aysan Abedinpoor[1] and Ping Zhang[1,2,3*]

Abstract

Background: Osteoporosis is a skeletal disease leading to an increased risk of bone fracture. Using a mouse osteoporosis model induced by administration of a receptor activator of nuclear factor kappa-B ligand (RANKL), salubrinal was recently reported as a potential therapeutic agent. To evaluate the role of salubrinal in cellular fates as well as migratory and adhesive functions of osteoclast/osteoblast precursors, we examined the development of primary bone marrow-derived cells in the presence and absence of salubrinal. We addressed a question: are salubrinal's actions more potent to the cells isolated from the osteoporotic mice than those isolated from the control mice?

Methods: Using the RANKL-injected and control mice, bone marrow-derived cells were harvested. Osteoclastogenesis was induced by macrophage-colony stimulating factor and RANKL, while osteoblastogenesis was driven by dexamethasone, ascorbic acid, and β-glycerophosphate.

Results: The results revealed that salubrinal suppressed the numbers of colony forming-unit (CFU)-granulocyte/macrophages and CFU-macrophages, as well as formation of mature osteoclasts in a dosage-dependent manner. Salubrinal also suppressed migration and adhesion of pre-osteoclasts and increased the number of CFU-osteoblasts. Salubrinal was more effective in exerting its effects in the cells isolated from the RANKL-injected mice than the control. Consistent with cellular fates and functions, salubrinal reduced the expression of nuclear factor of activated T cells c1 (NFATc1) as well as tartrate-resistant acid phosphatase.

Conclusions: The results support the notion that salubrinal exhibits significant inhibition of osteoclastogenesis as well as stimulation of osteoblastogenesis in bone marrow-derived cells, and its efficacy is enhanced in the cells harvested from the osteoporotic bone samples.

Keywords: Osteoporosis, RANKL, Salubrinal, Osteoclasts, Osteoblasts

Background

Osteoporosis is a common skeletal disease of bone loss, which leads to an increased risk of bone fractures, morbidity, mortality, and an economic burden to society [1-3]. In many cases it is a physiological consequence of the aging process [3,4], and in postmenopausal women it is induced by a decrease in the production of estrogen, a hormone known to maintain the appropriate ratio of bone-forming osteoblasts to bone-resorbing osteoclasts [5]. During the past 20 years, many therapeutic drugs have been developed to prevent osteoporotic bone loss. Bisphosphonates are the most widely prescribed medications to treat postmenopausal osteoporosis, but they may be associated with an increased risk of osteonecrosis of the jawbone and atypical femur fracture [6]. Other treatments include administration of estrogen and estrogen analogs, as well as parathyroid hormone. However, increased risks of breast cancers and blood clots have been reported as side effects of these treatments [7-9]. The aim of this study is to evaluate a therapeutic role of a chemical agent, salubrinal, in potential treatment of osteoporosis.

Salubrinal is a small chemical agent (480 Da, $C_{21}H_{17}Cl_3N_4OS$) known to block de-phosphorylation of

* Correspondence: hyokota@iupui.edu; pizhang@iupui.edu
[1]Department of Biomedical Engineering, Indiana University-Purdue University Indianapolis, 723 West Michigan Street, SL220, Indianapolis, IN 46202, USA
[3]School of Basic Medical Sciences, Tianjin Medical University, Tanjin 300070, People's Republic of China
Full list of author information is available at the end of the article

eukaryotic translation initiation factor 2 alpha (eIF2α) [10]. Salubrinal is also reported to attenuate molecular signaling mediated by nuclear factor kappa B (NFκB) [11]. The elevated phosphorylation level of eIF2α upregulates activating transcription factor 4 (ATF4), one of the key transcription factors in bone formation [12]. Salubrinal is shown to enhance healing of bone wounds and promotes differentiation of osteoblasts [13]. Little is known, however, about its effects on bone resorption, in particular developmental regulation of bone marrow-derived cells. Bone marrow-derived cells contain mesenchymal stem cells (MSCs) and hematopoietic stem cells that give rise to osteoblasts and osteoclasts, respectively [14]. The primary focus of this study is the potential role of salubrinal in the development of bone marrow-derived cells towards mature osteoclasts, as well as its role in development of mesenchymal stem cells and osteoblasts.

Experimental animal models are useful to evaluate therapeutic efficacy of chemical agents. Available osteoporosis models include ovariectomy (OVX) [15,16], tail suspension [17,18], denervation [19,20], a low-calcium diet [21,22], and administration of receptor activator of nuclear factor kappa-B ligand (RANKL) [23-25]. Any animal model may have its advantage and disadvantage. For instance, OVX-induced osteoporosis, which is currently considered as the gold standard for the evaluation of pharmaceuticals for postmenopausal osteoporosis, not only reduces the level of estrogen but also generates surgery-induced injury together with an increase in osteoblast activity. Furthermore, surgical induction of OVX requires consistency in the surgical procedure as well as a minimum of 4 weeks. The tail suspension model not only increases bone resorption but also reduces osteoblast differentiation. In the denervation model, surgery-induced injury is involved. In this study, we evaluated *in vivo* effects of salubrinal using the OVX mice and *in vitro* effects of salubrinal using bone marrow-derived cells isolated from the RANKL-injected mice.

In the RANKL administration model, RANKL is subcutaneously injected for as a short period as 3 days [26]. RANKL is a cytokine belonging to the tumor necrosis factor family. In the immune system, it is involved in dendritic cell maturation, while in the skeletal system it is a ligand for osteoprotegerin (OPG) and functions as a key regulator for osteoclast differentiation and activation [27,28]. RANKL deletion in mice leads to osteopetrosis and a decrease of osteoclasts, while RANKL overproduction is linked to a variety of degenerative bone diseases including osteoporosis and rheumatoid arthritis [29,30].

Focusing on the development of bone marrow-derived cells in the presence and absence of salubrinal, we addressed a pair of questions: Does administration of salubrinal modulate cellular fates and functions of bone marrow-derived cells in favor of prevention of bone loss? If so, are salubrinal's actions more potent to the cells isolated from the osteoporotic RANKL-injected mice than those isolated from the control mice? Because of the anticipated role of salubrinal that is potentially opposite to that of RANKL, we hypothesized that salubrinal is more effective in inhibiting development of osteoclasts and stimulating development of osteoblasts in the cells isolated from the RANKL-injected mice than those from the control mice. To test the hypothesis, we employed assays such as colony-forming unit - granulocyte/macrophages (CFU-GM), colony-forming unit - macrophages (CFU-M), and formation of multi-nucleated osteoclasts in an osteoclast differentiation medium, as well as assays for migration and adhesion of pre-osteoclasts. We also conducted assays for examining colony-forming unit – osteoblasts (CFU-OBL) in an osteoblast differentiation medium. To evaluate salubrinal's effects on expression of nuclear factor of activated T cells c1 (NFATc1), a master transcription factor for osteoclastogenesis, we conducted real-time PCR and Western blot analysis.

Methods

Animals and materials preparation

C57BL/6 female mice (7 weeks of age) were used. Each cage housed four to five mice at the Indiana University Animal Care Facility. They were fed with mouse chow and water *ad libitum*. Experimental procedures were approved by the Indiana University Animal Care and Use Committee and were in compliance with the Guiding Principles in the Care and Use of Animals endorsed by the American Physiological Society. Cytokines were purchased from PeproTech (Rocky Hills, NC, USA) and other chemicals from Sigma (St. Louis, MO, USA) unless otherwise stated. Salubrinal (R&D Systems, Minneapolis, MN, USA) was administered at 1 mg/kg to mice, and at 0.5 to 5 μM to cultured cells for the duration of each experiment.

Ovariectomy

The animal was anesthetized with 1.5% isoflurane at a flow rate of 0.5 to 1.0 L/min. After removing the hair, the skin at the operative sites was cleaned using 70% alcohol and 10% providoneiodine solution. An incision (~20 mm) was made at the midline dorsal skin, and the peritoneal cavity was incised to access the ovaries. After removing the ovaries, the wound was closed by suturing. In 4 weeks after surgery, subcutaneous injection of salubrinal was conducted daily at a dose of 1 mg/kg body weight for 4 weeks. The control OVX mice received an equal volume of vehicle.

RANKL administration for the bone loss model

Soluble recombinant murine RANKL (sRANKL; PeproTech) was injected subcutaneously using a 1 mg/kg dosage in 100 μl PBS at 24 h intervals for 3 days [26]. The same

volume of PBS was injected into vehicle control mice. At 90 min after the final injection, the mice were euthanized. Iliac bones, femora, and tibiae were harvested, and bone marrow-derived cells were collected.

Determination of bone mineral density (BMD) and bone mineral content (BMC)

The BMD (g/cm^2) and BMC (g) of an entire humerus and ulna were determined using peripheral dual energy X-ray absorptiometry (DXA; PIXImus II, Lunar Corp., Madison, WI, USA) and its software (version 1.47).

Colony-forming unit-granulocyte-macrophages (CFU-GM) assay

As previously described, a colony-forming unit-granulocyte-macrophage (CFU-GM) assay was conducted [31-33]. Approximately 2.5x10^4 bone marrow-derived cells were prepared from the vehicle control and RANKL-treated mice and seeded onto a 35-mm gridded dish composed of methylcellulose supplemented with 30 ng/ml murine macrophage-colony stimulating factor (M-CSF), and 20 ng/ml RANKL. Three dosages of salubrinal (1, 2, and 5 μM) were administered, and cells were cultured at 37°C in a 5% CO_2 incubator for 7 days.

Colony-forming unit-macrophage/mononuclear (CFU-M) assay

Using bone marrow mononuclear cells (BMMNCs), a colony-forming unit-macrophage/mononuclear (CFU-M) assay was conducted, as described previously [34-37]. From the vehicle control and RANKL administration mice, approximately 2.5x10^4 bone marrow-derived cells were prepared. Cells were seeded onto a 35-mm gridded dish, which was composed of methylcellulose supplemented with 30 ng/ml M-CSF and 20 ng/ml RANKL. Three dosages of salubrinal (1, 2, and 5 μM) were administered, and cells were cultured at 37°C in a 5% CO_2 incubator for 7 days.

Isolation of bone marrow-derived cells for osteoclast development

Bone marrow-derived cells were collected by flushing the iliac, femur and tibia with Iscove's MEM (Gibco-Invitrogen, Carlsbad, CA, USA) containing 2% fetal bovine serum using a 23-gauge needle, as described previously [34,38]. Low-density gradient centrifugation was used to separate the cells, which were then cultured in α-MEM supplemented with 10% FBS, 30 ng/ml M-CSF, and 20 ng/ml murine receptor activator of nuclear factor kappa-B ligand (RANKL). Culture medium was replaced by α-MEM supplemented with 10% FBS, 30 ng/ml M-CSF, and 60 ng/ml RANKL on the third day, and cells were then grown for an additional 3 days.

Osteoclast differentiation assay

Using bone marrow-derived cells isolated from the vehicle control and RANKL-treated mice with administration of salubrinal (0, 1, 2, and 5 μM) in 96-well plates, an osteoclast differentiation assay was performed, as described previously [34,39,40]. For one experimental condition, salubrinal was applied on day 0 to day 6 (6 days), while in the other experimental condition, it was applied on day 4 to day 6 (3 days). Culture medium was exchanged once on day 4 during the 6-day experiments. A tartrate resistant acid phosphate (TRACP)-staining kit was used according to the manufacturer's instructions to fix and stain adherent cells. TRACP-positive multinuclear cells (> 3 nuclei) were identified as osteoclasts, and their numbers were counted [39]. The osteoclast formation assay was performed at least 3 times using cells isolated independently from different cohorts of mice.

Osteoclast migration assay

Using a transwell assay, migration of osteoclasts was evaluated as described previously with minor modifications [41]. After isolating them from vehicle control and RANKL-treated mice, bone marrow-derived cells (2×10^6/ml) were cultured in M-CSF and RANKL in 6-well plates for 4 days, and then trypsinized in Hank's balanced salt solution. With and without salubrinal (2 μM), the osteoclast precursor cells (1×10^5 cells/well) were loaded onto the upper chamber of transwells and allowed to migrate to the bottom chamber through an 8-μm polycarbonate filter coated with vitronectin (Takara Bio Inc., Otsu, Shigma, Japan). α-MEM consisting of 1% bovine serum albumin (BSA) and 30 ng/ml of M-CSF was in the bottom chamber. After reacting for 6 h, the osteoclast precursor cells in the lower chamber was stained with crystal violet and counted.

Osteoclast adhesion assay

Ninety-six well plates were coated with 5 μg/ml vitronectin in α-MEM supplemented with 30 ng/ml M-CSF and were applied with osteoclast precursors (1×10^5 cells/well) in the presence and absence of salubrinal (2 μM), as described previously [41]. Cells were incubated for 30 min, then washed with PBS three times and fixed with 4% paraformaldehyde at room temperature for 10–15 min. After crystal violet staining, the number of cells adherent to $\alpha_v\beta_3$ integrin was counted.

Osteoblast differentiation assay

Bone marrow-derived cells were plated at 2×10^6/ml in 6-well plates in osteogenic differentiation medium (MesenCult proliferation kit) supplemented with 10 nM dexamethasone, 50 μg/ml ascorbic acid 2-phosphate, and 10 mM β-glycerophosphate to induce osteogenic differentiation, as described previously [39,41,42]. Cells were

cultured for 2 weeks in the presence and absence of salubrinal (0.5 μM), and medium was changed every other day. For alkaline phosphatase (ALP) staining, cells were fixed in citrate-buffered acetone for 30 s, incubated in the alkaline-dye mix for 30 min, and counterstained with Mayer's Hematoxylin for 10 min. Cells were then evaluated microscopically and the intensity of ALP staining was determined.

To evaluate the effects of RANKL administration on multiple developmental stages starting from bone marrow-derived cells to mature osteoclasts, the RANKL-driven alterations in CFU-GM, CFU-M, osteoclast formation, migration, and adhesion were determined as fold-changes of the RANKL-injected mice to the vehicle control mice. Furthermore, to quantify efficacy of salubrinal in various developmental stages in osteoclastogenesis, the degree of suppression was measured with reduction ratios between the samples treated with and without 2 μM salubrinal.

Expression analysis of NFATc1 in bone marrow-derived cells and RAW264.7 pre-osteoclast cells

For Western blot analysis, RAW264.7 mouse monocyte/macrophage cells (ATCC, Manassas, VA, USA) were grown in α–MEM containing 10% fetal bovine serum and antibiotics (50 units/ml penicillin, and 50 μg/ml streptomycin; Life Technologies, Grand Island, NY, USA). To induce osteoclastogenesis, 20 ng/ml of RANKL was administered. Bone marrow-derived cells or RAW264.7 cells were lysed in a radioimmunoprecipitation assay (RIPA) lysis buffer, containing protease inhibitors (Santa Cruz Biotechd, Santa Cruz, CA, USA) and phosphatase inhibitos (Calbiochem, Billerica, MA, USA). Isolated proteins were fractionated using 10% SDS gels and electro-transferred to Immobilon-P membranes (Millipore, Billerica, MA, USA). Antibodies specific to NFATc1 (Santa Cruz), and β-actin (Sigma) were employed. Protein levels were assayed using a SuperSignal west femto maximum sensitivity substrate (Thermo Scientific). The bands were scanned with Adobe Photoshop CS2 (Adobe Systems, San Jose, CA, USA) and their intensities were quantified using Image J.

In quantitative PCR, total RNA was extracted using an RNeasy Plus mini kit (Qiagen, Germantown, MD, USA) and reverse transcription was conducted with high capacity cDNA reverse transcription kits (Applied Biosystems, Carlsbad, CA, USA). Real-time PCR was performed using Power SYBR green PCR master mix kits (Applied Biosystems). The PCR primers were: NFATc1 (5′-GGT GCT GTC TGG CCA TAA CT-3′; and 5′-GCG GAA AGG TGG TAT CTC AA-3′), tartrate-resistant acid phosphatase (TRACP) (5′- TCC TGG CTC AAA AAG CAG TT -3′; and 5′- ACA TAG CCC ACA CCG TTC TC -3′); and GAPDH (5′-TGC ACC ACC AAC TGC TTA G-3′; and 5′-GGA TGC AGG GAT GAT GTT C-3′), in which GAPDH was used for internal control. Since TRACP is highly expressed in osteoclasts, we used its mRNA expression level as a marker for development of osteoclasts. The relative mRNA abundance for the selected genes with respect to the level of GAPDH mRNA was expressed as a ratio of $S_{\text{treated}}/S_{\text{control}}$, where S_{treated} is the mRNA level for the cells treated with salubrinal, and S_{treated} is the mRNA level for control cells.

Statistical analysis

The data were expressed as mean ± standard error of mean (SEM). Student's *t*-test was conducted for two-group comparisons. For many-group comparisons, one-way ANOVA was used, followed by a post-hoc test using Fisher's protected least significant difference. All comparisons were two-tailed, and statistical significance was assumed at $p < 0.05$. The asterisks (*, **, and ***) represent $p < 0.05$, $p < 0.01$, and $p < 0.001$, respectively.

Results

Evaluation of BMD and BMC of the OVX mice and RANKL-injected mice

Four-week daily administration of salubrinal at a dose of 1 mg/kg to the OVX mice significantly elevated both BMD and BMC of a whole body (Figure 1A-B). Three-day administration of RANKL at a dose of 1 mg/kg, however, significantly decreased BMD and BMC of the humerus and ulna (N = 6; both $p < 0.05$) (Figure 1C-D). Using the RANKL-injected mice, bones from the Iliac, femora, and tibiae were harvested. Bone marrow-derived cells were collected from those bones for examining the effects of salubrinal on developments of osteoclasts and osteoblasts.

Reduction in the number of CFU-GM by salubrinal in a dosage-dependent manner

To determine the effects of salubrinal on the proliferation of osteoclast progenitors, the CFU-GM assay was conducted using bone marrow-derived cells isolated from the RANKL-injected mice. Salubrinal at 1, 2, and 5 μM reduced the total number of CFU-GM in the femur in a dosage-dependent manner ($p < 0.05$ for 1 μM salubrinal; $p < 0.01$ for 2 μM; and $p < 0.001$ for 2 & 5 μM) in the RANKL-injected mice (Figure 2A). The CFU-GM numbers were 37,177 ± 1,919 (vehicle control) and 53,213 ± 3,545 (RANKL administration, $p < 0.001$) (Figure 2B). The CFU-GM numbers were reduced by administration of salubrinal at 2 μM for 7 days by 28.5% ($p < 0.001$) in vehicle control and 30.8% ($p < 0.001$) in the RANKL-injected mice.

Reduction in the number of CFU-M by salubrinal in a dosage –dependent manner

To determine the effects of salubrinal on the population of osteoclast progenitors, the CFU-M assay was performed using bone marrow-derived cells isolated from the

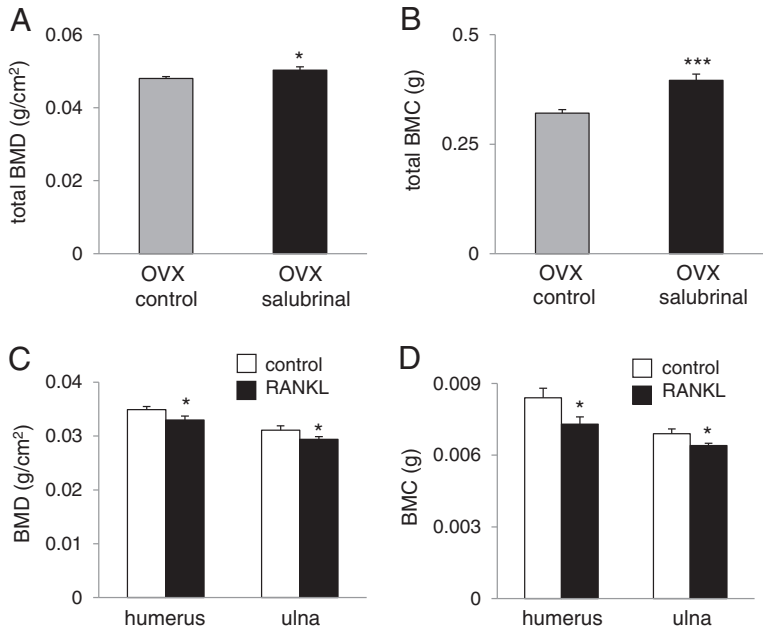

Figure 1 Determination of BMD and BMC in the OVX mice and RANKL-injected mice. A: Increase in BMD (g/cm^2) of the OVX mice by salubrinal (N = 8). **B**: Increase in BMC (g) of the OVX mice by salubrinal (N = 8). **C**: Decrease in BMD (g/cm^2) of the humerus and ulna of the RANKL-injected mice (N = 6). **D**: Decrease in BMC (g) of the humerus and ulna (N = 6).

RANKL-injected mice. Consistent with the CFU-M numbers, administration of salubrinal at 1, 2, and 5 μM reduced the total number of CFU-M in the femur in a dosage-dependent manner (all $p < 0.001$ in three dosages) (Figure 3A). The CFU-M numbers were 10,602 ± 396 (vehicle control) and 18,648 ± 760 (RANKL administration, $p < 0.001$) (Figure 3B). Administration of salubrinal at 2 μM for 7 days, for instance, reduced the CFU-M number by 41.2% ($p < 0.001$) in vehicle control and 43.1% ($p < 0.001$) in the RANKL-injected mice.

Suppression of osteoclast differentiation by salubrinal in a dosage– and time-dependent manner

Compared to the bone marrow-derived cells isolated from the vehicle control, the cells from the RANKL-injected mice exhibited an increase in the surface area occupied by multi-nucleated osteoclasts (24.8 ± 1.0% in vehicle control, and 36.5 ± 1.3% in RANKL administration) (Figure 4A). A series of images show that the process of osteoclast fusion was accelerated by administration of salubrinal. To evaluate the effects of salubrinal, three dosages of salubrinal (1, 2, and 5μM) were applied. In the cultures salubrinal was applied on day 0 for 6 days, administration of salubrinal resulted in a significant decrease in the surface area covered by multi-nucleated osteoclasts for vehicle control (all $p < 0.001$) and RANKL administration (all $p < 0.001$) (Figure 4A). In the cultures salubrinal was applied on day 3 for 4 days, the reduction of the area was also observed (all $p < 0.001$) (Figure 4B). A series of images indicate that the cellular fusion was reduced by salubrinal administration in a time-and dose-dependent manner.

To further evaluate potential effects of the period of salubrinal administration on osteoclast formation, we compared the results of two sets of experiments in which salubrinal at 2 μM was administered from days 0 to 6, and days 4 to 6. The result revealed that salubrinal administration at day 0 presented larger reduction in osteoclast formation than that at day 4 in the vehicle control and RANKL-injected groups (both $p < 0.001$) (Figure 4C).

Suppression of migration and adhesion of pre-osteoclasts by salubrinal

Pre-osteoclast cells isolated from the RANKL-injected mice were more migratory (304.1 ± 12.2 cells) than those from the vehicle control (190.4 ± 5.9 cells, $p < 0.001$), and the RANKL-driven increase was 37.4% (Figure 5A). However, salubrinal suppressed the amount of migration by 33.0% in vehicle control ($p < 0.001$) and by 53.2% in RANKL administration ($p < 0.001$). In the M-CSF mediated adhesion assay to $\alpha_V\beta_3$, the cells isolated from the RANKL-injected mice presented an increase in adhesion by 59.8% (142.5 ± 3.9 cells) over those from the vehicle control (57.3 ± 1.8 cells, $p < 0.001$) (Figure 5B). Administration of salubrinal presented significant reduction in cell adhesion by 32.4% in vehicle control ($p < 0.001$) and by 53.7% in RANKL administration ($p < 0.001$).

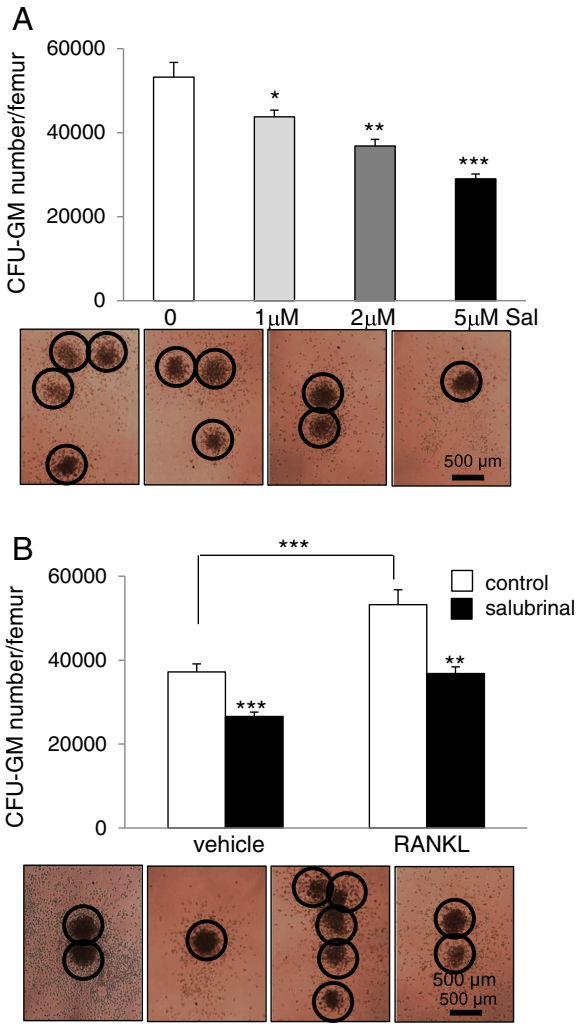

Figure 2 Effects of salubrinal on colony-forming unit-granulocyte-macrophage (CFU-GM). Approximately $2.5x10^4$ bone marrow-derived cells were prepared and seeded onto a 35-mm gridded dish supplemented with 30 ng/ml murine M-CSF and 20 ng/ml RANKL. Three dosages of salubrinal (1, 2, and 5 μM) were administered, and cells were cultured for 7 days. **A**: Salubrinal-induced reduction in CFU-GM numbers in the RANKL-injected mice using three dosage of salubrinal. The images exhibit the 4 different CFU-GM cultures, in which the circles indicate the colonies. **B**: Comparison of CFU-GM numbers in the vehicle control and RANKL-injected mice with and without *in vitro* administration of salubrinal. The representative microphotographs are shown, displaying 4 CFU-GM cultures with colonies in circle. Bar = 500 μm.

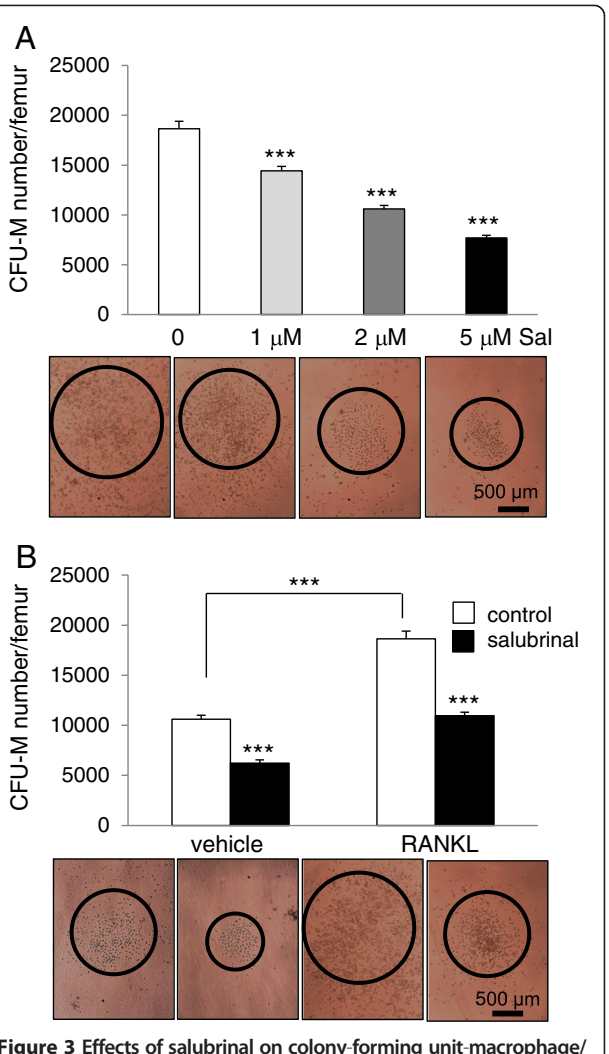

Figure 3 Effects of salubrinal on colony-forming unit-macrophage/monocyte (CFU-M). Approximately $2.5x10^4$ bone marrow mononuclear cells were prepared and seeded onto a 35-mm gridded dish supplemented with 30 ng/ml M-CSF and 20 ng/ml RANKL. Three dosages of salubrinal (1, 2, and 5 μM) were administered and cells were cultured for 7 days. **A**: Salubrinal-induced reduction in CFU-M numbers in the RANKL-injected mice using three dosage of salubrinal. The images exhibit the 4 different CFU-M cultures, in which the circles indicate the colonies. **B**: Comparison of CFU-M numbers in the vehicle control and RANKL-injected mice with and without *in vitro* administration of salubrinal. The representative microphotographs are shown, displaying 4 CFU-M cultures with colonies in circle. Bar = 500 μm.

Promotion of osteoblast differentiation by salubrinal

In the CFU-OBL assay, a significant increase in the number of ALP positive cells was detected by administration of salubrinal. Without salubrinal, the percentage of ALP-positive cells was 18.3 ± 2.3% in vehicle control and 20.4 ± 2.0% in RANKL administration ($p < 0.001$) (Figure 6). Administration of salubrinal at 0.5 μM increased the percentage of ALP-positive cells to 23.5 ± 1.1% in vehicle control ($p < 0.05$) and 28.8 ± 2.3% in RANKL administration ($p < 0.01$) (Figure 6).

Downregulation of NFATc1 by salubrinal in bone marrow-derived cells and RAW264.7 pre-osteoclast cells

Bone marrow-derived cells were incubated with RANKL in the presence and absence of salubrinal. Incubation with 20 ng/ml RANKL markedly increased the level of NFATc1, a master transcription factor for development of osteoclasts, and administration of 1 μM salubrinal

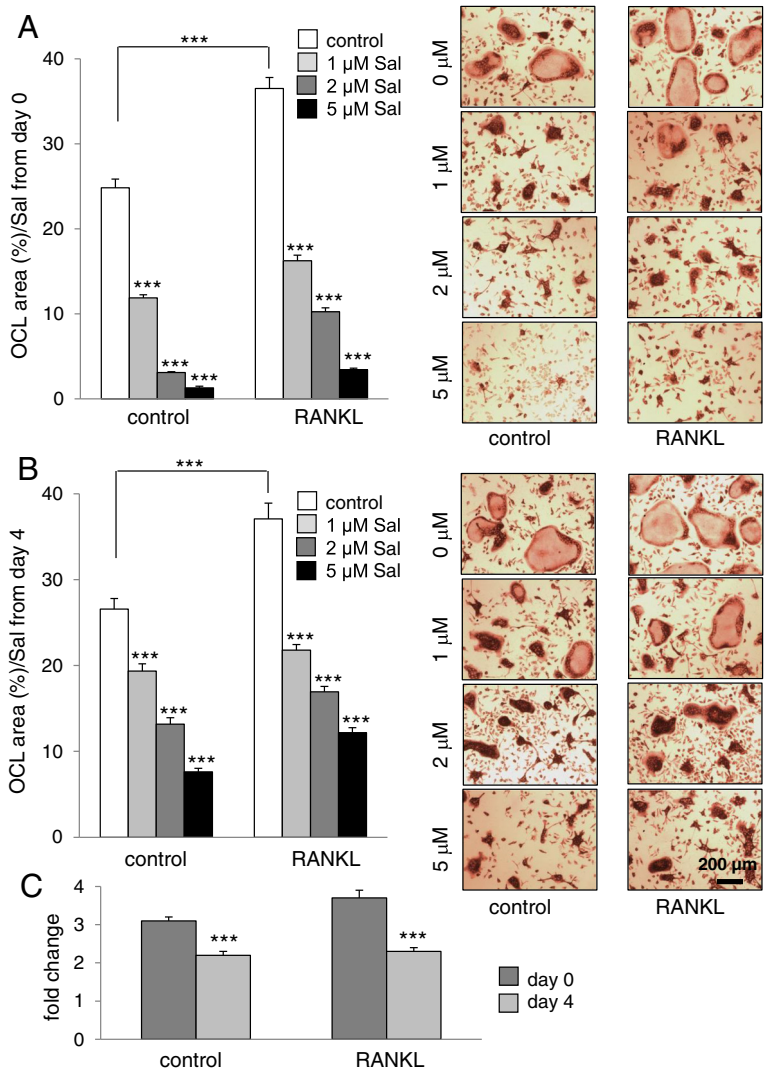

Figure 4 Effects of administration of salubrinal on multi-nucleated osteoclast formation. Using bone marrow-derived cells isolated from the vehicle control and RANKL-treated mice, an osteoclast differentiation assay was performed. The culture medium was exchanged once on day 4 during the 6-day experiments. TRACP-positive multinuclear cells (> 3 nuclei) were identified as osteoclasts. The areas covered by multi-nucleated osteoclasts are quantified in response to 3 doses of salubrinal (1, 2, and 5 μM). The microphotographs represent the two groups of osteoclast cultures (vehicle control and RANKL administration) with TRACP staining. Bar = 200 μm. **A**: Area covered by multi-nucleated osteoclasts in response to *in vitro* administration of salubrinal from day 0 to day 6 (6 days). **B**: Area covered by multi-nucleated osteoclasts in response to *in vitro* administration of salubrinal from day 4 to day 6 (3 days). **C**: Fold change in response to 2 μM salubrinal.

reduced the RANKL-driven increase in NFATc1 by 24% (Figure 7A). To further evaluate the effects of salubrinal, we employed RAW264.7 pre-osteoclast cells. Administration of 20 ng/ml RANKL elevated the level of NFATc1, and in response to 1–20 μM salubrinal the RANKL-induced elevation of NFATc1 was reduced in a dose dependent fashion (Figure 7B). Furthermore, the mRNA levels of NFATc1 and TRACP were increased by RANKL, and their elevation was suppressed by administration of salubrinal (Figure 7C).

Discussion

The present study presents the beneficial effect of *in vivo* administration of salubrinal on BMD and BMC of the OVX mice, and *in vitro* effects on the culture of bone marrow-derived cells isolated from the RANKL-injected and control mice. In the osteoclast assays of CFU-GM, CFU-M, and formation of multi-nucleation, salubrinal significantly reduced the numbers of osteoclastic colonies and cells isolated from both the vehicle control and RANKL-injected mice. In the two sets of maturation

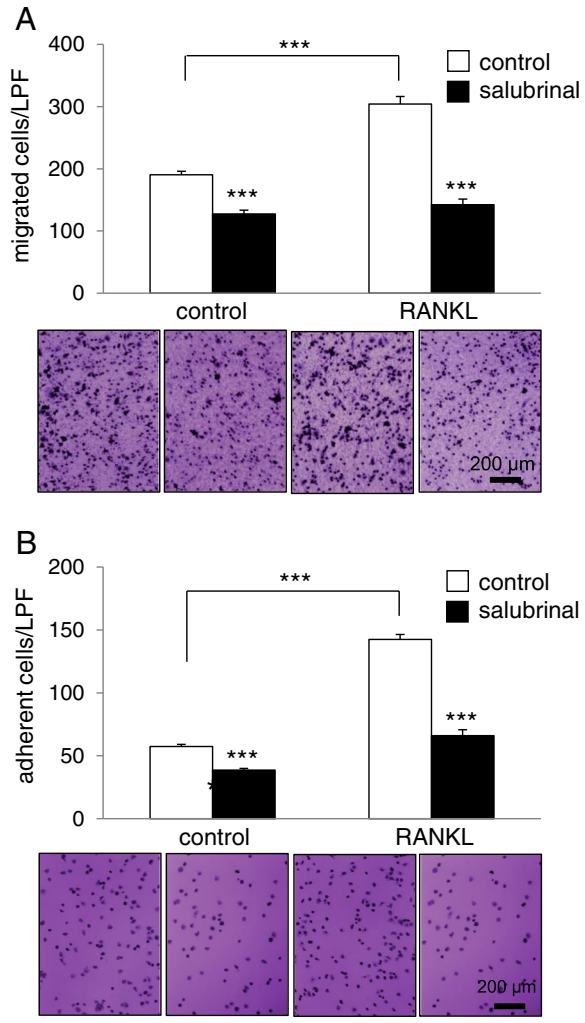

Figure 5 Effects of salubrinal on migration and adhesion of pre-osteoclasts. Bone marrow-derived cells (2×10^6/ml) were cultured in M-CSF and RANKL in 6-well plates for 4 days to obtain pre-osteoclasts used for the migration and adhesion assays. **A**: Number of migratory cells. Osteoclast precursor cells (1×10^5 cells/well) were loaded onto the upper chamber of transwells in the presence and absence of 2 μM salubrinal. The bottom chamber was filled with α-MEM consisting of 1% BSA and 30 ng/ml of M-CSF, and cells were allowed to migrate to the bottom chamber through an 8-μm polycarbonate filter coated with vitronectin. After reacting for 6 h, the cells in the lower chamber was stained with crystal violet and counted. The images display 2 pairs of osteoclast cultures. Bar = 200 μm. **B**: Number of adherent cells. Ninety-six well plates were coated with 5 μg/ml vitronectin and filled with α-MEM supplemented with 30 ng/ml M-CSF. Approximately 1×10^5 osteoclast precursor cells were cultured per well in the presence and absence of 2 μM salubrinal for 30 min. Cells were stained with crystal violet and the number of cells adherent to $\alpha_v\beta_3$ integrin was counted. Bar = 200 μm.

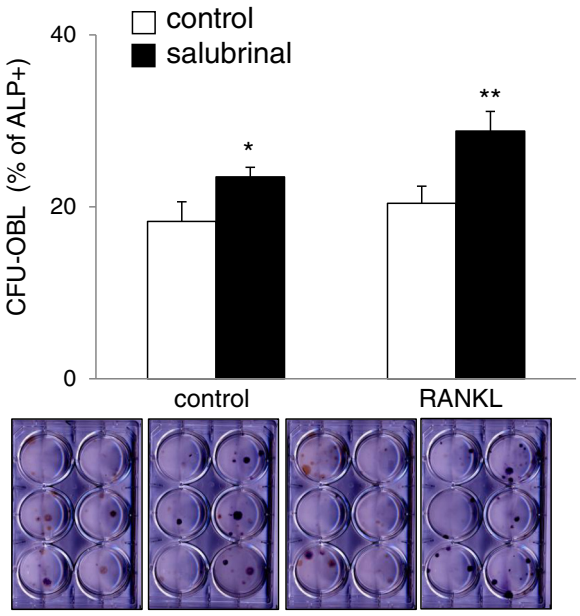

Figure 6 Enhanced osteoblast development by salubrinal in the CFU-OBL assay. Bone marrow-derived cells were plated at 2×10^6/ml in 6-well plates in osteogenic differentiation medium supplemented with 10 nM dexamethasone, 50 μg/ml ascorbic acid 2-phosphate, and 10 mM β-glycerophosphate. Cells were cultured for 2 weeks in the presence and absence of 0.5 μM salubrinal, and medium was changed every other day. For alkaline phosphatase (ALP) staining, cells were fixed in citrate-buffered acetone for 30 s, incubated in the alkaline-dye mix for 30 min, and counterstained with Mayer's Hematoxylin for 10 min. Cells were then evaluated microscopically and the intensity of ALP staining was determined. The images display 2 pairs of osteoblast cultures.

assays, in which salubrinal was applied from day 0 to 6 and from day 4 to 6, it suppressed both the early and late stages of osteoclastogenesis. This suppressive effect was larger in the cells isolated from the RANKL-injected mice than the vehicle control mice. In addition to attenuating osteoclastogenesis, salubrinal was able to reduce adhesion and migration of osteoclasts. Furthermore, it increased the number of CFU-OBL colonies suggesting that it not only inhibits development of osteoclasts but also promotes development of osteoblasts. Quantitative PCR and Western blot analysis revealed that the mRNA and protein levels of NFATc1 were elevated by RANKL, and this elevation was suppressed by administration of salubrinal in a dose dependent fashion.

In evaluating the effects of salubrinal on fates of HSCs and MSCs in bone marrow-derived cells, we employed the recently developed RANKL administration model of osteoporosis. An advantage of this RANKL administration model includes a short period (3 days in this study) for induction of osteoclastogenesis, and activation of multiple steps in the development of osteoclasts. In the RANK/RANKL/OPG signaling pathway, RANKL regulates not only development of osteoclasts but also their activation and survival [43]. RANKL is expressed in bone, bone marrow, and lymphoid tissues including spleen that houses osteoclast precursor cells as macrophages [44]. The RANKL administration model provided a platform to

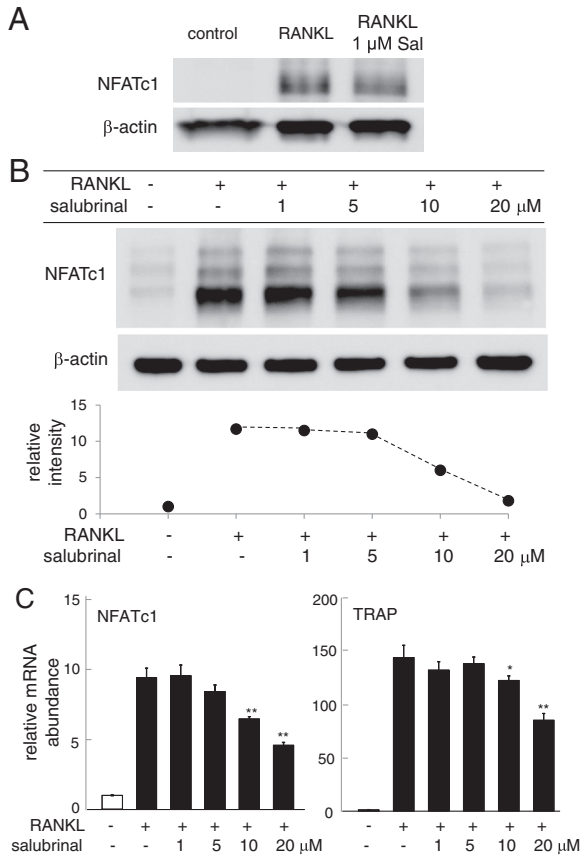

Figure 7 Suppression of RANKL-induced expression of NFATc1 and TRACP by salubrinal in RAW264.7 cells. A: Salubrinal-driven suppression of NFATc1 expression in RANKL-stimulated bone marrow-derived cells. **B**: Dose dependent suppression of NFATc1 in response to 1 – 20 μM salubrinal. β-actin was used as a loading control. **C**: Relative mRNA levels of NFATc1 and TRACP in response to 1 – 20 μM salubrinal. The mRNA levels are normalized by the mRNA level of the sample without salubrinal in the absence of RANKL stimulation.

evaluate efficacy of salubrinal as a potential therapeutic agent for preventing osteoclastogenesis and bone resorption. Besides bone resorption, however, RANKL is involved in multiple functions in the immune system such as proliferation of T cells and inhibition of apoptosis of dendritic cells [45]. It is reported that overproduction of RANKL induces inflammatory bone disorders [46,47]. Thus, the results from any animal model including the RANKL administration model should be confirmed by other animal models and eventually clinical trial.

The regulatory mechanism of salubrinal's action on osteoclastogenesis is not well understood. Salubrinal is known as an inhibitor of serine/threonine-protein phosphatase PP1 and it elevates the phosphorylation level of eIF2α (eIF2α-p) [48]. The level of eIF2α-p is upregulated in response to various stresses including viral infection, nutrient deprivation, radiation, and stress to the endoplasmic reticulum [49]. To cope with these cellular insults and reduce apoptosis, the elevated eIF2α-p in general lowers ribosome's efficiency of protein synthesis except for a group of proteins such as ATF4. Applications of salubrinal have been reported to reduce stress induced apoptosis [50]. We have previously shown that partial silencing of eIF2α by RNA interference reduces salubrinal-driven downregulation of NFATc1 in RAW264.7 cells [51], and the results in this study indicate that mRNA and protein expression of NFATc1 is downregulated by salubrinal. NFATc1 is a member of the NFAT transcription factor family and a master transcription factor for osteoclast development. It is reported that NFATc1-deficient embryonic stem cells are unable to differentiate into osteoclasts [52]. He et al. has recently shown that NFATc1 expression is regulated at a translational stage in bone marrow macrophage cells, and a phosphorylation mutant plasmid for eIF2α restored RANKL-induced NFATc1 expression [53]. MafB (V-maf musculoaponeurotic fibrosarcoma oncogene homolog B), IRF8 (interferon regulatory factor 8), and Bcl6 (V cell lymphoma) have been mentioned as inhibitors of NFATc1 [54-56]. Further analysis is necessary for identification of the mechanism of salubrinal's action on NFATc1, which is possibly regulated by eIF2α alone or any other mediators.

Conclusions

It is premature to draw any conclusion on development of a potential therapeutic agent for treatment of osteoporosis, but salubrinal possesses several unique features. First, it is a small synthetic chemical agent, which can be taken as an oral pill. Second, it has a dual role of stimulation of bone formation and attenuation of bone resorption. Third, its effects are stronger in the cells isolated from the osteoporotic RANKL-injected mice than those from the control mice. Fourth, it presents dose dependent efficacy in preventing osteoclastogenesis throughout a developmental stage including proliferation, multi-nucleation, and maturation, as well as migration and adhesion. The results herein support the possibility of preventing bone loss through salubrinal-driven regulation of bone marrow-derived cells.

Abbreviations

OVX: Ovariectomy; BMD: Bone mineral density; BMC: Bone mineral content; eIF2α: Eukaryotic translation initiation factor 2 alpha; eIF2α-p: Phosphorylated eIF2α; NFκB: Nuclear factor kappa B; ATF4: Activating transcription factor 4; NFATc1: Nuclear factor of activated T cells c1; OPG: Osteoprotegerin; RANKL: A Receptor activator of nuclear factor kappa-B ligand; M-CSF: Murine macrophage-colony stimulating factor; BMMNCs: Bone marrow mononuclear cells; MSCs: Mesenchymal stem cells; CFU-M: Colony forming-unit macrophages; CFU-GM: Colony forming-unit granulocyte/macrophages; CFU-OBL: Colony-forming unit – osteoblasts; ALP: Alkaline phosphatase; TRACP: Tartrate resistant acid phosphate; BSA: Bovine serum albumin.

Competing interests

The authors declare that they have no competing interests.

Authors' contributions

HY participated in experimental designs, and drafted a manuscript. KH conducted molecular experiments, performed data collection and analysis. AC and TD conducted animal experiments. NT and AA assisted data collection. PZ participated in experimental designs, performed animal and cell experiments, conducted data collection and interpretation, and drafted a manuscript. PZ accepted responsibility for integrity of data analysis. All authors read and approved the final manuscript.

Acknowledgements

The authors appreciated Enlin Qian for technical support.

Author details

[1]Department of Biomedical Engineering, Indiana University-Purdue University Indianapolis, 723 West Michigan Street, SL220, Indianapolis, IN 46202, USA. [2]Department of Anatomy and Cell Biology, Indiana University School of Medicine, Indianapolis, IN 46202, USA. [3]School of Basic Medical Sciences, Tianjin Medical University, Tanjin 300070, People's Republic of China.

Received: 26 April 2013 Accepted: 14 June 2013
Published: 1 July 2013

References

1. van den Bergh JP, van Geel TA, Geusens PP: **Osteoporosis, frailty and fracture: implications for case finding and therapy.** *Nat Rev Rheumatol* 2012, **8:**163–172.
2. Shiraki M, Kuroda T, Miyakawa N, Fujinawa N, Tanzawa K, Ishizuka A, Tanaka S, Tanaka Y, Hosoi T, Itoi E, Morimoto S, Itabashi A, Sugimoto T, Yamashita T, Gorai I, Mori S, Kishimoto H, Mizunuma H, Endo N, Nishizawa Y, Takaoka K, Ohashi Y, Ohta H, Fukunaga M, Nakamura T, Orimo H: **Design of a pragmatic approach to evaluate the effectiveness of concurrent treatment for the prevention of osteoporotic fractures: rationale, aims and organization of a Japanese Osteoporosis Intervention Trial (JOINT) initiated by the Research Group of Adequate Treatment of Osteoporosis (A-TOP).** *J Bone Miner Metab* 2011, **29:**37–43.
3. Vercini F, Grimaldi F: **PTH 1–84: bone rebuilding as a target for the therapy of severe osteoporosis.** *Clin Cases Miner Bone Metab* 2012, **9:**31–36.
4. Dempster DW, Lambing CL, Kostenuik PJ, Grauer A: **Role of RANK ligand and denosumab, a targeted RANK ligand inhibitor, in bone health and osteoporosis: a review of preclinical and clinical data.** *Clin Ther* 2012, **34:**521–536.
5. Yang Q, Jian J, Abramson SB, Huang X: **Inhibitory effects of iron on bone morphogenetic protein 2-induced osteoblastogenesis.** *J Bone Miner Res* 2011, **26:**1188–1196.
6. Khosla S, Bilezikian JP, Dempster DW, Lewiecki EM, Miler PD, Neer RM, Recker RR, Shane E, Shoback D, Potts JT: **Benefits and risks of bisphosphonate therapy for osteoporosis.** *J Clin Endocrinol Metab* 2012, **97:**2272–2282.
7. Riggs BL, Khosla S, Melton LJ III: **Sex steroids and the construction and conservation of the adult skeleton.** *Endocr Rev* 2002, **23:**279–302.
8. Valverde P: **Pharmacotherapies to manage bone loss-associated diseases: a quest for the perfect benefit-to-risk ratio.** *Curr Med Chem* 2008, **15:**284–304.
9. Boras-Granic K, Wysolmerski JJ: **PTHrP and breast cancer: more than hypercalcemia and bone metastases.** *Breast Cancer Res* 2012, **14:**307.
10. Boyce M, Bryant KF, Jousse C, Long K, Harding HP, Scheuner D, Kaufman RJ, Ma D, Coen DM, Ron D, Yuan J: **A selective inhibitor of eIF2alpha dephosphorylation protects cells from ER stress.** *Science* 2005, **307:**935–939.
11. Huang X, Chen Y, Zhang H, Ma Q, Zhang YW, Xu H: **Salubrinal attenuates β-amyloid-induced neuronal death and microglial activation by inhibition of the NF-κB pathway.** *Neurobiol Aging* 2012, **33:**1007.e9–1007.e17.
12. Saito A, Ochiai K, Kondo S, Tsumagari K, Murakami T, Cavener DR, Imaizumi K: **Endoplasmic reticulum stress response mediated by the PERK-eIF2 (alpha)-ATF4 pathway is involved in osteoblast differentiation induced by BMP2.** *J Biol Chem* 2011, **286:**4809–4818.
13. Zhang P, Hamamura K, Jiang C, Zhang L, Yokota H: **Salubrinal promotes healing of surgical wounds in rat femurs.** *J Bone Miner Metab* 2012, **30:**568–579.
14. Li X, Ling W, Khan S, Yaccoby S: **Therapeutic effects of intrabone and systemic mesenchymal stem cell cytotherapy on myeloma bone disease and tumor growth.** *J Bone Miner Res* 2012, **27:**1635–1648.
15. Sun L, Peng Y, Sharrow AC, Iqbal J, Zhang Z, Papachristou DJ, Zaidi S, Zhu LL, Yaroslavskiy BB, Zhou H, Zallone A, Sairam MR, Kumar TR, Bo W, Braun J, Cardoso-Landa L, Schaffler MB, Moonga BS, Blair HC, Zaidi M: **FSH directly regulates bone mass.** *Cell* 2006, **125:**247–260.
16. Weitzmann MN, Pacifici R: **Estrogen deficiency and bone loss: an inflammatory tale.** *J Clin Invest* 2006, **116:**1186–1194.
17. Shahnazari M, Wronski T, Chu V, Williams A, Leeper A, Stolina M, Ke HZ, Halloran B: **Early response of bone marrow osteoprogenitors to skeletal unloading and sclerostin antibody.** *Calcif Tissue Int* 2012, **91:**50–58.
18. Zhang P, Hammamura K, Yokota H: **A brief review of bone adaptation to unloading.** *Genomics Proteomics Bioinf* 2008, **6:**4–7.
19. Gaspar AP, Lazaretti-Castro M, Brandão CM: **Bone mineral density in spinal cord injury: an evaluation of the distal femur.** *J Osteoporos* 2012, **2012:**519754.
20. Jiang SD, Jiang LS, Dai LY: **Mechanisms of osteoporosis in spinal cord injury.** *Clin Endocrinol (Oxf)* 2006, **65:**555–565.
21. Omi N, Ezawa I: **Animal models for bone and joint disease. Low calcium diet-induced rat model of osteoporosis.** *Clin Calcium* 2012, **21:**173–180.
22. Chennaiah S, Vijayalakshmi V, Suresh C: **Effect of the supplementation of dietary rich phytoestrogens in altering the vitamin D levels in diet induced osteoporotic rat model.** *J Steroid Biochem Mol Biol* 2010, **121:**268–272.
23. Lo Iacono N, Blair HC, Poliani PL, Marrella V, Ficara F, Cassani B, Facchetti F, Fontana E, Guerrini MM, Traggiai E, Schena F, Paulis M, Mantero S, Inforzato A, Valaperta S, Pangrazio A, Crisafulli L, Maina V, Kostenuik P, Vezzoni P, Villa A, Sobacchi C: **Osteopetrosis rescue upon RANKL administration to Rankl (−/−) mice: A new therapy for human RANKL-dependent ARO.** *J Bone Miner Res* 2012, **27:**2501–2510.
24. Campbell GM, Ominsky MS, Boyd SK: **Bone quality is partially recovered after the discontinuation of RANKL administration in rats by increased bone mass on existing trabeculae: an in vivo micro-CT study.** *Osteoporosis Int* 2011, **22:**931–942.
25. Yasuda H: **Animal models for bone and joint disease. RANKL-injected bone loss model.** *Clin Calcium* 2011, **21:**197–208.
26. Tomimori Y, Mori K, Koide M, Nakamichi Y, Ninomiya T, Udagawa N, Yasuda H: **Evaluation of pharmaceuticals with a novel 50-hour animal model of bone loss.** *J Bone Miner Res* 2009, **24:**1194–1205.
27. Wasilewska A, Rybi-Szuminska AA, Zoch-Zwierz W: **Serum osteoprotegrin (OPG) and receptor activator of nuclear factor kappaB (RANKL) in healthy children and adolescents.** *J Pediatr Endocrinol Metab* 2009, **22:**1099–1104.
28. Takayanagi H: **Osteoimmunology and the effects of the immune system on bone.** *Nat Rev Rheumatol* 2009, **5:**667–676.
29. Nakamura M, Udagawa N: **Osteoporosis and RANKL signal.** *Clin Calcium* 2011, **21:**1149–1155.
30. Perlot T, Penninger JM: **Development and function of murine B cells lacking RANK.** *J Immunol* 2012, **188:**1201–1205.
31. Mun SH, Won HY, Hernandez P, Aguila HL, Lee SK: **Deletion of CD74, a putative MIF receptor, in mice enhances osteoclastogenesis and decreases bone mass.** *J Bone Miner Res* 2013, **28:**948–959.
32. Droxmeyer HE, Kappes F, Mor-Vaknin N, Legendre M, Kinzforql J, Cooper S, Hangoc G, Markovitz DM: **DEK regulates hematopoietic stem engraftment and progenitor cell proliferation.** *Stem Cells Dev* 2012, **21:**1449–1454.
33. Kroepfl JM, Pekovits K, Stelzer I, Fuchs R, Zelzer S, Hofmann P, Sedlmayr P, Dohr G, Wallner-Liebmann S, Domej W, Muller W: **Exercise increases the frequency of circulating hematopoietic progenitor cells, but reduces hematopoietic colony-forming capacity.** *Stem Cells Dev* 2012, **21:**2915–2925.
34. He Y, Rhodes SD, Chen S, Wu X, Yuan J, Yang X, Jiang L, Li X, Takahashi N, Xu M, Mohammad KS, Guise TA, Yang FC: **c-Fms Signaling Mediates Neurofibromatosis Type-1 Osteoclast Gain-In-Functions.** *PLoS One* 2012, **7:**e46900.
35. Yan D, Gurumurthy A, Wright M, Pfeiler TW, Loboa EG, Everett ET: **Genetic background influences fluoride's effects on osteoclastogenesis.** *Bone* 2007, **41:**1036–1144.
36. Broxmeyer HE, Mejia JA, Hangoc G, Barese C, Dinauer M, Cooper S: **SDF-1/CXCL12 enhances in vitro replating capacity of murine and human multipotential and macrophage progenitor cells.** *Stem Cells Dev* 2007, **16:**589–596.

37. McHugh KP, Shen Z, Crotti TN, Flannery MR, Fajardo R, Bierbaum BE, Goldring SR: **Role of cell-matrix interactions in osteoclast differentiation.** *Adv Exp Med Biol* 2007, **602:**107–111.
38. Wu X, Chen S, Orlando SA, Yuan J, Kim ET, Munugalavadla V, Mali RS, Kapur R, Yang FC: **p85α regulates osteoblast differentiation by cross-talking with the MAPK pathway.** *J Biol Chem* 2011, **286:**13512–13521.
39. Abdallah BM, Ditzel N, Mahmood A, Isa A, Traustadottir GA, Schilling AF, Ruiz-Hidalgo MJ, Laborda J, Amling M, Kassem M: **DLK1 is a novel regulator of bone mass that mediates estrogen deficiency-induced bone loss in mice.** *J Bone Miner Res* 2011, **26:**1457–1471.
40. Jansen ID, Vermeer JA, Bloemen V, Stap J, Everts V: **Osteoclast fusion and fission.** *Calcif Tissue Int* 2012, **90:**515–522.
41. Xiao G, Cheng H, Cao H, Chen K, Tu Y, Yu S, Jiao H, Yang S, Im HJ, Chen D, Chen J, Wu C: **Critical role of filamin-binding LIM protein 1 (FBLP-1)/migfilin in regulation of bone remodeling.** *J Biol Chem* 2012, **287:**21450–21460.
42. Nabavi N, Khandani A, Camirand A, Harrison RE: **Effects of microgravity on osteoclast bone resorption and osteoblast cytoskeletal organization and adhesion.** *Bone* 2011, **49:**965–974.
43. Boyce BF, Xing L: **The RANKL/RANK/OPG pathway.** *Curr Osteoporos Rep* 2007, **5:**98–104.
44. Graham LS, Tintut Y, Parhami F, Kitchen CM, Ivanov Y, Tetradis S, Effros RB: **Bone density and hyperlipidemia: the T-lymphocyte connection.** *J Bone Miner Res* 2010, **25:**2460–2469.
45. Akiyama T, Shinzawa M, Akiyama N: **RANKL-RANK interaction in immune regulatory systems.** *World J Orthop* 2012, **3:**142–150.
46. Chang SK, Noss EH, Chen M, Gu Z, Townsend K, Grenha R, Leon L, Lee SY, Lee DM, Brenner MB: **Cadherin-11 regulates fibroblast inflammation.** *Proc Natl Acad Sci U S A* 2011, **108:**8402–8407.
47. Belibasakis GN, Reddi D, Bostanci N: **Porphyromonas gingivalis induces RANKL in T-cells.** *Inflammation* 2011, **34:**133–138.
48. Vander Mierde D, Scheuner D, Quintens R, Patel R, Song B, Tsukamoto K, Beullens M, Kaufman RJ, Bollen M, Schuit FC: **Glucose activates a protein phosphatase-1-mediated signaling pathway to enhance overall translation in pancreatic beta-cells.** *Endocrinology* 2007, **148:**609–617.
49. Dey S, Baird TD, Zhou D, Palam LR, Spandau DF, Wek RC: **Both transcriptional regulation and translational control of ATF4 are central to the integrated stress response.** *J Biol Chem* 2010, **285:**33165–33174.
50. Dou G, Sreekumar PG, Spee C, He S, Ryan SJ, Kannan R, Hinton DR: **Deficiency of αB crystallin augments ER stress-induced apoptosis by enhancing mitochondrial dysfunction.** *Free Radic Biol Med* 2012, **53:**1111–1122.
51. Hamamura K, Tanjung N, Yokota H: **Suppression of osteoclastogenesis through phosphorylation of eukaryotic translation initiation factor 2 alpha.** *J Bone Miner Metab* 2013: . in press.
52. Takayanagi H: **The role of NFAT in osteoclast formation.** *Ann NY Acad Sci* 2007, **1116:**227–237.
53. He L, Lee J, Jang JH, Sakchaisri K, Hwang J, Cha-Molstad HJ, Kim KA, Ryoo IJ, Lee HG, Kim SO, Soung NK, Lee KS, Kwon YT, Erikson RL, Ahn JS, Kim BY: **Osteoporosis regulation by salubrinal through eIF2α mediated differentiation of osteoclast and osteoblast.** *Cell Signal* 2013, **25:**552–560.
54. Kim K, Kim JH, Lee J, Jin HM, Kook H, Kim KK, Lee SY, Kim N: **MafB negatively regulates RANKL-mediated osteoclast differentiation.** *Blood* 2007, **109:**3253–3259.
55. Zhao B, Takami M, Yamada A, Wang X, Koga T, Hu X, Tamura T, Ozato K, Choi Y, Ivashkiv LB, Takayanagi H, Kamijo R: **Interferon regulatory factor-8 regulates bone metabolism by suppressing osteoclastogenesis.** *Nat Med* 2009, **15:**1066–1071.
56. Miyauchi Y, Ninomiya K, Miyamoto H, Sakamoto A, Iwasaki R, Hoshi H, Miyamoto K, Hao W, Yoshida S, Morioka H, Chiba K, Kato S, Tokuhisa T, Saitou M, Toyama Y, Suda T, Miyamoto T: **The Blimp1-Bcl6 axis is critical to regulate osteoclast differentiation and bone homeostasis.** *J Exp Med* 2010, **207:**751–762.

doi:10.1186/1471-2474-14-197
Cite this article as: Yokota *et al.*: Effects of salubrinal on development of osteoclasts and osteoblasts from bone marrow-derived cells. *BMC Musculoskeletal Disorders* 2013 **14**:197.

Prevention of glucocorticoid induced-apoptosis of osteoblasts and osteocytes by protecting against endoplasmic reticulum (ER) stress.

Sato A.[1] Plotkin L. [1] Bellido T.[1,2,3]

[1]Department of Anatomy & Cell Biology, [2]Department of Medicine, Division of Endocrinology, Indiana University School of Medicine, Indianapolis, IN, [3]Roudebush Veterans Administration Medical Center, Indianapolis, IN.

Increased oxidative stress, such as with excess of glucocorticoids (GC) or during aging, has been associated with endoplasmic reticulum (ER) stress, due to accumulation of misfolded or unfolded proteins, leading to cellular apoptosis. The double-stranded RNA-activated protein kinase-like ER kinase (PERK) is activated to alleviate ER stress and phosphorylates the eukaryotic translation initiation factor 2 alpha subunit (eIF2α). Phosphorylated eIF2α in turn inhibits global protein translation to provide time to the ER to recover from the unfolded protein load, promoting cell viability. We hypothesized that the pro-apoptotic effect of GC on osteoblasts and osteocytes are at least in part due to induction of ER stress. To test this hypothesis, we used MLO-Y4 osteocytic cells, OB-6 osteoblastic cells, and primary osteoblastic cells derived from neonatal murine calvaria. We found that the synthetic GC dexamethasone (DEX) significantly increased the percentage of apoptotic cells in cultures of MLO-Y4, OB-6, and primary osteoblastic cells. Similarly, the specific ER-stress inducing agents brefeldin A, an inhibitor of ER-golgi apparatus vesicle transport, and tunicamycin, a protein glycosylation inhibitor, significantly increased OB-6 cell apoptosis. We then tested the effect of salubrinal, an agent that protects against ER stress by inhibiting the dephosphorylation of eIF2α, on bone cell apoptosis. Salubrinal blocked apoptosis induced by the ER stressors brefeldin A and tunicamycin in OB-6 cells. Salubrinal was also effective in blocking apoptosis induced by DEX in MLO-Y4, OB-6 and primary osteoblastic cells. Optimal responses were found at 10 μM salubrinal, after either 6 or 24 h. Guanabenz, another inhibitor of eIF2α dephosphorylation, also blocked DEX and tunicamycin-induced apoptosis of primary osteoblastic cells. Furthermore, addition of DEX to mineralizing OB-6 or primary osteoblastic cells markedly decreased mineral deposition and hydroxyapatite formation. In contrast, treatment with guanabenz increased mineralization of OB-6 cell cultures and prevented the inhibitory effect of DEX. We conclude that part of the pro-apoptotic actions of GC on osteoblastic cells are mediated through ER stress and that interventions that prevent dephosphorylation of eIF2α could potentially prevent the deleterious effects of GC on bone.

2478 characters including spaces (max 2500)

Bone 73 (2015) 60–68

Contents lists available at ScienceDirect

Bone

journal homepage: www.elsevier.com/locate/bone

Original Full Length Article

Prevention of glucocorticoid induced-apoptosis of osteoblasts and osteocytes by protecting against endoplasmic reticulum (ER) stress *in vitro* and *in vivo* in female mice ☆

Amy Y. Sato [a], Xiaolin Tu [a], Kevin A. McAndrews [a,c], Lilian I. Plotkin [a,c], Teresita Bellido [a,b,c,*]

[a] Department of Anatomy & Cell Biology, Indiana University School of Medicine, Indianapolis, IN, USA
[b] Department of Medicine, Division of Endocrinology, Indiana University School of Medicine, Indianapolis, IN, USA
[c] Roudebush Veterans Administration Medical Center, Indianapolis, IN, USA

ARTICLE INFO

Article history:
Received 27 October 2014
Revised 9 December 2014
Accepted 13 December 2014
Available online 19 December 2014

Edited by: J. Aubin

Keywords:
Glucocorticoid-induced osteoporosis
Osteoblasts
Osteocytes
Endoplasmic reticulum stress

ABSTRACT

Endoplasmic reticulum (ER) stress is associated with increased reactive oxygen species (ROS), results from accumulation of misfolded/unfolded proteins, and can trigger apoptosis. ER stress is alleviated by phosphorylation of eukaryotic translation initiation factor 2α (eIF2α), which inhibits protein translation allowing the ER to recover, thus promoting cell viability. We investigated whether osteoblastic cell apoptosis induced by glucocorticoids (GCs) is due to induction of ROS/ER stress and whether inhibition of eIF2α dephosphorylation promotes survival opposing the deleterious effects of GC *in vitro* and *in vivo*. Apoptosis of osteocytic MLO-Y4 and osteoblastic OB-6 cells induced by dexamethasone was abolished by ROS inhibitors. Like GC, the ER stress inducing agents brefeldin A and tunicamycin induced osteoblastic cell apoptosis. Salubrinal or guanabenz, specific inhibitors of eIF2α dephosphorylation, blocked apoptosis induced by either GC or ER stress inducers. Moreover, GC markedly decreased mineralization in OB-6 cells or primary osteoblasts; and salubrinal or guanabenz increased mineralization and prevented the inhibitory effect of GC. Furthermore, salubrinal (1 mg/kg/day) abolished osteoblast and osteocyte apoptosis in cancellous and cortical bone and partially prevented the loss of BMD at all sites and the decreased vertebral cancellous bone formation induced by treatment with prednisolone for 28 days (1.4 mg/kg/day). We conclude that part of the pro-apoptotic actions of GC on osteoblastic cells is mediated through ER stress, and that inhibition of eIF2α dephosphorylation protects from GC-induced apoptosis of osteoblasts and osteocytes *in vitro* and *in vivo* and from the deleterious effects of GC on the skeleton.

Introduction

Excess of glucocorticoids (GCs), either endogenous as in aging or due to glucocorticoid administration as immunosuppressants, leads to loss of bone [1]. Chronic GC therapy is prescribed for a multitude of medical conditions including autoimmune diseases such as rheumatoid arthritis, organ transplants, asthma, as a component of cancer chemotherapies, and a variety of inflammatory afflictions [2,3]. Patients with chronic GC exposure exhibit a consistent reduced bone formation rate and histomorphometric features of increased bone resorption [1,4,5]. Studies with experimental animals in which GC action is blocked in osteoclasts or in osteoblasts/osteocytes support the notion that GC-induced bone loss occurs in two phases: an early bone loss caused by osteoclast-driven bone resorption, followed by a steady decline in both bone formation and bone resorption [6–8]. Between 30 to 50% of patients experience at least one bone fracture, with the consequent morbidity and mortality. Approximately 25% of patients also develop osteonecrosis due to accumulation of apoptotic osteocytes, which increases the risk of femoral head collapse [9]. Thus, understanding the mechanisms of GC action on bone cells and designing therapeutic strategies that prevent the deleterious effects of these drugs are imperative.

Increased apoptosis of osteoblasts and osteocytes is one of the mechanisms that underlie the reduced bone formation and bone fragility that characterize GC-induced osteoporosis [1]. Apoptosis by GC is due to direct hormonal effects on osteoblasts and osteocytes [10–12] and is abolished by overexpressing in these cells the enzyme that inactivates GC, 11beta-hydroxysteroid dehydrogenase type 2 [7]. The pro-apoptotic effects of GC are mediated through the classical GC receptor and are triggered by rapid activation of the kinases Pyk2 and JNK [11]. GC-induced JNK phosphorylation lies downstream of increased reactive oxygen species (ROS) generation and subsequent activation of pro-apoptotic signaling in osteoblasts [13]. Phosphorylation of eukaryotic translation initiation factor 2α (eIF2α) by double-stranded RNA-activated protein

☆ Funding sources: This research was supported by the U.S. Department of Defense (DM102485), NIAMS (R01AR059357), and the Veterans Administration (Merit Review I01BX002104) to TB.

* Corresponding author at: Department of Anatomy & Cell Biology, and Department of Internal Medicine, Endocrinology, Indiana University School of Medicine, 635 Barnhill Drive, MS5045A, Indianapolis, Indiana 46202, USA. Fax: +1 317 278 2040.
E-mail address: tbellido@iupui.edu (T. Bellido).

http://dx.doi.org/10.1016/j.bone.2014.12.012
8756-3282/

kinase-like ER kinase (PERK) protects cells from oxidative stress and apoptosis under ER stress conditions [14]. Phosphorylated eIF2α slows global rate of protein translation to provide time for the ER to recover from the excessive protein load, allowing the cell to escape from apoptosis [14,15]. Earlier findings showed that selective inhibition of eIF2α phosphatases with salubrinal or guanabenz protects from apoptosis induced by ER stress [16,17]. Salubrinal increases the levels of phosphorylated eIF2α and protects PC12 pheochromocytoma cells from apoptosis induced by the ER stressor tunicamycin, in a dose dependent manner at concentrations varying from 1–100 μM [16]. Further, guanabenz, another eIF2α phosphatase inhibitor, antagonizes the effect of tunicamycin on several cell types at concentrations up to 50 μM [17]. We hypothesized that the pro-apoptotic effect of GC on osteoblasts and osteocytes is at least in part due to induction of ER stress, and we investigated here whether the compounds salubrinal and guanabenz that inhibit eIF2α dephosphorylation will promote osteoblastic cell viability and oppose the deleterious effects of GC *in vitro* and *in vivo*.

Materials and methods

Cell lines

Primary osteoblastic cells were isolated from the neonatal calvarial bones of C57BL/6 mice, as previously published [18]. Murine primary osteoblastic cells, bone marrow-derived OB-6 osteoblastic cells, and MLO-Y4 osteocytic cells were cultured as previously described [19,20].

Quantification of cell detachment, apoptosis, and cell viability

Cell and nuclear morphology was quantified in MLO-Y4 osteocytic cells stably transfected with green fluorescent protein targeted to the nucleus (nGFP), as published [11]. Briefly, cell detachment was assessed by quantifying the number of cytoplasmic processes per cell. Cells were then categorized into one of two groups: having 3 or less processes or having more than 3 processes; and data is reported as percentage of cells with 3 or less processes. Apoptosis was evaluated by quantifying the percentage of cells with chromatin condensation and nuclear fragmentation in the same cultures. Data is reported as percentage of apoptotic cells.

Cells were treated with the anti-oxidant agents N-acetyl cysteine (NAC, 10 mM), ebselen (20 μM), or catalase (1250 U/ml), the eIF2α phosphatase inhibitors salubrinal (1–100 μM) and guanabenz (10 μM) [16,17], the bisphosphonate alendronate (0.1 μM), or corresponding vehicle (named control in the figures), for 1 h. Subsequently, cells were exposed to the pro-apoptotic agents dexamethasone (1 μM), etoposide (50 μM), brefeldin A (2.7 μM), or tunicamycin (2.7 μM) or corresponding vehicle (named vehicle in the figures), for the indicated times. Cell viability was assessed by trypan blue uptake as previously published [11,18]. Cells that excluded the dye were considered alive, and stained cells were considered dead. Data is reported as the percentage of dead cells.

Mineralization assay

Primary osteoblasts or OB-6 cells were plated at a density of 5000 cells/cm^2 in growth medium consisting of MEM Alpha medium supplemented with 10% fetal bovine serum and 1% penicillin/streptomycin. Once cultures reached confluence, medium was replaced by osteogenic medium containing 50 μg/ml ascorbic acid and 10 mM β-glycerophosphate together with 1 μM dexamethasone or its corresponding vehicle (ethanol), and 10 μM salubrinal or guanabenz or the corresponding vehicle (DMSO). Medium was replaced every 2–3 days. Mineralization was visualized using von Kossa phosphate staining [21], Alizarin Red S (Sigma-Aldrich) staining [22], or OsteoImage Mineralization Assay Kit (Lonza). Mineralization was quantified using a microplate reader for Alizarin Red S staining (405 nm absorbance) and Lonza staining (492/520 nm excitation/emission fluorescence).

In vivo study

C57BL/6 female mice (n = 7–11 per group) were purchased from Harlan (Indianapolis, IN). After a 2 week acclimation period, four-month-old mice were implanted with 60 day slow-release pellets delivering placebo, 1.4 mg/kg/day (GC1) prednisolone, or 2.1 mg/kg/day (GC2) prednisolone (Innovative Research of America, Sarasota, FL) while under isoflurane anesthesia. For this, a small area between the shoulder blades was shaved and cleaned with 70% EtOH prior to incision. Daily subcutaneous injections of salubrinal (1 mg/kg/day, Tocris Bioscience, USA) or equal volume of vehicle (propylene glycol, Sigma-Aldrich, named control) began 3 days prior to pellet implantation and continued until experiment termination. An additional group of GC2 implanted mice (n = 10) received 5.25 mg/kg/week alendronate subcutaneous injections starting 3 days before pellet implantation. Mice were sacrificed 28 days after pellet implantation. Institutional Animal Care and Use Committee at Indiana University School of Medicine approved all animal procedures.

Bone mineral density (BMD) measurements

BMD was determined in live mice by dual-energy x-ray absorptiometry (DXA) scanning using a PIXImus II densitometer (G.E. Medical Systems, Lunar Division, Madison, WI) [23]. Experimental group assignment was randomized by basal spine BMD determined by DXA scanning performed 5 days prior to pellet implantation. DXA scanning was also performed 28 days after pellet implantation.

Bone histomorphometry and apoptosis

Distal femora were fixed in10% neutral buffered formalin. After 48 h in fixative, samples were transferred to 70% ethanol, and then embedded undecalcified in methyl methacrylate as previously described [12]. Dynamic histomorphometry measurements were performed in 7-μm unstained bone sections under epifluorescence microscopy. For this purpose, 0.6% calcein and 1.0% alizarin red solutions were intraperitoneally injected 8 and 3 days prior to sacrifice. Histomorphometric analysis was performed with a computer and digitizer tablet (OsteoMetrics, Decatur, GA) interfaced to an Olympus BX51 fluorescence microscope (Olympus America Inc., Melville, NY) with a drawing tube attachment [24]. Apoptotic cells were detected by transferase-mediated biotin-dUTP nick end-labeling (TUNEL) reaction in undecalcified longitudinal sections of the distal femur, as previously described [12]. Analysis was performed in cancellous and cortical bone, starting 200 μm below the growth plate and ending at the mid-diaphysis.

Statistical analysis

Data is expressed as means ± standard deviation (SD). Sample differences were assessed using SigmaPlot 12.0 (Systat Software Inc., San Jose, CA), following the appropriate method for each measurement, as indicated in the figure legends. Means were considered significantly different at $p < 0.05$.

Results

Glucocorticoids induce apoptosis of osteocytic and osteoblastic cells by generating ROS

The synthetic glucocorticoid dexamethasone induced retraction of osteocytic MLO-Y4 cytoplasmic processes, an early sign of cell detachment that triggers apoptosis (anoikis) [11], as revealed by a reduction

in the percentage of cells exhibiting 3 or more cytoplasmic projections (Fig. 1A). Dexamethasone also induced apoptosis of MLO-Y4 osteocytic cells, as quantified by evaluating chromatin condensation and nuclear fragmentation (Figs. 1B and C). Further, dexamethasone increased the percentage of MLO-Y4 and OB-6 osteoblastic cells exhibiting trypan blue uptake (Fig. 1D), another sign of apoptotic cell death induced by GC previously shown to be blocked by inhibiting caspase 3 activity [11,12,18]. Pre-treatment with the anti-oxidants NAC, ebselen, or catalase prevented GC-induced apoptosis of either cell type, although for OB-6 cells the inhibitory effect of catalase was incomplete.

Inhibition of eIF2α dephosphorylation with salubrinal and guanabenz prevents apoptosis induced by glucocorticoids, etoposide, and ER stressors in osteoblastic cells

Because ROS induce ER stress, we next investigated whether reduction of ER stress by inhibiting eIF2α dephosphorylation with salubrinal was able to prevent apoptosis induced by dexamethasone or etoposide, another proapoptotic stimulus that induces apoptosis by inhibiting topoisomerase II and DNA repair. Dexamethasone or etoposide consistently increased MLO-Y4 and OB-6 cell death (Fig. 2). Salubrinal did not significantly affect cell viability, except for increasing trypan blue uptake of MLO-Y4 cells at 100 μM for 6 h (Fig. 2A). The mechanism behind the decreased viability induced by high concentrations of salubrinal is not known. However, it might be related to a transient increase in the expression of pro-apoptotic protein CHOP as found by Zhang et al. in MC3T3 osteoblastic cells [25]. Further, 1–100 μM salubrinal prevented cell death induced by dexamethasone in both MLO-Y4 and OB-6 cells (Figs. 2A and B). Salubrinal also inhibited the effects of etoposide, but with less efficiency. The 10 μM salubrinal concentration was used for subsequent experiments as it consistently prevented dexamethasone-induced apoptosis in MLO-Y4 and OB-6 cells at both 6 and 24 h time points. Salubrinal and guanabenz, another inhibitor of eIF2α dephosphorylation, also inhibited apoptosis of OB-6 osteoblastic cells and primary osteoblasts induced by the inducers of ER stress brefeldin A, an inhibitor the ER/Golgi apparatus vesicle transport, and tunicamycin, a protein glycosylation inhibitor [16] (Figs. 3A–C). In contrast, alendronate, an agent previously shown to effectively inhibit apoptosis of osteocytic MLO-Y4 cells, osteoblastic OB-6 cells, and primary calvaria derived osteoblasts induced by dexamethasone or etoposide [12,23,26], was unable to prevent the increase in OB-6 cell death induced by the ER stress inducers (Fig. 3B).

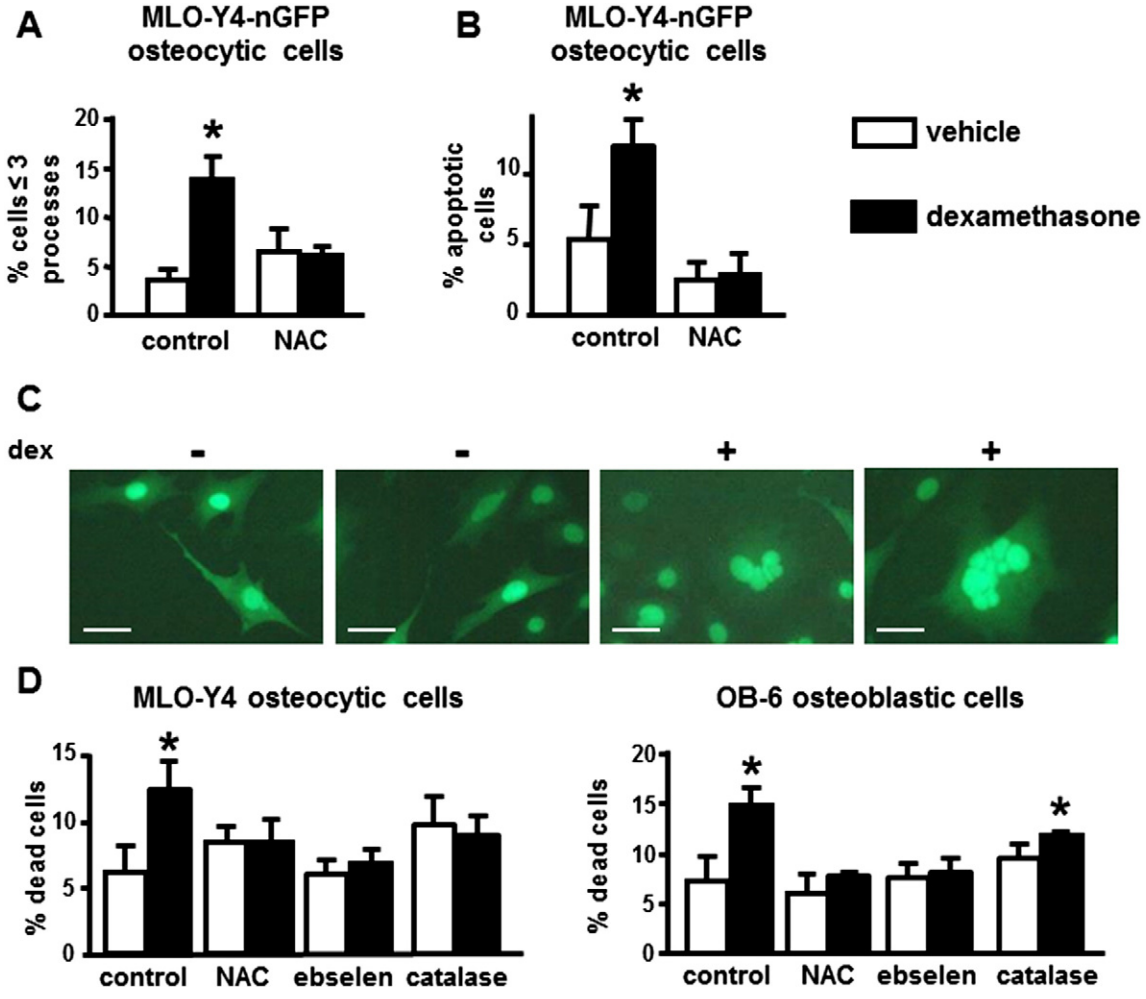

Fig. 1. Glucocorticoid-induced apoptosis of osteocytic and osteoblastic cells is prevented by inhibiting ROS generation. (A–D) Cells were exposed to vehicle (ethanol) or dexamethasone for 6 h. (A) Quantification of cytoplasmic retraction in stably transfected nGFP MLO-Y4 cells treated with or without NAC for 1 h prior to addition of dexamethasone. (B) Apoptosis quantification of nGFP-transfected MLO-Y4 cells. (C) Representative images of nGFP-expressing MLO-Y4 osteocytic cells treated with vehicle or dexamethasone showing changes in cell morphology, chromatin condensation, and nuclear fragmentation. Lines correspond to 200 μm. (D) Quantification of cell death in MLO-Y4 osteocytic or OB-6 osteoblastic cells with or without pretreatment of the indicated anti-oxidant agent, assessed by trypan blue uptake. Bars represent the means ± SD of N = 3 independent wells/treatment. *$p < 0.05$ *vs.* the corresponding vehicle-treated cells, by one-way ANOVA.

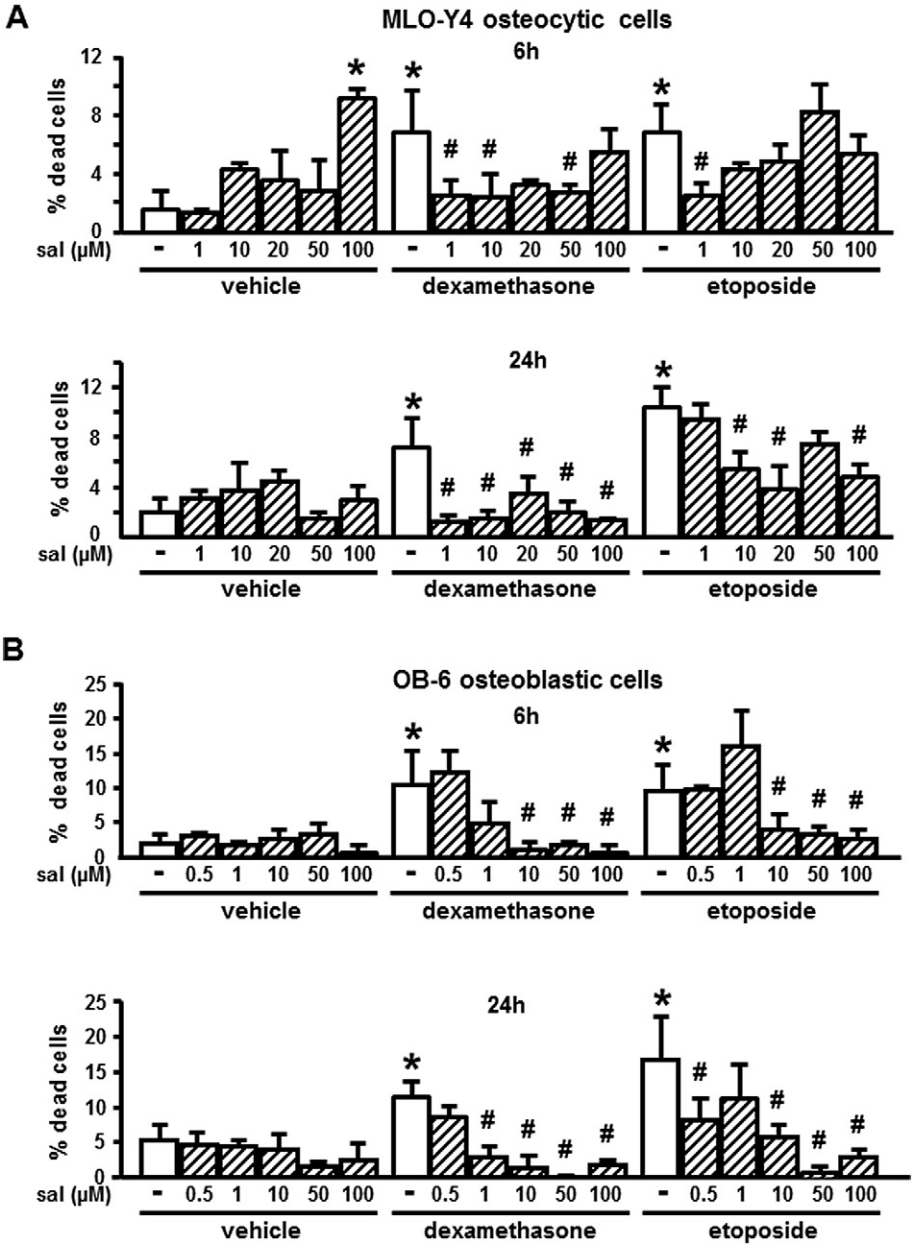

Fig. 2. Protection against ER stress with salubrinal prevents dexamethasone and etoposide induced apoptosis of osteocytic MLO-Y4 and osteoblastic OB-6 cells. Cell death quantification in MLO-Y4 osteocytic (A) or OB-6 osteoblastic (B) cells treated with or without salubrinal prior to addition of vehicle, dexamethasone, or etoposide, assessed by trypan blue uptake. Bars represent the means ± SD of N = 3 samples per treatment. *$p < 0.05$ *vs.* cells treated with vehicle without salubrinal and #$p < 0.05$ *vs.* corresponding apoptotic agent without salubrinal for each time point, by one-way ANOVA.

Salubrinal and guanabenz ameliorate the inhibitory effects of glucocorticoids on matrix mineralization

We next investigated whether inhibitors of the ER stress alter the effects of GC on matrix mineralization. GC decreased mineral deposition in OB-6 osteoblastic cells cultured under osteogenic conditions, as shown by staining with von Kossa (that detects phosphate) or Alizarin Red S (that detects calcium) (Figs. 4A and B), or in primary osteoblasts measured by hydroxyapatite accumulation (Fig. 4C). Treatment with salubrinal or guanabenz increased mineralization of OB-6 cells (Figs. 5A and B). Further, either compound partially prevented the decreased mineralization induced by GC in OB-6 or primary osteoblasts (Fig. 5). Thus, salubrinal increased mineral content in cells treated with GC compared to GC alone after 7 and 10 days of culture (Fig. 5A). However, salubrinal treatment could not block GC reductions in mineralization after 14 days of GC exposure, but guanabenz remained effective throughout the two week GC treatment period (Figs. 5A–C).

Salubrinal protects against osteoblast and osteocyte apoptosis in vivo and partially prevents the bone loss induced by glucocorticoids

We next investigated whether inhibition of eIF2α dephosphorylation promoted bone cell viability also *in vivo*. Guanabenz appeared to be more potent in opposing the *in vitro* effects of GC compared to salubrinal. However, guanabenz is also an α2 adrenergic receptor agonist used in the treatment of hypertension [27]. To avoid potential skeletal effects of activating these receptors, we decided to use salubrinal for the *in vivo* study. C57BL/6 female mice implanted with pellets containing two different doses of the GC prednisolone (GC1 = 1.4 or GC2 = 2.1 mg/kg/day) received daily injections of

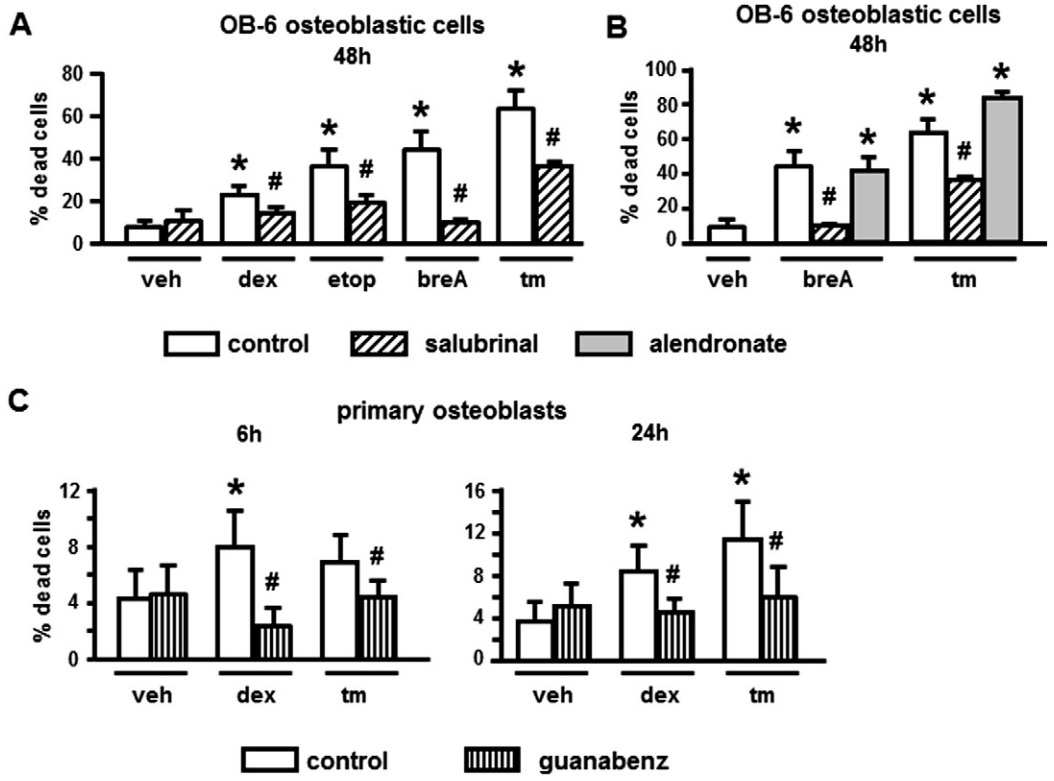

Fig. 3. Salubrinal or guanabenz protects from apoptosis induced by dexamethasone, etoposide, and ER stressors in osteoblastic cells. Cell death quantification in OB-6 osteoblastic (A and B) or primary osteoblastic (C) cells treated with or without anti-apoptotic agents salubrinal, alendronate, or guanabenz prior to addition of dexamethasone (dex), etoposide (etop), brefeldin A (breA), tunicamycin (tm), or vehicle (veh). Bars represent the means ± SD of N = 3 samples per group. *$p < 0.05$ *vs.* veh-treated cells and #$p < 0.05$ *vs.* corresponding apoptotic agent without designated eIF2α phosphatase inhibitor for each time point, by Student's *t*-test in (A) and (C) and by one-way ANOVA in (B).

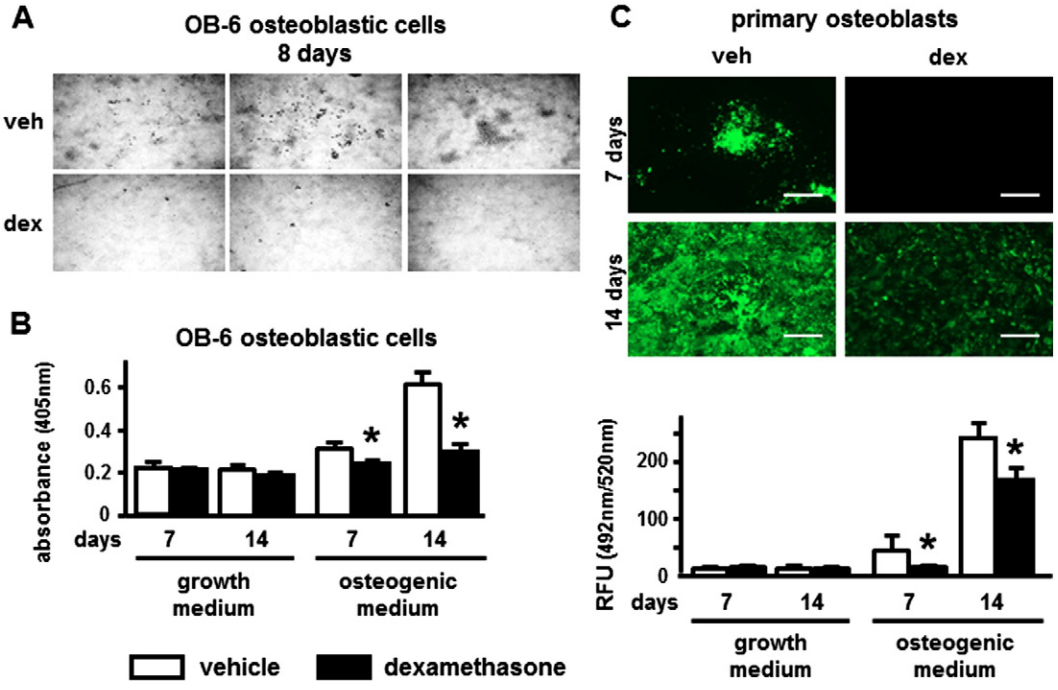

Fig. 4. Glucocorticoid decreases matrix mineralization in cultures of osteoblastic cells and primary osteoblasts. (A and B) OB-6 osteoblastic cells cultured with or without dexamethasone (dex) and the degree of mineralization was assessed by von Kossa staining for 8 days (A) and by Alizarin Red S staining for 1 or 2 weeks (B). (C) Calvaria-derived osteoblastic cells were cultured with or without osteogenic medium for 1 or 2 weeks together with vehicle (veh) or dexamethasone (dex) and mineralization was assessed using the OsteoImage Mineralization Assay Kit. Lines correspond to 200 μm. Bars represent the means ± SD of N = 3 for (A) and (B), N = 6 for (C) samples per group. *$p < 0.05$ *vs.* veh-treated cells in corresponding medium condition for each time point, by two-way ANOVA.

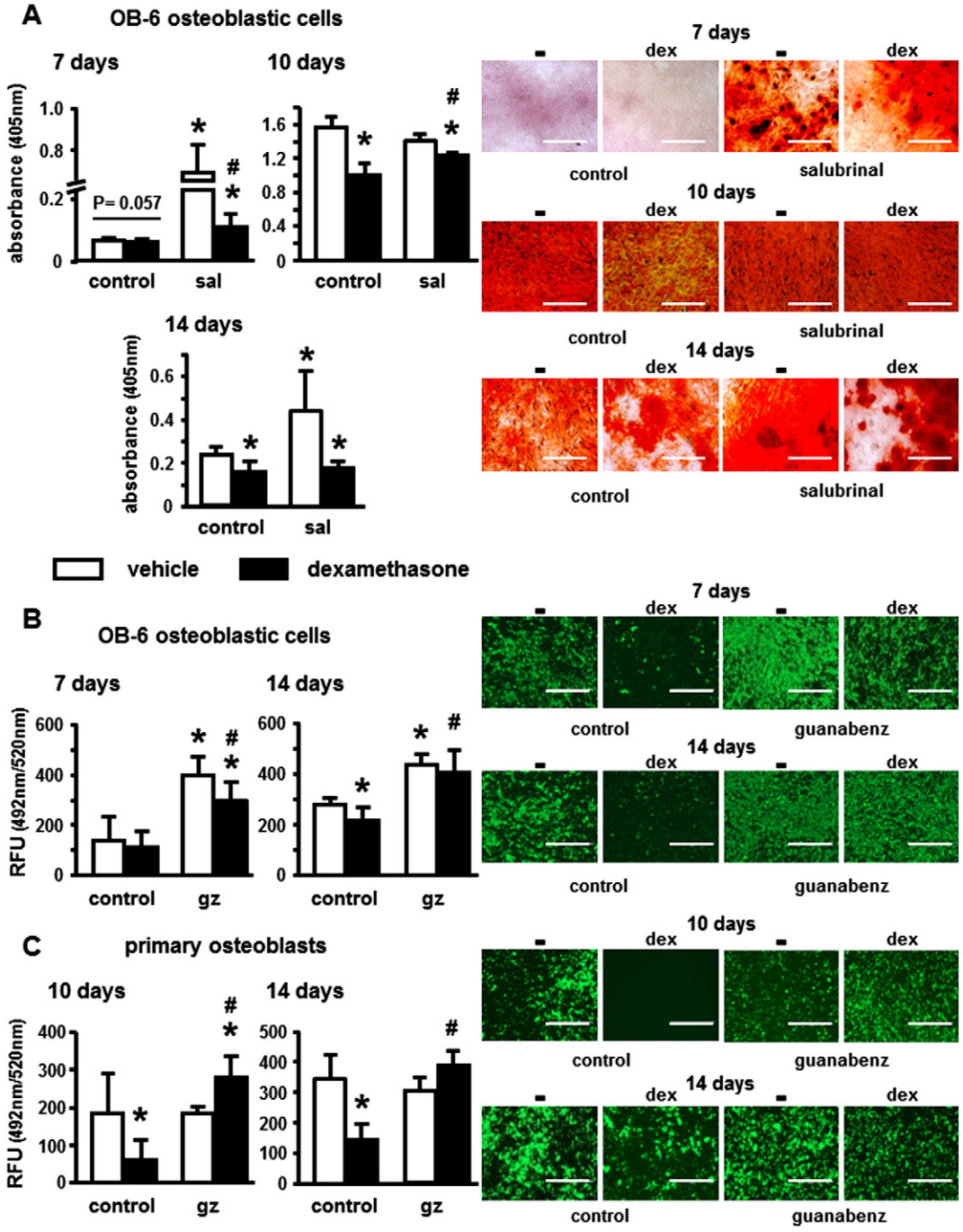

Fig. 5. Salubrinal and guanabenz ameliorate the inhibitory effects of GC on matrix mineralization. (A) Mineralization was determined in vehicle (veh) or dexamethasone (dex) treated differentiated OB-6 cells without (control) or with salubrinal (sal) pre-treatment for 7, 10, and 14 days by Alizarin Red S staining. (B) and (C) quantification of mineralization in OB-6 (B) and calvaria-derived (C) osteoblastic cells treated with vehicle or dexamethasone with or without guanabenz (gz) for the indicated incubation periods. Hydroxyapatite accumulation was measured by OsteoImage Mineralization Assay Kit. Lines correspond to 400 μm. Bars represent the means ± SD of N = 3 for (A) and N = 12 for (B–C). $^{*}p < 0.05$ *vs.* veh-treated control cells and $^{\#}p < 0.05$ *vs.* dex-treated control cells, by one-way ANOVA.

salubrinal (1 mg/kg/day). Mice treated with prednisolone exhibited increased apoptosis of osteoblasts in cancellous bone and of osteocytes in both cancellous and cortical bone (Fig. 6A). Salubrinal completely blocked GC1-induced apoptosis of both osteoblasts and osteocytes, whereas it only partially prevented the increase in GC2-induced apoptosis of osteoblasts and did not inhibit GC2-induced osteocyte apoptosis. On the other hand and consistent with previous findings [23], alendronate effectively prevented GC2-induced apoptosis of both osteoblasts and osteocytes in cancellous bone, although it did not inhibit GC2-induced cortical osteocyte apoptosis. Administration of prednisolone induced a significant decrease in BMD in total body, spine, and femur, at both doses compared to placebo (Fig. 6B). Mice implanted with placebo pellets and treated with salubrinal lost significantly less spinal BMD compared to those treated with vehicle. Similarly, mice implanted with GC1 pellets and injected with salubrinal lost significantly less bone compared to mice implanted with GC1 pellets and injected with vehicle. On the other hand, salubrinal did not prevent the loss of bone induced by GC2. In contrast, inhibition of resorption with alendronate not only prevented GC2-induced bone loss, as previously shown [23], but also increased BMD over placebo treated mice. Moreover, GC1 and GC2 reduced bone formation rate (BFR) in cancellous bone by a combination of reduction in MS/BS and in MAR (Fig. 6C).

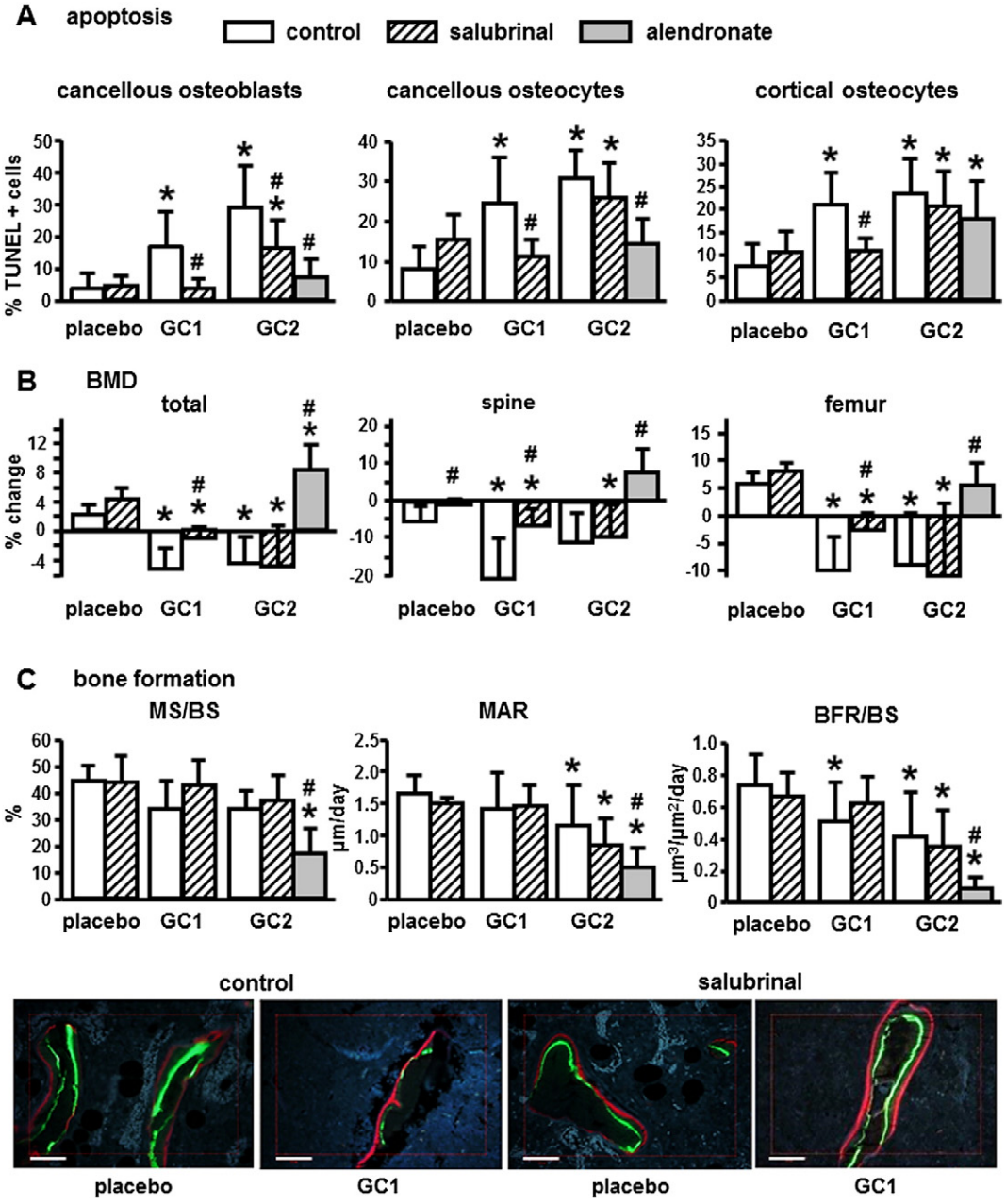

Fig. 6. Salubrinal protects against glucocorticoid-induced apoptosis and consequent bone loss *in vivo*. (A) TUNEL and (C) dynamic histomorphometric data was obtained from longitudinal distal femur sections. Representative images of fluorochrome labeled bones are shown. Bars correspond to 50 µm. (B) BMD percent changes for placebo, 1.4 mg/kg/day prednisolone (GC1), or 2.1 mg/kg/day prednisolone (GC2) pellet implanted mice with or without salubrinal intervention were determined by DXA analysis. Bars represent the means ± SD of N = 7–10 for (A) and (C) and N = 6–10 for (B). Statistical analysis for placebo, GC1, and GC2 treated mice treated with vehicle (control) or salubrinal was performed by two-way ANOVA. $^{*}p < 0.05$ *vs.* placebo mice injected with vehicle (control) or salubrinal. $^{\#}p < 0.05$ *vs.* the corresponding GC treated mice injected with vehicle (control). The effect of alendronate on GC2 treated mice was analyzed by comparing placebo, GC2, and GC2 plus alendronate by one-way ANOVA. $^{*}p < 0.05$ *vs.* placebo mice injected with vehicle (control) and $^{\#}p < 0.05$ *vs.* GC2 treated mice injected with vehicle (control).

Salubrinal reversed the decreased BFR induced by GC1 but not GC2. Alendronate reduced further GC2-mediated inhibition of BFR by decreasing both MS/BS and MAR.

Discussion

Apoptosis of osteoblasts and osteocytes contributes to the reduced bone formation and increased bone fragility in glucocorticoid-induced osteoporosis [6,7,9]. Therefore, understanding the mechanisms by which GCs induce apoptosis of osteoblastic cells is critical for the development of intervention therapies. Earlier studies demonstrated that apoptosis of osteocytes and osteoblasts is caused by loss of attachment to the extracellular matrix mediated by inside-out signaling downstream of Pyk2/JNK kinases [11] and that GCs increase ROS production in bone *in vivo* and in osteoblastic cells *in vitro* [13]. We investigated in this study the effect on GC action of salubrinal and guanabenz, eIF2α dephosphorylation inhibitors that block ROS-induced ER stress [16,17]. These compounds prevented the pro-apoptotic effect of GC on osteoblasts and osteocytes *in vitro* and the decreased in mineral deposition induced by GC in osteoblastic cell cultures. Further, salubrinal prevented apoptosis of osteoblasts and osteocytes induced by GC *in vivo* and the concomitant decrease in bone mass and bone formation.

Consistent with the current study demonstrating inhibition of apoptosis of osteoblasts and osteocytes and improved mineralization by

decreasing ER stress, recent evidence demonstrates increased apoptosis of osteoblastic cells and changes in osteoblast differentiation associated with elevated ER stress *in vitro* with thapsigargin or tunicamycin [28,29]. Remarkably, increased ER stress appears to have a time-dependent biphasic effect inducing rapid increase in osteoblast markers Runx2 and osterix, followed by a reduction in the expression of these transcription factors as well as osteocalcin [28]. Further, ER stress-mediated apoptosis of osteoblasts and impaired osteoblast differentiation was also demonstrated in a model of osteogenesis imperfecta [30] and in mice lacking the ER-localized protein Arl6ip5 in osteoblasts [31]. Consistent with the pro-apoptotic and inhibitory effect of ER stress on osteoblast differentiation, in the current manuscript we show that opposing ER stress by inhibiting eIF2α dephosphorylation prevents osteoblast and osteocyte apoptosis and the decrease in osteoblast function induced by GC *in vitro* and *in vivo*. Our findings agree with previous evidence showing that salubrinal increases the number of alkaline phosphatase positive colonies in bone marrow cell cultures [32] and osteocalcin expression in MC3T3-E1 cells [33].

In contrast to the protective effect of salubrinal against the action of low GC dose (GC1), salubrinal was unable to protect the skeleton from the high GC dose (GC2). Similarly, whereas salubrinal or guanabenz effectively prevented the inhibition of mineralization induced by short-term treatment of cultured osteoblasts with GC, only guanabenz was able to reverse the effects of prolonged treatment with GC. The mechanism of the different outcome of guanabenz compared to salubrinal is not known. It remains unclear also the reason for the incomplete inhibition of cortical osteocyte apoptosis by alendronate in this experiment, since in earlier studies alendronate completely prevented apoptosis of osteoblastic cells in both cancellous and cortical bone [23]. A potential explanation is that in the previous study alendronate was administered daily instead of in a weekly 7-day cumulative dose. Nevertheless, these findings suggest that the potency of the pro-apoptotic signals delivered by GC, either due to high dose or prolonged exposure, determines the ability of the protective compound to induced survival and that once a pro-apoptotic threshold is reached, salubrinal is not able to reverse it.

Consistent with the *in vitro* and *in vivo* data showing that inhibition of eIF2α dephosphorylation preserves osteoblast viability, treatment with salubrinal reversed the inhibition in BFR induced by low dose of GC mainly by reversing the decrease in MS/BS. These findings together with the demonstration that salubrinal prevents the reduction in mineralization induced by GC *in vitro* strongly suggest that the preservation of bone mineral density by salubrinal is due to its protective effects on osteoblasts. In contrast, alendronate further reduced BFR in GC treated animals, as expected due to its potent inhibitory effects on osteoclasts and resorption. Salubrinal, like alendronate, has been also shown to inhibit osteoclastogenesis [33] and to protect from ovariectomy-induced bone loss [34]. However, in the setting of GC excess, the main mechanism of salubrinal action appears to be related to osteoblasts. Thus, the bone sparing actions of salubrinal and bisphosphonates on GC excess are mediated by distinct cellular mechanisms. Whereas alendronate inhibits osteoclast activity and reduces bone turnover, salubrinal preserves the viability and the bone forming function of osteoblasts.

Protein misfolding is a common feature of several human diseases including neurodegenerative conditions such as Alzheimer's and Parkinson's diseases, as well as type 2 diabetes [35]. Lack of functional PERK, the sensor of the unfolded protein response and a major eIF2α kinase, causes the Wolcott–Rallison syndrome (WRS) in humans, which is characterized by early onset diabetes and aberrant skeletal development [36]. PERK deletion in the mouse prevents the unfolded protein response induced by ER stressors and inhibits phosphorylation of eIF2α [37]. Homozygous PERK null mice are born normal but loose β cells rapidly and develop early diabetes [38]. As with WRS patients, PERK knockout mice develop skeletal dysplasia and defective bone mineralization [39]. Osteoblast and osteocyte number, mineral appositional rate MAR, and markers of osteoblasts and osteocytes are decreased in PERK null mice. Osteoblast survival appears not to be affected *in vitro*, albeit *in vivo* studies were not shown. Together with the current study in which increased osteoblast and osteocyte apoptosis, decreased bone formation, and decreased bone mass induced by glucocorticoids are partially prevented by salubrinal, these findings suggest that inhibition of eIF2α dephosphorylation is a potential novel target for the treatment of glucocorticoid-induced osteoporosis and other conditions with deficient osteoblast differentiation and bone mineralization.

Acknowledgments

The authors thank Dr. Nicoletta Bivi and Meloney Cregor for their technical assistance, Dr. Ziyue Liu for the assistance with statistical analysis, and Dr. Hiroki Yokota for the advice. This research was supported by the U.S. Department of Defense (DM102485), National Institutes of Health (R01AR059357, R01 DK076007, and S10-RR023710 to TB), and the Veterans Administration (Merit Review I01BX002104 to TB).

Disclosure statement

The authors have nothing to disclose.

References

[1] Weinstein RS. Clinical practice. Glucocorticoid-induced bone disease. N Engl J Med 2011;365:62–70.
[2] Jin HO, Seo SK, Woo SH, Kim ES, Lee HC, Yoo DH, et al. Activating transcription factor 4 and CCAAT/enhancer-binding protein-beta negatively regulate the mammalian target of rapamycin via Redd1 expression in response to oxidative and endoplasmic reticulum stress. Free Radic Biol Med 2009;46:1158–67.
[3] Weinstein RS. Glucocorticoid-induced osteoporosis. Rev Endocr Metab Disord 2001;2:65–73.
[4] Dempster DW. Bone histomorphometry in glucocorticoid-induced osteoporosis. J Bone Miner Res 1989;4:137–41.
[5] Reid IR. Glucocorticoid osteoporosis—mechanisms and management. Eur J Endocrinol 1997;137:209–17.
[6] Weinstein RS, Jilka RL, Parfitt AM, Manolagas SC. Inhibition of osteoblastogenesis and promotion of apoptosis of osteoblasts and osteocytes by glucocorticoids: potential mechanisms of their deleterious effects on bone. J Clin Invest 1998;102:274–82.
[7] O'Brien CA, Jia D, Plotkin LI, Bellido T, Powers CC, Stewart SA, et al. Glucocorticoids act directly on osteoblasts and osteocytes to induce their apoptosis and reduce bone formation and strength. Endocrinology 2004;145:1835–41.
[8] Jia D, O'Brien CA, Stewart SA, Manolagas SC, Weinstein RS. Glucocorticoids act directly on osteoclasts to increase their lifespan and reduce bone density. Endocrinology 2006;147:5592–9.
[9] Weinstein RS, Nicholas RW, Manolagas SC. Apoptosis of osteocytes in glucocorticoid-induced osteonecrosis of the hip. J Clin Endocrinol Metab 2000;85:2907–12.
[10] Jilka RL, Weinstein RS, Bellido T, Roberson P, Parfitt AM, Manolagas SC. Increased bone formation by prevention of osteoblast apoptosis with parathyroid hormone. J Clin Invest 1999;104:439–46.
[11] Plotkin LI, Manolagas SC, Bellido T. Glucocorticoids induce osteocyte apoptosis by blocking focal adhesion kinase-mediated survival: evidence for inside-out signaling leading to anoikis. J Biol Chem 2007;282:24120–30.
[12] Plotkin LI, Weinstein RS, Parfitt AM, Roberson PK, Manolagas SC, Bellido T. Prevention of osteocyte and osteoblast apoptosis by bisphosphonates and calcitonin. J Clin Invest 1999;104:1363–74.
[13] Almeida M, Han L, Ambrogini E, Weinstein RS, Manolagas SC. Glucocorticoids and tumor necrosis factor (TNF) alpha increase oxidative stress and suppress WNT signaling in osteoblasts. J Biol Chem 2011;286:44326–35.
[14] Harding HP, Zhang Y, Zeng H, Novoa I, Lu PD, Calfon M, et al. An integrated stress response regulates amino acid metabolism and resistance to oxidative stress. Mol Cell 2003;11:619–33.
[15] Walter P, Ron D. The unfolded protein response: from stress pathway to homeostatic regulation. Science 2011;334:1081–6.
[16] Boyce M, Bryant KF, Jousse C, Long K, Harding HP, Scheuner D, et al. A selective inhibitor of eIF2alpha dephosphorylation protects cells from ER stress. Science 2005;307:935–9.
[17] Tsaytler P, Harding HP, Ron D, Bertolotti A. Selective inhibition of a regulatory subunit of protein phosphatase 1 restores proteostasis. Science 2011;332:91–4.
[18] Bellido T, Ali AA, Plotkin LI, Fu Q, Gubrij I, Roberson PK, et al. Proteasomal degradation of Runx2 shortens parathyroid hormone-induced anti-apoptotic signaling in osteoblasts. A putative explanation for why intermittent administration is needed for bone anabolism. J Biol Chem 2003;278:50259–72.
[19] Lecka-Czernik B, Gubrij I, Moerman EA, Kajkenova O, Lipschitz DA, Manolagas SC, et al. Inhibition of Osf2/Cbfa1 expression and terminal osteoblast differentiation by PPAR-gamma 2. J Cell Biochem 1999;74:357–71.
[20] Kato Y, Windle JJ, Koop BA, Mundy GR, Bonewald LF. Establishment of an osteocyte-like cell line, MLO-Y4. J Bone Miner Res 1997;12:2014–23.

[21] Ogawa R, Mizuno H, Watanabe A, Migita M, Shimada T, Hyakusoku H. Osteogenic and chondrogenic differentiation by adipose-derived stem cells harvested from GFP transgenic mice. Biochem Biophys Res Commun 2004;313:871–7.
[22] Tsai SW, Liou HM, Lin CJ, Kuo KL, Hung YS, Weng RC, et al. MG63 osteoblast-like cells exhibit different behavior when grown on electrospun collagen matrix versus electrospun gelatin matrix. PLoS One 2012;7:e31200.
[23] Plotkin LI, Lezcano V, Thostenson J, Weinstein RS, Manolagas SC, Bellido T. Connexin 43 is required for the anti-apoptotic effect of bisphosphonates on osteocytes and osteoblasts in vivo. J Bone Miner Res 2008;23:1712–21.
[24] Aguirre JI, Plotkin LI, Stewart SA, Weinstein RS, Parfitt AM, Manolagas SC, et al. Osteocyte apoptosis is induced by weightlessness in mice and precedes osteoclast recruitment and bone loss. J Bone Miner Res 2006;21:605–15.
[25] Zhang P, Hamamura K, Jiang C, Zhao L, Yokota H. Salubrinal promotes healing of surgical wounds in rat femurs. J Bone Miner Metab 2012;30:568–79.
[26] Bellido T, Plotkin LI. Novel actions of bisphosphonates in bone: preservation of osteoblast and osteocyte viability. Bone 2011;49:50–5.
[27] Holmes B, Brogden RN, Heel RC, Speight TM, Avery GS. Guanabenz. A review of its pharmacodynamic properties and therapeutic efficacy in hypertension. Drugs 1983;26:212–29.
[28] Hamamura K, Yokota H. Stress to endoplasmic reticulum of mouse osteoblasts induces apoptosis and transcriptional activation for bone remodeling. FEBS Lett 2007;581:1769–74.
[29] Saito A, Ochiai K, Kondo S, Tsumagari K, Murakami T, Cavener DR, et al. Endoplasmic reticulum stress response mediated by the PERK-eIF2(alpha)-ATF4 pathway is involved in osteoblast differentiation induced by BMP2. J Biol Chem 2011;286:4809–18.
[30] Lisse TS, Thiele F, Fuchs H, Hans W, Przemeck GKH, Abe K, et al. ER stress-mediated apoptosis in a new mouse model of osteogenesis imperfecta. PLoS Genet 2008;4(2):e7 [4:1-11].
[31] Wu Y, Yang M, Fan J, Peng Y, Deng L, Ding Y, et al. Deficiency of osteoblastic Arl6ip5 impaired osteoblast differentiation and enhanced osteoclastogenesis via disturbance of ER calcium homeostasis and induction of ER stress-mediated apoptosis. Cell Death Dis 2014;5:e1464.
[32] Yokota H, Hamamura K, Chen A, Dodge TR, Tanjung N, Abedinpoor A, et al. Effects of salubrinal on development of osteoclasts and osteoblasts from bone marrow-derived cells. BMC Musculoskelet Disord 2013;14:197.
[33] Hamamura K, Tanjung N, Yokota H. Suppression of osteoclastogenesis through phosphorylation of eukaryotic translation initiation factor 2 alpha. J Bone Miner Metab 2013;31:618–28.
[34] Zhang P, Chen A, Dodge TTN, Zheng Y, Fuqua C, Yokota H. Salubrinal regulates bone remodeling and fat metabolism in ovariectomized mice. Proceedings of the Orthopedic Research Society Annual Meeting; 2013.
[35] Fullwood MJ, Zhou W, Shenolikar S. Targeting phosphorylation of eukaryotic initiation factor-2alpha to treat human disease. Prog Mol Biol Transl Sci 2012;106:75–106.
[36] Delepine M, Nicolino M, Barrett T, Golamaully M, Lathrop GM, Julier C. EIF2AK3, encoding translation initiation factor 2-alpha kinase 3, is mutated in patients with Wolcott–Rallison syndrome. Nat Genet 2000;25:406–9.
[37] Harding HP, Zhang Y, Bertolotti A, Zeng H, Ron D. Perk is essential for translational regulation and cell survival during the unfolded protein response. Mol Cell 2000;5:897–904.
[38] Harding HP, Zeng H, Zhang Y, Jungries R, Chung P, Plesken H, et al. Diabetes mellitus and exocrine pancreatic dysfunction in perk−/− mice reveals a role for translational control in secretory cell survival. Mol Cell 2001;7:1153–63.
[39] Wei J, Sheng X, Feng D, McGrath B, Cavener DR. PERK is essential for neonatal skeletal development to regulate osteoblast proliferation and differentiation. J Cell Physiol 2008;217:693–707.

Role of miR-222-3p in c-Src-Mediated Regulation of Osteoclastogenesis

Shinya Takigawa[1,2], Andy Chen[1], Qiaoqiao Wan[1], Sungsoo Na[1], Akihiro Sudo[2],

Hiroki Yokota[1], and Kazunori Hamamura[1,3]

[1]Department of Biomedical Engineering, Indiana University-Purdue University Indianapolis,

Indianapolis, IN 46202 USA

[2]Department of Orthopaedic Surgery, Mie University Graduate School of Medicine,

Mie 514-8507, Japan

[3]Department of Pharmacology, School of Dentistry, Aichi-Gakuin University,

Nagoya 464-8650, Japan

Running Title: miR-222-3p in Osteoclastogenesis

Shinya Takigawa: stakigaw@iupui.edu

Andy Chen: andychen@umail.iu.edu

Qiaoqiao Wan: wanq@purdue.edu

Sungsoo Na: sungna@iupui.edu

Akihiro Sudo: a-sudou@clin.medic.mie-u.ac.jp

Hiroki Yokota: hyokota@iupui.edu

Corresponding Author:

Kazunori Hamamura, PhD/DDS (hamak@dpc.agu.ac.jp)

Department of Pharmacology

School of Dentistry, Aichi-Gakuin University,

1-100 Kusumoto-cho, Chikusa-ku, Nagoya 464-8650, Japan

Phone: +81-52-757-6743

Fax: +81-52-752-5988

Abstract

MicroRNAs (miRNAs) are small non-coding RNAs that play a mostly post-transcriptional regulatory role in gene expression. Using RAW264.7 pre-osteoclast cells and genome-wide expression analysis, we identified a set of miRNAs that are involved in osteoclastogenesis. Based on *in silico* analysis, we specifically focused on miR-222-3p and evaluated its role in osteoclastogenesis. The results show that the inhibitor of miR-222-3p upregulated the mRNA levels of nuclear factor of activated T-cells, cytoplasmic 1 (NFATc1) and tartrate-resistant acid phosphatase (TRAP), while its mimicking agent downregulated their mRNA levels. Western blot analysis showed that its inhibitor increased the protein levels of TRAP and cathepsin K, while its mimicking agent decreased their levels. Genome-wide mRNA expression analysis in the presence and absence of receptor activator of nuclear factor kappa-B ligand (RANKL) predicted c-Src as a potential regulatory target of miR-222-3p. Live cell imaging using a fluorescence resonance energy transfer (FRET) technique revealed that miR-222-3p acted as an inhibitor of c-Src activity, and a partial silencing of c-Src suppressed RANKL-induced expression of TRAP and cathepsin K, as well as the number of multi-nucleated osteoclasts and their pit formation. Collectively, the study herein demonstrates that miR-222-3p serves as an inhibitor of osteoclastogenesis and c-Src mediates its inhibition of cathepsin K and TRAP.

Keywords: microarray, miRNA, osteoclastogenesis, RAW264.7 cells, c-Src

1. Introduction

MicroRNAs (miRNAs) are small non-coding RNA molecules that participate in various gene regulatory processes. They may reorganize chromatin and silence specific genes, cleave and destabilize mRNAs, or inhibit transcriptional initiation and elongation [1]. Chronic lymphocytic leukemia is the first human disease that was shown to be associated with miRNA [2], and since then involvement of miRNAs in tumor growth and metastasis has been reported [2, 3]. The regulatory role of miRNAs has also been identified in homeostasis of organ systems such as the cardiovascular system, the nervous system, and musculoskeletal system [4-6], as well as in the maintenance and development of stem cells [7].

The specific aim of this study is to evaluate a potential role of miRNAs in osteoclastogenesis. Osteoclastogenesis is a developmental process of pre-osteoclast cells in the hematopoietic lineage. In the self-fusion process to form mature multinucleated cells, receptor activator of nuclear factor kappa-B ligand (RANKL) acts as a potent stimulator and activates nuclear factor kappa-B (NFκB) signaling and a transcription factor, nuclear factor of activated T-cells, cytoplasmic 1 (NFATc1) [8]. In the response to RANKL's stimulation, NFATc1 is considered to serve as a master transcription factor, and other regulatory factors such as macrophage colony-stimulating factor (M-CSF), c-Fos, PU.1, and TRAF6 are also known to be activated [8]. It is reported that miRNAs such as miR-34a, miR-99b, miR-223, miR-365, miR-378, and miR-451 are involved in osteoclastogenesis [9,10,11, 12,13,14]. However, little is known about the regulatory mechanism of their actions and the genes directly regulated by these miRNAs.

In this study, we conducted genome-wide expression profiling of both miRNAs and mRNAs using RAW264.7 pre-osteoclast cells, followed by *in silico* data analysis, primarily using principal component analysis. Expression analysis led us to focus on miR-222-3p, which presented a consistent expression profile during osteoclastogenesis. In the presence and absence of miR-222-3p's inhibitor and mimicking agent, its influence on the selected osteoclast marker genes such as TRAP and cathepsin K was examined. Furthermore, miR-222-3p's target genes were predicted using publicly available software tools, and the predicted regulatory pathway was evaluated using inhibitor and mimicking agents, as well as siRNA specific to miR-222-3p's target gene and FRET (fluorescence resonance energy transfer)-based live cell imaging.

2. Results

2.1. RANKL responsive miRNAs

In response to RANKL treatment for 2 days, expression levels of ~20 miRNAs were significantly altered in the microarray-based assay (Figure 1). In particular, the heat map of the selected miRNAs (signal value > 500 and $p < 0.05$) shows that miRNAs such as miR-221-3p and miR-222-3p were downregulated by RANKL, while miRNAs such as miR-125b-5p and miR-182-5p were upregulated (Figure 1A). Principal component analysis (PCA), a statistical technique for finding representative axes in multidimensional data, was used to examine 6 miRNA samples (C1-C3, and R1-R3) to reveal that three RANKL-treated samples had a larger value in the second principal axis than three control samples (Figure 1B). Among 17 miRNAs in Fig. 1A that significantly altered their expression levels by RANKL with high signal values (max signal > 500), two miRNAs (miR-221-3p and miR-222-3p) were positioned with the smallest second principal component values (Figure 1C).

2.2. PCR-based mRNA and miRNA expression levels

The expression of miRNA levels, initially determined with microarrays, were re-evaluated using qPCR (Figure 2). Consistent with the stimulation of osteoclastogenesis by RANKL treatment, the mRNA levels of NFATc1 and TRAP were elevated on days 2 and 4 (Figure 2A-B). The expression levels of three miRNAs (miR-125b-5p, miR-146a-5p, and miR-182-5p) in Fig. 1A were elevated by RANKL treatment on day 2, but their expression levels on day 4 were either up, down, or unchanged (Figure 2C-E). Consistency on days 2 and 4 were observed for three miRNA (miR-27b-3p, miR-221-3p, and miR-222-3p), which were continually downregulated by RANKL treatment (Figure 2F-H).

2.3. Effects of inhibitor and mimic miR221-3p and miR222-3p

Since RANKL-driven downregulation of miR-221-3p and miR-222-3p have not been reported, we further evaluated their potential roles in osteoclastogenesis using their inhibitors and mimicking agents. In response to the inhibitor of miR-221-3p, the levels of NFATc1 mRNA, TRAP mRNA, and cathepsin K mRNA were significantly elevated (Figure 3A, C). Consistently, the mimicking agent reduced the mRNA level of TRAP, although the levels of NFATc1 mRNA and cathepsin K mRNA were not significantly changed (Figure 3B, D). We then examined the role of miR-222-3p using its inhibitor and mimicking agent (Figure 4). The mRNA levels of NFATc1, TRAP, and cathepsin K were upregulated by its inhibitor. Furthermore, the mRNA levels of NFATc1 and TRAP were downregulated by its mimicking agent (Figure 4A-D). Hereafter, the regulatory analysis was mainly conducted focusing on miR-222-3p.

2.4. Western blot analysis of NFATc1, TRAP, and cathepsin K

The mRNA expression analysis of NFATc1 and TRAP predicted that miR-222-3p may act as an inhibitor of osteoclastogenesis. To further examine the role of miR-222-3p in osteoclast development, we determined the protein expression of NFATc1, TRAP, and cathepsin K in the presence of RANKL. In response to its inhibitor, the protein levels of TRAP and cathepsin K were increased (Figure 5A). Furthermore, its mimicking agent decreased the protein levels of TRAP and cathepsin K (Figure 5B). However, the level of NFATc1 protein was not altered in response to the inhibitor or mimicking agent.

2.5. RANKL responsive genes and the prediction of miRNA responsive genes

To predict potential target genes that are regulated by RANKL-responsive miRNAs, we conducted genome-wide mRNA analysis followed by *in silico* prediction. First, we selected 27 osteoclast-linked genes whose mRNA levels were altered more than 1.5-fold by RANKL treatment (Figure 6A). These genes are ordered according to the fold change in their mRNA expression levels in response to RANKL treatment. We then predicted whether those 27 genes were potentially downregulated by RANKL-responsive miRNAs 221-3p and 222-3p (Figure 6B). The target prediction algorithms revealed several potential targets of 222-3p (Ccr1, c-Src, Dcstamp, Gpr55, Car2, Itgb3, etc.). Given their relatively high fold-changes as well as confidence in prediction, c-Src and Dcstamp were chosen for further study.

2.6. c-Src expression and activity in response to the inhibitor of miR-222-3p

Since c-Src and Dcstamp were highly responsive to RANKL treatment and predicted to be linked to miR-222-3p, we determined the mRNA levels of these two genes in the presence and absence of the inhibitor of miR-222-3p. Consistent with the prediction by *in silico* analysis, the result showed that their mRNA levels were elevated in response to miR-222-3p's inhibitor agent (Figure 7A). To further test the involvement of miR-222-3p, the cells were co-transfected with a FRET-based c-Src biosensor and the inhibitor of miR-222-3p. The data revealed that, 24 hours post-transfection, c-Src activity was elevated by the inhibitory agent (Figure 7B).

2.7. Effects of silencing c-Src in RANKL-driven osteoclastogenesis

To evaluate the role of c-Src in RANKL-driven osteoclastogenesis, we employed siRNA specific to c-Src and determined the protein levels of NFATc1, TRAP, and cathepsin K. The significant reduction in the mRNA and protein levels of c-Src was confirmed (Figure 8A-C). The result

with c-Src siRNA showed that the protein level of NFATc1 was not significantly altered. However, in response to RANKL treatment, the protein levels of TRAP and cathepsin K were significantly reduced by c-Src siRNA (Figure 8B, D). Of note, the expression of miR-221-3p or miR-222-3p was not significantly affected by c-Src siRNA treatment (Figure 8E).

TRAP staining revealed that the number of multi-nucleated osteoclasts was significantly reduced in the presence of c-Src siRNA (Figure 9A, B). Furthermore, an osteoclast activity assay showed that the number of pits, formed by active osteoclasts, was lowered by c-Src siRNA treatment (Fig. 9C, D).

3. Discussion

This study revealed that miR-222-3p acts as an inhibitory regulator of RANKL-driven osteoclastogenesis in RAW264.7 pre-osteoclast cells. Through genome-wide miRNA and mRNA expression analysis together with *in silico* predictions, miR-221-3p and miR-222-3p were highlighted as regulatory candidates. These two miRNAs were positioned at the corner in the PCA plane, indicating that their predicted inhibitory actions were strongest among RANKL responsive miRNAs. The result with qPCR revealed that the inhibitors of miR221-3p and miR-222-3p upregulated the mRNA levels of NFATc1 and TRAP. The mimicking agent of miR-222-3p downregulated the mRNA levels of NFATc1 and TRAP, while that of miR-221-3p did not significantly alter the mRNA level of NFATc1. Consistent with mRNA analysis, the inhibitor of miR-222-3p increased the protein levels of TRAP and cathepsin K, while its mimicking agent decreased these protein levels. Collectively, RNA-based loss-of-function and gain-of-function assays supported the inhibitory role of miR-222-3p in RANKL-driven upregulation of TRAP and cathepsin K.

In order to determine a signaling mechanism directly driven by miR-222-3p, 27 RANKL-responsive genes were selected as potential targets of miR-222-3p. *In silico* prediction using publicly available algorithms in miRWalk2.0 [15] assigned a confidence measure to those genes. Two genes, which were upregulated more than 5-fold by RANKL and assigned a positive confidence measure in *in silico* prediction, were c-Src and Dcstamp. According to RNAhybrid software [16], a pairing of miR-222-3p (21 nucleotide long) and the 3'-end of c-Src's untranslated region (UTR) yields the minimum free energy of -26 kcal/mol with 18 matches and 3 mismatches. In the response to miR-222-3p's inhibitor and mimicking agent, we confirmed

that the upregulation of c-Src mRNA and Dcstamp mRNA by RANKL was mediated by miR-222-3p.

Src family kinases are non-receptor tyrosine kinases, and c-Src is its proto-oncogene that promotes cellular survival, proliferation, and migration. It is reported that deletion of c-Src impairs bone resorbing activities by osteoclasts [17,18,19]. Histological analysis using TRAP staining as well as the osteoclast activity assay using pit formation revealed that a partial silencing of c-Src by RNA interference reduced the number of multi-nucleated osteoclasts and suppressed bone-resorbing activity. Using FRET-based live cell imaging, we determined the activity of c-Src in the presence and absence of miR-222-3p's inhibitor agent. The FRET result showed that the baseline activity of c-Src was increased by the inhibitor agent. Furthermore, a partial silencing of c-Src by its siRNA suppressed miR-222-3p-driven downregulation of cathepsin K and TRAP. Dcstamp is also known to play a critical role in cell-cell fusion in osteoclasts [20], and miR-222-3p is involved in its regulation. Collectively, the proposed regulatory mechanism of miR-222-3p's action is illustrated (Figure 10). Our qPCR results support the notion that miR-222-3p is inhibitory to c-Src that does not directly alter expression of miR-222-3p. Of note, while the mRNA level of NFATc1 was significantly downregulated by miR-222-3p, a reduction in its protein level was not significant.

Although the involvement of c-Src in miR-222-3p-driven regulation of osteoclastogenesis was predicted and validated, the rate of false positive in the *in silico* prediction turned out to be high. For example, a transcription factor, Fos, was predicted by every algorithm to be a target gene of miR-222-3p, but its expression was unchanged by the stimulation and inhibition of miR-222-3p

(data not shown). A variety of prediction algorithms employs a combination of sequence matching, evolutionary conservation, adjacent nucleotide composition, sequence location, and the secondary structure of the targeted region [21], in which different weights and assumptions result in variations in predictions. It appears that most of these algorithms do not effectively take into account biological context such as dependence on cell types and physiological states [22].

In tumor proliferation and invasion, miRNAs play critical roles [23]. In various cancer types including colon, pancreas, prostate, and thyroid, the expression level of miR-222-3p is reported to be altered [3,24,25,26]. It is to be shown whether the observed modulation of miR-222-3p in tumor cells is induced by specific DNA mutations, and whether its modulation might be linked to metastasis to bone followed by osteolytic responses by osteoclasts.

Based on *in slico* predictions, we focused on miR-221-3p and miR-222-3p as two potential candidates for osteoclast regulation. These two miRNAs are known to form a cluster and regulate various genes [27], but it is also reported that they can act independently. For instance, miR-222 but not miR-221 is involved in neovascularization by regulating STAT5A [28]. Hydroxyurea, which is used for the treatment of neoplastic diseases, elevates expression of miR-221 but decreases that of miR-222 [29]. Furthermore, the inhibition of miR-221 but not miR-222 suppresses a release of IL6 in patients with severe asthma [30].

In summary, this study demonstrated an inhibitory role of miR-222-3p in RANKL-driven osteoclastogenesis. Genome-wide miRNA and mRNA analysis predicted c-Src as one of the miR-222-3p's target genes. A partial silencing of c-Src using RNA interference revealed that

miR-222-3p suppressed expression of the osteoclast marker genes such as TRAP and cathepsin K via c-Src. In bone-related metabolic diseases and cancer, the role of miRNAs has not been fully understood. By identifying miR-222-3p as a regulator of bone-resorbing osteoclasts, this study indicates a novel therapeutic direction in osteoporosis as well as osteolytic lesion in bone metastasis.

4. Experimental Section

4.1. Cell culture

RAW264.7 mouse pre-osteoclast (monocyte/macrophage) cells were cultured in αMEM containing 10% fetal bovine serum and antibiotics (50 units/ml penicillin, and 50 μg/ml streptomycin; Life Technologies, Grand Island, NY, USA). Cells were maintained at 37°C and 5% CO_2 in a humidified incubator. To induce differentiation, cells were treated with 50 ng/ml RANKL (PeproTech, Rocky Hills, NC, USA) [31].

4.2. Microarray experiments for genome-wide miRNAs and mRNAs

Genome-wide miRNA and mRNA expression analyses were conducted using μParaflo® High Performance Microfluidic Microarrays (LC Sciences, Houston, TX, USA) and Mouse Gene 2.0 ST arrays (Affymetrix, Santa Clara, CA, USA), respectively. RAW264.7 cells were harvested 48 h after incubation with and without RANKL, and miRNA was isolated with a miRNeasy mini kit (Qiagen, Germantown, MD, USA). The samples for miRNA were labeled as C1-C3 (control) and R1-R3 (RANKL-treated), while the samples for mRNA were CN1-CN3 (control) and RN1-RN3 (RANKL-treated). Signal values for miRNA were background subtracted and normalized using the locally weighted scatterplot smoothing (LOWESS) method, while signal values for mRNA were normalized using robust multiarray average (RMA). The data discussed in this publication have been deposited in NCBI's Gene Expression Omnibus [32] and are accessible through GEO Series accession number GSE74847 (http://www.ncbi.nlm.nih.gov/geo/query/acc.cgi?acc=GSE74847). The heatmaps were generated for differentially expressed miRNAs and mRNAs at $p < 0.05$.

4.3. Principal component analysis

After scaling raw expression data, principal component analysis (PCA) was performed for miRNAs using singular value decomposition, as outlined previously [33]. A set of highly expressed miRNAs whose minimum signal values were greater than 100 were selected, and principal component axes were defined. The six control and RANKL-treated samples (C1-C3 and R1-R3) as well as highly expressed miRNAs were mapped on the first and second principal component plane.

4.4. In silico prediction of miRNA target genes

In predicting miRNA target genes, we focused on miRNAs that were differentially expressed between the RANKL and control samples ($p < 0.05$) with a maximum signal value above 100. First, potential target genes were pre-selected, using the 3'-end of each gene's untranslated sequence using 10 different prediction algorithms (miRWalk [15], Microt4 [34], miRanda [35], miRDB [36], miRMap [37], miRNAMap [38], PITA [39], RNA22 [40], RNAhybrid [16], and Targetscan [41]). Second, from the above potential genes, we further chose the genes that were responsive to treatment with RANKL (FDR-corrected $p < 0.05$) and had fold change greater than 1.5. Lastly, using Gene Ontology annotations the genes relating to osteoclasts were filtered and selected as target genes. For each of the target genes, the number of positive hits among the 10 algorithms was grayscale-coded as a confidence measure of *in silico* prediction.

4.5. Transfection of the inhibitor and mimic of miR-221-3p, miR-222-3p and c-Src siRNA

Cells were treated with the inhibitor and mimicking agent of miR-221-3p and miR-222-3p, as well as siRNA specific to c-Src (Life Technologies). The selected target sequences were: 5'-

AGC UAC AUU GUC UGC UGG GUU UC -3' (inhibitor and mimic of miR-221-3p); 5'-AGC UAC AUC UGG CUA CUG GGU-3' (inhibitor and mimic of miR-222-3p); and 5'-GGA AGA ACC CAU UUA CAU U-3' (c-Src siRNA). As a nonspecific control, mirVana™ miRNA Inhibitor Negative Control #1 (5'- UUACGUCGUCGCGUCGUUAU -3'), mirVana™ miRNA Mimic Negative Control #1 (5'- UAACGACGCGACGACGUAA -3'), and a negative siRNA (5'-UGU ACU GCU UAC GAU UCG G-3') (Life technologies) were used. Cells were transiently transfected with siRNA for c-Src or control in Opti-MEM I medium with Lipofectamine RNAiMAX (Life Technologies). Twelve hours later, the medium was replaced by regular culture medium. The efficiency of silencing was assessed with immunoblotting or quantitative PCR 48-72 h after transfection.

4.6. Quantitative real-time PCR

Total RNA was extracted using an RNeasy Plus mini kit (Qiagen, Germantown, MD, USA). Reverse transcription was conducted with high capacity cDNA reverse transcription kits (Applied Biosystems, Carlsbad, CA, USA), and quantitative real-time PCR was performed using ABI 7500 with Power SYBR green PCR master mix kits (Applied Biosystems). We evaluated miRNA levels of miR-27b-3p, miR-125b-5p, miR-146a-5p, miR-182-5p, miR-221-3p, and miR-222-3p (Table 1), as well as mRNA levels of NFATc1, TRAP, cathepsin K, Dcstamp, and c-Src using primers listed in Table 2. SnoRNA202 (for miRNA) and GAPDH (for mRNA) were used for internal control.

4.7. Western Immunoblotting

Cells were lysed in a radioimmunoprecipitation assay (RIPA) buffer containing protease inhibitors (Santa Cruz Biotechnology, Santa Cruz, CA, USA) and phosphatase inhibitors (Calbiochem, Billerica, MA, USA). Isolated proteins were fractionated using 10-12% SDS gels and electro-transferred to Immobilon-P membranes (Millipore, Billerica, MA, USA). The membrane was incubated for 1 h with primary antibodies followed by 45 min incubation with goat anti-rabbit or anti-mouse IgG conjugated with horseradish peroxidase (Cell Signaling, Danvers, MA, USA). We used antibodies against NFATc1 and cathepsin K (Santa Cruz), TRAP (Abcam), c-Src (Cell Signaling), and β-actin (Sigma). Protein levels were assayed using a SuperSignal west femto maximum sensitivity substrate (Thermo Scientific), and signal intensities were quantified with a luminescent image analyzer (LAS-3000, Fuji Film, Tokyo, Japan).

4.8. Live cell imaging for c-Src activity using FRET

To visualize the activity of c-Src in response to the inhibitor of miR-222-3p, FRET imaging was conducted using cyan fluorescent protein (CFP)-yellow fluorescent protein (YFP) c-Src biosensor. The biosensors were transfected into the cells using a Neon transfection system (Life Technologies). Time-lapse images of c-Src FRET activity were acquired at an interval of 2 min using a fluorescence microscope (Nikon, Tokyo, Japan). The filter sets were chosen for CFP excitation at 438 ± 24 nm (center wavelength ± bandwidth), CFP emission at 483 ± 32 nm, and YFP emission at 542 ± 27 nm. The level of c-Src activity was determined by computing an emission ratio of CFP/YFP for individual cells using NIS-Elements software (Nikon). The FRET ratio images were scaled according to the color bar.

4.9. TRAP staining and bond resorption assay

For TRAP staining, RAW264.7 cells were transfected with non-specific control siRNA or Src siRNA and cultured for 4 days in a 96-well plate (0.5×10^4 cells/well) in the presence and absence of 50 ng/ml RANKL. Cells were then treated for TRAP staining using an acid phosphatase leukocyte kit (Sigma, St. Louis, MO, USA). The number of TRAP-positive cells containing three or more nuclei was determined. For a bone resorption assay, RAW264.7 cells were plated at 2.5×10^3 cells/well using a bone resorption assay plate (Cosmo Bio, Tokyo, Japan) and cultured with 50 ng/ml RANKL for 5 days. Cells were then removed from the plate, and the pit area generated by osteoclast activity was determined using an optical microscope (TS100, Nikon, Tokyo, Japan).

4.10. Statistical analysis

Three or four-independent experiments were conducted and data were expressed as mean ± S.D. For comparison among multiple samples, ANOVA followed by *post hoc* tests was conducted. For the mRNA microarray, a Benjamini-Hochberg correction was applied to determine the false detection rate. Statistical significance was evaluated at $p < 0.05$. The single and double asterisks and daggers indicate $p < 0.05$ and $p < 0.01$, respectively. To determine intensities in immunoblotting, images were scanned with Adobe Photoshop CS2 (Adobe Systems, San Jose, CA, USA) and quantified using Image J.

5. Conclusions

This study revealed that miR-222-3p suppresses RANKL-driven osteoclastogenesis. The observed suppression was mediated by c-Src, since inhibition of miR-222-3p elevated expression of c-Src and a partial silencing of c-Src reduced expression of the osteoclast marker genes such as TRAP and cathepsin K. The role of miRNAs has not been fully understood in bone-related metabolic diseases and cancer. The result in this study may contribute to developing a novel therapeutic strategy for prevention of bone loss in many skeletal diseases.

Acknowledgements

This study was supported by the grant DOD W81XWH-11-1-0716 (HY) and NIH AR065148 (SN). Microarray experiments were in part supported by the CTSA grant NIH U54 TR001012. All authors state that they have no conflicts of interest.

Authors' contributions

S.T., A.S., H.Y., and K.H. designed the research. S.T., A.C., Q.W., S.N., and K.H. performed the experiments and analyzed the data. S.T., A.C., H.Y., and K.H. wrote the manuscript. All authors read and approved the final manuscript.

Conflicts of Interest

The authors declare no conflict of interest.

References

1. Bartel, D.P. MicroRNAs: genomics, biogenesis, mechanism, and function. *Cell* **2004,** *116,* 281-297.
2. Calin, G.A.; Croce, C.M. MicroRNA signatures in human cancers. *Nat. Rev. Cancer* **2006,** *6,* 857-866.
3. Xu, Q.; Li, P.; Chen, X.; Zong, L.; Jiang, Z.; Nan, L.; Lei, J.; Duan, W.; Zhang, D.; Li, X.; *et al*. miR-221/222 induces pancreatic cancer progression through the regulation of matrix metalloproteinases. *Oncotarget.* **2015,** *6,* 14153-14164.
4. Corsten, M.F.; Dennert, R.; Jochems, S.; Kuznetsova, T.; Devaux, Y.; Hofstra, L.; Wagner, D.R.; Staessen, J.A.; Heymans, S.; Schroen, B.; *et al*. Circulating MicroRNA-208b and MicroRNA-499 reflect myocardial damage in cardiovascular disease. *Genet.* **2010,** *3,* 499-506.
5. Bak, M.; Silahtaroglu, A.; Møller, M.; Christensen, M.; Rath, M.F.; Skryabin, B.; Tommerup, N.; Kauppinen, S.; *et al*. MicroRNA expression in the adult mouse central nervous system. *RNA* **2008,** *14,* 432-444.
6. Rottiers, V.; Näär, A.M. MicroRNAs in metabolism and metabolic disorders. *Nat. Rev. Mol. Cell Biol.* **2012,** *13,* 239-250.
7. Hatfield, S.D.; Shcherbata, H.R.; Fischer, K.A.; Nakahara, K.; Carthew, R.W.; Ruohola-Baker, H. Stem cell division is regulated by the microRNA pathway. *Nature* **2005,** *435,* 974-978.
8. Takayanagi, H.; Kim, S.; Koga, T.; Nishina, H.; Isshiki, M.; Yoshida, H.; Saiura, A.; Isobe, M.; Yokochi, T.; Inoue, J.; *et al*. Induction and activation of the transcription factor

NFATc1 (NFAT2) integrate RANKL signaling in terminal differentiation of osteoclasts. *Dev. Cell* **2002,** *3,* 889-901.

9. Franceschetti, T.; Dole, N.S.; Kessler, C.B.; Lee, S.K.; Delany, A.M. Pathway analysis of microRNA expression profile during murine osteoclastogenesis. *PLoS One* **2014,** *9,* e107262.
10. Sugatani, T.; Hruska, K.A. MicroRNA-223 is a key factor in osteoclast differentiation. *J. Cell. Biochem.* **2007,** *101,* 996-999.
11. Ell, B.; Mercatali, L.; Ibrahim, T.; Campbell, N.; Schwarzenbach, H.; Pantel, K.; Amadori, D.; Kang, Y.; *et al*. Tumor-induced osteoclast miRNA changes as regulators and biomarkers of osteolytic bone metastasis. *Cancer Cell* **2013,** *24,* 542-556.
12. Krzeszinski, J.Y.; Wei, W.; Huynh, H.; Jin, Z.; Wang, X.; Chang, T.C.; Xie, X.J.; He, L.; Mangala, L.S.; Lopez-Berestein, G.; et al. miR-34a blocks osteoporosis and bone metastasis by inhibiting osteoclastogenesis and Tgif2. *Nature.* **2014,** *512,* 431-435.
13. M'Baya-Moutoula, E1.; Louvet, L.; Metzinger-Le, Meuth, V.; Massy, Z.A.; Metzinger, L. High inorganic phosphate concentration inhibits osteoclastogenesis by modulating miR-223. *Biochim Biophys Acta.* **2015,** *1852,*2202-2212.
14. Zhao, Z.J.; Shen, J. Circular RNA Participates in the Carcinogenesis and the Malignant Behavior of Cancer. *RNA Biol.* **2015,** Dec 9:0. [Epub ahead of print]
15. Dweep, H.; Sticht, C.; Pandey, P.; Gretz, N. miRWalk--database: prediction of possible miRNA binding sites by "walking" the genes of three genomes. *J. Biomed. Inform.* **2011,** *44,* 839-847.
16. Rehmsmeier, M.; Steffen, P.; Hochsmann, M.; Giegerich, R. Fast and effective prediction of microRNA/target duplexes. *RNA* **2004,** *10,* 1507-1517.

17. Boyce, B.F.; Yoneda, T.; Lowe, C.; Soriano, P.; Mundy, G.R.; Requirement of pp60c-src expression for osteoclasts to form ruffled borders and resorb bone in mice. *J. Clin. Invest.* **1992,** 90, 1622-1627.

18. Schwartzberg, P.L.; Xing, L.; Hoffmann, O.; Lowell, C.A.; Garrett, L.; Boyce, B.F.; Varmus, H.E.; Rescue of osteoclast function by transgenic expression of kinase-deficient Src in src-/- mutant mice. *Genes Dev.* **1997,** 11, 2835-2844,

19. Miyazaki, T.; Sanjay, A.; Neff, L.; Tanaka, S.; Horne, W.C.; Baron, R. Src kinase activity is essential for osteoclast function. *J. Biol. Chem.* **2004,** *279,* 17660-17666.

20. Yagi, M.; Miyamoto, T.; Sawatani, Y.; Iwamoto, K.; Hosogane, N.; Fujita, N.; Morita, K., Ninomiya, K.; Suzuki, T.; Miyamoto, K.; Oike, Y.; Takeya, M.; Toyama, Y.; Suda, T.; DC-STAMP is essential for cell-cell fusion in osteoclasts and foreign body giant cells. *J. Exp. Med.* **2005,** 202, 345-351.

21. Peterson, S.M.; Thompson, J.A.; Ufkin, M.L.; Sathyanarayana, P.; Liaw, L.; Congdon, C.B. Common features of microRNA target prediction tools. *Front. Genet.* **2014,** *5,* 23.

22. Witkos, T.M.; Koscianska, E.; Krzyzosiak, W.J. Practical aspects of microRNA target prediction. *Cur. Mol. Med.* **2011,** *11,* 93-109.

23. Ohtsuka, M.; Ling, H.; Doki, Y.; Mori, M.; Calin, G.A. MicroRNA processing and human cancer. *J. Clin. Med.* **2015,** *4,* 1651-1667.

24. Saiselet, M.; Gacquer, D.; Spinette, A.; Craciun, L.; Decaussin-Petrucci, M.; Andry, G.; Detours, V.; Maenhaut, C. New global analysis of the microRNA transcriptome of primary tumors and lymph node metastases of papillary thyroid cancer. *BMC Genomics.* **2015,** *16,* 828.

25. Kara, M.; Yumrutas, O.; Ozcan, O.; Celik, O.; Bozgeyik, E.; Bozgeyik, I.; Tasdemir, S. Differential expressions of cancer associated genes and their regulatory miRNA in colorectal carcinoma. *Gene* **2015,** *567,* 81-86.

26. Song, C.; Chen, H.; Wang, T.; Zhang, W.; Ru, G.; Lang, J. Expression profile analysis of microRNAs in prostate cancer by next-generation sequencing. *Prostate* **2015,** *75,* 500-516.

27. Goto, Y.; Kojima, S.; Nishikawa, R.; Kurozumi, A.; Kato, M.; Enokida, H.; Matsushita, R.; Yamazaki, K.; Ishida, Y.; Nakagawa, M.; et al. MicroRNA expression signature of castration-resistant prostate cancer: the microRNA-221/222 cluster functions as a tumour suppressor and disease progression marker. *Br J Cancer.* **2015,** *113,* 1055-1065.

28. Dentelli, P.; Rosso, A.; Orso, F.; Olgasi, C.; Taverna, D.; Brizzi, M.F. microRNA-222 controls neovascularization by regulating signal transducer and activator of transcription 5A expression. *Arterioscler Thromb Vasc Biol.* **2010,** *30,* 1562-1568.

29. Lopes, F.C.; Ferreira, R.; Albuquerque, D.M.: Silveira, A.A.; Costa, R.; Soares, R.; Costa, F.F.; Conran, N. In vitro and in vivo anti-angiogenic effects of hydroxyurea. *Microvasc Res.* **2014,** *94,* 106-113.

30. Perry, M.M.; Baker, J.E.; Gibeon, D.S.; Adcock, I.M.; Chung, K.F. Airway smooth muscle hyperproliferation is regulated by microRNA-221 in severe asthma. *Am J Respir Cell Mol Biol.* **2014,** *50,* 7-17.

31. Hamamura, K.; Chen, A.; Tanjung, N.; Takigawa, S.; Sudo, A.; Yokota, H. In vitro and in silico analysis of an inhibitory mechanism of osteoclastogenesis by salubrinal and guanabenz. *Cell. Signal.* **2015,** *27,* 353-362.

32. Edgar, R.; Domrachev, M.; Lash, A.E. Gene Expression Omnibus: NCBI gene expression and hybridization array data repository. *Nucl. Acids Res.* **2002,** *30,* 207-210.

33. Hamamura, K.; Chen, A.; Nishimura, A.; Tanjung, N.; Sudo, A.; Yokota, H. Predicting and validating the pathway of Wnt3a-driven suppression of osteoclastogenesis. *Cell. Signal.* **2014,** *26,* 2358-2369.

34. Maragkakis, M.; Vergoulis, T.; Alexiou, P.; Reczko, M.; Plomaritou, K.; Gousis, M.; Kourtis, K.; Koziris, N.; Dalamagas, T.; Hatzigeorgiou, A.G. DIANA-microT Web server upgrade supports Fly and Worm miRNA target prediction and bibliographic miRNA to disease association. *Nucl. Acids Res.* **2011,** *39,* W145-148.

35. Betel, D.; Koppal, A.; Agius, P.; Sander, C.; Leslie, C. Comprehensive modeling of microRNA targets predicts functional non-conserved and non-canonical sites. *Genome Biol.* **2010,** *11,* R90.

36. Wang, X.; EI, Naqa, IM. Prediction of both conserved and nonconserved microRNA targets in animals. *Bioinformatics.* **2008,** *24,* 325-332.

37. Vejnar, C.E.; Blum, M.; Zdobnov, E.M. miRmap web: Comprehensive microRNA target prediction online. *Nucleic. Acids Res.* **2013,** *41,* W165-168.

38. Hsu, S.D.; Chu, C.H.; Tsou, A.P.; Chen, S.J.; Chen, H.C.; Hsu, P.W.; Wong, Y.H.; Chen, Y.H.; Chen, G.H.; Huang, H.D. miRNAMap 2.0: genomic maps of microRNAs in metazoan genomes. *Nucleic. Acids Res.* **2008,** *36,* D165-169.

39. Kertesz, M.; Iovino, N.; Unnerstall, U.; Gaul, U.; Segal, E. The role of site accessibility in microRNA target recognition. *Nat. Genet.* **2007,** *39,* 1278-1284.

40. Loher, P.; Rigoutsos, I. Interactive exploration of RNA22 microRNA target predictions. Bioinformatics. *Bioinformatics* **2012,** *28,* 3322-3323.

41. Friedman, R.C.; Farh, K.K.; Burge, C.B.; Bartel, D.P. Most mammalian mRNAs are conserved targets of microRNAs. *Genome Res.* **2009,** *19,* 92-105.

Tables

Table 1. Targeted miRNA sequences.

miRNA	targeted miRNA sequences
27b-3p	5’- UUCACAGUGGCUAAGUUCUGC -3’
125b-5p	5’- UCCCUGAGACCCUAACUUGUGA -3’
146a-5p	5’- UGAGAACUGAAUUCCAUGGGUU -3’
182-5p	5’- UUUGGCAAUGGUAGAACUCACACCG -3’
221-3p	5’- AGCUACAUUGUCUGCUGGGUUUC -3’
222-3p	5’- AGCUACAUCUGGCUACUGGGU -3’
SnoRNA202	5’- GCTGTACTGACTTGATGAAAGTACTTTTGAACCCTTTTCCATCTGATG -3’

Table 2. Real-time PCR primers for mRNAs.

gene	forward primer	backward primer
c-Src	5’- TCCTTTGGGATTCTGCTGAC -3’	5’- TGTGGCTCAGTGGACGTAAA -3’
cat K	5’- CAGCTTCCCCAAGATGTGAT -3’	5’- AGCACCAACGAGAGGAGAAA -3’
Dcstamp	5’-AAAACCCTTGGGCTGTTCTT-3’	5’-AATCATGGACGACTCCTTGG-3’
NFATc1	5’- GGTGCTGTCTGGCCATAACT -3’	5’- GCGGAAAGGTGGTATCTCAA -3’
TRAP	5’- TCCTGGCTCAAAAAGCAGTT -3’	5’- ACATAGCCCACACCGTTCTC -3’
GAPDH	5’- TGCACCACCAACTGCTTAG -3’	5’- GGATGCAGGGATGATGTTC -3’

Figure Legends

Figure 1. Microarray-based miRNA expression analysis. Cells were stimulated with 20 ng/ml RANKL for 2 days. (A) Heat map of the selected miRNAs (signal values < 500 and $p < 0.05$) in response to RANKL. The green and red colors indicate downregulation and upregulation, respectively. Of note, C1, C2, and C3 are control samples, and R1, R2, and R3 are RANKL-treated samples. (B) PCA for 6 samples (C1-C3, and R1-R3) in the first and second principal plane. (C) PCA for miRNAs in the first and second principal plane. Two miRNAs (221-3p and 222-3) are positioned with the smallest values along the second principal axis.

Figure 2. PCR-based mRNA and miRNA expression levels on days 2 and 4 after RANKL addition (n = 5). CN = control sample; and RANKL = RANKL-treated sample (20 ng/ml). (A) NFATc1 mRNA level. (B) TRAP mRNA level. (C) miR-125b-5b level. (D) miR-146a-5p level. (E) miR-182-5p level. (F) miR-27b-3p level. (G) miR-221-3p level. (H) miR-222-3p level.

Figure 3. Effects of miR221-3p inhibitor and mimicking agent. Of note, 50 ng/ml RANKL was used for 1 day in (C) and (D). The sample number was 3 in (A) and (B), 4 in (C), and 6 in (D). NC = non-specific control. (A) miR-221-3p level in response to its inhibitor. (B) miR-221-3p level in response to its mimicking agent. (C) NFATc1, TRAP, and cathepsin K mRNA levels in response to miR-221-3p inhibitor. (D) NFATc1, TRAP, and cathepsin K mRNA levels in response to miR-221-3p mimic.

Figure 4. Effects of miR222-3p inhibitor and mimicking agent. Of note, 50 ng/ml RANKL was used for 1 day in (C) and (D). The sample number was 3 in (A) and (B), and 4 in (C) and (D). NC = non-specific control. (A) miR-222-3p level in response to its inhibitor. (B) miR-222-3p level in response to its mimicking agent. (C) NFATc1, TRAP, and cathepsin K mRNA levels in response to miR-222-3p inhibitor. (D) NFATc1, TRAP, and cathepsin K mRNA levels in response to miR-222-3p mimic.

Figure 5. Western blot analysis of NFATc1, TRAP, and cathepsin K in response to the inhibitor or mimic specific to miR-222-3p. Of note, 50 ng/ml RANKL was used for 3 days in all cases. The sample number was 3 in (C) and (D). NC = non-specific control; inh = inhibitor; and mim = mimicking agent. (A) Expression of NFATc1, TRAP, and cathepsin K in response to the inhibitor of miR-222-3p. (B) Expression of NFATc1, TRAP, and cathepsin K in response to the mimic of miR-222-3p. (C & D) Quantified expression levels of TRAP and cathepsin K, respectively, in response to the inhibitor and mimic of miR-222-3p.

Figure 6. RANKL responsive genes and their potential link to miRNAs. (A) Heat map of RANKL-responsive genes that are related to osteoclasts. The blue and red colors indicate downregulation and upregulation, respectively. Note that CN1, CN2, and CN3 are control samples, and RN1, RN2, and RN3are RANKL-treated samples. (B) Predicted link between RANKL-responsive genes and miRNAs. The grey code indicates a confidence measure of *in silico* prediction.

Figure 7. Responses of c-Src and Dcstamp to the inhibitor of miR-222-3p. Of note, 50 ng/ml RANKL was used for 1 day. The sample number was 4 in (A), and the scale bar is 10 μm in (B). NC = non-specific control; and inh = inhibitor of miR-222-3p. (A) c-Src and Dcstamp mRNA levels in response to the inhibitor of miR-222-3p. (B) c-Src activity levels in response to the inhibitor of miR-222-3p.

Figure 8. Effects of c-Src siRNA. Of note, 50 ng/ml RANKL was used for 2 days in (B) – (E). The sample number was 3 in all cases. NC = non-specific control siRNA. (A) c-Src mRNA levels in response to c-Src siRNA. (B) Western blot analysis of c-Src, NFATc1, TRAP, and cathepsin K in response to c-Src siRNA. (C) Quantified protein levels of c-Src in response to c-Src siRNA. (D) Quantified protein levels of NFATc1, TRAP and cathepsin K in response to c-Src siRNA. (E) Levels of miR-221-3p and miR-222-3p in response to c-Src siRNA.

Figure 9. TRAP staining and osteoclast activity in the presence of c-Src siRNA. NC = non-specific control siRNA. (A & B) Number of multi-nucleated cells and TRAP staining in the presence and absence of 50 ng/ml RANKL for 4 days. (C & D) Number of pits and their images in the presence and absence of 50 ng/ml RANKL for 5 days.

Figure 10. Schematic illustration of the role of miR-222-3p in RANKL-stimulated osteoclastogenesis.

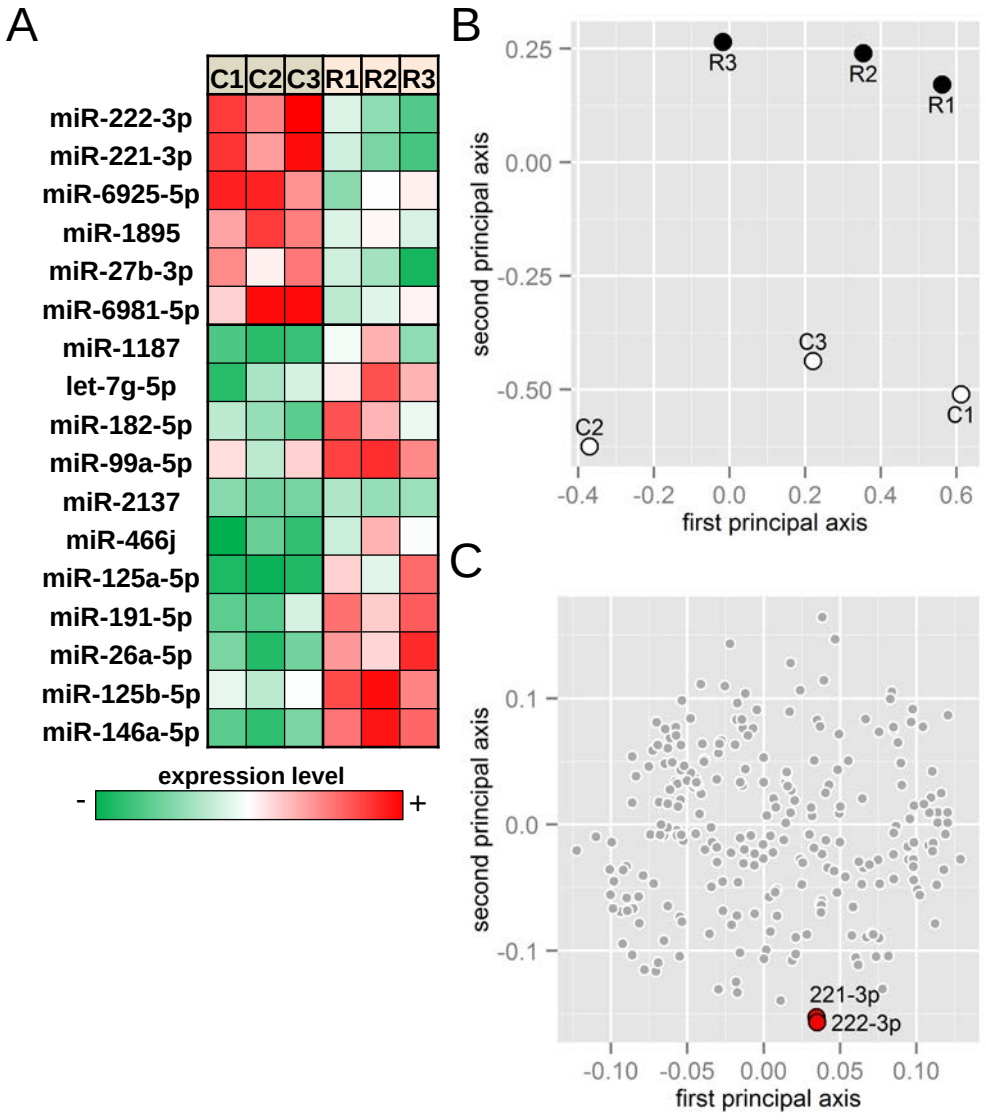
A
C1
C2
C3
R1
R2
R3
miR-222-3p
miR-221-3p
miR-6925-5p
miR-1895
miR-27b-3p
miR-6981-5p
miR-1187
let-7g-5p
miR-182-5p
miR-99a-5p
miR-2137
miR-466j
miR-125a-5p
miR-191-5p
miR-26a-5p
miR-125b-5p
miR-146a-5p
expression level
-
+
B
second principal axis
first principal axis
0.25
0.00
-0.25
-0.50
-0.4
-0.2
0.0
0.2
0.4
0.6
C
second principal axis
first principal axis
0.1
0.0
-0.1
-0.10
-0.05
0.00
0.05
0.10
221-3p
222-3p

Figure 1

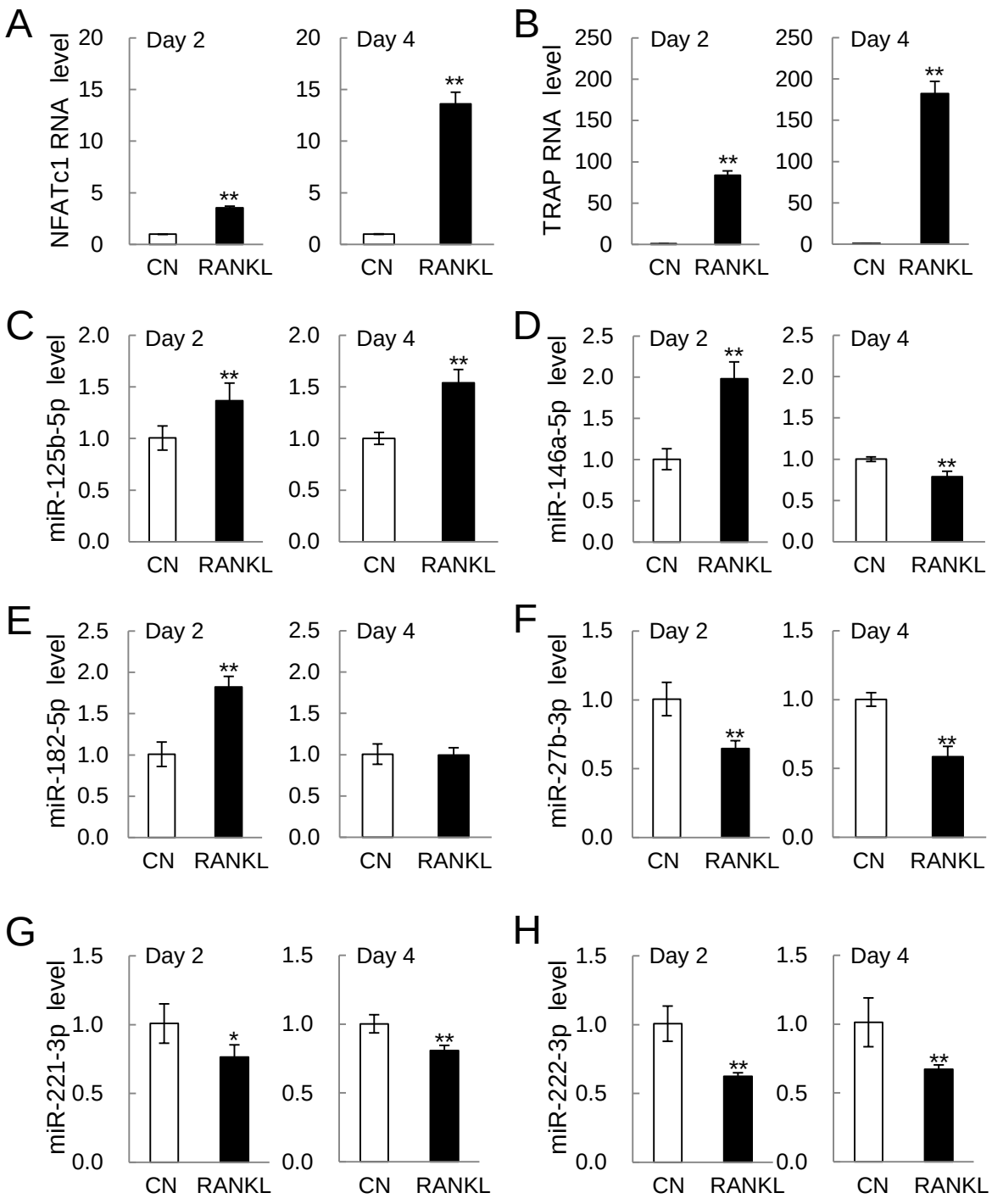
A
NFATc1 RNA level
Day 2
Day 4
CN
RANKL
B
TRAP RNA level
C
miR-125b-5p level
D
miR-146a-5p level
E
miR-182-5p level
F
miR-27b-3p level
G
miR-221-3p level
H
miR-222-3p level

Figure 2

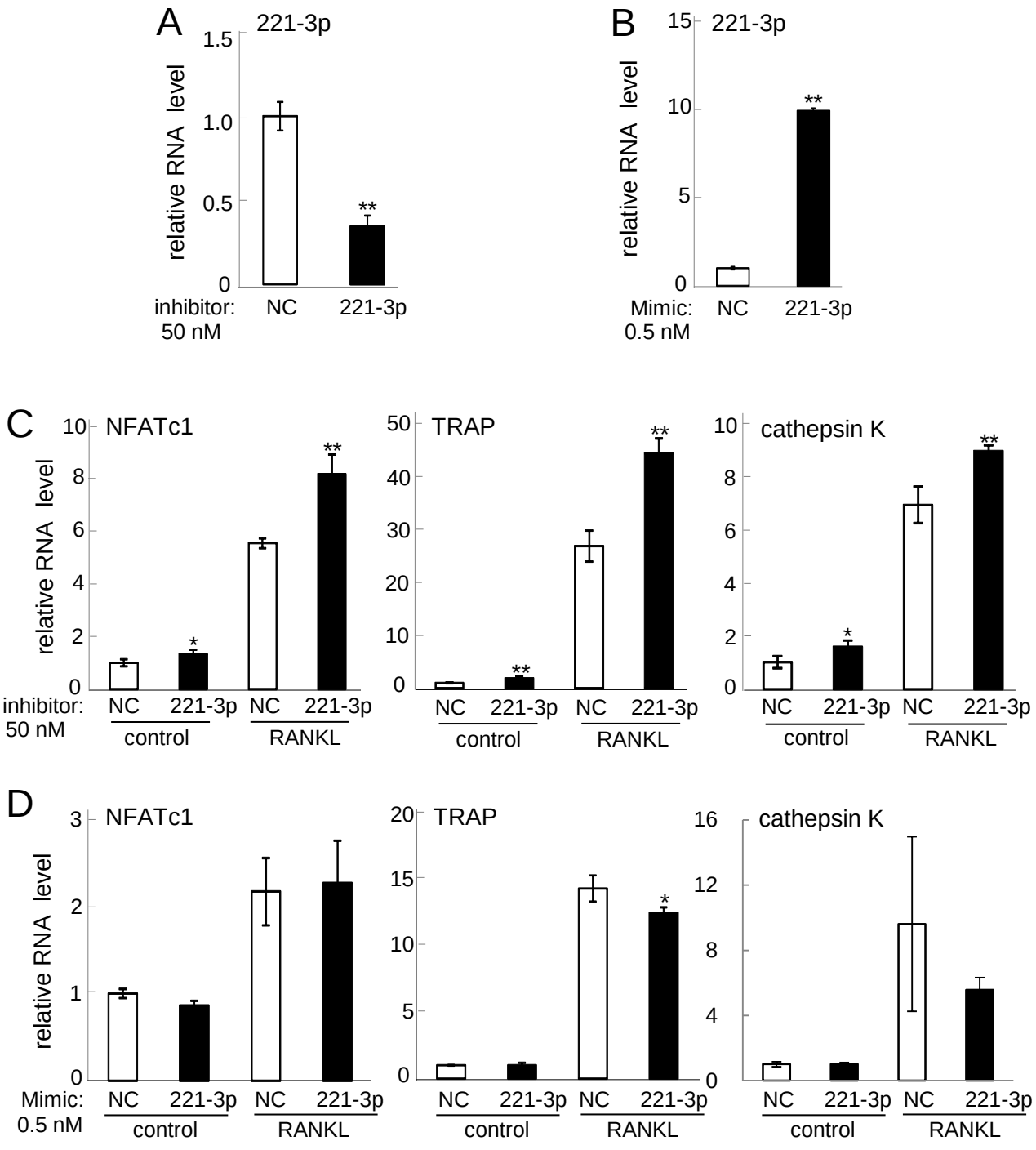
A
221-3p
relative RNA level
1.5
1.0
0.5
0
**
inhibitor:
50 nM
NC
221-3p
B
221-3p
relative RNA level
15
10
5
0
**
Mimic:
0.5 nM
NC
221-3p
C
NFATc1
relative RNA level
10
8
6
4
2
0
*
**
TRAP
50
40
30
20
10
0
**
**
cathepsin K
10
8
6
4
2
0
*
**
inhibitor:
50 nM
NC
221-3p
NC
221-3p
control
RANKL
D
NFATc1
relative RNA level
3
2
1
0
TRAP
20
15
10
5
0
*
cathepsin K
16
12
8
4
0
Mimic:
0.5 nM
NC
221-3p
NC
221-3p
control
RANKL

Figure 3

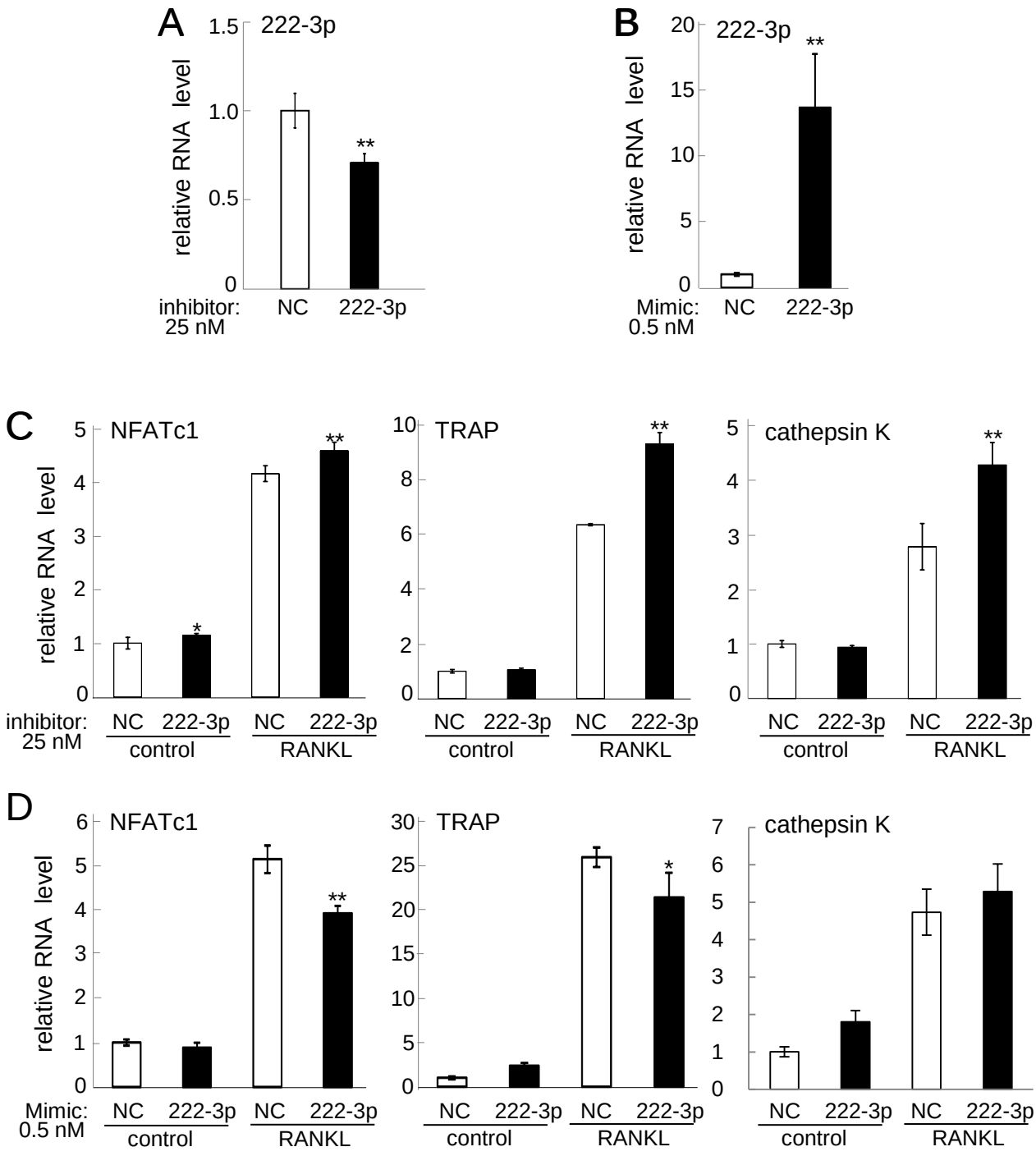
A
222-3p
relative RNA level
1.5
1.0
0.5
0
**
inhibitor:
25 nM
NC
222-3p
B
222-3p
relative RNA level
20
15
10
5
0
**
Mimic:
0.5 nM
NC
222-3p
C
NFATc1
relative RNA level
5
4
3
2
1
0
*
**
TRAP
10
8
6
4
2
0
**
cathepsin K
5
4
3
2
1
0
**
inhibitor:
25 nM
NC
222-3p
NC
222-3p
control
RANKL
D
NFATc1
relative RNA level
6
5
4
3
2
1
0
**
TRAP
30
25
20
15
10
5
0
*
cathepsin K
7
6
5
4
3
2
1
0
Mimic:
0.5 nM
NC
222-3p
NC
222-3p
control
RANKL

Figure 4

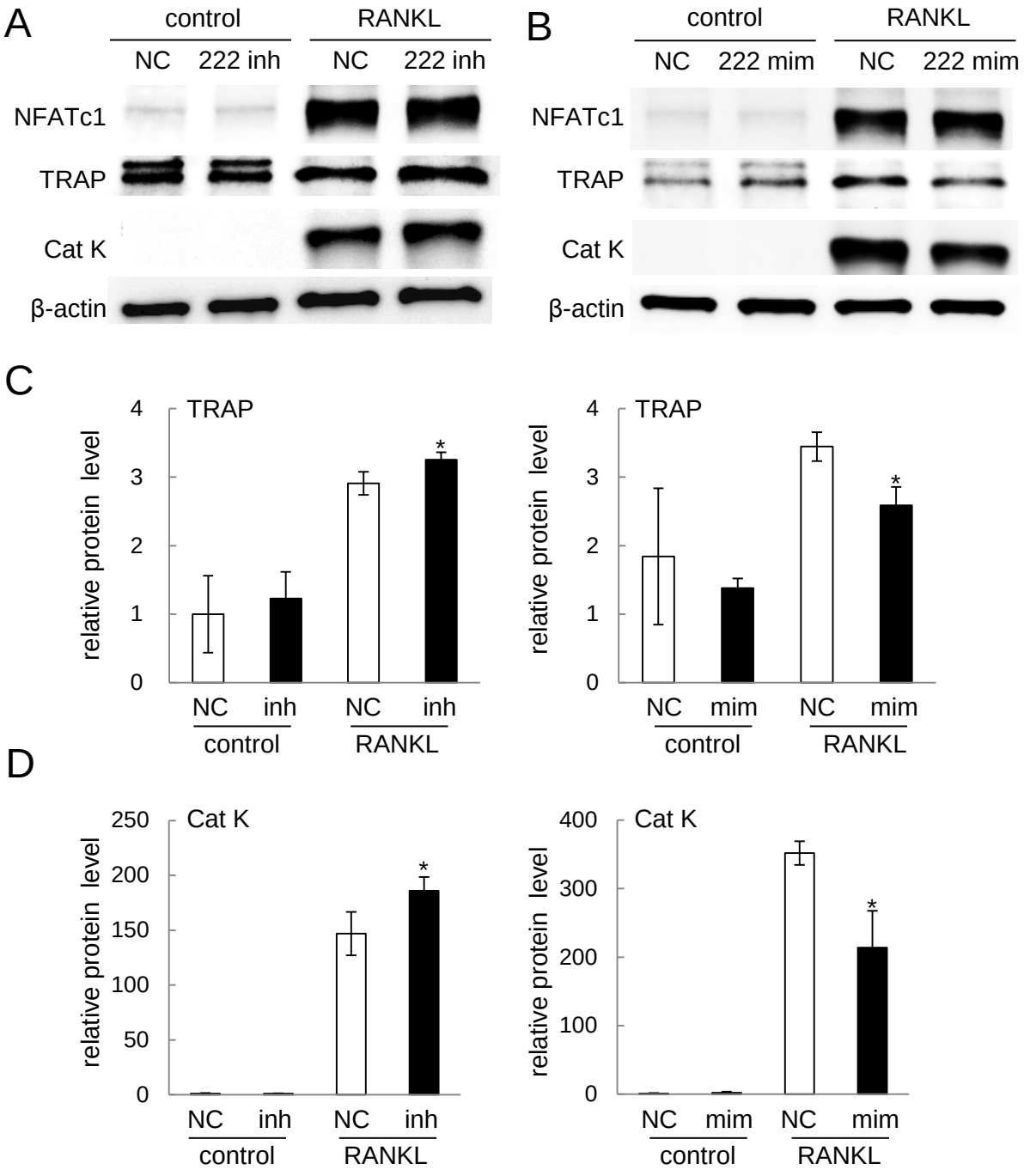
A
control
RANKL
NC
222 inh
NC
222 inh
NFATc1
TRAP
Cat K
β-actin
B
control
RANKL
NC
222 mim
NC
222 mim
NFATc1
TRAP
Cat K
β-actin
C
TRAP
relative protein level
0
1
2
3
4
*
NC
inh
NC
inh
control
RANKL
TRAP
relative protein level
0
1
2
3
4
*
NC
mim
NC
mim
control
RANKL
D
Cat K
relative protein level
0
50
100
150
200
250
*
NC
inh
NC
inh
control
RANKL
Cat K
relative protein level
0
100
200
300
400
*
NC
mim
NC
mim
control
RANKL

Figure 5

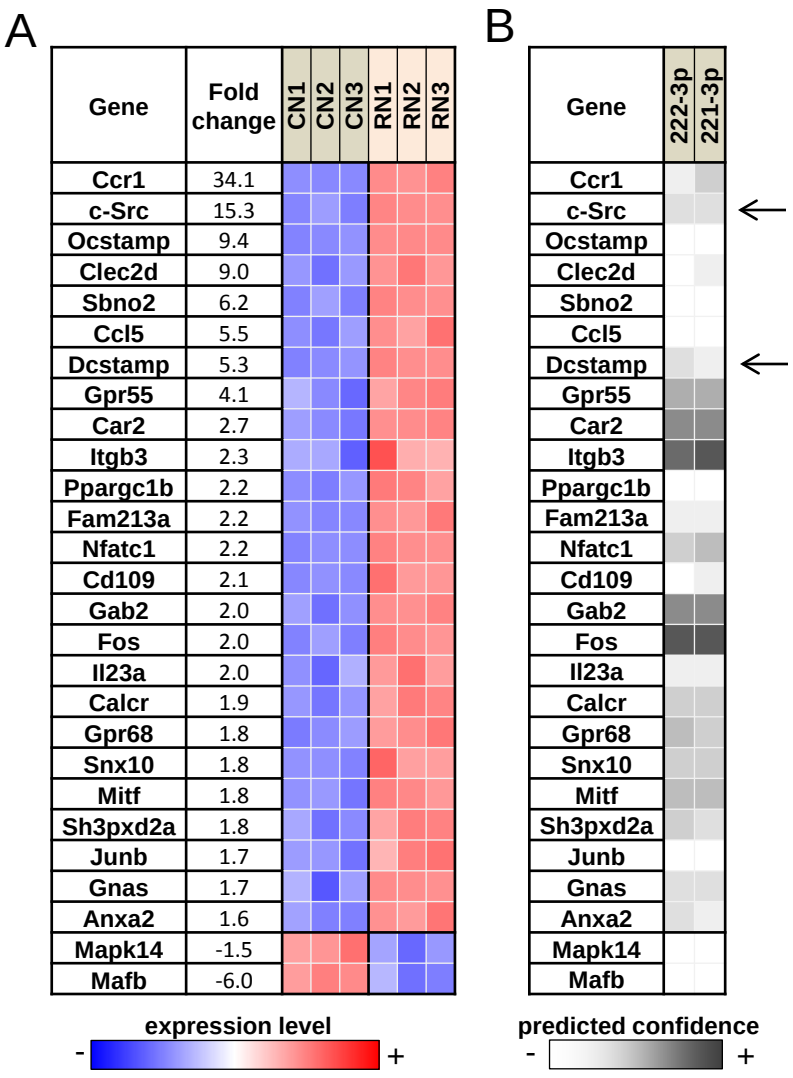
A
Gene
Fold change
CN1
CN2
CN3
RN1
RN2
RN3
Ccr1 34.1
c-Src 15.3
Ocstamp 9.4
Clec2d 9.0
Sbno2 6.2
Ccl5 5.5
Dcstamp 5.3
Gpr55 4.1
Car2 2.7
Itgb3 2.3
Ppargc1b 2.2
Fam213a 2.2
Nfatc1 2.2
Cd109 2.1
Gab2 2.0
Fos 2.0
Il23a 2.0
Calcr 1.9
Gpr68 1.8
Snx10 1.8
Mitf 1.8
Sh3pxd2a 1.8
Junb 1.7
Gnas 1.7
Anxa2 1.6
Mapk14 -1.5
Mafb -6.0
expression level
-
+
B
Gene
222-3p
221-3p
Ccr1
c-Src
Ocstamp
Clec2d
Sbno2
Ccl5
Dcstamp
Gpr55
Car2
Itgb3
Ppargc1b
Fam213a
Nfatc1
Cd109
Gab2
Fos
Il23a
Calcr
Gpr68
Snx10
Mitf
Sh3pxd2a
Junb
Gnas
Anxa2
Mapk14
Mafb
predicted confidence
-
+

Figure 6

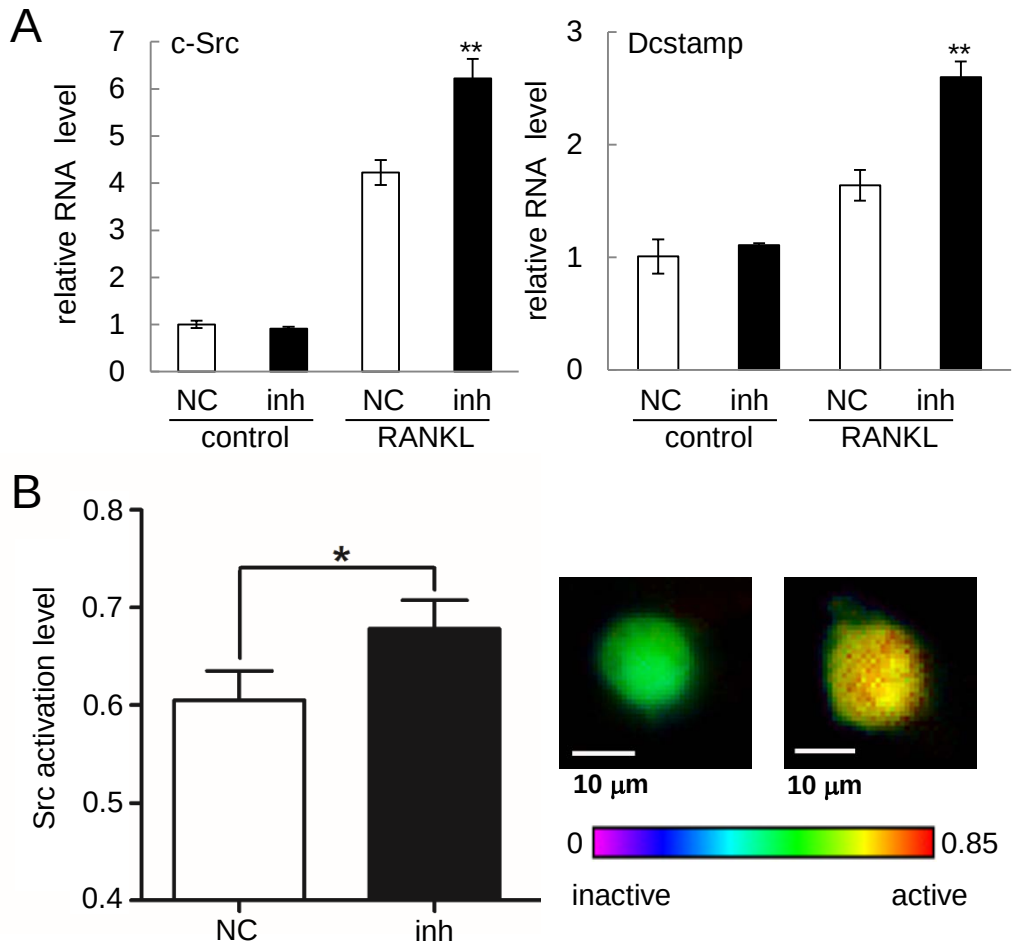
A
c-Src
relative RNA level
7
6
5
4
3
2
1
0
**
NC
inh
NC
inh
control
RANKL
Dcstamp
relative RNA level
3
2
1
0
**
NC
inh
NC
inh
control
RANKL
B
Src activation level
0.8
0.7
0.6
0.5
0.4
*
NC
inh
10 μm
10 μm
0
0.85
inactive
active

Figure 7

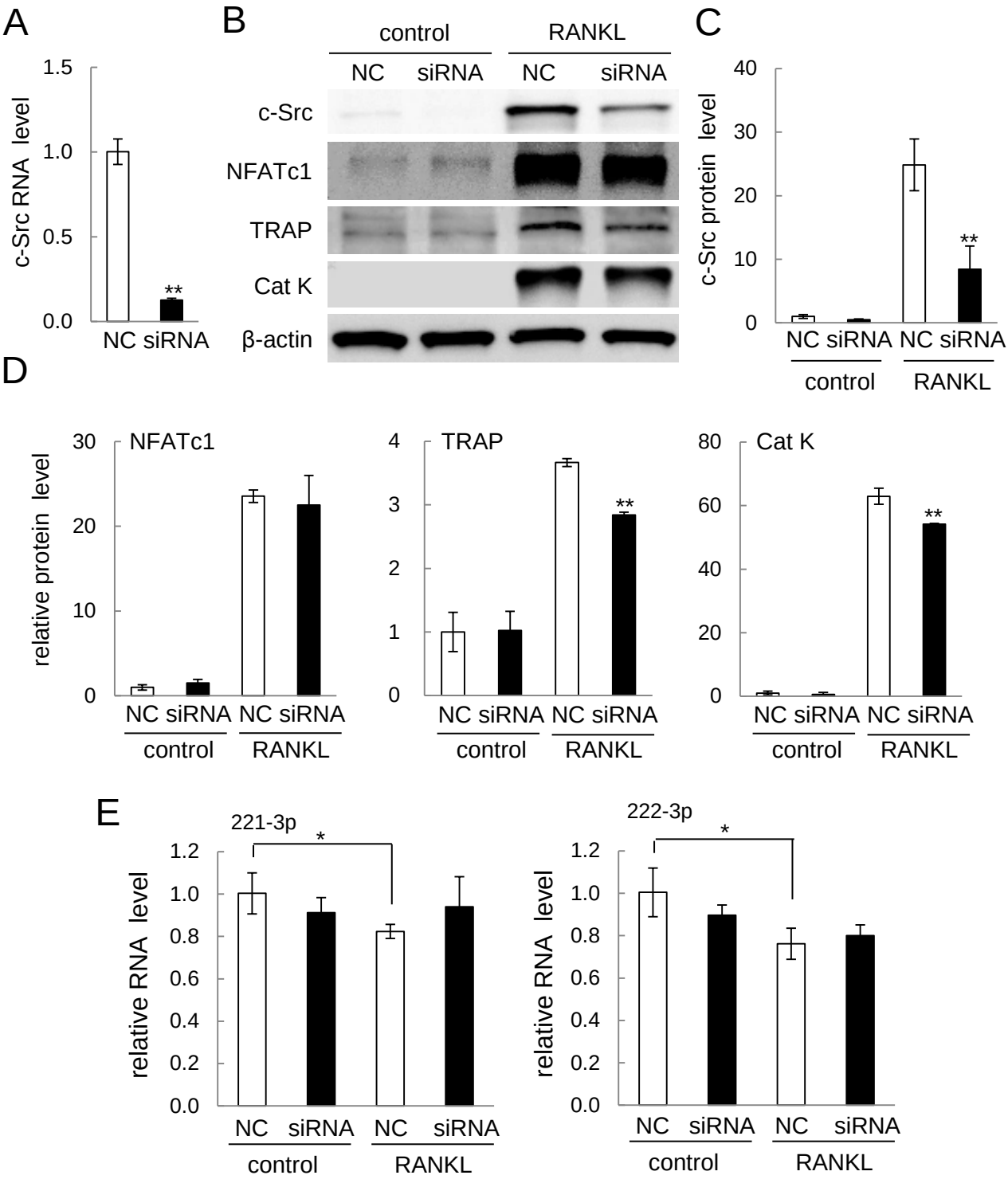
A
c-Src RNA level
1.5
1.0
0.5
0.0
**
NC siRNA
B
control
RANKL
NC
siRNA
NC
siRNA
c-Src
NFATc1
TRAP
Cat K
β-actin
C
c-Src protein level
40
30
20
10
0
**
NC siRNA NC siRNA
control
RANKL
D
relative protein level
NFATc1
30
20
10
0
NC siRNA NC siRNA
control
RANKL
TRAP
4
3
2
1
0
**
NC siRNA NC siRNA
control
RANKL
Cat K
80
60
40
20
0
**
NC siRNA NC siRNA
control
RANKL
E
221-3p
relative RNA level
1.2
1.0
0.8
0.6
0.4
0.2
0.0
*
NC siRNA NC siRNA
control
RANKL
222-3p
relative RNA level
1.2
1.0
0.8
0.6
0.4
0.2
0.0
*
NC siRNA NC siRNA
control
RANKL

Figure 8

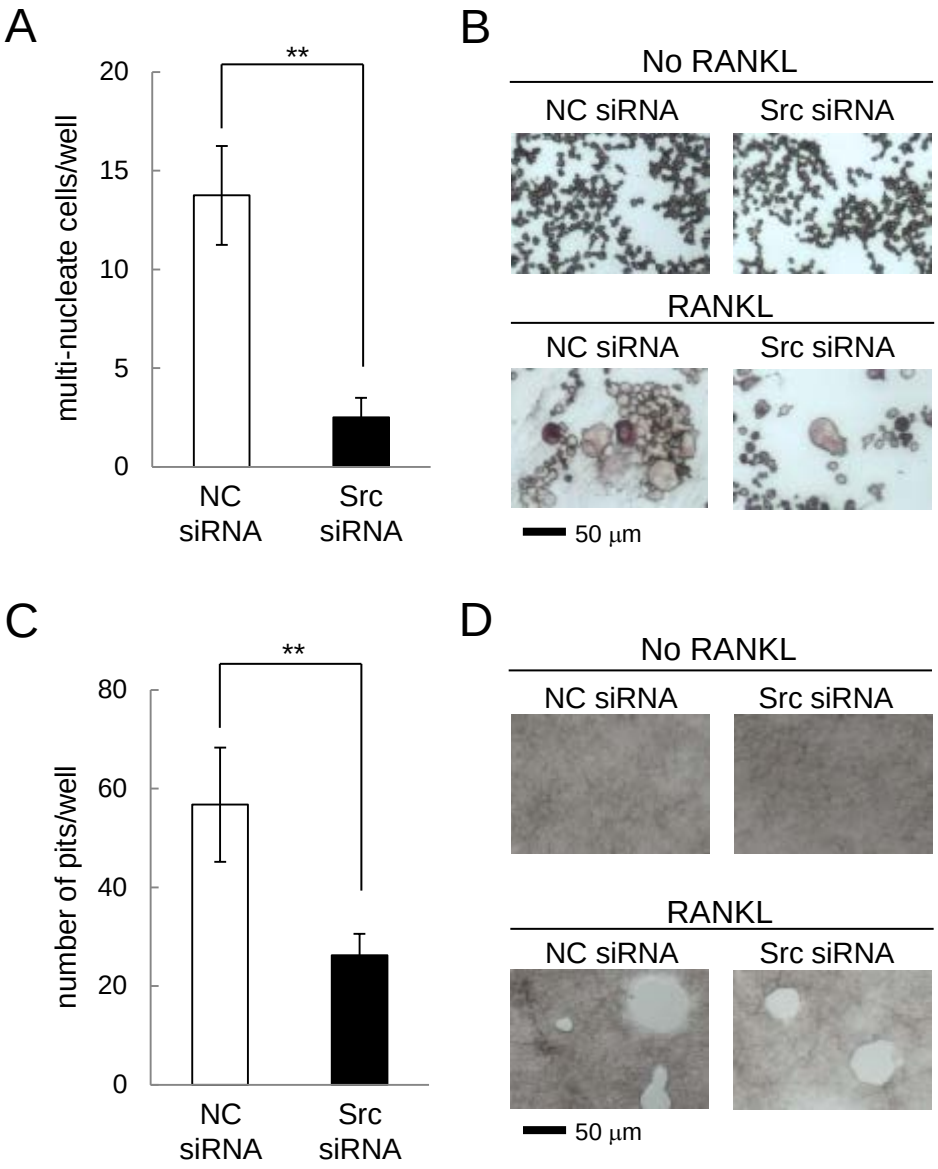
A
**
multi-nucleate cells/well
20
15
10
5
0
NC siRNA
Src siRNA
B
No RANKL
NC siRNA
Src siRNA
RANKL
NC siRNA
Src siRNA
50 μm
C
**
number of pits/well
80
60
40
20
0
NC siRNA
Src siRNA
D
No RANKL
NC siRNA
Src siRNA
RANKL
NC siRNA
Src siRNA
50 μm

Figure 9

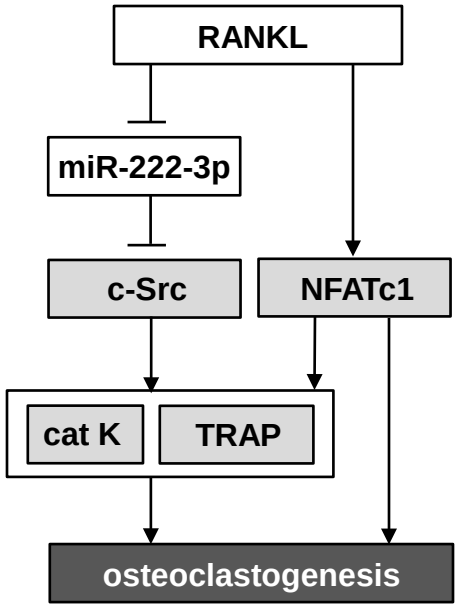

Figure 10

Salubrinal Attenuates Bone Loss in a Mouse Model of Postmenopausal Osteoporosis

Ping Zhang[1,2], Kazunori Hamamura[1], Andy Chen[1], Todd R. Dodge[1], Qiaoqiao Wan[1], Sungsoo Na[1], Munro Peacock[4], Teresita M. Bellido[3], Hiroki Yokota[1,3]

[1]Department of Biomedical Engineering, Indiana University-Purdue University Indianapolis, IN 46202 USA

[2]School of Basic Medical Sciences, Tianjin Medical University, Tanjin 300070, China

[3]Department of Anatomy and Cell Biology, Indiana University School of Medicine, Indianapolis, IN 46202 USA

[4]Department of Medicine, Indiana University School of Medicine, Indianapolis, IN 46202 USA

KEY WARDS: SALUBRINAL; OSTEOPOROSIS; OSTEOCLASTS; OSTEOBLASTS; BONE REMODELING; RAC1; FRET

Running title: Effects of Salubrinal on Ovariectomized Mice

Corresponding Author:

Hiroki Yokota, PhD

Department of Biomedical Engineering

Indiana University-Purdue University Indianapolis

723 West Michigan Street, SL220; Indianapolis, IN 46202

Phone: 317-278-5177

Email: hyokota@iupui.edu

ABSTRACT

Salubrinal is a synthetic chemical that inhibits de-phosphorylation of eukaryotic translation initiation factor 2 alpha (eIF2α). Salubrinal's effects on bone remodeling were studied using a mouse model of postmenopausal osteoporosis and primary and bone cell line cultures. Administration of salubrinal to ovariectomized (OVX) mice suppressed OVX-induced increase in body weight and decrease in bone mineral density. In cultures of primary bone marrow-derived cells, salubrinal increased the colony-forming unit-fibroblast (CFU-F) and osteoblasts (CFU-OBL). It also reduced the formation of mature osteoclasts and suppressed their migration and adhesion. In MC3T3 osteoblast-like cells, salubrinal increased phosphorylation of eIF2α and expression of Activating Transcription Factor 4 (ATF4). In RAW264.7 pre-osteoclasts, salubrinal reduced expression of Nuclear Factor of Activated T-cells cytoplasmic 1 (NFATc1), a master transcription factor for development of osteoclasts. Live cell imaging and a partial silencing by RNA interference demonstrated that suppression of osteoclastogenesis is in part mediated by Rac1 GTPase, which is downregulated by salubrinal-driven elevation of eIF2α phosphorylation. It is concluded that salubrinal attenuates OVX-induced bone loss by altering proliferation and differentiation of pre-osteoblasts and pre-osteoclasts downstream of eIF2α signaling.

Introduction

Bone remodeling is a continuous bone destroying and rebuilding process, undertaken mainly by bone-resorbing osteoclasts and bone-forming osteoblasts.[1] Diminished bone formation[2] and/or excessive bone resorption during bone remodeling results in osteoporosis, a common skeletal disease characterized by low bone mass and increased risk of fractures.[3] In postmenopausal women, bone loss is often induced by a decrease in the production of estrogen that is known to maintain the appropriate ratio of osteoblasts to osteoclasts.[4] Postmenopausal osteoporosis, can be treated by a variety of drugs including antiresorptive agents such as estrogen and estrogen analogs,[5] bisphosphonates,[6-8] denosumab,[9] and odancatib,[10] and anabolic agents including synthetic peptides derived from the parathyroid hormone sequence (Teriparatide),[11, 12] as well as emerging monoclonal therapies targeted to sclerostin.[13] None of them, however, provide an ideal therapeutic option because of side effects and/or limited efficacy.

Salubrinal is a synthetic chemical (480 Da, $C_{21}H_{17}Cl_3N_4OS$) known to block the de-phosphorylation of eukaryotic translation initiation factor 2 alpha(eIF2α).[14] The elevated phosphorylation level of eIF2αactivates translation of Activating Transcription Factor 4 (ATF4), which is one of the key transcription factors in bone formation.[15, 16] Little is known, however, on its effects on the development of bone marrow-derived cells, which give rise to both bone-forming osteoblasts and bone-resorbing osteoclasts. Furthermore, how eIF2α interacts with Rho family GTPases, such as Rac1, which play important roles in bone formation and resorption, remains elusive.[17-19]

The ovariectomized (OVX) mouse model mimics the increased bone turnover induced by menopause in humans.[20, 21] These mice exhibit significantly increased bone resorption, with a lesser increase in bone formation.[22] They also show an increase in body weight and a decrease in uterus weight.[23] We investigated here the effects of administration of salubrinal to ovariectomized mice, focusing on its dual effects regulating osteoblasts and osteoclasts. We also studied the *ex vivo* and *in vitro* effects of salubrinal on primary bone marrow-derived cells cultured in osteoblast or osteoclast differentiation media, as well as the drug's action on osteoblastic or pre-osteoclastic cell lines. Our study demonstrates that salubrinal attenuates the bone loss induced by estrogen deficiency by altering the proliferation and differentiation of osteoclasts and osteoblasts.

Materials and Methods

Ovariectomized mouse model and subcutaneous administration of salubrinal

Thirty-six C57BL/6 female mice (~12 weeks of age) were used. Four to five mice per cage were housed at the Indiana University Animal Care Facility and fed with mouse chow and water *ad libitum*. Experimental procedures were approved by the Indiana University Animal Care and Use Committee and were in compliance with the Guiding Principles in the Care and Use of Animals.

Twenty-four mice were ovariectomized. All animals were weighed prior to surgery and again before sacrifice. Anesthesia was induced with 1.5% isoflurane (IsoFlo, Abbott Laboratories, North Chicago, IL) at a flow rate of 0.5 to 1.0 L/min. After shaving the hair at the operative site (dorsal mid-lumbar area), the skin was cleaned with 70% alcohol and 10% povidone iodine solution. Using a scalpel, a 20 mm midline dorsal skin incision was made to access the ovaries. After they were excised with scissors, the wound was closed by suturing.[24, 25] For the sham control mice, the same procedure was conducted without removing the ovaries. At 4 weeks after surgery, half (24) of the OVX mice received subcutaneous injections of salubrinal (Tocris Bioscience, Ellisville, MO, USA) in 49.5% PEG400 and 0.5% Tween 80 daily at a dose of 1 mg/kg body weight for 4 weeks, while the other half received an equal volume of vehicle as control.[16] Mice were sacrificed at week 8.

Measurements of bone mineral density, bone mineral content, fat, and uterus weight

Using peripheral dual energy X-ray absorptiometry (DXA; PIXImus II, Lunar Corp., Madison, WI, USA), bone mineral density (BMD, g/cm^2) and bone mineral content (BMC, mg) of whole body (excluding the head), lumbar spine, femur, tibia, and percentage of total and abdominal fat were measured using mouse-specific software (version 1.47).[26, 27] Mice were anesthetized in an anesthetic induction chamber and then mask-anesthetized using 1.5% isoflurane, placed on the platform in the prone position, and images acquired in about 5 min. After sacrifice in week 8, the uteri were harvested and wet weight taken with an electronic balance. Dissected bones were cleaned of soft tissue and fixed in 10% neutral buffered formalin. After 48 h, bones were transferred to 70% alcohol for storage. BMD and BMC of isolated bone samples (lumbar spine, femur and tibia) were determined.

Bone histomorphometry

The femurs were fixed in 10% neutral buffered formalin for two days and decalcified in 14% EDTA for 2 weeks. Decalcified samples were embedded in paraffin, and 5-mm-thick coronal sections were cut with a Leica RM2255 microtome (Leica Microsystems Inc., Bannockburn, IL). The slides were then processed for hematoxylin and Eosin (H&E) staining. The images of the distal femur were captured with an Olympus BX53 microscope and Olympus DP73 camera. Measurements were performed within 2.6-mm^2 sample area on the proximal side of the growth plate, in which BV/TV (in %, TV, total tissue area, calculated from the total tissue area; and BV, trabecular bone area, calculated from the total trabecular area) was determined.

Isolation of bone marrow-derived cells for osteoclast development

Using a 23-gauge needle, bone marrow-derived cells were collected by flushing the iliac, femur, and tibia with Iscove's MEM (Gibco-Invitrogen, Carlsbad, CA, USA) containing 2% fetal bovine serum (FBS).[28] Cells were separated by low-density gradient centrifugation and cultured in α-MEM supplemented with 10% FBS, 30 ng/ml murine macrophage-colony stimulating factor (M-CSF), and 20 ng/ml murine receptor activator of nuclear factor kappa-B ligand (RANKL). On day 3, the culture medium was replaced by α-MEM supplemented with 10% FBS, 30 ng/ml M-CSF, and 60 ng/ml RANKL, and cells were grown for an additional 3 days.[29]

Assays for colony-forming unit-fibroblasts (CFU-F) and CFU-osteoblasts (CFU-OBL)

To evaluate the ability of fibroblast-like mesenchymal stem cell (MSC) colony formation in the CFU-F assay, bone marrow-derived cells were fractionated using a Ficoll-Hypaque density gradient. Approximately 2×10^6 cells/ml MSCs were cultured in 6-well culture plates in a complete MesenCult medium.[29-31] Fresh medium was exchanged every other day. On day 14, cells were rinsed with PBS and stained using a HEMA-3 quick staining kit (Fisher Scientific, Waltham, MA, USA). The number of CFU-F colonies with more than 50 cells was counted, and the clusters of cells that did not present fibroblast-like morphology were excluded.

In the CFU-OBL assay, bone marrow-derived cells isolated from three groups of mice (sham control, OVX, and salubrinal-injected OVX mice) were plated at 2×10^6 cells/ml in 6-well plates consisting of osteogenic differentiation medium (MesenCult proliferation kit, supplemented with 10 nM dexamethasone, 50 μg/ml ascorbic acid 2-phosphate, and 10 mM β-glycerophosphate).[30, 32, 33] The medium was changed every other day, and cells were cultured for 2 weeks. For alkaline phosphatase (ALP) staining, cells were fixed in citrate-buffered

acetone for 30 s, incubated in the alkaline-dye mix for 30 min, and counterstained with Mayer's Hematoxylin for 10 min. The intensity of ALP staining in cells was determined microscopically.

Colony-forming unit-macrophage/monocyte (CFU-M) assay

The CFU-M assay was conducted using bone marrow mononuclear cells as described previously.[29, 34-36] Approximately 2.5×10^4 bone marrow-derived cells from the femur were prepared from each of the sham control, OVX, and salubrinal-injected OVX mice. Cells were seeded onto a 35-mm gridded dish, which was composed of methylcellulose supplemented with 30 ng/ml M-CSF and 20 ng/ml RANKL. Cells were cultured at 37°C in a 5% CO_2 incubator for 7 days in the presence and absence of salubrinal. The colony numbers of CFU-M were converted to the numbers per femur.

Assay for differentiation to mature osteoclasts

The osteoclast differentiation assay was performed using bone marrow-derived cells in 96-well plates in the presence of 1, 2, or 5 μM salubrinal.[29, 37] During 6-day experiments, the culture medium was exchanged once on day 4. Adherent cells were fixed and stained with a tartrate resistant acid phosphate (TRACP)-staining kit according to the manufacturer's instructions. TRACP-positive multinucleated cells (>3 nuclei) were identified as mature osteoclasts, and the area covered by mature osteoclasts was determined.

Assays for the migration and adhesion of osteoclasts

Migration of osteoclasts was evaluated using a transwell assay as described previously with minor modifications.[28, 29] Bone marrow-derived cells (2×10^6 cells/ml in 6-well plates) were

cultured in M-CSF and RANKL for 4 days, and trypsinized in Hank's balanced salt solution. The osteoclast precursor cells (1×10^5 cells/well) were loaded onto the upper chamber of transwells and allowed to migrate to the bottom chamber through an 8-μm polycarbonate filter coated with vitronectin (Takara Bio Inc., Otsu, Shigma, Japan). The bottom chamber contained α-MEM consisting of 1% bovine serum albumin (BSA) and 30 ng/ml M-CSF. After 6 h reaction, the number of osteoclast precursor cells in the lower chamber (attached onto the bottom of the transwells) was counted. For assaying adhesion, osteoclast precursor cells (1×10^5 cells/well) were placed into 96-well plates coated with 5 μg/ml vitronectin in α-MEM supplemented with 30 ng/ml M-CSF.[28, 29] After 30 min of incubation, cells were washed with PBS three times and fixed with 4% paraformaldehyde at room temperature for 10–15 min. Cells were stained with crystal violet, and the number of cells adherent to $\alpha_v\beta_3$ was counted.[28, 29]

Quantitative PCR and Western blot analysis

RAW264.7 mouse monocyte/macrophage cells and MC3T3-E1 osteoblast-like cells (C14 clone) were grown in αMEM containing 10% FBS and antibiotics (50 units/ml penicillin, and 50 μg/ml streptomycin; Life Technologies, Grand Island, NY, USA).[38] To induce osteoclastogenesis, RAW264.7 cells were incubated with 20 ng/ml of RANKL. For quantitative PCR, total RNA was extracted using an RNeasy Plus mini kit (Qiagen, Germantown, MD, USA) and reverse transcription was conducted with high capacity cDNA reverse transcription kits (Applied Biosystems, Carlsbad, CA, USA). Real-time PCR was performed using Power SYBR green PCR master mix kits (Applied Biosystems). The PCR primers were: NFATc1 (5'-GGT GCT GTC TGG CCA TAA CT-3'; and 5'-GCG GAA AGG TGG TAT CTC AA-3'),osteocalcin (OCN, 5'- CCG GGA GCA GTG TGA GCT TA-3'; 5'- AGG CGG TCT TCA AGC CAT ACT-

3’), cathepsin K (5’- CAGCTTCCCCAAGATGTGAT -3’; and 5’-AGCACCAACGAGAGGAGA AA-3’); DcStamp (5’-AAAACCCTTGGGCTGTTCTT-3’; and 5’-AATCATGGACGACTCCTTGG-3’), and Atp6v0d2 (5’-AAGCCTTTGTTTGACGCTGT-3’; and 5’-TTCGATGCCTCTGTGAGATG-3’), and GAPDH (5’-TGC ACC ACC AAC TGC TTA G-3’; and 5’-GGA TGC AGG GAT GAT GTT C-3’) which was used as an internal control.

For Western blot analysis, bone marrow-derived cells, RAW264.7 cells, or MC3T3-E1 cellswere lysed in a RIPA lysis buffer containing protease inhibitors (Santa Cruz, Santa Cruz, CA, USA) and phosphatase inhibitors (Calbiochem, Billerica, MA, USA). Isolated proteins were fractionated using 10% SDS gels and electro-transferred to Immobilon-P membranes (Millipore, Billerica, MA, USA). Antibodies specific to ATF4, cathepsin K, NFATc1, and TRAP (Santa Cruz), eIF2α (Cell Signaling, Danvers, MA, USA), phospho-eIF2α (Thermo Scientific, Waltham, MA, USA), Rac1 (Millipore), and β-actin (Sigma) were used. Protein levels were assayed using a SuperSignal west femto maximum sensitivity substrate (Thermo Scientific) and signal intensities were quantified with a luminescent image analyzer (LAS-3000, Fuji Film, Tokyo, Japan).

Fluorescence-based osteoclast activity assay

Osteoclast activity was evaluated using a bone resorption assay kit (Cosmo Bio, Carlsbad, CA, USA). In brief, RAW264.7 cells were cultured for 7 days in each of 48 wells that were coated with fluoresceinamine-labeled calcium phosphate. The effects of RANKL and salubrinal on osteoclast activity were evaluated by measuring fluorescence intensity of the culture medium at an excitation wavelength of 485 nm and emission wavelength of 535 nm.

Fluorescence resonance energy transfer (FRET) imaging

In order to evaluate the effects of salubrinal on Rac1 activity, we conducted single live cell imaging using RAW264.7 cells and a Rac1 FRET biosensor.[39] The biosensor was composed of a binding domain of an effector protein for Rac1 (PAK1; p21 protein-activated kinase 1), together with a cyan fluorescent protein (CFP) and a yellow fluorescent protein (YFP). Rac1 activation results in conformational changes that shift FRET efficiency from CFP to YFP. Hence, the level of Rac1 activity can be determined by an intensity ratio of YFP/CFP in individual cells. The specificity of the biosensor has been well characterized.[17,39,40] The filter sets (Semrock) were chosen for exciting CFP at 438 ± 24 nm (center wavelength ± bandwidth), and emission for CFP and YFP at 483 ± 32 nm and 542 ± 27 nm, respectively. Fluorescent time-lapse images were acquired at an interval of 5 min using a Ti-E inverted microscope (Nikon) that was equipped with a 40× (0.75 numerical aperture) objective, a charge-coupled device (CCD) camera (Photometrics), and a filter wheel controller (Sutter). Final FRET images (emission ratios of YFP/CFP) were generated by NIS-Elements software (Nikon).

Knockdown of eIF2α and Rac1 by siRNA

RAW264.7 cells were treated with siRNA specific to eIF2α and Rac1 (Life Technologies). Selected target sequences for knockdown of eIF2αand Rac1 were: eIF2α, 5'-CGGUCAAAAUUCGAGCAGA-3', and Rac1, 5'-GCA UUU CCU GGA GAG UAC A -3'; as a nonspecific control, negative siRNAs (control siRNA-A, Santa Cruz;or 5'-UGU ACU GCU UAC GAU UCG G-3', Life Technologies) were used. Cells were transiently transfected with siRNA for eIF2α, Rac1, or control in Opti-MEM I medium with Lipofectamine RNAiMAX

(Life Technologies). Six hours later, the medium was replaced by regular culture medium. The efficiency of silencing was assessed with immunoblotting 48 h after transfection.

Statistical analysis

The data were expressed as mean ± standard error of mean (SEM). Statistical significance among the experimental groups was examined using one-way ANOVA. For pair-wise comparisons, a post-hoc test was conducted using Fisher's protected least significant difference. For the time-lapse FRET imaging data, mean activation levels of Rac1 were determined at each time point relative to time zero, and one-way ANOVA with Dunnett's post hoc test was used to determine the statistical differences. A paired *t*-test was employed to evaluate statistical significance between the salubrinal-injected and control samples. All comparisons were two-tailed and statistical significance was assumed at $p< 0.05$. The asterisks (*, **, and ***) represent $p< 0.05$, $p< 0.01$, and $p< 0.001$, respectively.

Results

Attenuation of OVX-induced effects in salubrinal-injected mice

OVX mice demonstrated an increase in body weight over the sham control mice, while subcutaneous administration of salubrinal in weeks 5 to 8 significantly suppressed the OVX-induced increase in body weight ($p < 0.001$) (Fig. 1*A*). Similarly, the uterus weight of OVX mice was significantly decreased compared to sham control mice, while salubrinal administration of OVX mice increased the uterus weight over untreated OVX mice, though this weight was still significantly lower than that of sham control mice (Fig. 1*B*). The percentage of both total fat and abdominal fat was increased in OVX mice when compared to the sham control group and decreased by the administration of salubrinal (Fig. 1*C&D*). OVX mice receiving salubrinal exhibited a statistically significant increase in BMD and BMC in the lumbar spine, femur, and tibia compared with OVX-only mice (Fig. 1*E&F*). The BMD of the lumbar, femur, and tibia in sham-operated mice were 0.0502 ± 0.0009 g/cm^2, 0.0521 ± 0.0016 g/cm^2, and 0.0492± 0.0009g/cm^2, respectively, while the BMC of the lumbar, femur, and tibia in sham-operated mice were 0.0693 ± 0.002 g, 0.024 ± 0.0008 g, and 0.0215 ± 0.0029 g.

Salubrinal-driven developmentof fibroblasts and osteoblasts

Ovariectomy did not induce a significant change in CFU-F or CFU-OBL colonies, representing the progenitors of fibroblasts and osteoblasts, respectively, as measured in cultures of bone marrow-derived cells (Fig. 2*A&B*). However, cells derived from OVX mice injected with salubrinal produced more CFU-F and CFU-OBL colonies when compared to cultures established from both sham-operated mice and ovariectomized mice (Fig. 2*A&B*).

Salubrinal's effects on BV/TV, BMD, and BMC of the femurs

To evaluate salubrinal's effect on bone architecture, the BV/TV ratio in the distal femur was evaluated among these three groups (Fig.2*C*). Compared to sham-control mice, ovariectomized mice presented a reduction in BV/TV ($p< 0.001$; 32.05 ± 1.5% in sham-control mice, and 19.31 ± 0.82% in OVX mice). However, salubrinal administration significantly restored BV/TV ($p< 0.001$; 25.5 ± 1.03% in salubrinal-treated OVX mice). In response to its daily administration, salubrinal's effects on femoral BMD and BMC differed between sham-control and OVX mice (Fig. 2*D*). OVX mice increased BMD and BMC of the femur by 11.8 ±2.7% and 11.8 ±0.8%, respectively. On the other hand, the elevation of BMD and BMC of sham OVX mice was significantly smaller, and they were 3.5 ±1.9% (BMD) and 3.7 ±0.8% (BMC).

Salubrinal-driven suppression in CFU-M, formation of mature osteoclasts, and migration and adhesion of osteoclasts

The number of CFU-M colonies, representing the number of osteoclast progenitors, developed from bone marrow cells isolated from ovariectomized mice was significantly higher than that of sham-operated animals. Cells derived from mice treated with salubrinal treatment had significantly lower numbers of CFU-M colonies (Fig. 3*A*). Cells isolated from the OVX mice exhibited an increase in the surface area (an index of formation of mature multinucleated osteoclasts) occupied by mature osteoclasts, whereas the cells isolated from the salubrinal-injected OVX mice presented a significant reduction in osteoclast surface area (Fig.3*B*).

Osteoclasts isolated from the OVX mice were more active in migration than those from the sham control, and osteoclasts isolated from the salubrinal-injected OVX mice showed

reduced migration compared to OVX mice (Fig. 3*C*). In M-CSF-mediated adhesion to αvβ3, cells isolated from OVX mice presented stronger adhesion than those from the sham control, while cells from salubrinal-injected OVX mice exhibited a reduction in osteoclast adhesion (Fig. 3*D*).

Effects of *in vitro* administration of salubrinal

We also conducted *in vitro* administration of salubrinal using cells isolated from the sham and OVX mice. First, *in vitro* administration of 2 μM salubrinal reduced the numbers of CFU-M colonies (Fig. 4*A*). Furthermore, incubation of sham-derived cells with salubrinal (in DMSO) at 1, 2, and 5 μM reduced the total number of CFU-M in a dosage-dependent manner (all $p < 0.001$ in three dosages) as well as the colony size (Fig. 4*B*). Second, in both the sham control and OVX mice, *in vitro* administration of salubrinal provided a slower migration rate (Fig. 4*C*). Third, *in vitro* administration of salubrinal also presented a significant reduction in cell adhesion ($p< 0.05$ in sham control, and $p< 0.001$ in OVX) (Fig. 4*D*).

Salubrinal's dose-dependent effect on formation of mature osteoclasts

To further evaluate the effects of salubrinal on the formation of mature osteoclasts, three dosages of salubrinal (1, 2, and 5 μM) were applied to the bone marrow-derived cells isolated from sham and OVX mice. Compared to the vehicle control, *in vitro* administration of salubrinal across a 6-day culture period (days 0–6) resulted in a significant decrease in the surface area covered by multinucleated osteoclasts (all $p < 0.001$) (Fig. 5*A*). To test the effects of salubrinal on the late development of osteoclasts, salubrinal was administered on days 4 to 6 only. This timeline was

also able to provide a significant decrease in the surface area of osteoclasts in a dosage-dependent manner ($p < 0.05$ for 1 μM, and $p < 0.001$ for 2and 5 μM) (Fig. 5*B*).

Elevation of phosphorylated eIF2α and ATF4 protein levels and osteocalcin mRNA level in MC3T3-E1 osteoblast-like cells by salubrinal

Using MC3T3-E1 osteoblast-like cells, the phosphorylation level of eIF2α, the expression level of ATF4, and the mRNA level of osteocalcin in response to administration of 5 μM salubrinal was evaluated. The results demonstrated that salubrinal increased the level of phosphorylated eIF2α (p-eIF2α) and ATF4 24 h (Fig. 6*A*), as well as the level of osteocalcin mRNA (32 h) by ~ 3.2 fold (Fig. 6*B*).

Reduction of NFATc1 in RAW264.7 monocyte/macrophage cells by salubrinal

To gain insight into the molecular mechanisms underlying the action of salubrinal on osteoclast generation, migration, and adhesion, the effect of salubrinal on cultures of RAW264.7 monocyte/macrophage cells was evaluated. Addition of RANKL to RAW264.7 cells in culture significantly increased the mRNA levels of the transcription factor essential for osteoclast differentiation NFATc1 and the osteoclast marker cathepsin K in 2 days (Fig. 6*C*). Furthermore, RANKL treatment elevated the mRNA levels of DcStamp and Atp6v0d2 that regulate cell fusion of osteoclasts. Administration of salubrinal at 5, 10, and 20 μM reduced RANKL-induced elevation of these mRNA levels in a dose-dependent manner. Furthermore, Western blot analysis demonstrated that salubrinal decreased the protein level of NFATc1 in a dose-dependent fashion (Fig. 6*D*). A fluorescence-based osteoclast activity assay showed that RANKL-driven increase in osteoclast activity was decreased by administration of salubrinal (Fig. 6*E*).

Inactivation of Rac1 GTPase by 10 or 20 μM salubrinal

Using FRET-based single cell imaging, the effect of salubrinal on the activity level of Rac1 GTPase was examined. In response to 10 and 20 μM salubrinal, the emission ratio of YFP/CFP was decreased, indicating that administration of salubrinal reduced the activity level of Rac1 (Fig. 7*A&B*). When RAW264.7 cells were treated with siRNA specific to eIF2α, salubrinal-driven down-regulation of Rac1 activity was significantly diminished ($p< 0.05$) compared to the cells treated with non-specific control siRNA (Fig. 7*C&D*).

Suppression of TRAP mRNA and cathepsin K mRNA by Rac1 siRNA

Using siRNA specific to Rac1, the role of Rac1 in expression of NFATc1, TRAP, and cathepsin K was examined using RAW264.7 cells. The result showed that the protein levels of TRAP and cathepsin K were downregulated by RNA inhibition of Rac1 (Fig. 8*A*). Consistent with its effects on protein levels, a partial silencing of Rac1 suppressed RANKL-driven upregulation of TRAP mRNA and cathepsin K mRNA but did not alter the mRNA level of NFATc1 (Fig. 8*B*).

Discussion

This study demonstrates that salubrinal is able to prevent bone loss in OVX mice and induce suppression of osteoclast development as well as promotion of osteoblast differentiation. In 4 weeks following ovariectomy, the OVX mice lost 14% of BMC in the whole body and approximately 10% of BMD in the spine and femur. Daily subcutaneous administration of salubrinal for 4 weeks significantly suppressed OVX-induced bone loss in the spine, femur, and tibia. Consistent with its effects on BMD and BMC, salubrinal reduced OVX effects, including increased body weight and decreased uterus weight.[41, 42] An increase in both BMD and BMC by salubrinal contributes to the elevation of not only Young's modulus but also an effective cross-sectional moment of inertia, both of which positively affect the prevention of fracture.

The results of the CFU-F and CFU-OBL assays are consistent with salubrinal-driven augmentation of bone formation in the OVX mice. The increase in CFU-F by salubrinal suggests a stimulated proliferation of MSCs in bone marrow-derived cells, while the elevated number of ALP-positive cells in CFU-OBL indicates an enhancement of osteoblast development. Salubrinal preserves eIF2α phosphorylation as a selective inhibitor of a phosphatase complex of eIF2α, protein phosphatase 1 (PP1),[14, 43, 44] and it is reported to accelerate the healing of bone wounds[16], enhance bone formation[45, 46], and increase the mineralization of MC3T3 cells[38]. The elevated level of p-eIF2α contributes to suppression of cellular stress, such as stress to the endoplasmic reticulum, radiation, and unloading, by decreasing translational efficiency in general, except for a set of proteins that includes ATF4. Since ATF4 is a transcription factor that is critical for osteoblastogenesis and bone formation, the increased p-eIF2α followed by the elevated level of ATF4 is consistent with the role of salubrinal as an inhibitor of PP1.

Regarding the development of osteoclasts in the OVX mice, subcutaneous injection of salubrinal as well as *in vitro* incubation of bone marrow-derived cells with salubrinal suppressed the proliferation of pre-osteoclasts as well as their differentiation to mature multinucleated osteoclasts.[47] Western blot analysis revealed that salubrinal reduced the expression of NFATc1 in RANKL-stimulated RAW264.7 pre-osteoclast cells, though this effect occurred at different concentrations than the anti-differentiation effects seen in bone marrow-derived cells. The difference in cell origin may cause the difference in dosage response. Because of the role of phosphorylated eIF2α in retarding translational efficiency, suppression of NFATc1 by salubrinal is likely to be regulated at least in part at the level of translation.[46] We observed, however, that both the mRNA and protein levels of NFATc1 were reduced by salubrinal. These results, together with previous studies, [38] suggest a mechanism for osteoclast regulation by salubrinal through p-eIF2α and NFATc1. Further studies will be necessary to establish other genes that mediate the response of NFATc1 to salubrinal treatment.

Live cell imaging using RAW264.7 cells revealed that salubrinal downregulates activity of Rac1 GTPase, which is involved in various functions including cell migration. Based on the result with eIF2α siRNA, this downregulation was in part mediated by eIF2α signaling. The observed result is consistent with salubrinal's action on inhibiting migration of pre-osteoclast cells. Furthermore, RNA silencing with siRNA specific to Rac1 showed that Rac1 also mediates salubrinal-driven downregulation of TRAP and Cathepsin K although expression of NFATc1 is not directly regulated by Rac1 (Fig. 8*B*).

The mechanism of salubrinal's effects on body weight and uterus weight is yet to be determined, but there may be a selective estrogen-receptor modulator (SERM)-like effect. Of note, the effect on uterine weight was much less than the effect on bone. Subcutaneous injection of salubrinal reduced both total and abdominal fat in the OVX mice, which might be associated with the observed changes in body weight. To clarify this mechanism, future studies may measure the serum levels of involved proteins, such as leptin, or isolate tissues and organs affected by OVX and measure their gene and protein expression.

This study demonstrates the potential of salubrinal as a therapy for reversing bone loss from osteoporosis. The study establishes salubrinal's effect at multiple levels, from improving body weight and BMD to promoting osteoblast formation and suppressing osteoclast formation. Additionally, its counteraction on increased body fat and decreased uterine weight, two conditions suffered by post-menopausal women, points to non-skeletal therapeutic uses for salubrinal. However, this study did not explore the mechanism of fat and uterine recovery by salubrinal. The mechanism of salubrinal's action was explored on bone cells using FRET and RNA inhibition to identify Rac1 GTPase as a mediator of its osteoclast suppression separate from NFATc1 (Fig. 8*C*). Mediators of p-eIF2α's regulation of Rac1 GTPase and NFATc1, however, have not been identified. Two notable features in anabolic responses with salubrinal are its effects on potential risk of cancer induction and bone formation in non-osteoporotic mice. Unlike PTH, salubrinal reduces proliferation and migration of breast cancer cells in a murine model of mammary tumor by eIF2α-mediated suppression of Rac1 GTPase.[48] Furthermore, although salubrinal treatment on bone marrow-derived cells from sham-operated mice decreased osteoclastogenesis, the effects of salubrinal to non-osteoporotic mice were significantly smaller

than those to OVX mice. In sham-control mice, no detectable changes are observed on body weight and fat content. Thus, potential side effects or unneeded bone growth of salubrinal might be smaller than PTH.

Currently, few drugs and chemical agents are available for both stimulation of osteoblasts and inhibition of osteoclasts. This study presented the possibility of a drug therapy to not only prevent bone loss but also regulate whole body and uterus weights. The results herein utilizing both an OVX mouse model and an *in vitro* analysis of primary bone marrow-derived cells, as well as cell line-based cultures, demonstrate that administration of salubrinal is effective in attenuating OVX-associated symptoms, as well as stimulating development of osteoblasts and inhibiting development of osteoclasts. Further analysis targeted to the molecular mechanism of salubrinal's action warrants the potential development of a novel therapeutic strategy for combating postmenopausal osteoporosis through eIF2α signaling.

Disclosures

All authors state that they have no conflicts of interest.

Acknowledgements

We appreciate X. Tu and M. Hamamura for technical assistance. This study was supported by grant DOD W81XWH-11-1-0716.

Author's roles: PZ participated in experimental designs, performed animal and cell experiments, conducted data collection and interpretation and drafted a manuscript. KH conducted molecular experiments, performed data collection and analysis. AC and TD conducted animal experiments. QW and SN conducted FRET experiments using Rac1 biosensor. HY, TB, and MP participated in experimental designs, and drafted a manuscript. PZ and HY accepted responsibility for integrity of data analysis. All authors read and approved the final manuscript.

References

1. Zaidi M. Skeletal remodeling in health and disease. Nat Med. 2007;13:791-801.
2. Chen AB, Zhang P, Yokota H. Evaluating treatment of osteoporosis using particle swarm on a bone remodelling mathematical model. IET Syst Biol. 2013;7:231-42.
3. Rachner TD, Khosla S, Hofbauer LC. Osteoporosis: now and the future. Lancet. 2011;377:1276-87.
4. Yang Q, Jian J, Abramson SB, Huang X. Inhibitory effects of iron on bone morphogenetic protein 2-induced osteoblastogenesis. J Bone Miner Res. 2011;26:1188-96.
5. Pinkerton JV, Harvey JA, Lindsay R, Pan K, Chines AA, Mirkin S, Archer DF, SMART-5 Investigators. Effects of bazedoxifene/conjugated estrogens on the endometrium and bone: a randomized trial. J Clin Endocrinol Metab. 2014;99:E189-98.
6. Khosla S, Bilezikian JP, Dempster DW, Lewiecki EM, Miler PD, Neer RM, Recker RR, Shane E, Shoback D, Potts JT. Benefits and risks of bisphosphonate therapy for osteoporosis. J Clin Endocrinol Metab. 2012;97:2272-82.
7. Gander T, Obwegeser JA, Zemann W, Grätz KW, Jacobsen C. Malignancy mimicking bisphosphonate-associated osteonecrosis of the jaw: a case series and literature review. Oral Surg Oral Med Oral Pathol Oral Radiol. 2014;117:32-6.
8. Valverde P. Pharmacotherapies to manage bone loss-associated diseases: a quest for the perfect benefit-to-risk ratio. Curr Med Chem. 2008;15:284-304.
9. Diab DL, Watts NB. Denosumab in osteoporosis. Expert Opin Drug Saf. 2014;13:247-53.
10. Zerbini CA, McClung MR. Odanacatib in postmenopausal women with low bone mineral density: a review of current clinical evidence. Ther Adv Musculoskelet Dis. 2013;5:199-209.

11. Han SL, Wan SL. Effect of teriparatide on bone mineral density and fracture in postmenopausal osteoporosis: meta-analysis of randomised controlled trials. Int J Clin Pract. 2012;66:199-209.
12. Boras-Granic K, Wysolmerski JJ. PTHrP and breast cancer: more than hypercalcemia and bone metastases. Breast Cancer Res. 2012;14:307.
13. Becker CB. Sclerostin inhibition for osteoporosis--a new approach. N Engl J Med. 2014;370:476-7.
14. Boyce M, Bryant KF, Jousse C, Long K, Harding HP, Scheuner D, Kaufman RJ, Ma D, Coen DM, Ron D, Yuan J. A selective inhibitor of eIF2alpha dephosphorylation protects cells from ER stress. Science. 2005;307:935-9.
15. Saito A, Ochiai K, Kondo S, Tsumagari K, Murakami T, Cavener DR, Imaizumi K. Endoplasmic reticulum stress response mediated by the PERK-eIF2(alpha)-ATF4 pathway is involved in osteoblast differentiation induced by BMP2. J Biol Chem.2011; 286:4809-18.
16. Zhang P, Hamamura K, Jiang C, Zhao L, Yokota H. Salubrinal promotes healing of surgical wounds in rat femurs. J Bone Miner Metab. 2012;30:568-79.
17. Wan Q, Cho E, Yokota H, Na S. Rac1 and Cdc42 GTPases regulate shear stress-driven ß-catenin signaling in osteoblasts. Biochem Biophys Res Commun. 2013; 433: 502-7.
18. Wang Y, Lebowitz D, Sun C, Thang H, Grynpas MD, Glogauer M. Identifying the relative contributions of Rac1 and Rac2 to osteoclastogenesis. J Bone Miner Res. 2008; 23: 260-70.
19. Fukuda A, Hikita A, Wakeyama H, Akiyama T, Oda H, Nakamura K, Tanaka S. Regulation of osteoclast apoptosis and motility by small GTPase binding protein Rac1. J Bone Miner Res. 2005;20: 2245-53.

20. Wright LE, Christian PJ, Rivera Z, Van Alstine WG, Funk JL, Bouxsein ML, Hoyer PB. Comparison of skeletal effects of ovariectomy versus chemically induced ovarian failure in mice. J Bone Miner Res. 2008;23:1296-303.
21. Chen WF, Gao QG, Dai ZJ, Kung AW, Guo DA, Wong MS. Estrogenic effects of ginsenoside Rg1 in endometrial cells in vitro were not observed in immature CD-1 mice or ovariectomized mice model. Menopause. 2012;19:1052-61.
22. Jilka RL, Takahashi K, Munshi M, Williams DC, Roberson PK, Manolagas SC. Loss of estrogen upregulates osteoblastogenesis in the murine bone marrow. Evidence for autonomy from factors released during bone resorption. J Clin Invest. 1998;101:1942-50.
23. Pirro M, Fabbriciani G, Leli C, Callarelli L, Manfredelli MR, Fioroni C, Mannarino MR, Scarponi AM, Mannarino E. High weight or body mass index increase the risk of vertebral fractures in postmenopausal osteoporotic women. J Bone Miner Metab. 2010;28:88-93.
24. McMillan J, Kinney RC, Ranly DM, Fatehi-Sedeh S, Schwartz Z, Boyan BD. Osteoinductivity of demineralized bone matrix in immunocompromised mice and rats is decreased by ovariectomy and restored by estrogen replacement. Bone. 2007;40:111-21.
25. Ström JO, Theodorsson A, Ingberg E, Isaksson IM, Theodorsson E. Ovariectomy and 17β-estradiol replacement in rats and mice: a visual demonstration. J Vis Exp. 2012;64:e4013.
26. Zhang P, Yokota H. Elbow loading promotes longitudinal bone growth of the ulna and the humerus. J Bone Miner Metab. 2012;30:31-9.
27. Zhang P, Yokota H. Knee loading stimulates healing of mouse bone wounds in a femur neck. Bone. 2011;49:867-72.

28. Xiao G, Cheng H, Cao H, Chen K, Tu Y, Yu S, Jiao H, Yang S, Im HJ, Chen D, Chen J, Wu C. Critical role of filamin-binding LIM protein 1 (FBLP-1);/migfilin in regulation of bone remodeling. J Biol Chem. 2012;287:21450-60.

29. He Y, Childress P, Hood M Jr, Alvarez M, Kacena MA, Hanlon M, McKee B, Bidwell JP, Yang FC. Nmp4/CIZ Suppresses the Parathyroid Hormone Anabolic Window by Restricting Mesenchymal Stem Cell and Osteoprogenitor Frequency. Stem Cells Dev. 2013;22:492-500.

30. Wu X, Chen S, Orlando SA, Yuan J, Kim ET, Munugalavadla V, Mali RS, Kapur R, Yang FC. p85α regulates osteoblast differentiation by cross-talking with the MAPK pathway. J Biol Chem. 2011;286:13512-21.

31. Uveges TE, Collin-Osdoby P, Cabral WA, Ledgard F, Goldberg L, Bergwitz C, Forlino A, Osdoby P, Gronowicz GA, Marini JC. Cellular mechanism of decreased bone in Brtl mouse model of OI: imbalance of decreased osteoblast function and increased osteoclasts and their precursors. J Bone Miner Res. 2008;23:1983-94.

32. Nabavi N, Khandani A, Camirand A, Harrison RE. Effects of microgravity on osteoclast bone resorption and osteoblast cytoskeletal organization and adhesion. Bone. 2011;49:965-74.

33. Liu Y, Berendsen AD, Jia S, Lotinun S, Baron R, Ferrara N, Olsen BR. Intracellular VEGF regulates the balance between osteoblast and adipocyte differentiation. J Clin Invest. 2012;122:3101-13.

34. Yan D, Gurumurthy A, Wright M, Pfeiler TW, Loboa EG, Everett ET. Genetic background influences fluoride's effects on osteoclastogenesis. Bone. 2007;41:1036-44.

35. Broxmeyer HE, Mejia JA, Hangoc G, Barese C, Dinauer M, Cooper S. SDF-1/CXCL12 enhances in vitro replating capacity of murine and human multipotential and macrophage progenitor cells. Stem Cells Dev. 2007;16:589-96.

36. McHugh KP, Shen Z, Crotti TN, Flannery MR, Fajardo R, Bierbaum BE, Goldring SR. Role of cell-matrix interactions in osteoclast differentiation. AdvExp Med Biol. 2007;602:107-11.

37. Abdallah BM, Ditzel N, Mahmood A, Isa A, Traustadottir GA, Schilling AF, Ruiz-Hidalgo MJ, Laborda J, Amling M, Kassem M. DLK1 is a novel regulator of bone mass that mediates estrogen deficiency-induced bone loss in mice. J Bone Miner Res. 2011;26:1457-71.

38. Hamamura K, Tanjung N, Yokota H. Suppression of osteoclastogenesis through phosphorylation of eukaryotic translation initiation factor 2 alpha. J Bone Miner Metab. 2013;31:618-28.

39. Itoh RE, Kurokawa K, Ohba Y, Yoshizaki H, Mochizuki N, Matsuda M. Activation of Rac and Cdc42 video imaged by fluorescent resonance energy transfer-based single-molecule probes in the membrane of living cells. Mol Cell Biol. 2002;22:6582-91.

40. Poh YC, Na S, Chowdhury S, Ouyang M, Wang Y, Wang N. Rapid activation of Rac GTPase in living cells by force is independent of Src. PLoS One. 2009;4:e7886.

41. Fujioka M, Uehara M, Wu J, Adlercreutz H, Suzuki K, Kanazawa K, Takeda K, Yamada K Ishimi Y. Equol, a metabolite of daidzein, inhibits bone loss in ovariectomized mice. J Nutr. 2004;134:2623-7.

42. Rogers NH, Perfield JW 2nd, Strissel KJ, Obin MS, Greenberg AS. Reduced energy expenditure and increased inflammation are early events in the development of ovariectomy-induced obesity. Endocrinology. 2009;150:2161-8.

43. Tréton X, Pedruzzi E, Guichard C, Ladeiro Y, Sedghi S, Vallée M, Fernandez N, Bruyére E, Woerther PL, Ducroc R, Montcuquet N, Freund JN, Van Seuningen I, Barreau F, Marah A, Hugot JP, Cazals-Hatem D, Bouhnik Y, Daniel F, Ogier-Denis E. Combined NADPH oxidase 1 and interkeukin 10 deficiency induces chronic endoplasmic reticulum stress and causes ulcerative colitis-like disease in mice. PLoS One. 2014;9:e101669.

44. Schewe DM, Aguirre-Ghiso JA. Inhibition of eIF2α dephosphorylation maximizes bortezomib efficiency and eliminates quiescent multiple myeloma cells surviving proteasome inhibitor therapy. Cancer Res. 2009; 69:1545-52.

45. Chen A, Hamamura K, Zhang P, Chen Y, Yokota H. Systems analysis of bone remodelling as a homeostatic regulator. IET Syst Biol. 2010;4:52-63.

46. He L, Lee J, Jang JH, Sakchaisri K, Hwang JS, Cha-Molstad HJ, Kim KA, Ryoo IJ, Lee HG, Kim SO, Soung NK, Lee KS, Kwon YT, Erikson RL, Ahn JS, Kim BY. Osteoporosis regulation by salubrinal through eIF2α mediated differentiation of osteoclast and osteoblast. Cellular Signaling. 2013;25:552-60.

47. Yokota H, Hamamura K, Chen A, Dodge TR, Tanjung N, Abedinpoor A, Zhang P. Effects of salubrinal on development of osteoclasts and osteoblasts from bone marrow-derived cells. BMC Musculoskelet Dis. 2013;14:197.

48. Hamamura K, Minami K, Tanjung N, Wan Q, Koizumi M, Matsuura N, et al. Attenuation of malignant phenotypes of breast cancer cells through eIF2α-mediated downregulation of Rac1 signaling. Int J Oncol. 2014;44:1980-8.

Figure legends

Fig. 1. Effects of ovariectomy and salubrinal on body weight, uterus weight, total fat, abdominal fat, BMD, and BMC.

(A) Salubrinal-driven suppression of OVX-induced gain of body weight. (B) Salubrinal-driven partial recovery of OVX-induced loss of uterine weight. (C) Salubrinal-induced reduction in total fat (%). Total fat, when compared to sham control (20.3 ± 2.0%), was increased by OVX (to 27.6 ± 1.3%) and decreased by salubrinal (to 24.0 ± 1.0%). (D) Salubrinal-induced reduction in abdominal fat (%). OVX increased abdominal fat over sham (23.0 ± 3.1% to 36.2 ± 1.8%), while salubrinal treatment decreased it (to 27.4 ± 1.1%). (E and F) Suppression of OVX-induced reduction of BMD and BMC, respectively, in the lumbar spine, femur and tibia. Salubrinal increased BMD compared to OVX in the lumbar spine (0.0396 ± 0.0004 g/cm^2 to 0.0453 ± 0.0004 g/cm^2), femur (0.0431 ± 0.0007 g/cm^2 to 0.0482 ± 0.0007 g/cm^2), and tibia (0.0421 ± 0.0005 g/cm^2 to 0.0467 ± 0.0005 g/cm^2). BMC was similar (lumbar spine: 0.0451 ± 0.0011 g to 0.0519 ± 0.0015 g; femur: 0.0195 ± 0.0004 g to 0.0217 ± 0.0004 g; tibia: 0.0142 ± 0.0002 g to 0.0184 ± 0.0003 g).Asterisks (*, **, and ***) represent statistical significance at$p< 0.05$, $p< 0.01$, and $p< 0.001$, respectively (n=12).

Fig. 2. Effects of subcutaneous administration of salubrinal on CFU-F, CFU-OBL, and femoral bone. (A& B) Comparison of CFU-F and CFU-OBL, respectively. Bone marrow-derived cells were isolated from 3 groups of mice (sham, OVX, and salubrinal-injected OVX mice). The representative photographs are shown (n=12). (C) BV/TV ratio in the distal femur (n=6). (D) Comparison of salubrinal-driven increases in femoral BMD and BMC between sham

control (n=6) and OVX mice (n=12). The representative photographs are shown. Asterisks (**, and ***) represent statistical significance at $p< 0.01$ and $p< 0.001$, respectively.

Fig. 3. Effects of subcutaneous administration of salubrinal on CFU-M and osteoclast activity by bone marrow-derived cells.

The CFU-M numbers, area coverage by mature osteoclasts, and the migration and adhesion of osteoclasts wereevaluated. Bone marrow-derived cells were isolated from 3 groups of mice (sham, OVX, and salubrinal-injected OVX mice). (A) CFU-M numbers (sham: 9892 ± 383, OVX: 13526 ± 330, OVX+sal: 8,041 ± 282 colonies/femur). Salubrinal attenuated an OVX-induced increase in CFU-M. (B) Coverage area of mature osteoclasts (sham: 46.1 ± 1.0%, OVX: 64.6 ± 1.6%, OVX+sal: 24.9 ± 1.8%). Salubrinal suppressed an OVX-induced increase in osteoclast area. (C) Migration assay of osteoclasts (sham: 38.7 ± 2.0 cells/LPF, per low-power field, OVX: 86.0 ± 5.6 cells/LPF, OVX+sal: 56.6 ± 4.1 cells/LPF). Salubrinal administration decreased an OVX-induced increase in osteoclast migration. (D) Adhesion assay of osteoclasts (sham: 62.0 ± 2.5 cells/LPF, OVX: 72.1 ± 4.5 cells/LPF, OVX+sal: 55.3 ± 1.8 cells/LPF). Salubrinal reduced an OVX-induced increase in osteoclast adhesion. Asterisks (*, **, and ***) represent statistical significance at$p< 0.05$, $p< 0.01$, and $p< 0.001$, respectively (n=12).

Fig. 4. Effects of *in vitro* salubrinal administration on CFU-M, and the migration and adhesion of osteoclasts.

Bone marrow-derived cells were isolated from the sham and OVX mice, then cultured in the presence and absence of salubrinal. (A) Salubrinal-induced reduction in CFU-M numbers in both sham cells (from 9892 ± 383 to 6002 ± 531) and OVX cells (from 13526 ± 330 to 6334 ±

346). (B) Dose-dependent reduction in sham-derived CFU-M numbers in response to 0, 1, 2, and 5 μM salubrinal (9892 ± 383, 6962 ± 450, 6002 ± 531, and 5423 ± 451, respectively). The images exhibit representative sizes of CFU-M colonies (circled) at each dosage. (Bar = 500 μm, for scale). (C) Salubrinal-induced reduction in the migration of osteoclasts in both sham-derived cells (from 38.7 ± 2.0 to 26.5 ± 1.1) and OVX-derived cells (from 86.0 ± 5.6 to 31.9 ± 2.0). (D) Salubrinal-induced suppression of the adhesion of osteoclasts in both sham-derived cells (62.0 ± 2.5 to 51.9 ± 3.8) and OVX-derived cells (72.1 ± 4.5 to 34.9 ± 3.5). Asterisks (* and ***) represent statistical significance at $p< 0.05$ and $p< 0.001$, respectively (n=12).

Fig. 5. Effects of*in vitro* salubrinal administration on the formation of mature osteoclasts. Salubrinal was administeredat 3 dosages (1, 2, and 5 μM) for days 0–6 or days 4–6 to bone marrow-derived cells harvested from sham and OVX mice. Four pairs of images on the bottom showrepresentative osteoclasts stained with TRAP. (Bar = 200 μm, for scale). Experiments were conducted in triplicates per condition. Five fields were counted per well. Three independent experiments were performed with similar results. (A) Effects of *in vitro* salubrinal administration during days 0–6. (B) Effects of *in vitro* salubrinal administration during days 4–6. Asterisks (* and ***) represent statistical significance at $p< 0.05$ and $p< 0.001$, respectively (n=6).

Fig. 6. Effects of salubrinal on expression of NFATc1, cathepsin K, DcStamp, Atp6v0d2, p-eIF2α, ATF4, and osteocalcin, as well as osteoclast activity.

(A) Elevation of p-eIF2α and ATF4 by 5μM salubrinal in MC3T3-E1 cells. (B) Increase in osteocalcin (OCN) mRNA by 5μM salubrinal at 32 h in MC3T3-E1 cells. (C) Reduction of the

mRNA levels of NFATc1, cathepsin K, DcStamp, and Atp6v0d2 in RAW264.7 cells by 5–20 μM salubrinal. (D) Dose-dependent decrease in NFATc1 in RAW264.7 cells by 5–20 μM salubrinal. (E) Reduction in fluorescence-based osteoclast activity by salubrinal administration. Asterisks (*, **, and ***) represent statistical significance at $p< 0.05$, $p< 0.01$, and $p< 0.001$, respectively(n=3).

Fig.7. FRET-based detection of downregulation of Rac1 GTPase in RAW264.7 cells by salubrinal.

YFP/CFP emission ratios were averaged over the whole cell and normalized to time -10 min (10 min before Sal treatment). (Scale bars are 10μm). (A, B) Rac1 activity in response to 10 μM (n = 10) and 20 μM salubrinal (n = 9), respectively. (C) Level of eIF2α protein by partial silencing, and resultant Rac1 activity in response to 20 μM salubrinal (n=9). (D) Rac1 activity in response to 20 μM salubrinal in the cells transfected with NC (non-specific control) siRNA (n=6). An asterisk (*) represents statistical significance at $p< 0.05$.

Fig. 8. Effects of Rac1 siRNA on expression of NFATc1, TRAP and cathepsin K in RAW264.7 cells.

(A) Partial silencing of Rac1 protein level by Rac1 siRNA, and protein expression of NFATc1, TRAP, and cathepsin K. NC = treatment with non-specific control siRNA. (B) Relative mRNA levels of NFATc1, TRAP, and cathepsin K in response to Rac1 siRNA. TRAP and cathepsin K expressions are reduced by Rac1 siRNA, but NFATc1 expression remains unchanged. (C) Proposed mechanism of salubrinal's action in bone remodeling.

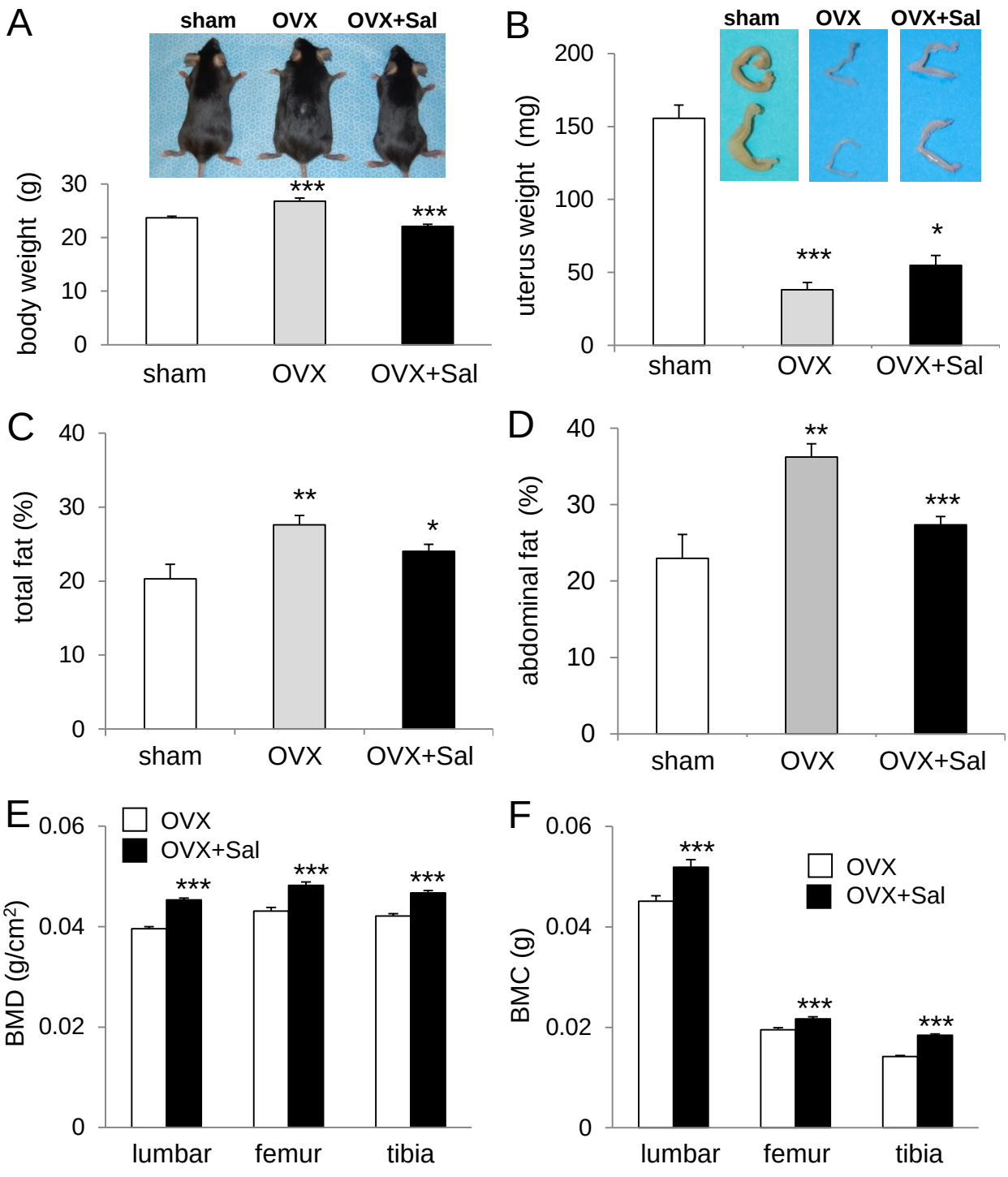
A
sham
OVX
OVX+Sal
body weight (g)
30
20
10
0
***
***
sham
OVX
OVX+Sal
B
sham
OVX
OVX+Sal
uterus weight (mg)
200
150
100
50
0
***
*
sham
OVX
OVX+Sal
C
total fat (%)
40
30
20
10
0
**
*
sham
OVX
OVX+Sal
D
abdominal fat (%)
40
30
20
10
0
**
***
sham
OVX
OVX+Sal
E
OVX
OVX+Sal
BMD (g/cm2)
0.06
0.04
0.02
0
***
***
***
lumbar
femur
tibia
F
BMC (g)
0.06
0.04
0.02
0
***
***
***
OVX
OVX+Sal
lumbar
femur
tibia

Figure 1

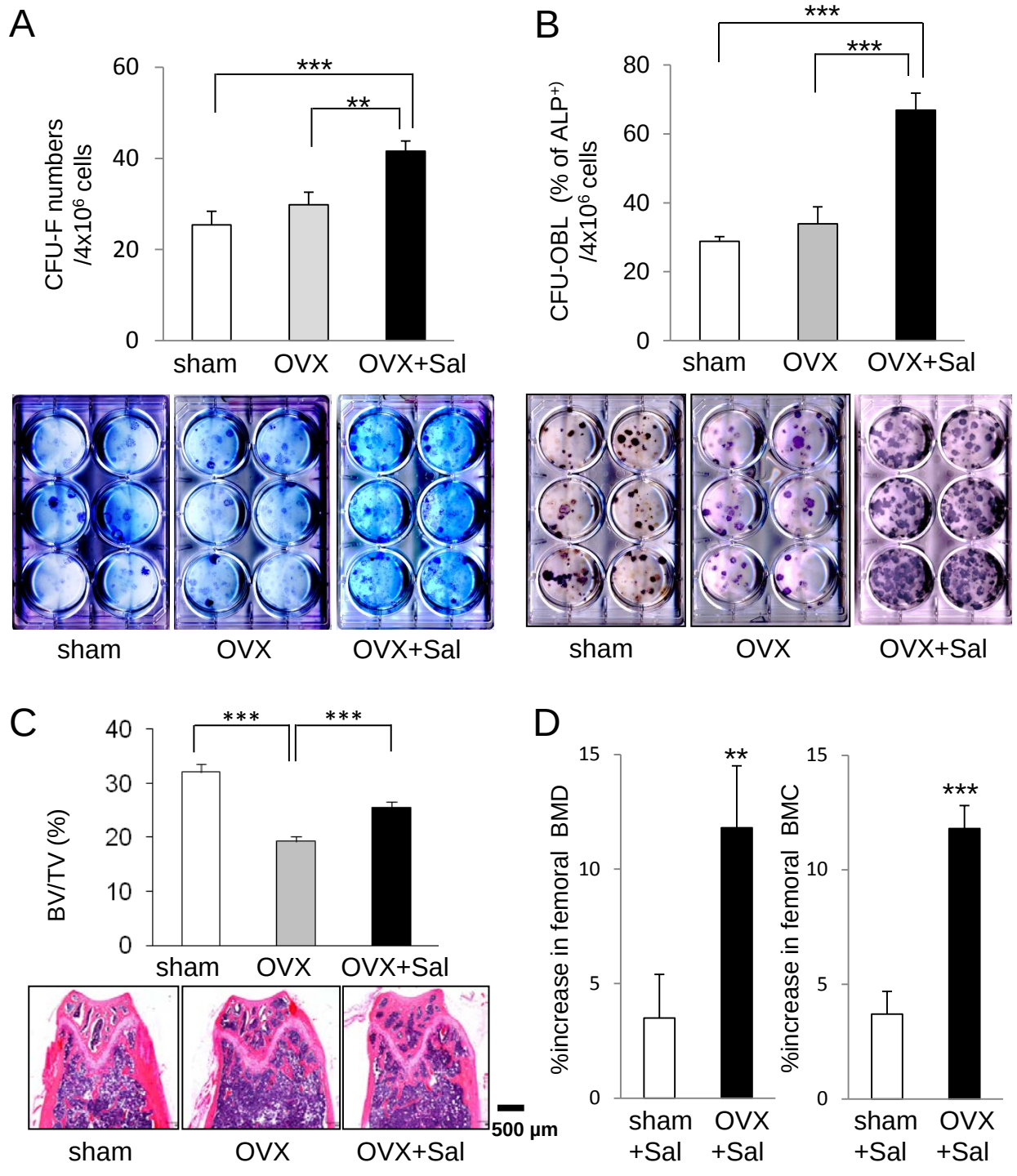
A
CFU-F numbers /4x10⁶ cells
60
40
20
0
***
**
sham
OVX
OVX+Sal
B
CFU-OBL (% of ALP+) /4x10⁶ cells
80
60
40
20
0
***
***
sham
OVX
OVX+Sal
sham
OVX
OVX+Sal
sham
OVX
OVX+Sal
C
BV/TV (%)
40
30
20
10
0
***
***
sham
OVX
OVX+Sal
500 μm
sham
OVX
OVX+Sal
D
%increase in femoral BMD
15
10
5
0
**
sham +Sal
OVX +Sal
%increase in femoral BMC
15
10
5
0
***
sham +Sal
OVX +Sal

Figure 2

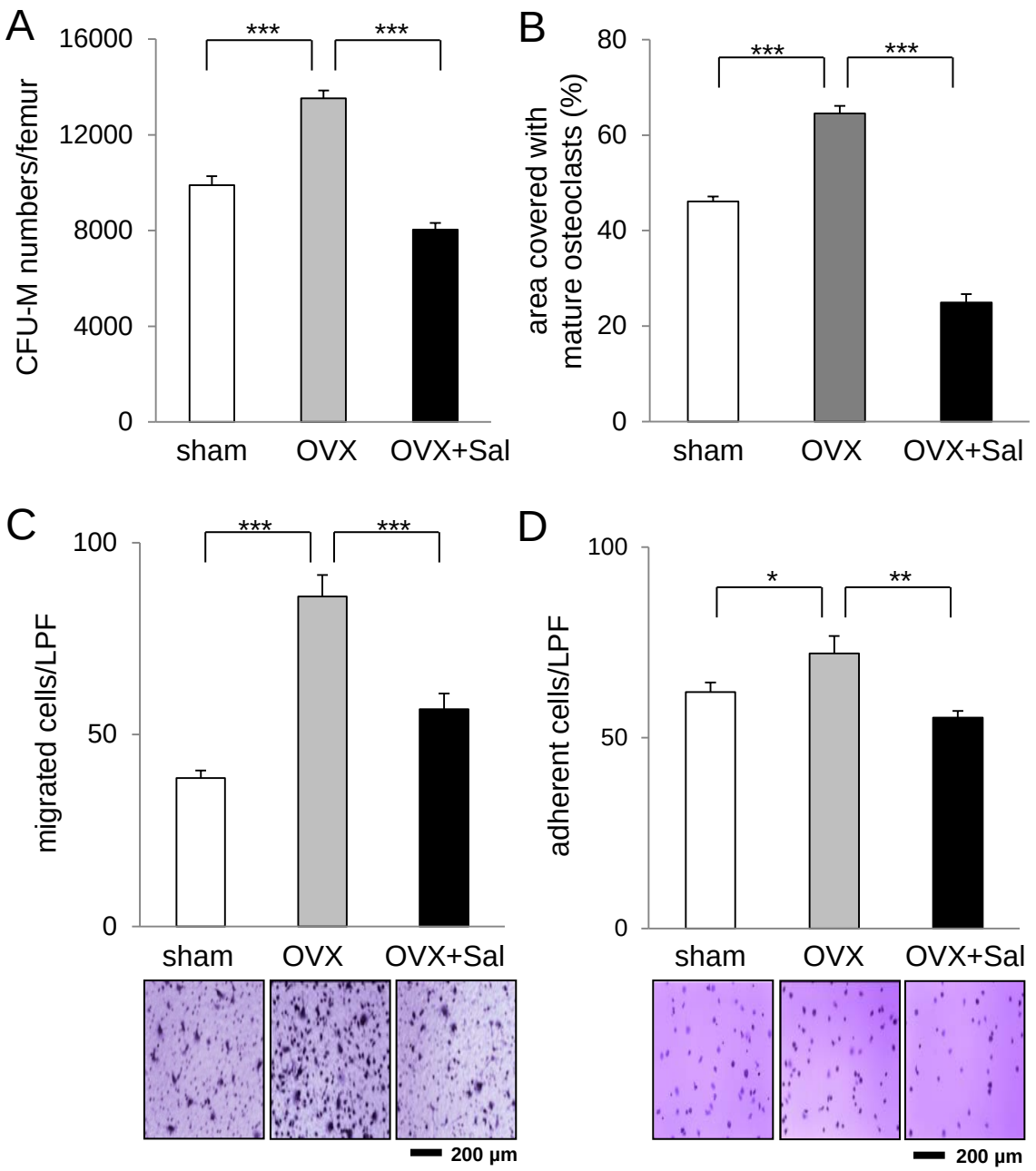
A
CFU-M numbers/femur
16000
12000
8000
4000
0
***
***
sham
OVX
OVX+Sal
B
area covered with mature osteoclasts (%)
80
60
40
20
0
***
***
sham
OVX
OVX+Sal
C
migrated cells/LPF
100
50
0
***
***
sham
OVX
OVX+Sal
200 μm
D
adherent cells/LPF
100
50
0
*
**
sham
OVX
OVX+Sal
200 μm

Figure 3

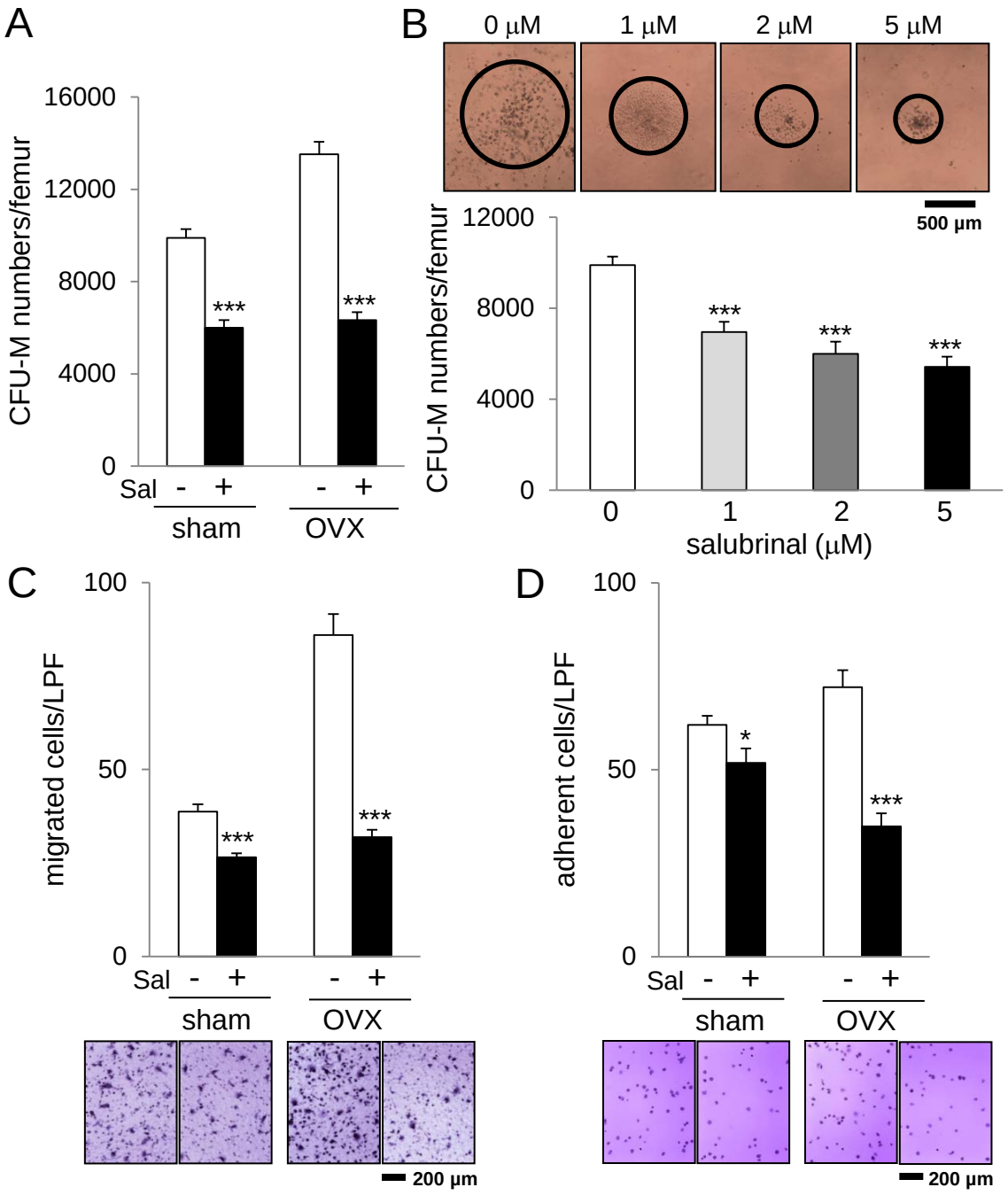
A
16000
12000
8000
4000
0
CFU-M numbers/femur
***
***
Sal - + - +
sham
OVX
B
0 μM
1 μM
2 μM
5 μM
500 μm
12000
8000
4000
0
CFU-M numbers/femur
***
***
***
0 1 2 5
salubrinal (μM)
C
100
50
0
migrated cells/LPF
***
***
Sal - + - +
sham
OVX
200 μm
D
100
50
0
adherent cells/LPF
*
***
Sal - + - +
sham
OVX
200 μm

Figure 4

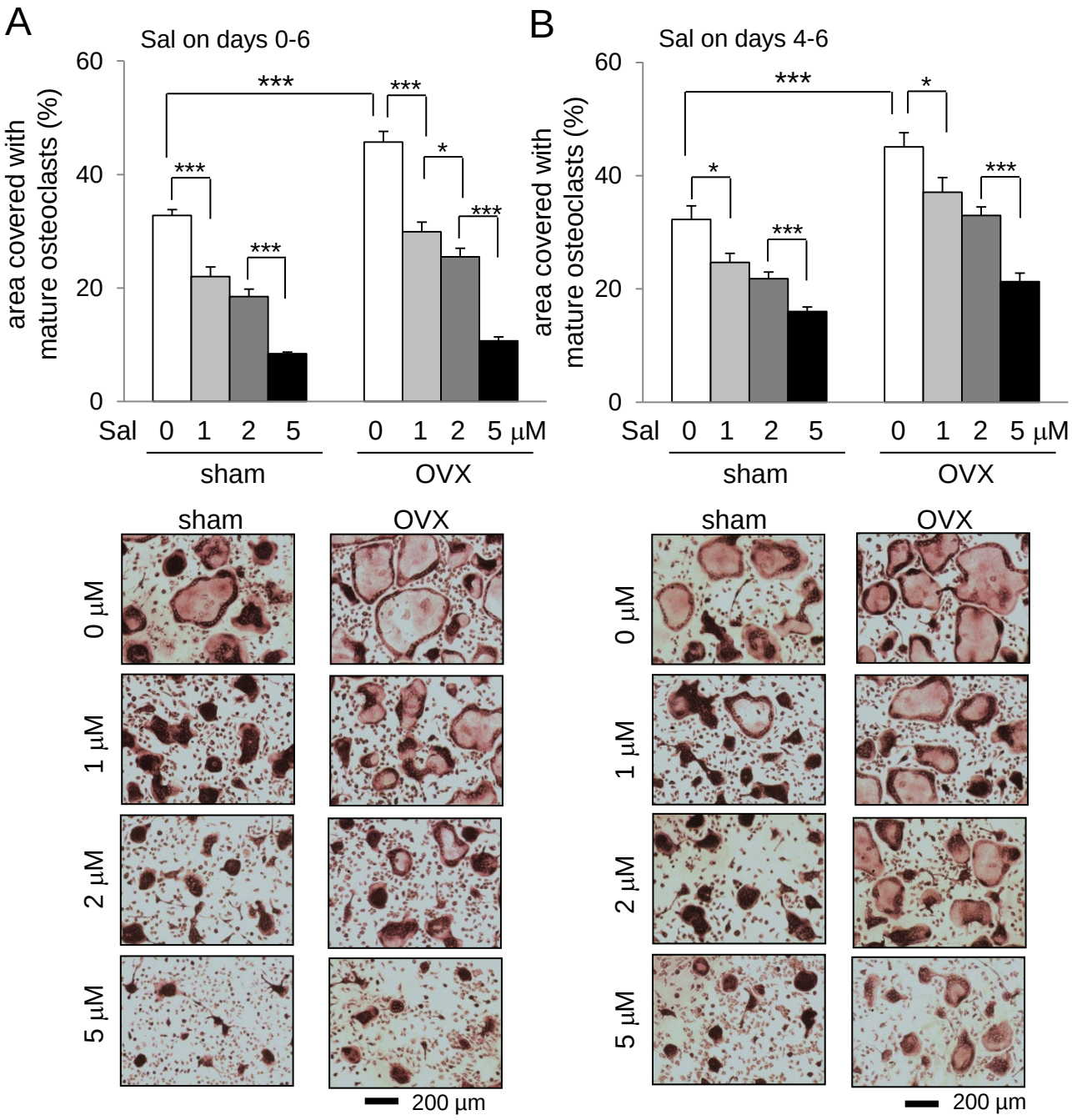
A
Sal on days 0-6
area covered with mature osteoclasts (%)
60
40
20
0
***
***
***
***
*
***
Sal 0 1 2 5 0 1 2 5 μM
sham
OVX
B
Sal on days 4-6
area covered with mature osteoclasts (%)
60
40
20
0
***
*
*
***
***
Sal 0 1 2 5 0 1 2 5 μM
sham
OVX
sham
OVX
0 μM
1 μM
2 μM
5 μM
200 μm
sham
OVX
0 μM
1 μM
2 μM
5 μM
200 μm

Figure 5

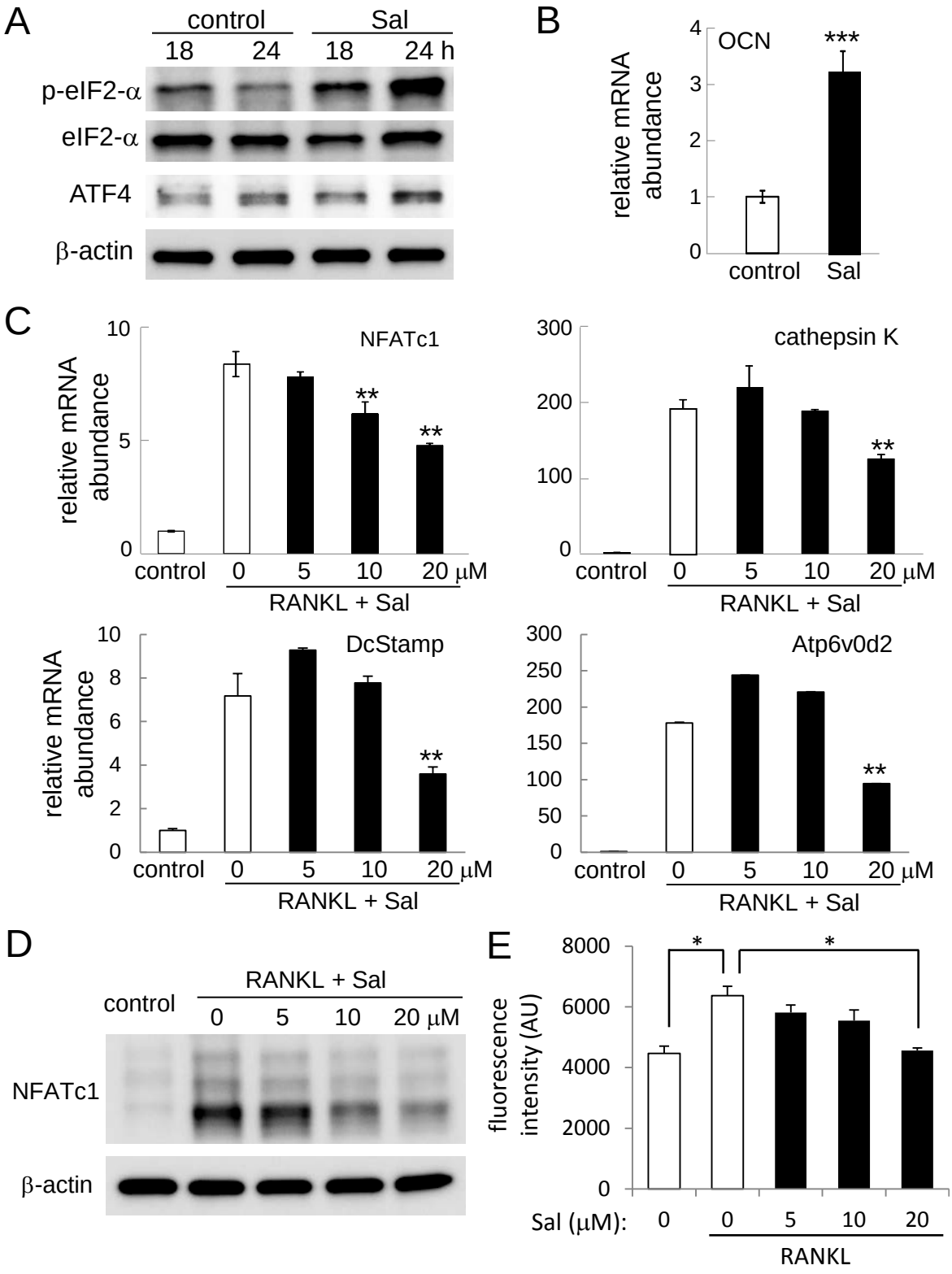
A
control
Sal
18
24
18
24 h
p-eIF2-α
eIF2-α
ATF4
β-actin
B
OCN
***
relative mRNA abundance
control
Sal
C
NFATc1
cathepsin K
DcStamp
Atp6v0d2
relative mRNA abundance
control
0
5
10
20 μM
RANKL + Sal
D
control
RANKL + Sal
0
5
10
20 μM
NFATc1
β-actin
E
fluorescence intensity (AU)
Sal (μM):
0
0
5
10
20
RANKL

Figure 6

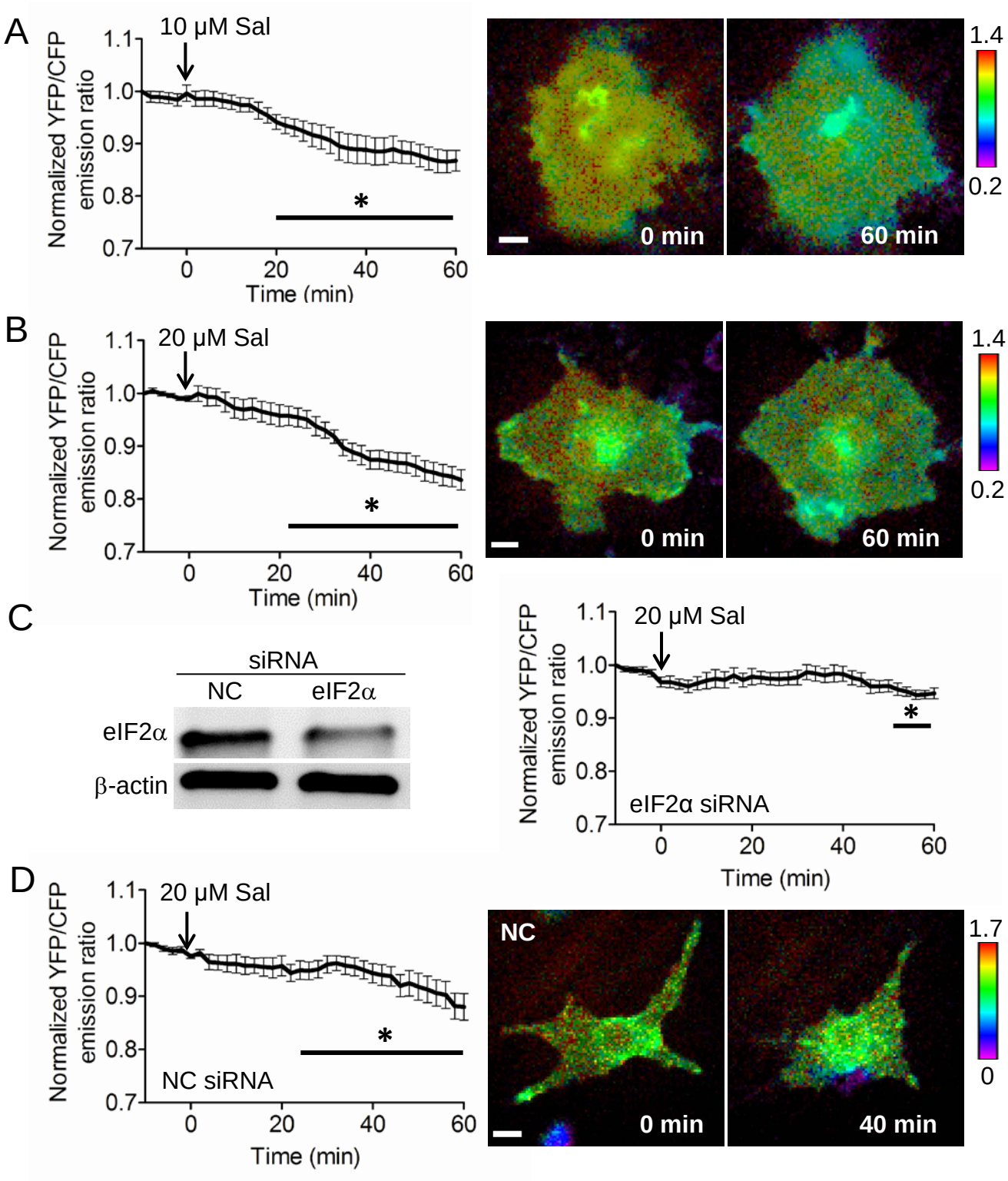
A
10 μM Sal
Normalized YFP/CFP emission ratio
1.1
1.0
0.9
0.8
0.7
0
20
40
60
Time (min)
*
0 min
60 min
1.4
0.2
B
20 μM Sal
Normalized YFP/CFP emission ratio
Time (min)
*
0 min
60 min
1.4
0.2
C
siRNA
NC
eIF2α
eIF2α
β-actin
20 μM Sal
Normalized YFP/CFP emission ratio
eIF2α siRNA
Time (min)
*
D
20 μM Sal
Normalized YFP/CFP emission ratio
NC siRNA
Time (min)
*
NC
0 min
40 min
1.7
0

Figure 7

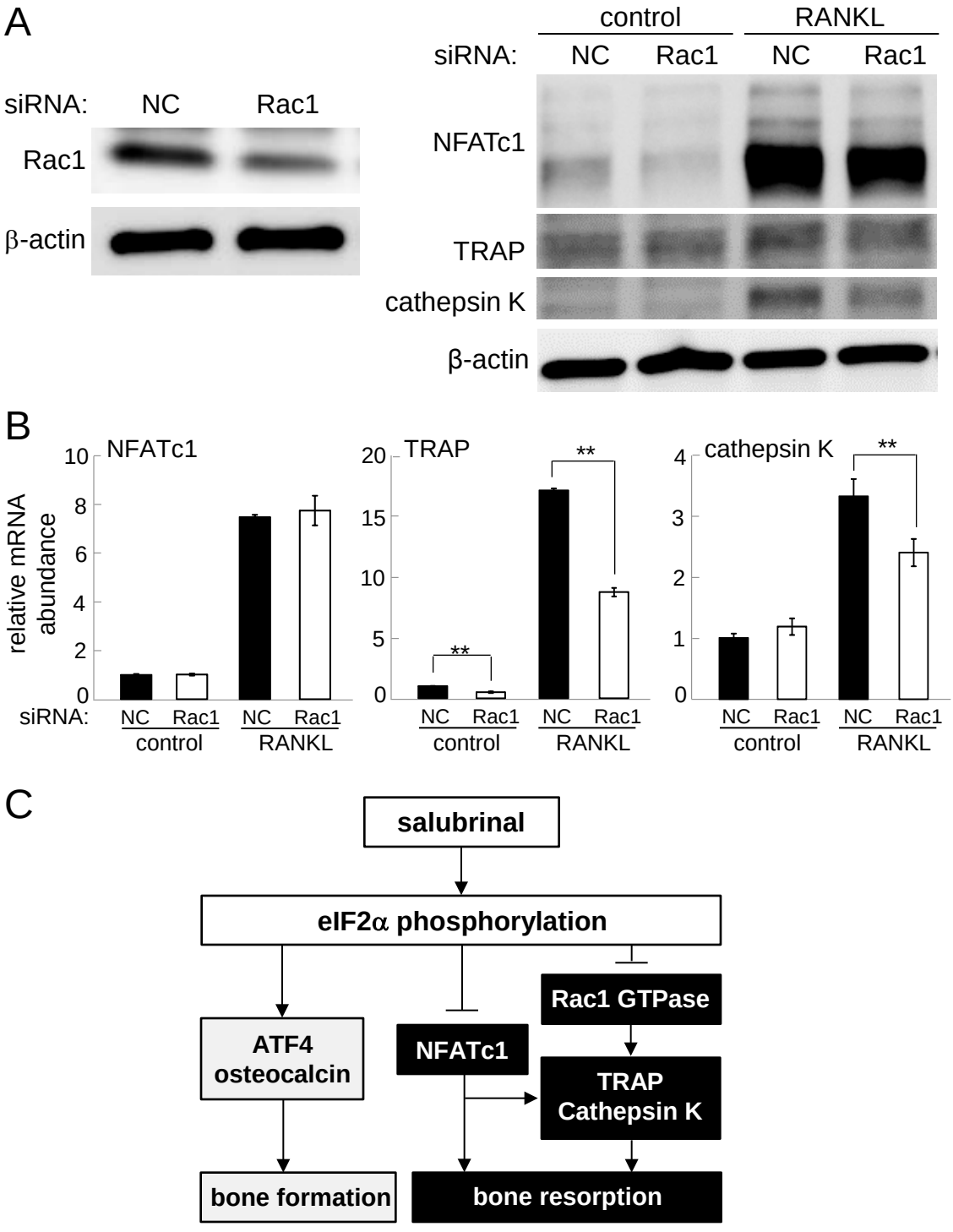
A
siRNA: NC Rac1
Rac1
β-actin
control RANKL
siRNA: NC Rac1 NC Rac1
NFATc1
TRAP
cathepsin K
β-actin
B
relative mRNA abundance
NFATc1
TRAP
cathepsin K
**
siRNA: NC Rac1 NC Rac1
control RANKL
C
salubrinal
eIF2α phosphorylation
ATF4
osteocalcin
NFATc1
Rac1 GTPase
TRAP
Cathepsin K
bone formation
bone resorption

Figure 8

2016 MILITARY SUPPLEMENT

Hydrogel-Based Local Release of Salubrinal Stimulates Healing of Mouse Tibia Fracture

Wenxiao Xu[1, 2], Andy Chen[3], Yijia Zhang[1], Jiliang Li[4], Chien-Chi Lin[1], Jing-long Yan[2], and Hiroki Yokota[1]

[1]Department of Biomedical Engineering, Indiana University Purdue University Indianapolis, Indianapolis, IN 46202, USA
[2]Department of Orthopedics, Second Affiliated Hospital of Harbin Medical University, Harbin, Heilongjiang 150086, China
[3]Weldon School of Biomedical Engineering, Purdue University, West Lafayette, IN 47907, USA
[4]Department of Biology, Indiana University Purdue University Indianapolis, Indianapolis, IN 46202, USA

Keywords: bone fracture, tibia, salubrinal, hydrogel, mechanical test

Running title: Salubrinal and Bone Fracture Healing

Corresponding Author:

Hiroki Yokota, PhD
Department of Biomedical Engineering
Indiana University Purdue University Indianapolis
723 West Michigan Street, SL220
Indianapolis, IN 46202
Phone: 317-278-5177
Fax: 317-278-2455
Email: hyokota@iupui.edu

Abstract

Salubrinal is a small synthetic agent that presents beneficial effects on skeletal diseases and tumor progression. It is reported to stimulate bone formation and suppress bone resorption. In this study, we examined whether salubrinal administration can stimulate the healing of bone fracture using a mouse model of closed tibia fracture. In particular, we administered salubrinal in two different routes: one-time hydrogel injection with salubrinal-loaded poly(lactic-co-glycolic acid (PLGA) microparticles; and daily subcutaneous injection for 4 weeks. A subcutaneous injection of bone morphogenetic protein 2 (BMP2) was used as a positive control. The results showed that 4 weeks after the induction of tibia fracture no groups including the BMP2 control group elevated bone mineral density (BMD) or bone mineral content (BMC). Hydrogel-based injection of salubrinal showed a higher stiffness than that of the placebo, as well as significant elevation of ultimate force. Although daily subcutaneous injection of BMP2 increased stiffness and ultimate, daily injection of salubrinal did not show any significant improvement of mechanical properties. Of note, the total salubrinal dose in the hydrogel group was approximately 18% of that in the subcutaneous group. Collectively, the study herein demonstrates that salubrinal is capable of stimulating the healing of tibia fracture in a single application when locally administered via PLGA microparticles.

Introduction

In order to stimulate the healing of bone fracture, various pharmacological therapies have been investigated. The administration of bone morphogenetic proteins (BMPs), transforming growth factor β (TGFβ) superfamily of proteins, has been shown in randomized controlled trials to be efficient in tibial fracture healing (1, 2), and vascular endothelial growth factor (VEGF) is also reported to enhance bone healing (3). Systemic therapy with agents such as parathyroid hormone (PTH), growth hormone (GH), and the HMG-CoA reductase inhibitors are under investigation. Through Wnt signaling, systemic administration of sclerostin monoclonal antibody was shown to increase bone formation, bone mass, and bone strength (4). Molecules such as prostaglandin E receptor agonists and the thrombin-related peptide, TP508, have presented promise in animal models of fracture repair (5, 6), and a possibility of gene therapy such as BMP2-transfected bone marrow was demonstrated (7). However, difficult healing problems such as delayed union, nonunion, growth abnormalities, and infection require much more effort to confirm the safety and therapeutic efficacy to further improve existing therapies in clinic.

Salubrinal is a synthetic compound ($C_{21}H_{17}Cl_3N_4OS$; 480 Da) which is known to reduce various cellular stresses including stress to the endoplasmic reticulum (8, 9). It inhibits serine/threonine protein phosphatase 1alpha (PP1α), followed by the elevation of phosphorylated eukaryotic translation initiation factor 2 alpha (eIF2α) (10). Salubrinal is reported to enhance bone formation by stimulating activating transcription factor 4 (ATF4), one of the transcription factors for bone formation, via eIF2α mediated signaling and stimulating development of bone-forming osteoblasts (11). It also suppresses nuclear factor of activated T-cells, cytoplasmic 1 (NFATc1),

a master transcription factor for osteoclastogenesis, and inhibits development of bone-resorbing osteoclasts (12, 13). Furthermore, salubrinal reduces inflammation and degradation of cartilage tissues (14, 15), and it is capable of attenuating proliferation and migration of breast cancer cells (16). While salubrinal can add calcified mass to osteoporotic bone, its effect on the healing of bone fracture has not been tested using a closed fracture model. A closed tibial shaft fracture is the most common long-bone fracture, often caused by sport-related injuries as well as simple falls (17). The current study investigated efficacy of salubrinal in the healing of tibia fracture using a mouse closed fracture model.

Bone fracture healing is an orchestrated process by many types of cells, including mesenchymal stem cells, hematopoietic stem cells, inflammatory cells (macrophages, monocytes, lymphocytes, etc.), fibroblasts, osteoblasts, and osteoclasts (18). It consists of three major phases (19), the reactive, reparative, and remodeling phases, and there is evidence salubrinal may play a role in these phases. In the early reactive phase immediately after fracture, a hematoma develops at the fracture site, and inflammatory responses are induced by cells such as macrophages, monocytes, and lymphocytes (19). It is yet to be examined whether the observed anti-inflammatory effects of salubrinal provides positive influence in this reactive phase. In the second reparative phase, a collagen matrix is actively synthesized and mineralized mainly by osteoblasts, whose proliferation and differentiation is affected by salubrinal (11). The third phase is bone remodeling, in which the transient form of calcified tissue is remodeled to form a stiffer matrix, and the original shape and structure is restored (20). It is not clear whether salubrinal's inhibitory effect on bone-resorbing osteoclasts accelerate both the reparative and remodeling phases.

A specific question, addressed herein, was: does salubrinal's delivery method change its efficacy? Two different routes were employed in this study: one-time injection of *in situ* gelled poly(ethylene glycol) (PEG) hydrogel that contained salubrinal-loaded poly(lactic-co-glycolic acid) (PLGA) microparticles; and daily subcutaneous injection of salubrinal for 4 weeks. Hydrogels are highly hydrated networks of crosslinked polymer chains, which are formed from either natural (e.g. collagen and hyaluronic acid) or synthetic (e.g. PEG) polymeric materials (21). PEG-based hydrogels provide high degrees of tunability in matrix crosslinking, degradation, and modification (22), and might have the benefits to emulate native matrix mechanics as well as to deliver bone anabolic agents locally for fracture healing. PLGA microparticles loaded with salubrinal were expected to serve as a carrier for salubrinal's sustained delivery. In this study, salubrinal-loaded PLGA microparticles were mixed with PEG macromers capable of *in situ* gelling, and the composite were injected and cured *in situ*.

Materials and Methods

Animal Preparation

Seventy-two C57BL/6 female mice (14 weeks, body weight ~20 g; Harlan Sprague–Dawley Inc., Indianapolis, IN, USA) were used in the study. All procedures performed in this study were approved by the Indiana University Animal Care and Use Committee and were in compliance with the *Guiding Principles in the Care and Use of Animals* endorsed by the American Physiological Society. Five mice were housed together in a cage. Animals were fed with standard laboratory chow and water *ad libitum*, and they were allowed to acclimate for 1 week before experimentation. Mice were allowed full unrestricted cage activity, and they were weighed weekly. We employed visual inspection of food and water consumption, any signs of inflammation or infection, and walking patterns. Mice were divided into 6 groups, in which group 1 was treated as normal control (no induction of tibia fracture). Groups 2 and 3 were used for testing hydrogel-based administration of placebo and salubrinal (experiment 1), while groups 4-6 for examining subcutaneous injection of placebo, BMP2 and salubrinal (experiment 2). Experiments 1 and 2 were conducted separately using different batches of animals.

Surgical procedure for induction of the closed tibia fracture

Prior to the induction of closed fracture in the right tibia, mice were anesthetized using 1.5% isoflurane. To mice in groups 2-5, a stainless steel wire (30-gauge needle) was inserted into the intramedullary cavity of the right tibia through its proximal end (Fig. 1C & D). The wire extending beyond the tibia condyles was cut, and the patella was properly repositioned. A closed diaphyseal fracture was then induced in the right distal tibia using a custom made 3-point bending device with a consistent force (Fig. 1A) (23). Radiographic images were taken

(Faxitron, Tucson, AZ, USA) on day 0, as well as weeks 1, 2, 3 and 4 after fracture induction (Fig. 1C & D).

Fabrication of Salubrinal-loaded PLGA microparticles

Salubrinal loaded PLGA (50:50, MW: 30-60 kDa, Sigma) microparticles were prepared using oil-in-water emulsion method (24). First, 100 mg/ml of PLGA was dissolved in dichloromethane (DCM). Next, 2 mg of salubrinal was added to 1 ml of PLGA/DCM solution, followed by vortexing for 1 minute. The primary emulsion was added to 2 ml of 1% poly(vinyl alcohol) (PVA) solution and vortexed for 3 minutes. The secondary emulsion was poured into 20ml of aqueous solution containing 0.5% PVA and 450 mM sodium chloride. The emulsion was stirred for 4 hours at 700 rpm to allow the evaporation of DCM, and the hardened microparticles were collected by centrifugation (2000 rpm, 5 min) and washed three times with ddH_2O. The drug-loaded PLGA microparticles were then freeze dried and stored at -20°C until use.

In situ rheometry of PEG hydrogelation with and without drug-loaded PLGA microparticles

In situ cured PEG hydrogels were prepared by reacting four-arm PEG-acrylate (PEG4A, 20 kDa, synthesized using published protocol) (22) and four-arm PEG-thiol (PEG4SH, 10 kDa, purchased from JenKem Technology USA) (Fig. 2A) through Michael-type addition reaction (25) (Fig. 2B). Briefly, stock solutions of PEG4A and PEG4SH (both at 20 wt%) were mixed at equal volume and pipetted onto the platform of a digital rheometer (CVO 100, Malvern). Eight-mm parallel plate geometry was used, and the gelation was monitored using single frequency rheometry (1 Hz) operated at 5% strain. In one group, PLGA microparticles (10 wt%) were mixed with the PEG solutions prior to *in situ* rheometry measurement.

Administration of salubrinal and BMP2

In experiment 1, 12 mice in group 2 (hydrogel placebo) were given hydrogel without any agent on day 1, while 12 mice in group 3 (hydrogel salubrinal) received a single administration of salubrinal loaded hydrogel (100μg of salubrinal in 50 μl of gel). In experiment 2, 12 mice in group 4 (subcutaneous placebo) received daily subcutaneous injections of the vehicle (50 μl) to the fracture site. Twelve mice in group 5 (subcutaneous BMP2) were given daily injections of BMP2 (10 μg/kg in 50 μl of vehicle) as a positive control, and 12 mice in group 6 (subcutaneous salubrinal) received daily injections of salubrinal (1 mg/kg in 50 μl of vehicle).

Measurements of bone mineral density (BMD) and bone mineral content (BMC)

Mice were sacrificed 4 weeks after the fracture induction, and tibiae were harvested. Isolated tibiae were cleaned of soft tissues and stored at -20°C in gauze that was moisturized with PBS. The BMD and BMC of the entire tibia and callus region at the fracture site were determined using a PIXImus densitometer with a threshold value of 1800 (software version 1.4; GE Medical System Lunar, Madison, WI, USA) (26). The callus region was defined as a fixed rectangle region of interest (20 pixels X 20 pixels) that covered the callus center.

Fracture score

The fracture scores were defined from 0 to 3: “0” for no fracture, “1” for minor fracture, “2” for moderate fracture, and “3” for major fracture. X-ray images of the fractured tibia at weeks 0 - 4 were randomly labeled, and eight independent scorers participated in the evaluation. All scores were collected and averaged for each sample and time point.

Micro CT imaging

Micro-computed tomography was performed using Skyscan 1172 (Bruker-MicroCT, Kontich Belgium) (27). The harvested tibiae were wrapped in parafilm to maintain hydration and placed in a plastic tube and oriented vertically. Scans were performed at pixel size 8.99 μm. Using manufacturer-provided software, the images were reconstructed (nRecon v1.6.9.18), cross sections were obtained (Dataviewer, v1.5.0), and 3D models were generated (CT Analyser, v1.11.4.2) and visualized (CTvol, v2.2.3.0).

Mechanical testing of the tibia

Tibiae were tested to failure by four-point bending using a voltage-regulated mechanical loading device (ElectroForce 3100, Bose, Inc.), with a loading span of 2.3 mm and a support span of 7 mm (Fig. 1B) (28). The load was applied to the medial tibia such that the right span was located just inside of the tibia-fibula junction. After preloading to 0.5 N, the bone was twice loaded with a sinusoidal regimen of 0.5 Hz, 1 Hz, and 2 Hz at amplitude 1 N. The bone was then loaded monotonically at 0.005 mm/s until failure. Load and displacement were recorded and used to calculate stiffness and ultimate force.

Statistical analysis

The data were expressed as mean ± SEM. Statistical significance among groups was examined using one-way analysis of variance (ANOVA), and a *post hoc* test was conducted using Fisher's protected least significant difference (PLSD) for the pairwise comparisons. A paired *t*-test was

employed to evaluate statistical significance between the loaded and control samples. All comparisons were two tailed, and statistical significance was assumed for $p < 0.05$.

Results

In situ *rheometry of gelation with and without drug-loaded PLGA microparticles*

We first monitored the gelation process through *in situ* rheometry either in the absence (Fig. 2C) or presence (Fig. 2D) or PLGA microparticles. As expected, the two PEG macromers, PEG4A and PEG4SH, reacted to form a crosslinked network, demonstrated by rapid crossover of hydrogel elastic modulus (G') and viscous modulus (G") with a gel point of less than 1 minute regardless of the presence of PLGA microparticles. The gelation reached near completion within a few minutes of mixing the two macromer components. This timing is ideal as it allowed sufficient time to mix the essential components (i.e., PEG4A, PEG4SH, and PLGA microparticles) while permitting rapid gelation locally at the fracture site. It was worth noting that the addition of PLGA microparticles increased the Young's modulus (E_0) of the resulting hydrogels from ~33 kPa to ~96 kPa (Fig. 2C & D).

No significant change in BMD/BMC by hydrogel-based salubrinal administration

In experiment 1 with hydrogel-based administration of salubrinal, X-ray images in weeks 1, 2, 3, and 4, as well as micro CT images of the representative tibia samples after harvest in week 4 were captured (Fig. 3A - D). Although X-ray images in week 4 indicated a complete bridge of the fracture site with calcified tissue, the sagittal sections of micro CT images revealed discontinuous cortical bone at the fracture site. The BMD and BMC measurement of the entire tibia in week 4 did not show any significant changes in the hydrogel placebo (group 2) and salubrinal (group 3) samples. The same measurement in the restricted callus region in week 4 presented a tendency of increase in the salubrinal treated group, but the difference was not statistically significant ($p = 0.2$ for BMD, and $p = 0.09$ for BMC) (Fig. 3E & F).

The fracture score, which indicated the degree of discontinuity in the cortical bone at the fracture site, decreased in groups 2 and 3 (Fig. 4A). No statistical difference was observed during the 4-week healing period between the two groups except for week 2.

Elevated ultimate force by hydrogel-based salubrinal administration

The force-displacement relationship for 3 groups showed a distinctively different profile in response to a sinusoidal load (0.5 N, peak-to-peak) at 0.5, 1, and 2 Hz (Fig. 4B – G). The ascending and descending loads exhibited the same pattern, in which the intact control (group 1) was the stiffest and the hydrogel placebo (group 3) was the softest with the hydrogel salubrinal (group 2) in between. The ultimate force was 11.64 ± 5.48 N (hydrogel placebo, n = 12) and 16.99 ± 5.41 N (hydrogel salubrinal, n = 12) with $p = 0.03$, while stiffness was 81.55 ± 23.58 N/mm (hydrogel placebo, n = 12) and 106.73 ± 32.81 N/mm (hydrogel salubrinal, n = 12) with $p = 0.05$.

Differential effects of hydrogel-based administration and subcutaneous salubrinal injection

In experiment 2 with daily subcutaneous injection of vehicle (group 4), BMP2 (group 5), and salubrinal (group 6), the fracture score was determined for weeks 0 to 4 using longitudinal X-ray images (Fig. 6A & B). Images collected by PIXImus densitometer were used for determining BMD and BMC (Fig. 6C & D). The image analysis revealed that no statistical difference was detected among three groups for the fracture score, BMD, and BMC. Mechanical test using 4-point bending revealed that ultimate force and stiffness were significantly elevated in group 5 (subcutaneous BMP2), but no statistical difference was detected between group 4 (subcutaneous

control) and group 6 (subcutaneous salubrinal). Between experiments 1 and 2, no direct comparison of the mechanical testing results is possible since two experiments were conducted independently using different batches of animals.

Discussion

This study demonstrates that hydrogel-based administration of salubrinal in PLGA microparticles elevates the ultimate force in the four-point bending test and improves mechanical strength of the fractured tibia. Injectable and biodegradable hydrogels are excellent matrices for temporarily filling critical size bone defects and for delivering therapeutically relevant agents to facilitate/accelerate the healing process. The injectable PEG-based hydrogels used in this study were prepared using multi-arm PEG macromers (i.e., PEG4A and PEG4SH, Fig. 2A) with mutually reactive acrylate and thiol moieties. *In situ* gelation was achieved through a Michael-type addition reaction (Fig. 2B), and the resulting thiolether ester bonds could be degraded hydrolytically and/or enzymatically by esterases (Fig. 2B). We fabricated degradable PLGA microparticles for loading and subsequently releasing salubrinal *in vivo*. After injecting the precursor solution in the fracture site, hydrogel hardened and effectively entrapped the drug-loaded microparticles. Instead of delivering as daily systemic injections, the hydrogel served as void filling matrices, whereas the PLGA microparticles carried salubrinal and released it locally and gradually. Ideally, the PEG hydrogels and the PLGA microparticles would degrade slowly as the new bone formed and regenerated.

In experiment 1, salubrinal was loaded in PLGA microparticles and given one day after the induction of tibia fracture as a single injection at a dose of 5 mg/kg. In this administration, two solutions (PEG4SH and PEG4A) were mixed and the liquid mixture was quickly injected into the site of fracture within 30 sec. When salubrinal was applied as a daily subcutaneous injection at a dose of 1 mg/kg in experiment 2, no significant improvement of mechanical parameters such as the ultimate force and stiffness was observed. Since the subcutaneous injection was

conducted 28 times during the 4-week healing period, the total dose became 28 mg/kg. Collectively, efficacy of salubrinal in fracture healing significantly depends on its delivery method. A local delivery with a dose of 5 mg/kg was found to be more effective than a systemic delivery with a total dose of 28 mg/kg.

Agents for the healing of bone fracture are primarily screened and selected based on their efficacy in bone formation and bone remodeling (29). Salubrinal is a unique compound that affects inflammatory responses as well as skeletal preservation and reconstruction. In the reactive phase of fracture healing, previous studies strongly indicate that salubrinal acts as an anti-inflammatory agent. For instance, salubrinal is reported to suppress lipopolysaccharide (LPS)-stimulated inflammatory responses in macrophages (14), reduce orofacial inflammatory pain (30), and alleviates colitis through suppression of pro-inflammatory cytokines (31). Furthermore, it attenuates inflammatory cytokines such as IL1β, Cox2, IL2, TNF, and IL13 in macrophages, T lymphocytes, and mast cells (14). The mechanism of salubrinal's anti-inflammatory action and its link to eIF2α regulation are not satisfactorily understood (32). Besides eIF2α-mediated signaling, salubrinal is reported to downregulate NFκB signaling in an eIF2α independent fashion (15). Although inflammatory responses are a critical phase in fracture healing, the results with hydrogel-based administration of salubrinal indicate that suppression of inflammatory responses, at least in part, may accelerate an overall healing of fractured bone.

While BMP2 mainly enhances bone formation without directly affecting bone resorption, salubrinal not only stimulates osteoblastogenesis but also inhibits osteoclastogenesis in the

reparative and remodeling phases of fracture healing. Furthermore, salubrinal's action is mediated using its unique signaling pathway. Regarding bone formation, salubrinal activates development of osteoblasts by upregulating ATF4, followed by ATF4-mediated elevation of osteocalcin. Upregulation of ATF4 is primarily driven by the elevated eIF2α phosphorylation (10), while BMP2 activates many other signaling pathways including Smad, mitogen-activated protein kinase (MAPK), Wnt, Hedgehog, Notch, and fibroblast growth factor (FGF) (33). Regarding bone resorption, salubrinal suppresses the proliferation and maturation of osteoclasts by downregulating AP-1 proteins such as c-Fos and JunB, as well as NFATc1 (12). The mechanistic differences in the actions of BMP2 and salubrinal may result in their differential effects on malignant tumor. BMP2 has a risk of inducing cancer (34), but salubrinal is reported to present an inhibitory role in growth and migration of breast cancer cells (16). Bisphosphonates are anti-resorptive agents which have been frequently administered for treatment of osteoporosis. In bone fractured animals treated with bisphosphonates, an increase in callus size and bone strength is reported (35). A comparative study between bisphosphonates and salubrinal might help understand significance of anti-resorptive actions in the fracture healing.

There are several factors that might contribute to further elevating salubrinal's efficacy. First, the most effective release rate of salubrinal might be determined by adjusting its loading condition to PLGA. Second, the size of PEG molecules (currently 10 kDa and 20 kDa) might be altered to control PLGA retention in a hydrogel and salubrinal's release rate. Third, salubrinal's efficacy will be evaluated in each of the three healing phases separately. In summary, we demonstrated that a single hydrogel-based administration of salubrinal increased mechanical

strength of the fractured tibia. Further analysis regarding administration frequency and most effective dosage may warrant a future clinical trial to the common closed tibial shaft fracture.

Acknowledgements

The authors appreciate Kazumasa Minami, Yu Sun, Shinya Takigawa, Shengzhi Liu, Allen Zhang, and Allen Zhou for technical support. This study was supported by DOD W81XWH-11-1-0716 (HY).

References

1. Govender S, Csimma C: Recombinant human bone morphogenetic protein-2 for treatment of open tibial fractures: a prospective, controlled, randomized study of four hundred and fifty patients. *J Bone Joint Surg Am* 84:2123 – 2134, 2002.
2. Schmidmaier G, Wildemann B, Ostapowicz D, Kandziora F, Stange R, Haas NP, Raschke M: Long-term effects of local growth factor (IGF-I and TGF-beta1) treatment on fracture healing. A safety study for using growth factors. *J Orthop Res* 22(3):514−519, 2004.
3. Eckardt H, Ding M, Lind M, Hansen ES, Christensen KS, Hvid I: Recombinant human vascular endothelial growth factor enhances bone healing in an experimental nonunion model. *J Bone Joint Surg Br* 87(10):1434−1438, 2005.
4. Li X, Ominsky MS, Warmington KS: Sclerostin antibody treatment increases bone formation, bone mass, and bone strength in a rat model of post-menopausal osteoporosis. *J Bone Miner Res* 24:578-588, 2009.
5. Paralkar VM, Borovecki F, Ke HZ, Cameron KO, Lefker B, Grasser WA, Owen TA, Li M, DaSilva-Jardine P, Zhou M, Dunn RL, Dumont F, Korsmeyer R, Krasney P, Brown TA, Plowchalk D, Vukicevic S, Thompson DD: An EP2 receptor-selective prostaglandin E2 agonist induces bone healing. *Proc Natl Acad Sci USA* 100(11):6736−6740, 2003.
6. Sheller MR, Crowther RS, Kinney JH, Yang J, Di Jorio S, Breunig T, Carney DH, Ryaby JT: Repair of rabbit segmental defects with the thrombin peptide, TP508. *J Orthop Res* 22(5):1094−1099, 2004.
7. Lieberman JR, Daluiski A, Stevenson S, Wu L, McAllister P, Lee YP, Kabo JM, Finerman GA, Berk AJ, Witte ON: The effect of regional gene therapy with bone morphogenetic

protein-2-producing bone-marrow cells on the repair of segmental femoral defects in rats. *J Bone Joint Surg Am* 81(7):905−917, 1999.

8. Boyce M, Bryant KF, Jousse C, Long K, Harding HP, Scheuner D, Kaufman RJ, Ma D, Coen DM, Ron D, Yuan J: A selective inhibitor of eIF2alpha dephosphorylation protects cells from ER stress. *Science* 307: 935-939, 2005.
9. Ron D: Translational control in the endoplasmic reticulum stress response. *J Clin Invest* 110:1383-1388, 2002.
10. Wek RC, Jiang HY, Anthony TG: Coping with stress: eIF2 kinases and translational control. *Biochem Soc Trans* 34: 7-11, 2006.
11. Yokota H, Hamamura K, Chen A, Dodge TR, Tanjung N, Abedinpoor A, Zhang P: Effects of salubrinal on development of osteoclasts and osteoblasts from bone marrow-derived cells. *BMC Musculoskeletal Disorders* 14:197, 2013.
12. Hamamura K, Tanjung N, Yokota H: Suppression of osteoclastogenesis through phosphorylation of eukaryotic translation initiation factor 2 alpha. *J Bone Miner Metab* 31: 618-628, 2013.
13. Hamamura K, Chen A, Tanjung N, Takigawa S, Sudo A, Yokota H: *In vitro* and *in silico* analysis of an inhibitory mechanism of osteoclastogenesis by salubrinal and guanabenz. *Cell Signal* 27: 353-362, 2015.
14. Hamamura K, Nishimura A, Chen A, Takigawa S, Sudo A, Yokota H: Salubrinal acts as a Dusp2 inhibitor and suppresses inflammation in anti-collagen antibody-induced arthritis. *Cellular Signaling* 27:828-835, 2015.
15. Hamamura K, Nishimura A, Iino T, Takigawa S, Sudo A Yokota H: Chondroprotective effects of salubrinal in a mouse model of osteoarthritis. *Bone Joint Res* 4:84-92, 2015.

16. Hamamura K, Minami K, Tanjung N, Wan Q, Koizumi M, Matsuura N, Na S, Yokota H: Attenuation of malignant phenotypes of breast cancer cells through eIF2α-mediated downregulation of Rac1 signaling. *Int. J. Oncology* 44:1980-1988, 2014.
17. Antonova E, Le TK, Burge R, Mershon J: Tibia shaft fractures: costly burden of nonunions. *BMC Musculoskelet Disord* 14:42, 2013.
18. Burr DB, Allen MR: Basic and Applied Bone Biology. Academic Press, San Diego, USA, pp 205-223, 2013.
19. Whener T, Gruchenberg K, Bindl R, Recknagel S, Steiner M, Ignatius A, Claes L: Temporal delimitation of the healing phases via monitoring of fracture callus stiffness in rats. *J. Orthop Res* 32:1589-1595, 2014.
20. Marsell R, Einhorn TA: The biology of fracture healing. *Injury* 42:551-555, 2011.
21. Gibbs DMR, Dawson JI, Black CRM, Oreffo ROC: A review of hydrogel use in fracture healing and bone regeneration, *J Tissue Eng Regen Med*, doi: 10.1002/term.1968, 2014.
22. Lin CC: Recent advances in crosslinking chemistry of biomimetic poly(ethylene glycol) hydrogels, *RSC Adv* 5(50):39844-398583, 2015.
23. Manigrasso MB, O'Connor JP: Characterization of a closed femur fracture model in mice. *J. Orthop. Trauma* 18:687-695, 2004.
24. Ito F, Fujimori H, Honnami H, Kawakami H, Kanamura K, Makino K: Control of drug loading efficiency and drug release behavior in preparation of hydrophilic-drug-containing monodisperse PLGA microspheres. *J Mater Sci: Mater Med* 21:1563–1571, 2010.
25. Hao Y, Shih H, Munoz Z, Kemp A, Lin CC: Visible light cured thiol-vinyl hydrogels with tunable degradation for 3D cell culture. *Acta Biomaterialia* 10:104-114, 2014.

26. Zhang P, Hamamura K, Turner CH, Yokota H: Lengthening of mouse hindlimbs with joint loading. *J Bone Miner Metab* 28:268-275, 2010.

27. Berman, AG, Clauser, CA, Wunderlin, C, Hammond, MA, Wallace, JM: Structural and Mechanical Improvements to Bone Are Strain Dependent with Axial Compression of the Tibia in Female C57BL/6 Mice. *PLoS One* 10:e0130504, 2015.

28. Hiltunen A, Vuorio E, Aro HT: A standardized experimental fracture in the mouse tibia. *J Orthop Res* 11:305-312, 1993.

29. Bukara SV: Systemic administration of pharmacological agents and bone repair: what can we expect. *Injury* 42:605-608, 2011.

30. Yang ES, Bae JY, Kim TH, Kim YS, Suk K, Bae YC: Involvement of endoplasmic reticulum stress response in orofacial inflammatory pain. *Exp Neurobiol* 23:372-380, 2014.

31. Okazaki T, Nishio A, Takeo M, Sakaguchi Y, Fukui T, Uchida K, Okazaki K: Inhibition of the dephosphorylation of eukaryotic initiation factor 2a ameliorates murine experimental colitis. *Digestion* 90:167-178, 2014.

32. Hamamura K, Chen A, Uto Y, Yokota H: Potential therapeutic applications of salubrinal for skeletal diseases and beyond. *J. Nat. Sci*. 1:e151, 2015.

33. Wan M, Cao X: BMP signaling in skeletal development. *Biochem Biophy Res Com* 328:651-657, 2005.

34. Carragee EJ, Chu G, Rohatgi R, Hurwitz EL, Weiner BK, Yoon ST, Comer G, Kopjar B: Cancer risk after use of recombinant bone morphogenetic protein 2 for spinal arthrodesis. *J Bone Joint Surg Am* 95:1537-1545, 2013.

35. Li J, Mori S, Kaji Y, Mashiba T, Kawanishi J, Norimatsu H: Effect of bisphosphonate (incadronate) on fracture healing of long bones in rats. *J Bone Miner Res* 14:969-979, 1999.

Figure Legends

Figure 1. Tibia fracture study. (A) Custom-made 3-point bending device for inducing closed tibia fracture. (B) Four-point bending setup for mechanical testing. (C & D) X-ray images of the fractured tibiae. Of note, a stainless steel rod was inserted in the medullary cavity of the tibia.

Figure 2. Hydrogel based delivery. (A) Chemical structure of two PEG derivatives (PEG4SH and PEG4A). (B) Chemical reactions for *in situ* gelation and overtime hydrolysis. (C) Changes in moduli during gelation without PLGA particles. (D) Changes in moduli during gelation with salubrinal-loaded PLGA particles.

Figure 3. X-ray images, micro CT images, and BMD and BMC for experiment 1. (A) X-ray images of the fractured tibiae for the hydrogel placebo (group 2) and hydrogel salubrinal (group 3) in weeks 0, 1, 2, 3, and 4. (B) Micro CT images of the intact control sample (group 1). Scale bar indicates 1 mm. (C) Micro CT images of the hydrogel placebo sample (group 2). (D) Micro CT images of the hydrogel salubrinal sample (group 3). (E) BMD for the whole tibia and callous near the fracture site for groups 2 and 3. (F) BMC for the whole tibia and callous near the fracture site for groups 2 and 3.

Figure 4. Fracture score and force-displacement relationship for experiment 1. (A) Fracture score in weeks 0 – 4 for the hydrogel control and hydrogel salubrinal groups. Of note, fracture score = "0" (no obvious fracture), "1" (minor fracture), "2" (moderate fracture), and "3" (severe fracture). (B – D) Force-displacement relationship for groups 1-3 in response to an increasing

sinusoidal force (0.5 N, peak-to-peak) at 0.5, 1, and 2 Hz, respectively. (E – G) Force-displacement relationship for groups 1-3 in response to a decreasing sinusoidal force (0.5 N, peak-to-peak) at 0.5, 1, and 2 Hz, respectively.

Figure 5. Mechanical strength 4 weeks after fracture induction for experiment 1. (A) Force-displacement relationship for the hydrogel control group in response to a linearly increasing displacement. The cross indicates the site of ultimate force. (B) Force-displacement relationship for the hydrogel salubrinal group. (C) Ultimate force of the hydrogel control and hydrogel salubrinal groups. (D) Stiffness of the hydrogel control and hydrogel salubrinal groups.

Figure 6. Administration of BMP2 and salubrinal as subcutaneous injection near the fracture site in experiment 2. (A) X-ray images of the fractured tibiae for the subcutaneous control (group 4), subcutaneous BMP2 (group 5), and subcutaneous salubrinal (group 6) in weeks 0, 1, 2, 3, and 4. (B) Fracture score in weeks 0 – 4 for the subcutaneous control, BMP2, and salubrinal groups. (C & D) BMD and BMC of the fractured tibia, respectively. (E) Ultimate force of the subcutaneous control, BMP2, and salubrinal samples. (F) Stiffness of the subcutaneous control, BMP2, and salubrinal samples.

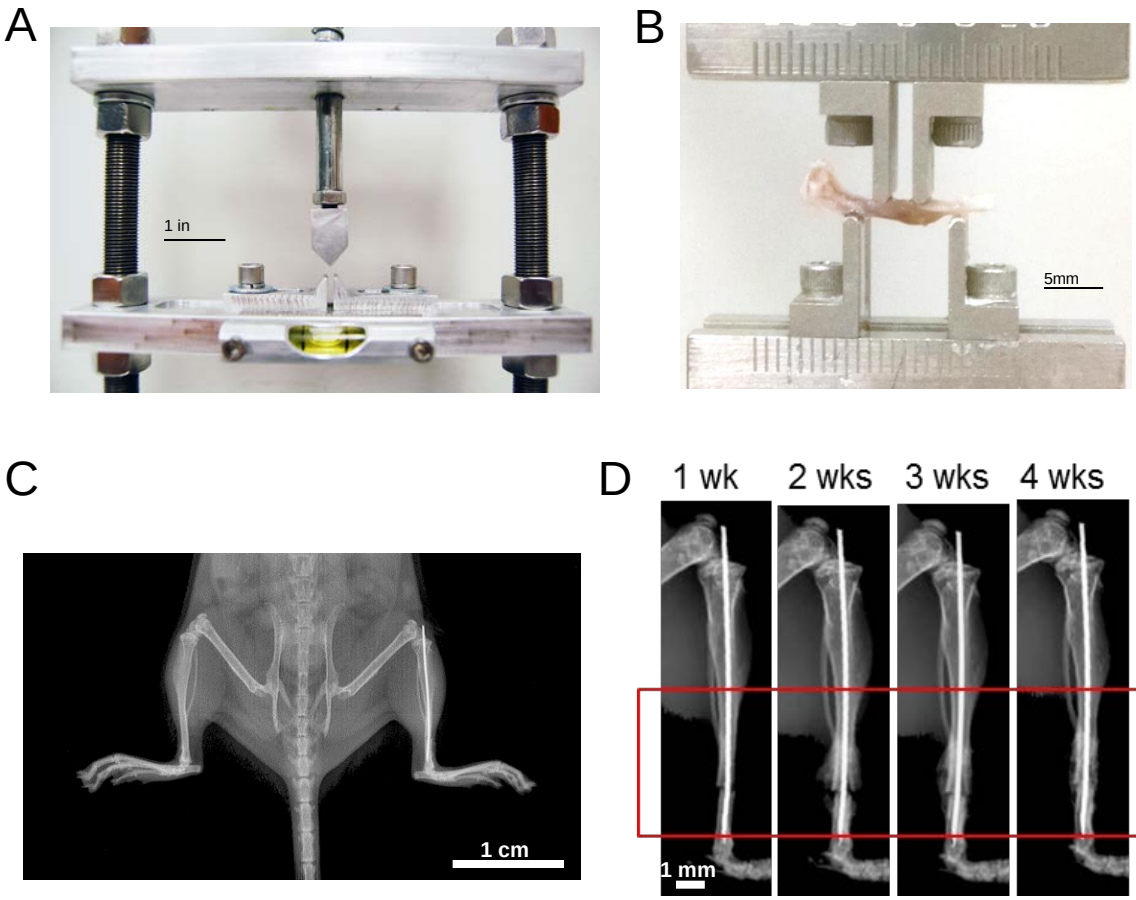

Figure 1

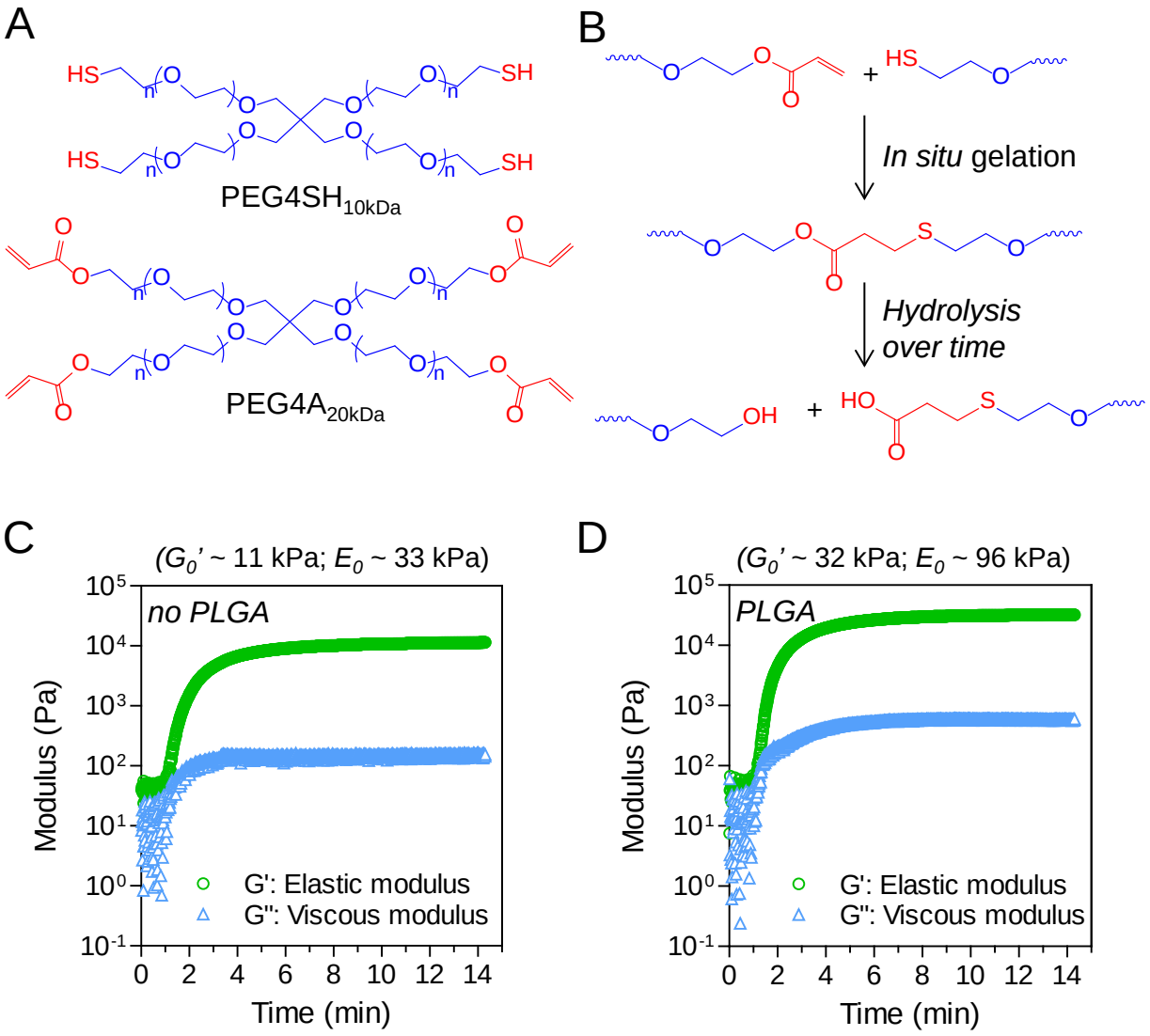
A
HS
SH
PEG4SH10kDa
PEG4A20kDa
B
HS
In situ gelation
Hydrolysis
over time
OH
HO
C
(G0' ~ 11 kPa; E0 ~ 33 kPa)
no PLGA
Modulus (Pa)
G': Elastic modulus
G": Viscous modulus
Time (min)
D
(G0' ~ 32 kPa; E0 ~ 96 kPa)
PLGA
Modulus (Pa)
G': Elastic modulus
G": Viscous modulus
Time (min)

Figure 2

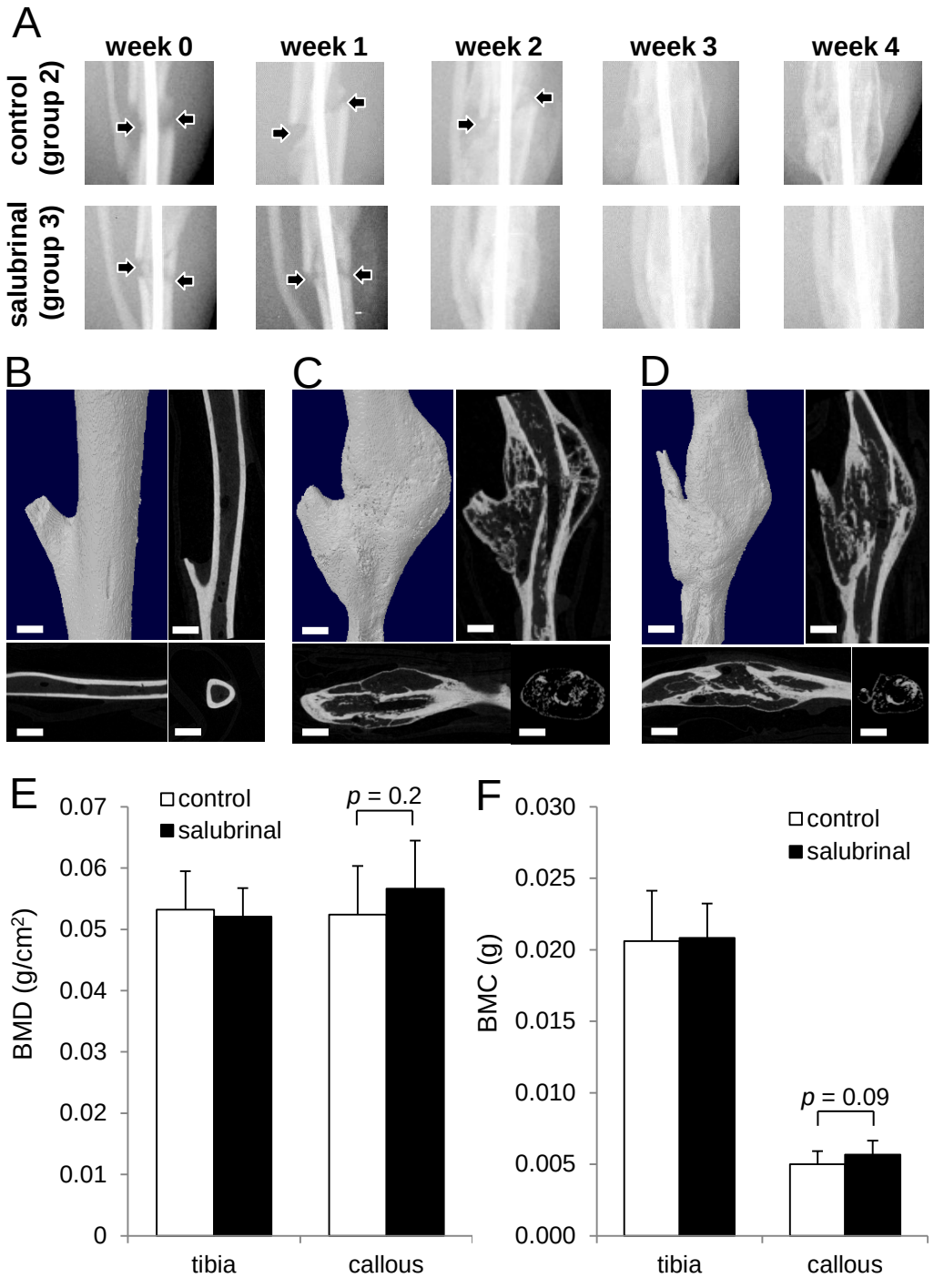
A
week 0
week 1
week 2
week 3
week 4
control (group 2)
salubrinal (group 3)
B
C
D
E
control
salubrinal
p = 0.2
BMD (g/cm²)
0.07
0.06
0.05
0.04
0.03
0.02
0.01
0
tibia
callous
F
control
salubrinal
p = 0.09
BMC (g)
0.030
0.025
0.020
0.015
0.010
0.005
0.000
tibia
callous

Figure 3

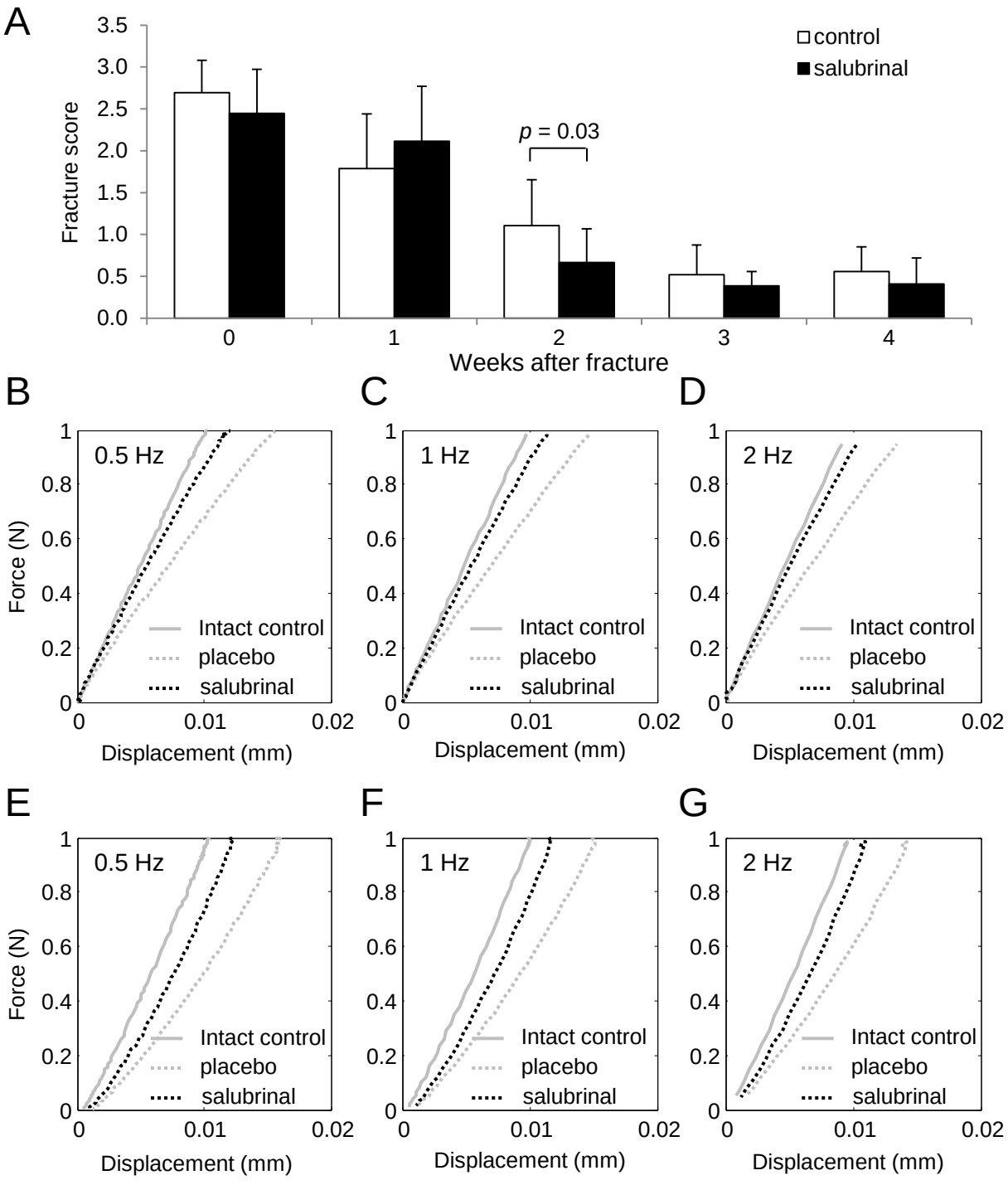
A
Fracture score
3.5
3.0
2.5
2.0
1.5
1.0
0.5
0.0
control
salubrinal
p = 0.03
0
1
2
3
4
Weeks after fracture
B
C
D
0.5 Hz
1 Hz
2 Hz
Force (N)
Intact control
placebo
salubrinal
0
0.01
0.02
Displacement (mm)
E
F
G

Figure 4

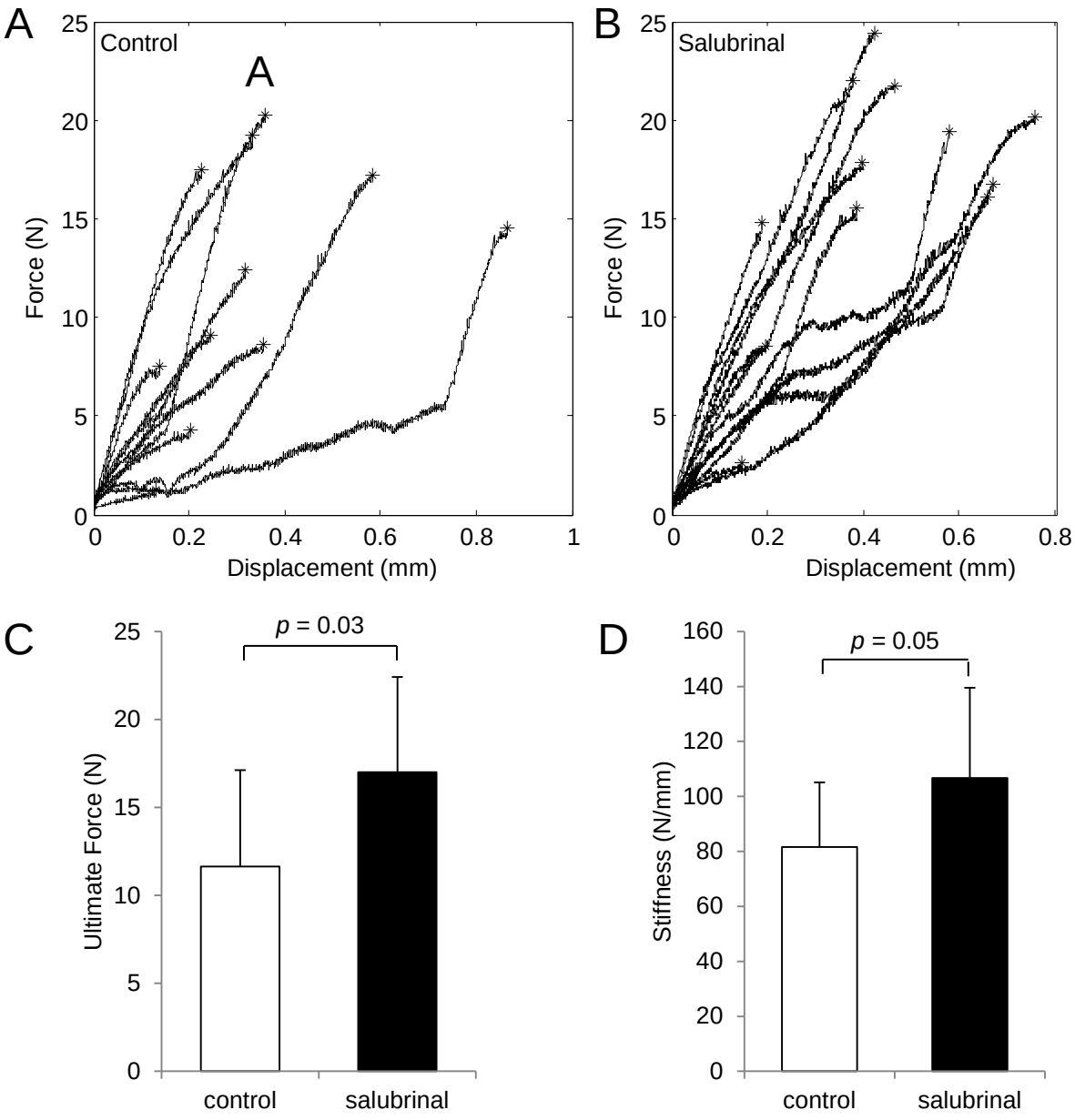
A
Control
A
Force (N)
Displacement (mm)
B
Salubrinal
Force (N)
Displacement (mm)
C
p = 0.03
Ultimate Force (N)
control
salubrinal
D
p = 0.05
Stiffness (N/mm)
control
salubrinal

Figure 5

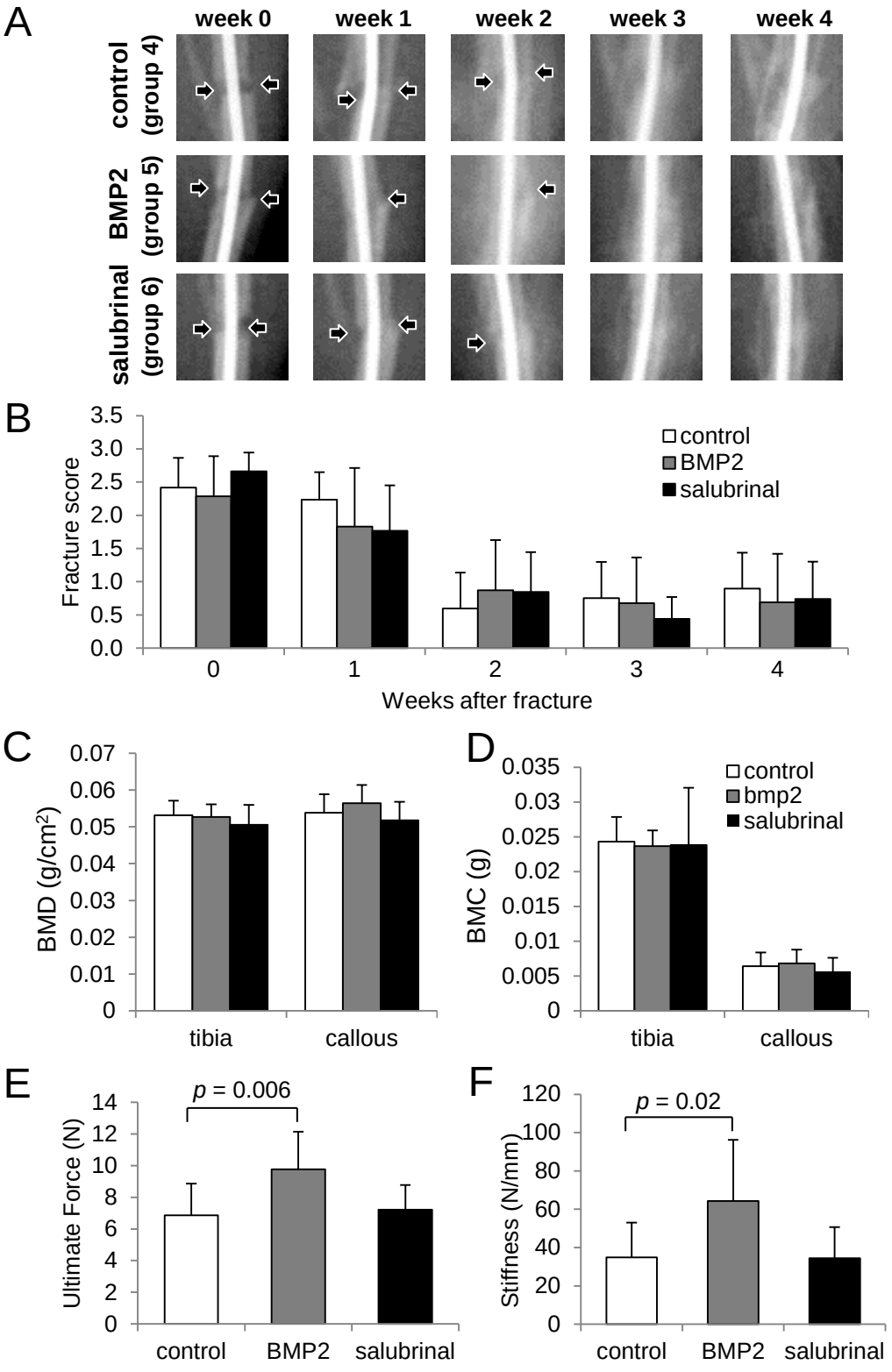
A
week 0
week 1
week 2
week 3
week 4
control (group 4)
BMP2 (group 5)
salubrinal (group 6)
B
Fracture score
control
BMP2
salubrinal
Weeks after fracture
C
BMD (g/cm²)
tibia
callous
D
BMC (g)
control
bmp2
salubrinal
tibia
callous
E
p = 0.006
Ultimate Force (N)
control
BMP2
salubrinal
F
p = 0.02
Stiffness (N/mm)
control
BMP2
salubrinal

Figure 6